

Fundamental Characterization of Photodegradable Hydrogels:
Spatiotemporal Control of the Cellular Microenvironment

by

Mark William Tibbitt

B.A., Northwestern University, 2007

A thesis submitted to the
Faculty of the Graduate School of the
University of Colorado in partial fulfillment
of the requirement for the degree of
Doctor of Philosophy
Department of Chemical and Biological Engineering
2012

This thesis entitled:
Fundamental Characterization of Photodegradable Hydrogels:
Spatiotemporal Control of the Cellular Microenvironment

written by Mark William Tibbitt

has been approved for the Department of Chemical and Biological Engineering

Kristi S. Anseth, Ph.D.

Christopher N. Bowman, Ph.D.

Date: November 30th, 2012

The final copy of this thesis has been examined by the signatories, and we find that both the content and the form meet acceptable presentation standards of scholarly work in the above mentioned discipline.

Abstract

Tibbitt, Mark W. (Ph.D., Chemical Engineering)

Department of Chemical and Biological Engineering, University of Colorado at Boulder.

Fundamental Characterization of Photodegradable Hydrogels: Spatiotemporal Control of the Cellular Microenvironment

Thesis directed by Professor Kristi S. Anseth

Synthetic hydrogels are an attractive class of materials for the design of well-defined cell culture platforms to better understand how cells receive and integrate signals present in the extracellular environment. Within this class, responsive hydrogels have emerged to investigate questions as to how cells sense and respond to dynamic changes in the mechanical and biochemical nature of the cell niche. To complement this growing body of research, this thesis aimed to develop photoresponsive, synthetic hydrogels that enable experimenters to explore how spatiotemporally varying cues from the extracellular matrix influence biological function in real time. Specifically, cytocompatible, chain and step polymerized hydrogels were fabricated from a photolabile, divinyl poly(ethylene glycol) monomer that enable user-defined modulation of gel properties with light in the presence of mammalian cells. A fundamental and quantifiable characterization of how light-induced property changes alter the structure and function of these photodegradable hydrogels was conducted through experimental and modeling approaches. Similarly, the chemically similar chain and step polymerized hydrogels were employed to better understand how network connectivity affects mechanical integrity and degradation in water-swollen polymer networks. Based on this thorough characterization of how light can be exploited to modulate the structure of photodegradable hydrogels, several experiments were conducted to study how dynamic alterations in the mechanics and biochemistry of the

extracellular matrix influence and direct specific cell function. For this, cytocompatible gelation and irradiation conditions that enable light-induced material property changes in the presence of cells were determined. Gradients in gel density were photopatterned into three-dimensional hydrogels to explore how encapsulated cells respond to changes in the elasticity of the surrounding environment, while micron-scale regions of two-dimensional hydrogels were photoeroded to disrupt cell-material interactions on the subcellular length scale, inducing dynamic cell retraction. Photodegradable hydrogels were further processed into protein-laden microspheres to enable the spatially and temporally defined release of bioactive factors to cells during culture. Finally, unique photodegradable materials were engineered based on the principles developed in this thesis that enable the selective culture or capture of mammalian cells that can subsequently be liberated or released from the hydrogel material. Collectively, this thesis research developed a fundamental understanding of light-induced structure and function changes in photodegradable, poly(ethylene glycol) hydrogels through experimental characterization and modeling. This knowledge was then applied to modulate both the physical and chemical nature of the cellular microenvironment in real time and in the presence of cells with spatial and temporal control. The ability to modulate gel properties in a defined and predictable manner enabled unique studies of how cellular function is related to dynamic signals from the extracellular matrix. This approach and characterization should prove useful for those seeking to investigate complex biological questions that depend on dynamic signaling from the extracellular microenvironment and should further the development of responsive materials that enable precise and predictable user-defined changes in structure and function.

To Grammy Tibbitt

Acknowledgements

This thesis work would not have been possible without the generous guidance and support from a great number of individuals. There is no way that I can express my full gratitude to everyone who has helped me throughout my thesis work, but I do sincerely appreciate all the help and friendship I have received from all of you. Specifically, I would like to thank my research advisor, Prof. Kristi Anseth, for providing incredible support and guidance throughout my thesis work both in and out of the research setting. I have thoroughly enjoyed working with you on this thesis research, and your incessant excitement, generosity, and creativity has made all of the work that went into this a true joy. I would also like to thank my thesis committee, Profs. Christopher Bowman, Jeffrey Stansbury, Stephanie Bryant, Brad Olwin, and Joel Kaar, for your helpful guidance and insightful feedback during the time of this thesis work.

I have had the distinct pleasure of working with many exemplary students, post-doctoral fellows, and professors while performing this thesis research, without whom this all would have been much more difficult and much less enjoyable. Thank you to my mentees, Bruce Han, Emily Maginnis, Kiran Dyamenahalli, Cara Florance, Caroline Szczepanski, Kayla Culver, Donna Kuntzler, Lisa Sawicki, Kristen Feaver, Austin Healey, and Paige Fischer, for being patient with me and teaching me more than I could have imagined. I have enjoyed working with each of you. To those who have mentored me, thank you for your wisdom and guidance and for helping shape me into the scientist that I am today: Drs. April Kloxin, Chris Kloxin, Cole DeForest, Alex Aimetti, Pat Hume, Chien-Chi Lin, Mirza Peljto, Malar Azagarsamy, and Daniel Alge. To those who I have had the opportunity of collaborating with, thank you for allowing me to explore the broader applications of my thesis research and for strengthening the work therein, Dr. April Kloxin, Ajay Shah (Massachusetts General Hospital), Ivan Grubisic (UC-Berkeley),

Quinn Fleming, Dr. Mirza Peljto, Dr. Malar Azagarsamy, Dr. Cole DeForest, Katie Lewis, Prof. John Oakey (University of Wyoming), and Prof. Mehmet Toner (Massachusetts General Hospital).

This thesis would not have been possible without the financial support of a number of funding agencies, including the Howard Hughes Medical Institute, the National Science Foundation (DMR 1006711), and the National Institutes of Health. Fellowship assistance for this work was kindly provided by the U.S. Department of Education's Graduate Assistantships in Areas of National Need (GAANN) program, the National Institutes of Health Molecular Biophysics training grant (T32 GM-065103), and the Teets Family Endowed Doctoral Fellowship.

Finally, I would like to thank my close friends and family for their support and encouragement throughout the journey to get here, especially the past five years. To Tania, thank you for your friendship and unparalleled support over the years, without which this would not have been possible or nearly as fun. To my roommates and friends, past and present, thank you for keeping me grounded and for keeping life outside of the lab a joy. To my parents Peggy and Jim, thank you so much for all of the tremendous love and support you have given me throughout my life and for fostering my early desires that allowed me to accomplish this. To the Tiblings, Dan and Laura, thank you for always being best friends that I could lean on when needed and for teaching me the importance and value of family. Without all of you I would not be the person that I am today.

TABLE OF CONTENTS

LIST OF FIGURES	IV
CHAPTER I – INTRODUCTION AND BACKGROUND	1
1.0 Overview	1
1.1 Hydrogels as extracellular matrix mimics for cell culture	2
1.1.1 The cell culture context matters	4
1.1.2 Hydrogels as 3D culture platforms	6
1.1.3 Permissive and promoting hydrogels	8
1.1.4 Native extracellular matrix	9
1.1.5 Design criteria	11
1.1.6 Bridging the gap	12
1.1.7 Current directions	15
1.2 Poly(ethylene glycol) hydrogels for cell culture	18
1.3 Hydrogel material properties	22
1.4 Photoreactions for dynamic control of hydrogel properties	24
1.5 Research summary	29
1.6 References	31
CHAPTER II – THESIS OBJECTIVES	42
2.1 Overview	42
2.2 References	46
CHAPTER III – SYNTHESIS OF PHOTODEGRADABLE HYDROGELS AS DYNAMICALLY TUNABLE MATERIALS FOR 2D AND 3D CELL CULTURE.....	49
3.1 Abstract	49

3.2 Introduction	49
3.2.1 Background	50
3.2.2 Development of the protocol	51
3.2.3 Application of the method	52
3.2.4 Comparison with other methods	55
3.3 Experimental	57
3.3.1 Monomer synthesis	57
3.3.1a Photodegradable acrylate	57
3.3.1b Photodegradable crosslinker	58
3.3.1c Photoreleasable tether	58
3.3.2 Hydrogel synthesis	59
3.3.3 Cell encapsulation	61
3.3.4 Photodegradation of hydrogels	62
3.3.4a Photolithography	62
3.3.4b Single-photon confocal microscope	63
3.3.4c Degradation parameter overview	64
3.4 Materials	64
3.4.1 Reagents	64
3.4.1a Monomer synthesis	64
3.4.1b Gel synthesis	66
3.4.2 Equipment	67
3.4.3 Equipment setup	70
3.5 Procedure	71

3.5.1 Monomer synthesis	71
3.5.2 Hydrogel synthesis	82
3.5.3 Hydrogel degradation and patterning	90
3.5.4 Timing	94
3.6 NMR reference spectra	96
3.6.1 Synthesis of photolabile group (reaction a)	96
3.6.2 Synthesis of photolabile group (reaction b)	96
3.6.3 Synthesis of photolabile group (reaction c)	96
3.6.4 Synthesis of photolabile group (reaction d)	96
3.6.5 Photodegradable acrylate (reaction e and f)	97
3.6.6 Photodegradable crosslinker	97
3.7 References	97

CHAPTER IV – MODELING CONTROLLED PHOTODEGRADATION IN OPTICALLY THICK HYDROGELS..... 101

4.1 Abstract	101
4.2 Introduction	102
4.3 Materials and Methods	104
4.3.1 Synthesis of nitrobenzyl ether photolabile moiety	105
4.3.2 Acrylation of nitrobenzyl ether photolabile moiety	105
4.3.3 Synthesis of photolabile crosslinker	106
4.3.4 Synthesis of photolabile hydrogels	106
4.3.5 Measurement of molar absorptivities	107
4.3.6 Measurement of quantum yield via photorheometry	107
4.3.7 Measurement of quantum yield via NMR	108

4.3.8 Fractional mass loss in PEGdiPDA hydrogels.....	109
4.3.9 Channel patterning in PEGdiPDA hydrogels.....	109
4.3.10 Surface gradient patterning in PEGdiPDA hydrogels.....	110
4.3.11 Model calculations	111
4.4 Model development	111
4.4.1 Modeling light intensity and photoactive species profiles	111
4.4.2 PEGdiPDA photodegradable hydrogels	114
4.4.3 Statistical model of degradation and erosion in the gel	115
4.5 Results and Discussion	119
4.6 Conclusions	132
4.7 References	133
CHAPTER V – MECHANICAL PROPERTIES AND DEGRADATION OF CHAIN AND STEP POLYMERIZED PHOTODEGRADABLE HYDROGELS	136
5.1 Introduction	136
5.2 Materials and Methods	139
5.2.1 Synthesis of gel forming monomers	139
5.2.2 Fabrication of chain polymerized hydrogels	140
5.2.3 Fabrication of step polymerized hydrogels	140
5.2.4 Modulus measurements of hydrogels	141
5.2.5 Tensile testing of hydrogels	142
5.2.6 Degradation of hydrogels	142
5.2.7 Degradation with collimated light	143
5.2.8 Erosion of channels into hydrogel surfaces	143
5.2.9 Model predictions	144

5.2.10 Statistics	144
5.3 Results and Discussion	145
5.3.1 Formation of chain and step polymerized hydrogels	145
5.3.2 Mechanical analysis of chain and step polymerized hydrogels	147
5.3.3 Photodegradation of chain and step polymerized hydrogels	148
5.4 Conclusion	154
5.5 References	154
CHAPTER VI – TUNABLE HYDROGELS FOR EXTERNAL MANIPULATION OF CELLULAR MICROENVIRONMENTS THROUGH CONTROLLED PHOTODEGRADATION	159
6.1 Introduction	159
6.2 Results and Discussion	162
6.2.1 Synthesis of photodegradable, three-dimensional culture platforms	162
6.2.2 Degradation of three-dimensional, photodegradable hydrogels	164
6.2.3 Spatially defined erosion of three-dimensional hydrogels	169
6.2.4 Cell response to dynamic changes in gel microenvironment	170
6.3 Conclusion	172
6.4 References	172
6.5 Supplemental Information	175
CHAPTER VII – CONTROLLED TWO-PHOTON DEGRADATION OF PEG HYDROGELS TO STUDY AND MANIPULATE SUBCELLULAR INTERACTIONS ON SOFT MATERIALS	188
7.1 Abstract	188
7.2 Introduction	189
7.3 Results and Discussion	191

7.3.1 Preparation of a two-photon degradable hydrogel	191
7.3.2 Resolution of two-photon erosion of PEGdiPDA hydrogels	194
7.3.3 Critical exposure time for two-photon erosion	194
7.3.4 Irradiation conditions for <i>in situ</i> degradation	198
7.3.5 Two-photon control of ECM context and geometry	199
7.3.6 Erosion of PEGdiPDA hydrogels to study subcellular detachment	202
7.4 Conclusion	205
7.5 Experimental	205
7.5.1 Synthesis of a photodegradable crosslinker	205
7.5.2 Fabrication of PEGdiPDA hydrogels	207
7.5.3 Culture and transfection of hMSCs	208
7.5.4 Laser setup and power measurement	208
7.5.5 Gel characterization	209
7.5.6 Quantification of subcellular detachment	209
7.5.7 Statistical analysis	210
7.6 References	210
7.7 Supplemental Information	213
CHAPTER VIII – DYNAMIC SUBSTRATES TO PROBE MESENCHYMAL STEM CELL MECHANOTRANSDUCTION AND PLASTICITY	215
8.1 Introduction	215
8.2 Materials and Methods	217
8.2.1 Hydrogel preparation	217
8.2.2 Hydrogel film characterization with rheometry	218
8.2.3 Cell culture	219

8.2.4 Immunostaining for myogenic and osteogenic lineages	219
8.2.5 Statistics	220
8.3 Results and Discussion	220
8.3.1 Fabrication of hydrogels with tunable mechanics <i>via</i> light	220
8.3.2 Dynamic moduli to direct hMSC plasticity	221
8.4 Current and future work	223
8.5 Conclusion	224
8.6 References	224
CHAPTER IX – SYNTHESIS AND APPLICATION OF PHOTODEGRADABLE MICROSPHERES FOR SPATIOTEMPORAL CONTROL OF PROTEIN DELIVERY	227
9.1 Abstract	227
9.2 Introduction	228
9.3 Materials and Methods	230
9.3.1 Microsphere preparation	230
9.3.2 Absorbance of PEGdiPDA	231
9.3.3 Microsphere characterization with image analysis	231
9.3.4 Degradation of microspheres	232
9.3.5 Quantification of BSA-488 release	233
9.3.6 Diffusion in fibrin gels	233
9.3.7 Cell culture	233
9.3.8 TGF- β 1 delivery	234
9.3.9 Fluorescently labeled Annexin V delivery	234
9.4 Results and Discussion	235

9.4.1 Synthesis and characterization of microspheres	235
9.4.2 Photodegradation of microspheres	236
9.4.3 Selective release of proteins	238
9.4.4 Release of proteins in 3D culture platforms	239
9.4.5 Release of bioactive proteins to direct cell function	241
9.4.6 Release of bioactive proteins to assay cell function	242
9.5 Conclusion	243
9.6 References	244
CHAPTER X – THREE-DIMENSIONAL CULTURE PLATFORMS FOR THE ENCAPSULATION AND RECOVERY OF MAMMALIAN CELLS	247
10.1 Introduction	247
10.2 Materials and Methods	249
10.2.1 Synthesis of click-functionalized polymer precursors	249
10.2.2 Hydrogel formation and photodegradation	250
10.2.3 Cell culture	250
10.3 Results and Discussion	251
10.4 Current and future work	254
10.5 Conclusion	255
10.6 References	256
CHAPTER XI – MICROFLUIDIC DEVICES FOR THE SELECTIVE CAPTURE AND RELEASE OF MAMMALIAN CELLS WITH PHOTODEGRADABLE HYDROGELS	258
11.1 Introduction	258
11.2 Materials and Methods	260
11.2.1 Hydrogel precursor synthesis	260

11.2.2 PEGdiPDA hydrogel fabrication	261
11.2.3 Hydrogel fabrication in microfluidic devices	261
11.2.4 Fabrication of multifaceted PEGdiPDA hydrogels	262
11.2.5 PEGdiPDA hydrogel functionalization	263
11.2.6 Cell culture, capture, and release	263
11.3 Results and Discussion	264
11.3.1 Photopolymerization of PEGdiPDA films	264
11.3.2 Functionalizing gels with biotinylated molecules	265
11.3.3 Multifaceted capture device	266
11.3.4 Flow capture and release of cells	268
11.3.5 Current studies and future directions	269
11.4 Conclusion	270
11.5 References	271
CHAPTER XII – CONCLUSIONS AND FUTURE DIRECTIONS	273
12.1 References	287
CHAPTER XIII – BIBLIOGRAPHY	289

LIST OF FIGURES AND SCHEMES

Figure 1.1 Cell culture in two-dimensional and three-dimensional platforms. Cells experience a drastically different environment between 2D and 3D culture. For instance, neural cells cultured in monolayer (a) are constrained to extend processes in the plane. Cell bodies are stained green and β -tubulin in axonal extensions is stained red. When cultured within hydrolytically degradable poly(ethylene glycol) based hydrogels (b) the same cells form neurospheres and extend processes isotropically in three dimensions. Images taken by M.J. Mahoney.

Figure 1.2 Permissive and promoting hydrogels. Permissive hydrogels (a) composed of synthetic polymers (yellow mesh) provide a 3D environment for culturing cells; however, they fail to activate integrins (brown) and other surface receptors (orange). The synthetic environment simply permits viability as cells remodel their surrounding microenvironment. On the other hand, promoting hydrogels (b) formed from naturally derived polymers present a myriad of integrin-binding sites (green) and growth factors (red) coordinated to the ECM (yellow fibers), which direct cell behavior through signaling cascades that are initiated by binding events with cell surface receptors.

Figure 1.3 The native extracellular matrix. The native ECM is the prototypical hydrogel that regulates cell function on many length scales. (A) Integrin-binding with ECM proteins (green ligands and tan receptors), growth factor sequestration within proteoglycans (red), and cell-cell contact via cadherins (purple) occur on the scale of tens of nanometers to microns. (B) Migration, which is critical in tissue regeneration, cancer metastasis, and wound healing, initiates on the scale of tens to hundreds of microns. Paracrine signaling that directs differentiation (pink growth factors) and proliferation (red growth factors) is also mediated on this length scale. (C) Tissue homeostasis, development, and wound healing are regulated over hundreds of microns to centimeters. Here, we illustrate neutrophils being recruited to the site of a wound in the epithelium.

Figure 1.4 Synthetic-biologic hydrogels. Synthetic biologic hydrogels that incorporate several well-defined and orthogonal chemistries serve as robust ECM mimics for 3D cell culture. Depending on the application, it may be advantageous to incorporate cell- or user-defined regulation of the material properties to emulate the native dynamic environment. However, in many cases, synthetic hydrogels that incorporate both cell- and user-defined chemistries will be necessary. Here, we illustrate a cell cleaving MMP degradable crosslinks (yellow circles) that allow it to access sequestered growth factors (red) and integrin-binding sites, such as RGD (green circles). Ultimately, this cleavage allows cell motility and the deposition of ECM proteins (orange fiber). User-defined chemistries, such as photodegradable crosslinks (blue ellipses) and post-gelation attachment of RGD to the network backbone, afford facile control of the dynamic biochemical and biophysical properties of the gel, thereby directing cell attachment and motility. Further, exogenous application of enzymes (brown) can allow user-defined release of sequestered growth factors.

Figure 1.5 Chain and step polymerized hydrogels. (A) Hydrogels formed by a radical initiated chain polymerization are comprised of networks with heterogeneous structure of dense

kinetic chains (yellow) connected by crosslinking polymers (blue). **(B)** Hydrogels formed by step polymerization, in this case of a tetrafunctional monomer (red) with a difunctional monomer (blue), form a more homogeneous network with increased cooperativity between elastically active network strands.

Figure 1.6 Photochemical patterning in hydrogels. **(a)** Fluorescently-labeled, acrylated RGD was swollen into a preformed PEGDA gel and selectively coupled within the network *via* photopolymerization. In this manner, fibroblast migration was confined to regions of a gel that was patterned with RGD (blue = cell nuclei; red = cell actin; green = RGD). **(b)** Photodeprotection of thiols was employed to selectively couple maleimide-functionalized peptides to hydrogel. Here, the outgrowth of dorsal root ganglia cells was confined to adhesively patterned regions of the gel (green = patterned peptide; red = dorsal root ganglia cells). **(c)** A similar approach coupled fluorescently-labeled peptides to a hydrogel network through photoinitiated thiol-ene chemistry. This afforded the sequential addition of multiple biochemical signals with spatial and temporal control. **(d)** Recent work has demonstrated the photoaddition of multiple full-length proteins in three-dimensional hydrogels using photodeprotection of thiols and maleimide-functionalized molecules that capture proteins orthogonally. Scale bars = 100 μm .

Figure 1.7 Photochemical patterning of hydrogel mechanics. **(a)** Sequential crosslinking reactions have been employed to photochemically alter the mechanics of a hydrogel. Here, a Michael-addition between dithiol peptides and methacrylated-hyaluronic acid is used to form a gel, which can undergo secondary photochemical crosslinking through unreacted methacrylate groups. In this experiment, cell spreading was prohibited in regions where the gel density was increased *via* photopolymerization. **(b)** Further, this technique was extended to spatially pattern the mechanics of a hydrogel for cell culture, whereby cell spreading was similarly restricted to regions of lower gel density (red = photocrosslinked gel; green = cells). Scale bars, 100 μm .

Figure 1.8 Proposed mechanism of *o*-nitrobenzyl ether photocleavage. When an *o*-nitrobenzyl ether moiety is photoexcited, it forms an intermediate five-member ring *via* proton exchange that can result in molecular scission. This results in the release of X, which is typically terminated in a carboxylic acid or amine functionality. Figure adapted from Li *et al.*

Figure 1.9 Photodegradable hydrogels for spatiotemporal control of the cell microenvironment thesis organization. This thesis focuses on the development of photodegradable hydrogels that enable user-defined control over the mechanics and biochemical nature of the cell microenvironment. The general approach is to develop a fundamental and quantifiable understanding of light-induced property changes on the structure and function of photodegradable gels through characterization and modeling. Using this knowledge, photodegradable hydrogels will be employed to probe the cellular response to dynamic mechanical signals, to direct and assay cell function through the spatiotemporally controlled release of trophic factors, and to engineer unique materials for the culture and capture of mammalian cells that enable subsequent cell release.

Figure 3.1 Photolabile hydrogels for cell culture. Recent work has emphasized the importance of cues from the extracellular matrix in directing cell function. Namely, the elasticity, adhesive

context, geometry, and biochemical nature of the cellular microenvironment have been shown to direct cell migration, differentiation, and fate. Photolabile hydrogels are a dynamic class of cell culture materials that can be exploited to precisely and predictably alter the cellular microenvironment in both space and time. By incorporating photolabile functionalities into the gels, the user can tune dynamically the elasticity/polymer density, biochemical nature, or geometry of the cell culture platform in real time with light. **(a)** Dynamic changes in the adhesive context influence cell morphology and cytoskeletal organization. Here, light-induced changes in polymer density or ligand concentration are employed to control cell spreading and cytoskeletal organization. **(b)** Cells can be seeded within wells of photoactive hydrogels and subsequent changes to the geometry of the cellular microenvironment can be introduced with light. Here, a channel is introduced between two wells, encouraging cells to migrate out of their niche. These patterning strategies can be extended easily to tune the cellular microenvironment around encapsulated cells or to connect encapsulated cells in 3D cell culture.

Figure 3.2 Photodegradable hydrogel synthesis and patterning. **(a)** Photodegradable hydrogels are formed by redox initiated, free radical chain polymerization of PEGdiPDA crosslinking molecules, rapidly forming an insoluble hydrogel. The resultant network structure is comprised of polyacrylate kinetic chains (green) connected by PEG-based crosslinks (black) with photocleavable *o*-nitrobenzylether moieties (blue) in the backbone. **(b)** Chrome masks (black and white layer) can be placed at the surface of photodegradable gels (orange) to selectively occlude incident light (purple). With sufficient irradiation time (*t*) features are formed at the surface of PEGdiPDA gels, where the depth of feature formation depends on the duration of exposure. This photolithographic degradation can be used to generate features in the surface of a gel with minutes of irradiation time. **(c)** The focal point of a laser can be used to pattern features *within* PEGdiPDA hydrogels. Here, a laser scanning microscope (LSM) with a 405 nm laser is used to draw regions of interest (ROI) in the material. The laser focal point is rastered through the ROI and into the *z*-dimension to completely erode 3D features within the hydrogel in seconds. Both of these patterning strategies can be translated for spatiotemporally controlled presentation of biochemical ligands with gels containing the photoreleasable tether. **(d)** An overview of irradiation parameters for degradation and complete erosion of photodegradable hydrogels. Ultimately, these patterning approaches allow the rapid, *in situ* creation of micron-scale features in the presence or absence of cells in 2D and 3D.

Figure 3.3 Photodegradable acrylate monomer synthetic scheme. Synthetic route for preparing photodegradable acrylate. Reagents and conditions: **(a)** DMF, ethyl-4-bromobutyrate, Ar, K₂CO₃; **(b)** HNO₃, ~ 5 °C → ~ 32 °C; **(c)** EtOH, Ar, NaBH₄, 38 °C; **(d)** DI H₂O, TFA, ~ 90 °C; **(e)** Ar, DCM, TEA, AC, 0 °C → room temperature; **(f)** acetone, DI H₂O.

Figure 3.4 Photodegradable acrylate. **(a)** The reaction set-up for the acrylation of the photolabile group. The photolabile group is added to a round-bottomed flask with DCM and a stir bar and chilled to 0 °C in an ice bath. TEA is added to the round-bottomed flask while AC is mixed with DCM in an addition funnel under Ar purge. The AC/DCM is added dropwise to the round-bottomed flask. **(b)** In response to light, the photodegradable acrylate (blue) undergoes irreversible cleavage, producing the cleaved photolabile group and acrylic acid (green). **(c)** The molar absorptivities of photodegradable acrylate (blue) and the cleaved photolabile group (green)

from 300 to 600 nm. **(d)** ^1H NMR shifts for the photodegradable acrylate monomer for synthetic verification.

Figure 3.5 Macromolecular monomer synthetic schemes. **(a)** Synthetic route for preparing the photodegradable crosslinker (a) and photoreleasable tether (b). (a) NMP, HBTU, HOBt, DIEA, and PEG-*bis*-amine. (b) NMP, HBTU, HOBt, DIEA, and RGDS peptide. **(b)** ^1H NMR shifts for the photodegradable crosslinker for synthetic verification. **(c)** MALDI-TOF spectrum for the photoreleasable tether for synthetic verification.

Figure 3.6 Hydrogel synthesis. **(a)** A schematic of the network structure of photodegradable hydrogels formed via free-radical chain polymerization of the photodegradable crosslinker: polyacrylate kinetic chains (green coils), PEG-based crosslinks (black lines), and photolabile moieties (blue circles). **(b)** A schematic of the network structure of photoreleasing hydrogels formed via free-radical chain co-polymerization of the non-degradable crosslinker with the photoreleasable tether: polyacrylate kinetic chains (green coils), PEG-based crosslinks (black lines), photolabile moieties (blue circles), and pendant peptides (orange hexagons). **(c)** Photolabile hydrogels are formed between an acrylated cover glass and a non-acrylated cover glass in a silicon mold (spacer). The silicon mold is placed on the acrylated cover glass (1) and set-up next to the non-acrylated cover glass. The macromer solution is initiated by adding TEMED to the solution while mixing (2), and this solution is quickly pipetted onto the acrylated cover glass (3) in the void of the mold. The non-acrylated cover glass is used to cover the solution, and the sandwich is clamped shut with binder clips (4). After ~ 5 min, the sandwich is opened with a razor blade (5), and the formed gel (6) is placed in PBS.

Figure 3.7 Cell encapsulation within photodegradable hydrogels. **(a)** Cells are encapsulated within photolabile hydrogels by resuspending a cell pellet in the macromer solution just before the addition of TEMED. Cell viability is verified after polymerization using a LIVE/DEAD Cytotoxicity Assay and confocal imaging. Here hMSCs exhibit good viability within the photodegradable hydrogel after encapsulation (live cells stained green, dead cells stained red, day 1, confocal z-projection). Scale bar, $100\ \mu\text{m}$. **(b)** Cell function after irradiation and gel degradation can be assessed by measuring metabolic activity with the alamarBlue assay. Metabolic activity of hMSCs encapsulated in a photodegradable gel increases slightly on irradiation and degradation (8 min of $10\ \text{mW}/\text{cm}^2$ at 365 nm), compared with photodegradable gels without irradiation (control) ($P < 0.001$), but the two conditions are similar ~ 24 h after irradiation (48 h in 3D culture). **(c)** Irradiation of the hydrogels for up to 8 min ($10\ \text{mW}/\text{cm}^2$ at 365 nm) creates z-gradient in degradation and gel cross-linking density (ρ_x). Cells were imaged on day 4 in culture after irradiation for 8 min on day 1. This 3D gradient in cross-linking density can be used to study how gel density influences cell function in 3D culture. hMSCs labeled with CellTracker Green are observed spreading in lower cross-linking density regions of the gel (right, confocal slice overlaid with bright field) as compared with regions with high cross-linking density (left), and increasing cell area in response to this z-direction gradient is observed and quantified with image analysis (table, ρ_x normalized to its initial, nondegraded value, ρ_{x0}). Scale bars, $50\ \mu\text{m}$.

Figure 3.8 Photopatterning with photolithography. **(a)** To pattern photolabile hydrogels with standard photolithography, a mask is placed between a collimated light source and the gel

surface. For proper pattern transfer, it is important that the light be well collimated with a collimating lens and that the mask be appropriately placed above the hydrogel surface. **(b)** Photopatterning can be used to form gradients in elasticity or biochemical signals in photolabile hydrogels via gradient masking. Briefly, the sample is placed in a PBS/media filled chamber, and a syringe pump is used to slowly cover the sample so that the sample receives a gradient of light, which induces a gradient in photocleavage. **(c)** Photopatterning can also be employed to generate features at the surface of photolabile hydrogels using a chrome mask. To ensure pattern transfer, use a well-collimated light source and rest the chrome mask just above the gel surface on glass slides or cover glass. Here, we used a mask with square features to pattern positive square pillars at the surface of photodegradable hydrogels. Features are shown in a confocal surface image (upper left), brightfield image (upper right), and confocal cross section image (bottom).

Figure 3.9 3D photopatterning with a confocal microscope. Focused, 405 nm laser light can be used on a confocal microscope to completely erode features within photodegradable hydrogels. **(a)** To maintain sterility the prepared gel is sealed within a liquid filled chamber that fits onto the stage of a confocal microscope. ROI software is used to raster the focal point of the 405 nm laser through defined geometries within photolabile hydrogels. **(b)** Here, cylindrical wells (5, 25, and 50 μm diameter, left to right) are degraded into the surface of a photodegradable gel and imaged in brightfield (middle, scale bar 100 μm) and confocal fluorescence (right, y-cross section, scale bar 50 μm). Such surface features can be used for cell aggregation, studying cell connectivity and migration, and manipulation of cell adhesion. **(c)** Further, channels can be created *within* photodegradable hydrogels on size scales relevant to mammalian cells to study 3D migration and connectivity. Here, we show a bifurcating channel patterned 50 μm below the gel surface as imaged in brightfield (middle, scale bar 100 μm) and confocal fluorescence (right, z-cross section, scale bar 50 μm). Note that there is non-specific degradation in the z-dimension owing to overlapping regions of out-of-focus light.

Figure 4.1 Photodegradable hydrogel system. **(a)** Photodegradable PEG based hydrogels were formed through redox-initiated free radical polymerization of the photodegradable crosslinker (PEGdiPDA) with a co-monomer (PEGA). **(b)** Upon exposure to collimated irradiation, these gels degrade as the photolabile *o*-nitrobenzyl ether (NBE) cleaves leading to mass loss and, ultimately, erosion. **(c)** Mass loss results from the release of cleavage products from the network that predominantly fall into three categories: i. free PEGdiPDA crosslinks, ii. kinetic chains, and iii. kinetic chains with pendant crosslinks. Once a sufficient fraction of NBE moieties are cleaved in a local region, the gel undergoes reverse gelation where the polymers no longer form an infinite molecular weight network and the local material erodes from the gel. **(d)** Photodegradation can be achieved at wavelengths where NBE absorbs light (solid line). In this work, 365 nm, 405 nm, and 436 nm were employed for degradation. The mechanism of mass loss of the gels was dictated by the total absorptivity of the degradable hydrogels, which depends on the molar absorptivity of NBE (solid line), the molar absorptivity of the cleavage product (NBP; dashed line), the concentrations of photoactive species, the thickness of the gel, and the wavelength of irradiation. Molar absorptivity data previously reported in ref. 29.

Figure 4.2 Model predictions of light intensity profiles and kinetic rates. The incident irradiation is attenuated in the hydrogel on account of the absorbing NBE within the PEGdiPDA

hydrogels. **(a)** Increased thickness of the hydrogel ($[NBE] = 0.04 \text{ M}$; $\lambda = 365 \text{ nm}$; $I_0 = 10 \text{ mW cm}^{-2}$) leads to decreased penetration depth of the light through the gel ($z = 10 \text{ }\mu\text{m}$, dash-dot line; $z = 100 \text{ }\mu\text{m}$, solid line; $z = 1000 \text{ }\mu\text{m}$, dashed line). **(b)** Similarly, increased concentration of the NBE moieties in the gel ($z = 100 \text{ }\mu\text{m}$; $\lambda = 365 \text{ nm}$; $I_0 = 10 \text{ mW cm}^{-2}$) leads to decreased penetration depth of the light through the gel ($[NBE] = 0.004\text{M}$, dashed line; $[NBE] = 0.04\text{M}$, solid line; $[NBE] = 0.4\text{M}$, dash-dot line). **(c)** The penetration depth of the light in the gel is also dependent on the wavelength of incident irradiation ($[NBE] = 0.04 \text{ M}$; $z = 100 \text{ }\mu\text{m}$; $I_0 = 10 \text{ mW cm}^{-2}$). Here, 365 nm irradiation (solid line) is strongly attenuated owing to the high molar absorptivity of NBE at 365 nm ($\epsilon_{NBE} = 4300 \text{ L mol}^{-1} \text{ cm}^{-1}$). 405 nm irradiation (dashed line) leads to increased penetration depth ($\epsilon_{NBE} = 720 \text{ L mol}^{-1} \text{ cm}^{-1}$) while 436 nm irradiation (dash-dot line) is nearly uniform through the depth of the gel ($\epsilon_{NBE} = 16 \text{ L mol}^{-1} \text{ cm}^{-1}$). **(d)** The initial photocleavage rate as a function of depth is dependent on the local light intensity and the wavelength of irradiation, through changes in absorbance and quantum yield. ($[NBE] = 0.04 \text{ M}$; $I_0 = 10 \text{ mW cm}^{-2}$; $z = 100 \text{ }\mu\text{m}$; $\lambda = 365 \text{ nm}$, solid line; $\lambda = 405 \text{ nm}$, dashed line; $\lambda = 436 \text{ nm}$, dash-dot line)

Figure 4.3 Model predictions of surface and bulk erosion of photodegradable hydrogels.

Surface erosion and bulk degradation are both observed *in silico* for photodegradable hydrogels depending on the total absorbance of the material. **(a)** PEGdiPDA hydrogels with high absorbance ($A = 10$; $[NBE] = 0.23 \text{ M}$; $z = 100 \text{ }\mu\text{m}$) severely attenuate the incident irradiation ($\lambda = 365 \text{ nm}$; $I_0 = 10 \text{ mW cm}^{-2}$), which leads to a front of light moving through the depth of the material as degradation proceeds. (arrows indicate the direction of increasing time; $t = 0 \text{ min}$, solid line; $t = 22.5 \text{ min}$, dashed line; $t = 45 \text{ min}$, dotted line; $t = 67.5 \text{ min}$, dash-dot line; $t = 90 \text{ min}$, dash-double dot line) **(b)** Photodegradation erodes the surface of the material, where light remains at a high intensity. Erosion is indicated by $C/C_0 = 0$. In this surface erosion case, the strongly coupled equations (Eqs. 1 - 3) lead to a propagation of light and mass loss through the depth of the gel with time. ($t = 0 \text{ min}$, solid line; $t = 22.5 \text{ min}$, dashed line; $t = 45 \text{ min}$, dotted line; $t = 67.5 \text{ min}$, dash-dot line; $t = 90 \text{ min}$, dash-double dot line) **(c)** PEGdiPDA hydrogels with low absorbance ($A = 0.01$; $[NBE] = 0.0056 \text{ M}$; $z = 25 \text{ }\mu\text{m}$) allow incident irradiation ($\lambda = 405 \text{ nm}$; $I_0 = 25 \text{ mW cm}^{-2}$) to penetrate through the full depth of the gel uniformly, which results in bulk degradation of the material. ($t = 0 \text{ min}$, solid line; $t = 7.5 \text{ min}$, dashed line; $t = 15 \text{ min}$, dotted line; $t = 22.5 \text{ min}$, dash-dot line; $t = 30 \text{ min}$, dash-double dot line) **(d)** As light penetrates the material uniformly, the reaction rate is uniform through the depth of the gel, which results in an even decrease in $[NBE]$ through the depth of the gel, which is indicative of bulk degradation. At late time points, the whole material erodes. ($t = 0 \text{ min}$, solid line; $t = 7.5 \text{ min}$, dashed line; $t = 15 \text{ min}$, dotted line; $t = 22.5 \text{ min}$, dash-dot line; $t = 30 \text{ min}$, dash-double dot line) For all model calculations $N = 20$.

Figure 4.4 Model predictions of photodegradation in PEGdiPDA hydrogels.

For PEGdiPDA hydrogels with intermediate absorbance ($A \sim 0.1 - 10$), degradation is observed to be a mixture of surface erosion and bulk degradation. **(a)** In these materials, light is mostly confined to the surface volume of the gel, while a portion of the light is able to penetrate the full thickness, leading to non-negligible cleavage of NBE moieties. **(b)** As time progresses the light front moves through the gel surface, eroding the material while anisotropically patterning the full depth of the gel. (arrows indicate the direction of increasing time; $t = 0 \text{ min}$, solid line; $t = 7.5 \text{ min}$, dashed line; $t = 15 \text{ min}$, dotted line; $t = 22.5 \text{ min}$, dash-dot line; $t = 30 \text{ min}$, dash-double dot line) **(c)** The

anisotropic patterning caused by this phenomenon is predicted to generate materials with gradients in crosslinking density as a function of depth. ($t = 0$ min, solid line; $t = 2$ min, dashed line; $t = 6$ min, dashed-dot line) **(d)** Since the volumetric swelling ratio, Q , and Young's modulus, E , of PEG hydrogels depend on the crosslinking density, ρ_x , anisotropies in crosslinking density are readily generated to create spatially varying materials, that can be difficult to synthesize through traditional fabrication routes. For all model calculations, $N = 20$; $[NBE] = 0.04$ M; $z = 100$ μm ; $\lambda = 365$ nm; $I_0 = 10$ mW cm^{-2} ; $A = 1.7$.

Figure 4.5 Model predictions compared to experimental degradation of PEGdiPDA hydrogels. The photodegradation model was employed to predict mass loss and material property changes in chain polymerized, PEGdiPDA hydrogels. **(a)** Fractional mass loss for two formulations ($[NBE] = 0.04$ M; $z = 1500$ μm ; triangles – experimental, previously reported data found in ref. 20; dashed line – prediction and $[NBE] = 0.058$ M; $z = 1500$ μm ; squares – experimental, previously reported data found in ref. 20; solid line – prediction) in response to irradiation ($\lambda = 365$ nm; $I_0 = 20$ mW/cm^2) was predicted by the statistical-kinetic mass loss model. **(b)** Fractional mass loss for PEGdiPDA hydrogels ($[NBE] = 0.04$ M) in response to irradiation ($\lambda = 405$ nm at $I_0 = 25$ mW/cm^2) also compared well with predictions. (triangles – experimental; solid line – prediction) **(c)** The depth of channels patterned into the surface of PEGdiPDA hydrogels ($[NBE] = 0.04$ M; $\lambda = 365$ nm; $I_0 = 10$ mW/cm^2) was predicted, except at short irradiation times. (triangles – experimental, previously reported data found in ref. 20; solid line – prediction) **(d)** A gradient in surface elasticity generated by photomasking was also predicted by the statistical-kinetic model. (triangles – experimental, previously reported data found in ref. 21; solid line – prediction, line connects discrete model predictions) For all model calculations, $N = 20$.

Figure 5.1 Fabrication of chain and step polymerized photodegradable hydrogels. **(a)** Chain polymerized and step polymerized hydrogels were formed with the same photolabile monomer, PEGdiPDA. Chain polymerized hydrogels (CP gels) were fabricated through the co-polymerization of PEGdiPDA with PEGA via free-radical polymerization, resulting in a heterogeneous network structure. Step polymerized hydrogels (SP gels) were fabricated through the co-polymerization of PEGdiDPA with PEG4SH via Michael-addition polymerization. **(b)** Chain polymerized and step polymerized hydrogels form in minutes, $t_f = 370 \pm 1$ s for CP gels and $t_f = 1470 \pm 60$ s for SP gels. **(c)** Chain polymerized and step polymerized hydrogels form with similar shear storage moduli, $G'_f = 4140 \pm 130$ Pa for CP gels and $G'_f = 3680 \pm 90$ Pa for SP gels.

Figure 5.2 Mechanical analysis of chain and step polymerized hydrogels. **(a)** Uniaxial extension of CP and SP gels was conducted to measure the percent strain to failure and modulus of toughness from the stress-strain curves. Solid black line is a representative stress-strain curve for the CP gels. Dotted grey line is a representative stress-strain curve for the SP gels. **(b)** The average percent strain to failure was significantly higher for SP (grey) gels as compared to CP (black) gels, $129 \pm 11\%$ compared to $33 \pm 4\%$. **(c)** The SP (grey) gels also demonstrated a significantly increased tensile toughness as compared to CP (black) gels, 4130 ± 370 Pa compared to 1250 ± 300 Pa.

Figure 5.3 Photodegradation of chain and step polymerized hydrogels. (a) and (b) The *o*-nitrobenzyl ether moieties (orange ring structures) in PEGdiPDA undergo an irreversible cleavage in response to irradiation (one-photon: $\lambda \sim 320\text{-}436$ nm, two-photon: $\lambda \sim 740$ nm), breaking elastically active network strands in the hydrogel backbone. In this manner, light can be employed to degrade and, ultimately, erode the CP and SP hydrogels. (c) Owing to the inclusion of the same photolabile monomer into the network backbone, the initial effective cleavage kinetic constant, defined as the opposite of the slope of $\ln(G/G_0)$ as a function of irradiation time divided by the incident irradiation intensity, was similar for the CP (black) and SP (grey) gels.

Figure 5.4 Modeling erosion in chain and step polymerized hydrogels. (a) The erosion depth of photopatterned channels as a function of irradiation time was plotted for the CP (black) and SP (grey) photodegradable hydrogels. A statistical-kinetic photodegradation model based on the photocleavage reaction and network connectivity predicted these functions over the 30 minute exposure time. (b) The critical extent of NBE moieties that need to be cleaved to reach reverse gelation governs the rate at which features can be patterned into photodegradable gels. P_{rg} is a function of network connectivity in both CP and SP gels. Here, $P_{rg}(N)$ is plotted for CP gels (solid black line) and $P_{rg}(f_A)$ is plotted for SP gels with $f_B = 2$ (grey circles), $f_B = 3$ (grey squares), and $f_B = 4$ (grey triangles).

Figure 6.1 Photodegradable hydrogel synthesis and degradation schematics. (a) Photodegradable hydrogels were synthesized by redox-initiated radical chain polymerization of PEGdiPDA (top left) with PEGA (bottom left) (15 wt% total macromer in water). The resulting swollen polymer network consists of polyacrylate chains (green coils) linked by degradable PEG (black lines with red boxes). The initial gel crosslinking density (ρ_x) is varied with crosslinker concentration. (b) Upon irradiation, the photolabile moiety is cleaved (open red boxes), releasing PEG (black) and decreasing the gel crosslinking density. With flood irradiation, light can either penetrate the gel uniformly, causing bulk degradation (top), or be attenuated with absorption by the photolabile group, causing gradient changes in the crosslinking density (middle) or surface erosion (bottom). The intensity profile within the gel is dictated by the irradiation wavelength and the photolabile group concentration. (c) Three-dimensional structures are eroded in a hydrogel using focused light directed by a single photon LSM, where desired shapes are drawn using region of interest software and subsequently scanned with a laser within the hydrogel.

Figure 6.2 Photolysis kinetics and gradient photodegradation. (a) Degradation of these hydrogels was characterized using the more loosely crosslinked gel composition (10 mol % : 90 mol % PEGdiPDA : PEGA). Photodegradation rates were characterized via rheometry, where the natural log of the storage modulus G' normalized to its initial value G'_0 decreases with 365 nm irradiation. Fits of this data yield the characteristic degradation time, τ , which varies with the irradiation intensity (inset) and was used in conjunction with a photodegradation model to predict changes in the hydrogel crosslinking as well as gel mass loss. (b) The experimentally-determined τ values were used to predict the hydrogel's crosslinking density with time during bulk degradation (normalized to initial value, (a) 10 mW cm⁻² and (b) 5 mW cm⁻² at 365 nm). (c) A gradient in the hydrogel's crosslinking density within the top 50 μm of the gel was created with an irradiation gradient across the surface. No degradation occurs on the left, 5 min of degradation occurs on the right, and a continuous and linear gradient of exposure times occurs

between these two extremes (365 nm at 10 mW cm⁻²). The resulting crosslinking density gradient was measured with AFM (blue triangles) and compares well to predicted values based on τ (solid curve). **(d)** Flood irradiating a thick hydrogel with a highly absorbed wavelength creates a degradation gradient in the z-direction within the hydrogel. This degradation gradient was visualized with a confocal LSM (left), where decreased fluorescence indicates loss of backbone chains. The effect of this degradation gradient on the material properties can be estimated through predicted changes in the crosslinking density (normalized to its initial value) with irradiation: (a) 2.5, (b) 5, and (c) 8 min (right). Scale bars are 100 μ m.

Figure 6.3. Hydrogel spatial erosion. **(a)** Mass loss profile and time to complete degradation with irradiation (365 nm at 20 mW cm⁻²) were adjusted with the initial crosslinker concentration and agree well with predictions based on τ (solid lines): 15 wt% total macromer and (a) 10 mol% and (b) 25 mol% photodegradable crosslinker. **(b)** Photolithography (365 nm at 10 mW cm⁻² through 400 μ m clear lines separated by 400 μ m black lines) was used for spatially-specific erosion, creating channels of increasing depth with increasing irradiation, (confocal images of the gel cross-section with irradiation time noted). **(c)** The observed eroded channel depth (squares) compares well with channel depths predicted with τ and the photodegradation model (solid line). **(d)** Spatial erosion of cylinders within a hydrogel was achieved using 405 nm laser on a LSM (top-down view of confocal stack with corresponding cross-sections marked by blue and green lines). Each column of cylinders is a different irradiation condition with decreasing scan speed and increasing laser power resulting in increased mass loss (left to right, scan time per plane and laser power (a) 10 s and 25%, (b) 16 s and 25%, (c) 28 s and 25%, and (d) 10 s and 10%). **(e)** Similarly, vertical cylinders were degraded within a hydrogel (scan time 2 s per plane, 25% laser power, 100 μ m z-scan) and subsequently connected with a horizontal channel within the hydrogel (scan time 16 s per plane, 1 μ m z-scan) (confocal slices false colored to aid in visualization, with red indicating most fluorescence intensity (no degradation) and yellow to green least fluorescence (most degradation and mass loss). The presence of the structure within the hydrogel was verified in brightfield. All scale bars are 100 μ m.

Figure 6.4 Cell area and morphology in gradient degraded hydrogels. hMSCs were encapsulated in photodegradable hydrogels and irradiated (365 nm at 10 mW cm⁻² for 8 min) on Day 1 to create a crosslinking density gradient in the z-direction. **(a)** By Day 4, cell spreading is observed within the upper portion of the irradiated hydrogel (top \sim 100 μ m), which possesses a significantly decreased crosslinking density based on predictions shown in Fig. 2, whereas limited spreading is observed in **(b)** degradable gels without irradiation (top down view of confocal LSM stack). Changes in cell morphology were confirmed with brightfield images (right). Scale bars are 50 μ m. **(c)** No change in cell area was observed over 4 days without irradiation (Day 1 prior to irradiation, Day 4 no light). In contrast, an increase in cell area was observed with irradiation and degradation (Day 4 light) as compared to these controls (* $p < 0.1$). **(d)** Spreading in response to the crosslinking density gradient ($\rho_x/\rho_{x_0} = 0.1 - 0.9$, $\rho_{x_0} = 0.006$ M) was examined by splitting the 100- μ m thick confocal stack into 20- μ m thick confocal projections (top 20 μ m of the gel = position 1). On Day 4, increased cell area was observed in the top of the gel as compared to the lower regions in irradiated samples (blue squares), whereas no change in cell area was observed in the z-direction without irradiation (red diamonds, $\rho_x/\rho_{x_0} = 1$ at all positions).

Figure 6.5 Cell viability with photodegradation. hMSCs encapsulated in photodegradable PEGdiPDA hydrogels were exposed to flood irradiation (365 nm at 10 mW cm⁻² for 8 min). Upon exposure to light, cell viability is maintained throughout the hydrogel, where live cells fluoresce green and dead cells fluoresce red (top down view of confocal LSM stack). Scale bar is 100 μm.

Figure 6.6 Cell morphology in non-degradable hydrogel. (a) hMSCs were encapsulated in non-degradable PEGDA hydrogels and exposed to flood irradiation (365 nm at 10 mW cm⁻² for 8 min). Prior to light exposure (Day 1), cells exhibit small and rounded morphologies (left, top down view of confocal LSM stack; right, representative cells imaged with brightfield and fluorescence), where cells are fluorescently labeled green. (b) After light exposure (Day 4), cells persist in their small and rounded morphologies. (c) No significant difference in cell area is observed between encapsulated hMSCs in non-degradable PEGDA hydrogels at Day 1 (prior to light exposure) and at Day 4 (after light exposure). Scale bars are 50 μm.

Figure 6.7 Cell morphology progression. hMSCs were encapsulated in photodegradable PEGdiPDA (a,b) and non-degradable PEGDA (c) hydrogels. The progression of cell morphology over the course of four days in culture was monitored by confocal LSM imaging of cell morphology on each day, where cells are fluorescently labeled green, and of phalloidin staining for the presence of f-actin (red) coupled with brightfield imaging on day 4. (a) hMSCs encapsulated in photodegradable hydrogels that were exposed to flood irradiation (365 nm at 10 mW cm⁻² for 8 min) exhibit a small and rounded morphology prior to light exposure (Day 1). After light exposure (Days 2-4), the cells begin to spread and increase in cell area. hMSCs encapsulated in photodegradable hydrogels that were not exposed to flood irradiation (b) and in non-degradable hydrogels that were exposed to flood irradiation (365 nm at 10 mW cm⁻² for 8 min) (c) persist in a small and rounded morphology throughout the four days in culture. Corresponding phalloidin staining on Day 4 (right) indicates diffuse f-actin presence around the exterior of the cells for all conditions. Scale bars are 50 μm.

Figure 6.8 Fibronectin presentation with degradation. Fluorescein labeled fibronectin was entrapped in photodegradable PEGdiPDA hydrogels and confocal image stacks of the fibronectin presence were taken prior to (Day 1) and post (Day 4) light exposure. Image analysis of the mean fluorescent intensity of the LSM stacks reveals no significant difference in fibronectin presentation between the PEGdiPDA hydrogel prior to light exposure (Day 1) and after light exposure (Day 4).

Figure 7.1 Two-photon induced degradation and complete erosion of photodegradable hydrogels. (a) Poly(ethylene glycol) (PEG)-based photodegradable hydrogels were formed (a, left) by redox-initiated free radical chain polymerization of PEGdiPDA (a, right) with PEGA. The crosslinking density of these gels corresponds to a mesh size (ξ) of approximately 10 nm (a, left), and the gels allow fibronectin to be physically entrapped within or covalently linked to the gel structure. (b) Focused, two-photon irradiation induces complete gel erosion when the focal point (red circle) dwells for enough time ($t = t_c$) such that a sufficient fraction of PEGdiPDA crosslinks can be cleaved locally ($p = p_c$) for a given average laser power. This photocleavage releases the polymer chains that comprise the hydrogel selectively from irradiated regions (b, right).

Figure 7.2 Parameter space for two-photon induced erosion of PEGdiPDA hydrogels. (a) Critical exposure times (t_c) for irradiation to induce complete erosion of PEGdiPDA hydrogels were determined experimentally for a broad range of average laser powers (P_{avg}) (solid circles) and plotted with model predictions (dashed line). (b) The pulse energy (E_{pulse}) for each average laser power used was calculated and combined with t_c to determine the total dosage required to erode the material and these data were plotted (solid circles). Previous studies have concluded that pulse energies above 1.5 nJ thermally ablate intracellular components (gray vertical line), demonstrating that complete erosion can be performed below the cut-off for laser-induced ablation of intracellular components. (c) Locally confined erosion of PEGdiPDA hydrogels was imaged in brightfield (outside images, black corner marks indicate the region of erosion) and with cross-sections of fluorescent confocal stacks (central images) and was confirmed with profilometry (data not shown). For the pulse energy used in cells studies and feature formation ($E_{\text{pulse}} = 1.25$ nJ, left outside image and top central image), selective erosion was achieved with an average depth of 8 ± 1 μm for 7 μm deep scans. At the highest pulse energies studied ($E_{\text{pulse}} = 2.3$ nJ, right outside image and bottom central image), nonspecific erosion was induced with an average depth of 11 ± 1 μm for 7 μm deep scans. Furthermore, cavitation was observed within the hydrogels at such high pulse energies as evidenced by bubble formation in the material. Scale bars represent 20 μm in the fluorescent images and 50 μm in the brightfield images.

Figure 7.3 Feature formation to control ECM context and geometry. (a) Defined features can be patterned at the surface or within PEGdiPDA hydrogels by rastering the focal point of a two-photon laser scanning microscope (LSM, Zeiss LSM 710) through specific geometries using region of interest software. (b) Surface feature formation can be performed on size scales relevant to the cell (~ 1 -100 μm) and spatially confined to desired regions to disrupt adhesion at the anterior or posterior of adhered cells (purple oval and yellow circle) or to disrupt adhesion at individual filopodia (red triangle). To demonstrate this strategy, feature formation was performed in the absence of cells on the order of microns (red triangle) to 100 μm (purple oval) and was monitored with confocal microscopy (3D renderings of fluorescent confocal stacks and the corresponding cross-sections, green and blue lines). (c) Features were also patterned within the bulk of PEGdiPDA hydrogels to motivate the utility of this approach for directing encapsulated cells (c.i) to migrate down specific channels (c.ii) or for defining the geometry of the cell niche (c.iii). 20 μm and 30 μm wide channels were patterned into PEGdiPDA gels (c.ii) for representative channel formation, and a 45 μm wide square cylinder was patterned into a gel (c.iii) as a representative change to the geometry of the cell niche. Scale bars represent 20 μm , except as noted.

Figure 7.4 Two-photon erosion of PEG substrates induces subcellular detachment. (a) Specific regions of cell-material interactions between GFP-actin transfected MSCs and PEGdiPDA hydrogels were disrupted by two-photon erosion ($t = 0$ s, region outlined in gray). This spatiotemporal erosion induced cell retraction, which was monitored with confocal microscopy (representative images of the first 400 s for an individual cell are shown). (b) Using confocal microscopy, cell area was monitored in response to subcellular detachment, and a fractional area decrease ($\Delta A(t)/A_0$) was calculated via image analysis. The solid line is a fit to the equation $\Delta A(t)/A_0 = \Delta A_{\text{max}}/A_0[1 - \exp(-(t-t_0)/\tau_c)]$, and good agreement is observed. (c) Average values for the induction time (t_0), retraction time (τ_c), and the maximum fractional area

change ($\Delta A_{\max}/A_0$) were compiled for retracting cells ($n = 6$, mean \pm s.e.m), where slowed induction and retraction times were observed on these soft hydrogels as compared to stiff culture substrates. Scale bars represent 20 μm .

Figure 7.5 MSCs on non-photodegradable PEG hydrogels exhibit no retraction in response to light exposure. Here, we present the fractional decrease in cell area for each of the control cells studied ($n = 4$) and in each scenario there is no retraction observed. Instead, the cells undergo fluctuations in cell area as expected for cells actively sensing a substrate. The average maximum fractional area change ($\Delta A_{\max}/A_0$) was -0.02 ± 0.04 (mean \pm s.e.m.), which is not significantly different from zero, indicating random fluctuations in cell area and not a concerted retraction mechanism.

Figure 8.1 Fabrication of PEGdiPDA hydrogels with tunable elasticity. (a) Photodegradable hydrogels were fabricated *via* the co-polymerization of PEGdiPDA with PEGA under redox-initiated, free radical chain polymerization. (b) The initial elasticity of these samples was $E \sim 32$ kPa and irradiation ($\lambda = 365$ nm; $I_0 = 10$ mW/cm²) lead to a monotonic decrease in substrate elasticity. With 5 minutes of irradiation, samples with a softer elasticity, $E \sim 7$ kPa, were formed.

Figure 8.2 Experimental design for probing hMSC plasticity. Cells were seeded on stiff PEGdiPDA samples at Day 0, where they remain RunX2 positive. At Day 1, 4, or 7+, a subset of the gels was softened *in situ* with light to generate soft substrates. After another 3-14 Days in culture, cells were assayed for osteogenic or myogenic transcription factors and compared to Day 0 levels.

Figure 8.3 Dynamic elasticity changes induce a cell differentiation response. (a) hMSC expression of RunX2, an early osteogenic transcription factor, was monitored over the course of two weeks after stiff substrates were softened *in situ* to generate soft substrates. Nuclear co-localization of RunX2 was compared to control samples, cells on a stiff substrate at Day 1. By Day 14, the RunX2 expression was suppressed on soft substrates. (b) hMSC expression of MyoD1, an early myogenic transcription factor, was monitored over the course of two weeks after stiff substrates were softened *in situ* to generate soft substrates. Nuclear co-localization of MyoD1 was compared to control sample, cells on a stiff substrate at Day1. On Day 7, the MyoD1 expression was upregulated on soft substrates but returned to basal levels by Day 14. (* indicates significance, $p < 0.05$)

Figure 9.1 Photodegradable microparticle fabrication. (a) Photodegradable particles were synthesized by reacting PEG4SH with PEGdiPDA via base-catalyzed Michael addition in an inverse-phase, suspension polymerization. The aqueous phase, consisting of macromers, the base catalyst triethanolamine, and the target protein, was suspended in an organic phase of hexanes and stabilized by surfactants. Upon completion of the polymerization, the particles were purified via centrifugation resulting in spherical particles, as imaged by SEM. The reaction of the PEG4SH with the PEGdiPDA forms a step-growth network, and owing to the presence of nitrobenzyl ether (NBE) moieties in the PEGdiPDA, the network degrades in response to light. (b) The NBE moiety absorbs light strongly at 365 nm with a tail out past 405 nm. This allows both single photon irradiation at 365 nm or 400-500 nm to be used to degrade the particles, as

well as two-photon irradiation using a wavelength of 740 nm.

Figure 9.2 Size and degradation characteristics of photodegradable microparticles. (a) BSA-488 was entrapped within photodegradable microspheres. (b) Image analysis was used to quantify the size distribution of the particles synthesized by this method ($n = 3130$). The particles were formed with a number average diameter of 22 μm and a diameter average diameter of 42 μm , which resulted in a polydispersity index of 1.9. Over 80% of the particles had a diameter less than 50 μm . (c) Photodegradable particles swell and, ultimately, erode in response to flood irradiation ($\lambda = 365$ nm; $I_0 = 13.5 \pm 0.5$ mW/cm²) over the time course of a minute. (d) The swelling was quantified with image analysis and plotted as normalized volume (V/V_0) as a function of irradiation time. Particles were exposed to 365 nm ($I_0 = 13.5 \pm 0.5$ mW/cm²; circles) and 400-500 nm ($I_0 = 20.0 \pm 0.5$ mW/cm²; triangles) irradiation, and the particles eroded at 55 ± 5 s and 300 ± 30 s for the two conditions, respectively (indicated by the dashed gray lines). (e) The release of BSA-488 as a function of irradiation time was quantified as the particles swelled and dissolved. Prior to dissolution (indicated by the dashed gray line), BSA-488 began diffusing out as the particles swelled, and after dissolution the majority of the payload was released into solution. Scale bars, 100 μm .

Figure 9.3 Spatially controlled degradation of photodegradable particles. (a) BSA-488 loaded microparticles were combined with BSA-594 loaded particles in a single system and focused irradiation from an LSM ($\lambda = 740$ nm; two-photon) was used to erode individual particles selectively. Here, a BSA-594 loaded particle was dissolved (t_1 to t_2) followed by the erosion of a BSA-488 loaded particle (t_2 to t_3) without disrupting neighboring particles. (b) Photodegradable particles can also be encapsulated within three-dimensional hydrogels and selectively photodegraded with focused light from an LSM ($\lambda = 405$ nm). Here, BSA-488 loaded particles were encapsulated within fibrin hydrogels and eroded with focused LSM irradiation after the image $t = 0$ s was taken. Images were captured after erosion to monitor diffusion of the protein through the fibrin gel. (c) Profiles of the diffusing protein were quantified over the time course of imaging and demonstrate that the BSA-488 diffused radially at a detectable level to a distance of 50 μm from the edge of the original particle. (d) Multiple protein loaded particle populations were encapsulated within a single fibrin gel and individual particles were eroded selectively as was demonstrated in 2D. Scale bars, 100 μm .

Figure 9.4 Release of bioactive proteins in the presence of cells. (a) Protein-loaded, photodegradable microparticles were incorporated into cell culture with plated cells. Collimated irradiation ($\lambda = 365$ nm; $I_0 = 13.5 \pm 0.5$ mW/cm²) was used to release the entrapped protein to direct or detect cell function. (b) TGF- β 1 loaded particles were added to the media of plated PE25 cells, a TGF- β 1 responsive reporter cell line, and compared to conditions: media with blank particles, media with soluble TGF- β 1, and plain media. All samples were irradiated with the same dose used to erode particles and release the TGF- β 1, and the response of the PE25 cells was compared between each condition. The TGF- β 1 loaded particles had a significantly higher response than negative controls (blank particles and media alone), though not as strong a response as the positive control of soluble TGF- β 1. This demonstrates that a significant fraction of the TGF- β 1 remained bioactive upon entrapment and photorelease. (c) Fluorescently-labeled Annexin V loaded particles were added to the media on plated 3T3 cells. (+)Camptothecin was

used to induce apoptosis and selected samples were irradiated to release the Annexin V. The samples were imaged to visualize cells labeled as apoptotic. Samples exposed to soluble Annexin V and photoreleased Annexin V stained positively for apoptosis (indicated by arrows at regions of red staining on the cell membranes), while there was no staining in the sample that was exposed to particles that were not photoreleased (particles are still visible in this image, denoted by the asterisk). Scale bar, 100 μm .

Figure 10.1. Formation of click-based hydrogels. (a) Photodegradable, MMP-degradable hydrogels were synthesized from the copolymerization of PEGtetra-yne and MMPdiN₃. (b) These gels were degraded with 365 nm light to fully erode the gel into soluble branched polymer chains, referred to as the degradation products.

Figure 10.2 Polymerization of click-based hydrogels. Rheometric monitoring of the shear storage modulus (G') evolution during polymerization indicated that a gel is formed by combining the PEGtetra-yne and the MMPdiN₃ (10 wt% monomer reacted on stoichiometry) over the course of ~ 10 minutes with $G' = 1.7 \pm 0.2$ kPa.

Figure 10.3 Cell culture in click-based hydrogels. (a) hMSCs (1×10^6 cells/mL) and (b) neural precursor embryoid bodies (500 EBs/mL) were encapsulated within the photodegradable, MMP-degradable hydrogels and spread after 24 h in the gel or extended axons during culture after 7 days in the gel, respectively. Scale bars, 50 μm

Figure 10.4 Cell recovery from click-based hydrogels. (a) hMSCs encapsulated within photodegradable, MMP-degradable hydrogels can be liberated from the gel with light ($\lambda = 365$ nm; $I_0 = 10$ mW/cm²). (b) 6 hours after liberation from the gel, hMSCs begin to spread on tissue-culture polystyrene, indicating viability and functionality after the recovery process. Scale bars, 50 μm

Figure 11.1 Photopolymerization of PEGdiPDA hydrogels for microfluidic capture devices. (a) PEGdiPDA-based, photodegradable hydrogels were photopolymerized using the visible light photoinitiator LAP within microfluidic channels to develop selective capture and release devices. (b) PEGdiPDA hydrogels (13.2 wt% monomer; 3 wt% LAP) were photopolymerized with 2 min of visible light exposure ($\lambda = 400\text{-}500$ nm; $I_0 = 20$ mW/cm²) resulting in a final shear modulus $G' = 8200 \pm 200$ Pa. (c) After complete polymerization, continued exposure of PEGdiPDA gels to light exposure ($\lambda = 400\text{-}500$ nm; $I_0 = 20$ mW/cm²) completely degraded the film over the course of an hour, demonstrated by the monotonic decrease in the normalized shear modulus.

Figure 11.2 Functionalization of PEGdiPDA hydrogel films. (a) Acrylated-NeutrAvidin (AcryINA) was incorporated into PEGdiPDA hydrogels at a range of concentrations (0 to 0.9 mg/mL). Biotinylated-fluorescein was coupled to the available AcryINA in the gels, and the incorporation of NeutrAvidin led to a dose-dependent increase in biotin binding. This demonstrates that a range of concentrations in surface functionality can be presented using AcryINA into PEGdiPDA hydrogels. (b) PEGdiPDA hydrogels were also functionalized with a cell capture antibody (biotinylated anti-EpCAM), and EpCAM expressing cancer cells (1×10^6 cells/mL) were only captured on anti-EpCAM functionalized gels in static capture experiments. Scale bars, 100 μm .

Figure 11.3 Multifaceted capture devices. Dual-layer PEGdiPDA hydrogels were photopolymerized into the microfluidic channels functionalized with BSA-488 (green) and BSA-594 (red), demonstrating the ability to present multiple, disparate surfaces to a cell suspension during flow. In this manner, the ability to spatially capture separate populations of cells from a single cell suspension could be realized. Scale bar, 400 μm .

Figure 11.4 Cell capture and release with PEGdiPDA microfluidic devices. (a) PC3 prostate cancer cells, which express EpCAM, were captured with anti-EpCAM functionalized PEGdiPDA hydrogels under continuous flow (i). UV light ($\lambda = 350\text{-}370\text{ nm}$) was employed to degrade the thin film selectively under specific cells to release them from the capture surface. Cells initially began to release from the capture location (ii), then began to roll away in the direction of continuous flow (iii), and finally became entrained in the flow for full release (iv). (b) PC3 cells were completely released in regions of degradation, curved feature on the top of the picture, but remained attached to the non-degraded regions of the film. Scale bars, 60 μm .

Figure 12.1 Photodegradable hydrogels for spatiotemporal control of the cell microenvironment thesis organization. This thesis focused on the development of photodegradable hydrogels that enable user-defined control over the mechanics and biochemical nature of the cell microenvironment. The general approach was to develop a fundamental and quantifiable understanding of light-induced property changes on the structure and function of photodegradable gels through characterization and modeling. Using this knowledge, photodegradable hydrogels were employed to probe the cellular response to dynamic mechanical signals, to direct and assay cell function through the spatiotemporally controlled release of trophic factors, and to engineer unique materials for the culture and capture of mammalian cells that enable subsequent cell release.

Figure 12.2 Subset of photocleavable moieties for photodegradable hydrogel synthesis. Organic synthesis is enabling the development of a broad range of cytocompatible, photolabile molecules, based on nitrobenzyl ether (a-c)⁸ or coumarin chemistries (d)⁷, that can be used to form photodegradable gels similar to the PEGdiPDA gels presented in this work. Similar fundamental characterization should be applied to these gels as they become synthetically available.

Figure 12.3 Modifications to statistical-kinetic model of photodegradation. (a) Erosion depth is predicted to trend linearly with irradiation time when diffusion and dissolution are assumed to occur instantaneously (solid black line); however, the inclusion of a simple dissolution assumption (dashed black line) changes the qualitative shape of the erosion depth trend line as well as the quantitative rate of erosion. These assumptions should be included in future developments of statistical-kinetic models of photodegradation. (b) Step polymerized gels are being developed from many multifunctional monomers, such as eight-arm norbornene-functionalized PEG and difunctional thiol-terminated PEG,⁹ and as photodegradable gels are synthesized with these network connectivities, new characterization and modeling should be applied to these systems.

Figure 12.4 Single cell analyses with photodegradable hydrogels. (a) Softening of 2D substrate modulus should be combined with single-cell analyses to further investigate the molecular mechanisms by which mammalian cells integrate mechanical signals from the extracellular matrix. (b) Micron-scale two-photon erosion of 3D hydrogels proximal to encapsulated cells should be explored to investigate how cells respond to changes in cell geometry in a 3D context.

Figure 12.5 Delivery of trophic factors from photodegradable microspheres. (a) Sonic hedgehog (Shh) loaded particles were employed to release Shh in the presence of neural precursor embryoid bodies to direct them toward a ventral motor neuron phenotype. *In vivo*, Shh patterns the CNS from ventral to dorsal with a gradient of Shh. Similarly, Shh released from photodegradable microspheres upregulated ventral genes (Nkx2.2, Olig2, and Nkx6.1) compared to un-treated, control embryoid bodies. *Work done in collaboration with Quinn Fleming and Mirza Peljto. (b) The chemokine SDF-1 α was loaded into photodegradable microspheres to develop a system to study hMSC chemotaxis in response to spatial release of SDF-1 α . SDF-1 α loaded microspheres were encapsulated in a small fibrin clot, which was surrounded by an hMSC laden fibrin gel. The SDF-1 α was released with photodegradation of the microspheres and the hMSCs preferentially migrated in the direction of released chemokine. *Work done in collaboration with Bruce Han and Kyle Kyburz.

Figure 12.6 Templated cyst-like structures from photodegradable microspheres. (a) Adhesive proteins, such as fibronectin and laminin, were entrapped within photodegradable hydrogels to enable coating with A549 cells. These cell coated particles were entrapped within MMP-degradable and RGD-functionalized hydrogels and the inner photodegradable microspheres were ablated to generate hollow, cyst-like structures. (b) A549 cells coat particles over the course of 18 h and remain attached during encapsulation. (c) Immunostaining for cytoskeleton (red = actin) and nuclei (blue = nuclei) illustrated that the cyst-like structures remain intact after cell encapsulation and photodegradation of the microspheres. *Work done in collaboration with Katie Lewis and Dr. Vivek Balasubramaniam.

Figure 12.7 Selective recovery of encapsulated cells for downstream analysis. Cells encapsulated in MMP-degradable and photodegradable, click-based hydrogels are selectively released by photodegradation of regions of the gel. Released cells are then recovered for subsequent culture or analysis.

CHAPTER I

INTRODUCTION AND BACKGROUND

Sections as published in *Biotechnology and Bioengineering*, **103**, 655-663 (2009)

1.0 Overview

Methods for culturing mammalian cells *ex vivo* are increasingly needed to study cell and tissue physiology and to grow replacement tissue for regenerative medicine. Two-dimensional, static culture has been the paradigm for typical *in vitro* cell culture; however, it has been demonstrated that cells behave more natively when cultured in environments that recapitulate the three-dimensionality and/or dynamics of the *in vivo* environment. Permissive, synthetic hydrogels and promoting, natural hydrogels have become popular as three-dimensional cell culture platforms; yet, neither of these systems provides the user with full control over the biochemical and biophysical nature of the extracellular space during culture. Synthetic hydrogels that incorporate sophisticated chemistries that enable cell-defined or user-defined changes in material properties during cell culture have begun to bridge the gap between blank slate, *in vitro* culture and the native, *in vivo* environment. A major goal of this thesis is the development and characterization of photoresponsive hydrogel platforms that enable user-programmable control over the physical and biochemical environment that cells interact with during culture to understand how cells integrate information from their dynamic surroundings.

While the biology and tissue engineering communities seek to better understand how cells receive information from their extracellular niche and integrate the signals to modulate output cell function, unique materials that enable hypothesis testing of how specific interactions influence cell fate are increasingly required. In this thesis, easily synthesized, light responsive biomaterials are characterized and applied to control the mechanical and chemical nature of cell-laden hydrogels in all three-dimensions and in real time. The overall goal of this thesis is the development of chain polymerized and step polymerized poly(ethylene glycol) (PEG) based hydrogels that undergo degradation upon exposure to appropriate wavelengths and intensities of light, affording the user full control over the extracellular niche in both space and time. The precise nature in which the light modifies hydrogel properties is characterized for both gel systems, while models are developed to predict how irradiation conditions and network connectivity influence evolving material properties. This precise and predictable control over material properties is then exploited to investigate how dynamic mechanical and biochemical extracellular environments influence and direct cell function.

This introductory chapter begins with a review of the use of hydrogels as extracellular matrix mimics for cell culture, focusing on the materials and methods commonly used for *in vitro* cell culture. Subsequently, the formation mechanisms of PEG based hydrogels are discussed, as well as the relevant material properties of hydrogels. Finally, photoreactions and photolabile chemistries for user-defined, dynamic property control in PEG hydrogels are presented.

1.1 Hydrogels as extracellular matrix mimics for cell culture

The culture of mammalian cells *in vitro* provides a defined platform for investigating cell and tissue physiology and pathophysiology outside of the organism. Traditionally, this has been done by culturing single cell populations on two-dimensional (2D) substrates such as tissue culture polystyrene (TCPS) or the surface of tissue analogs. Experiments with these 2D constructs have provided the basis for our nascent interpretation of complex biological phenomena, including molecular biology, stem cell differentiation,¹ and tissue morphogenesis.² Furthermore, 2D experiments have given rise to seminal findings in the dynamic relationship between cell function and interactions with the cellular microenvironment. For example, Discher and coworkers demonstrated that the differentiation of human mesenchymal stem cells (hMSCs) is dependent on the mechanical stiffness of the 2D culture platform.^{3,4} Further, Ingber and coworkers have shown that the degree to which a cell is mechanically distended on a 2D scaffold dictates relative growth and apoptotic rates.^{5,6} Thus, *in vitro* cell constructs can be used to examine how epigenetic factors affect physiological phenomena; however, recent work has shown that cells often exhibit unnatural behavior when they are excised from native three-dimensional (3D) tissues and confined to a monolayer.

In their groundbreaking work, Bissell and coworkers demonstrated that human breast epithelial cells develop like tumor cells when cultured in two dimensions, but revert to normal growth behavior when cultured in 3D analogs of their native microenvironment.⁷ Also, enhanced chondrogenesis of embryonic stem cells has been observed when cells are cultured in 3D embryoid bodies as compared to monolayer culture.⁸ These findings in oncogenesis and stem cell differentiation elucidate acute disparities in cell function between 2D and 3D culture and suggest that examining hierarchical biology in just two dimensions is insufficient.

As a result, biologists and bioengineers alike have investigated many three-dimensional scaffolds that recapitulate aspects of the native cellular microenvironment for *in vitro* cell culture. Among these, hydrogels – crosslinked networks that possess high water contents – demonstrate a distinct efficacy as matrices for 3D cell culture. Currently, the gamut of hydrogels used for mammalian cell culture ranges from purely natural to purely synthetic materials with each hydrogel system possessing its own advantages and limitations. As the field moves forward, the need for matrices that combine the benefits of natural and synthetic materials is becoming more apparent, along with identifying the essential biophysical and biochemical signals to incorporate in these synthetic extracellular matrix (ECM) analogs.

1.1.1 The cell culture context matters

The paradigm that cellular scaffolds serve solely as passive vehicles with which to study the relationship between gene expression and cell function has become outdated. It is now evident that the cellular microenvironment contributes to the spatially and temporally complex signaling domain that directs cell phenotype. In fact, Bissell's work established that phenotype can supersede genotype simply on account of interactions with the ECM. Thus, a cell can no longer be thought of as a solitary entity defined by its genome, but must be evaluated in the context of the ECM, soluble growth factors, hormones, and other small molecules that regulate organ, and ultimately organism, formation and function. This dynamic, extracellular environment orchestrates an intracellular signaling cascade that influences phenotypic fate by altering gene and protein expression.⁹ The differences in cell behavior observed between 2D and 3D cultures come from perturbations in gene expression that stem from how the cell experiences

its microenvironment differently in two dimensions as compared to the natural 3D surroundings (Figure 1.1).

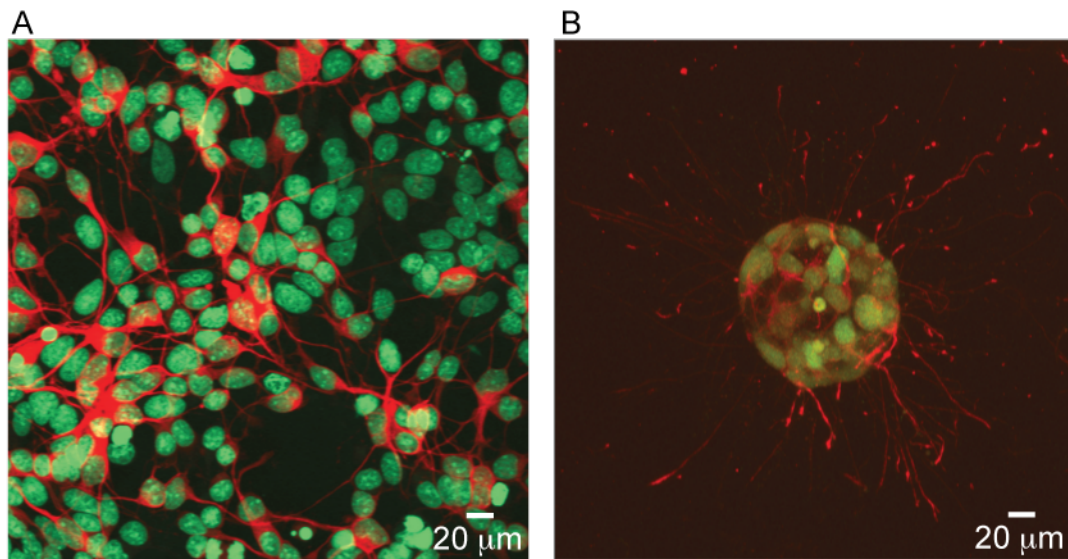


Figure 1.1 Cell culture in two-dimensional and three-dimensional platforms. Cells experience a drastically different environment between 2D and 3D culture. For instance, neural cells cultured in monolayer (a) are constrained to extend processes in the plane. Cell bodies are stained green and β -tubulin in axonal extensions is stained red. When cultured within hydrolytically degradable poly(ethylene glycol) based hydrogels (b) the same cells form neurospheres and extend processes isotropically in three dimensions. Images taken by M.J. Mahoney.

For instance, 2D culture can polarize cells, such that only a segment of the cell's membrane can interact with the ECM and neighboring cells, while the rest of the cell is exposed to the bulk culture media.¹⁰ This polarization often leads to unnatural integrin binding and mechanotransduction, which both affect intracellular signaling and phenotypic fate.¹¹ The inherent polarity also leads to unnatural interactions with soluble factors. In 2D culture, cells experience a relatively homogenous concentration of nutrients, growth factors, and cytokines present in the bulk media with the section of the membrane that contacts the surrounding media. In contrast, the concentrations of soluble factors that influence cell migration, cell-cell communication, and differentiation possess dynamic spatial gradients *in vivo*.¹²

Morphology alone has been shown to influence subtle cellular processes such as global histone acetylation,¹³ as well as proliferation, apoptosis,⁶ differentiation,¹⁴ and gene expression.⁹ 2D culture confines cells to a planar environment and restricts the more complex morphologies observed *in vivo*.

Furthermore, differences in migration exist between a 2D surface and a 3D environment. Not only is a cell confined to a plane in 2D, but also encounters little to no resistance to migration from a surrounding ECM. This applies to other phenomena that occur over longer length scales, such as cancer metastasis and tissue organization, where the behavior is regulated by mechanical interactions with the surrounding cellular microenvironment. Thus, to properly study cell physiology, mechanotransduction, and tissue morphogenesis *in vitro*, cells should be cultured in model microenvironments that more precisely recapitulate critical mechanical and biochemical cues present in the native ECM, while facilitating hierarchical processes such as migration and tissue organization.

1.1.2 Hydrogels as 3D culture platforms

Over the past few decades, tissue engineers and cell biologists have begun to develop material systems to culture mammalian cell within 3D ECM mimics to circumvent the limitations posed by traditional 2D cell culture. To this end, cells have been encapsulated within microporous,¹⁵⁻¹⁷ nanofibrous,^{18,19} and hydrogel scaffolds.²⁰ Microporous scaffolds allow for convenient encapsulation of cells, but they contain porosities ($\sim 100 \mu\text{m}$) greater than the average cell diameter ($\sim 10 \mu\text{m}$); thus, they effectively serve as 2D scaffolds with curvature. Nanofibrous scaffolds provide a 3D topology that better mimics the architecture formed by fibrillar ECM proteins; however, many are too weak to handle the stress needed for proper

mechanotransduction. These limitations are not found in hydrogels, which capture numerous characteristics of the architecture and mechanics of the native cellular microenvironment.²¹

Owing to their ability to simulate the nature of most soft tissues, hydrogels are a highly attractive material for developing synthetic ECM analogs. These reticulated structure of crosslinked polymer chains possess high water contents, facile transport of oxygen, nutrients and waste, as well as realistic transport and/or binding of soluble factors.²² Furthermore, many hydrogels can be formed under mild, cytocompatible conditions and are easily modified to possess cell adhesion ligands, desired viscoelasticity, and degradability.²³

Hydrogels used for cell culture can be formed from a vast array of natural and synthetic materials, offering a broad spectrum of mechanical and chemical properties. For excellent reviews of the materials and methods used for hydrogel synthesis see Lee and Mooney 2001 and Peppas *et al.* 2006 and 2009.^{20,24,25} At the simplest deconstruction, hydrogels are promoting of cell function when formed from natural materials and permissive to cell function when formed from synthetic materials (**Figure 1.2**).

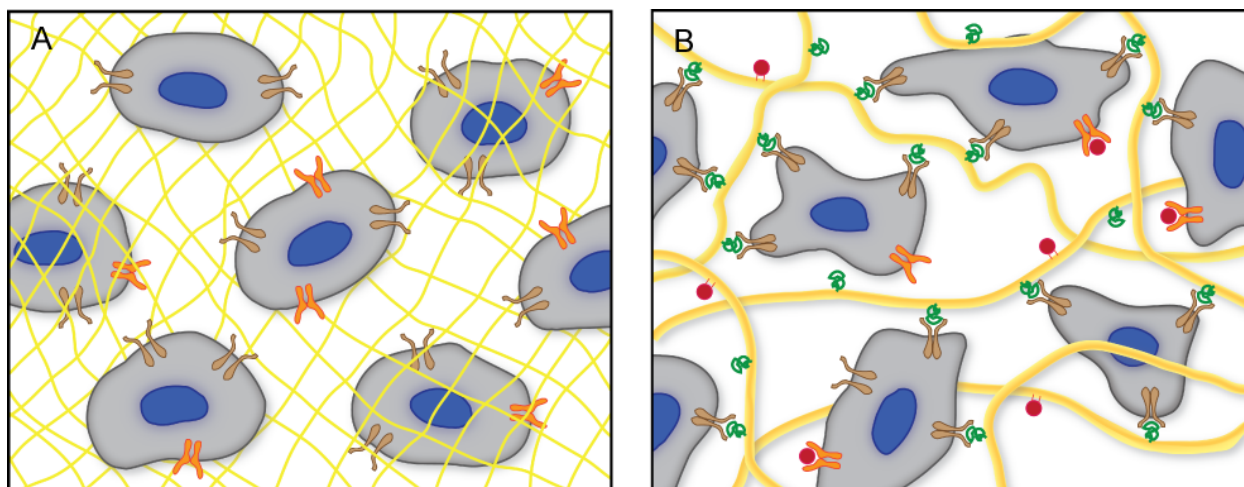


Figure 1.2 Permissive and promoting hydrogels. Permissive hydrogels (a) composed of synthetic polymers (yellow mesh) provide a 3D environment for culturing cells; however, they fail to activate integrins (brown) and other surface receptors (orange). The synthetic environment simply permits viability as cells remodel their surrounding microenvironment. On

the other hand, promoting hydrogels (**b**) formed from naturally derived polymers present a myriad of integrin-binding sites (green) and growth factors (red) coordinated to the ECM (yellow fibers), which direct cell behavior through signaling cascades that are initiated by binding events with cell surface receptors.

1.1.3 Permissive and promoting hydrogels

Natural gels for cell culture are typically formed of proteins and ECM components such as collagen,²⁶ fibrin,²⁷ hyaluronic acid,^{28,29} or Matrigel, as well as materials derived from other biological sources such as chitosan,³⁰ alginate,^{31,32} or silk fibrils.³³ Since they are derived from natural sources, these gels are inherently biocompatible and bioactive.³⁴ They also promote many cellular functions due to the myriad of endogenous factors present, which can be advantageous for the viability, proliferation, and development of many cell types. However, such scaffolds are complex and often ill-defined, making it difficult to determine exactly which signals are promoting cellular function.³⁵ Furthermore, tuning their material properties such as mechanics and biochemical presentation can be difficult; there is risk of contamination, they can be degraded or contracted too quickly, and they possess an inherent batch-to-batch variability that confounds the effect of the scaffold on cell proliferation, differentiation, and migration.

On the other hand, hydrogels can be formed of purely non-natural molecules such as poly(ethylene glycol) (PEG),³⁶ poly(vinyl alcohol),³⁷ and poly(2-hydroxy ethyl methacrylate).³⁸ PEG hydrogels have been shown to maintain the viability of encapsulated cells and allow for ECM deposition as they degrade,³⁹ demonstrating that synthetic gels can function as 3D cell culture platforms even without integrin-binding ligands. Such inert gels are highly reproducible, allow for facile tuning of mechanical properties, and are simply processed and manufactured. However, they lack endogenous factors that promote cell behavior and act mainly as a template to register cells in 3D and permit their function.³⁵

These synthetic scaffolds offer a minimalist approach to the culture of mammalian cells outside of the body and have been used for clinical applications, as well as for fundamental studies of cell physiology.⁴⁰ However, in order to properly mimic the native ECM, some of its complexity must be integrated into these permissive hydrogel.

1.1.4 Native extracellular matrix

In vivo, cells grow within a complex and bioactive hydrogel scaffold that provides mechanical support while directing cell adhesion, proliferation, differentiation, morphology, and gene expression – the ECM. Functional scaffolds for three-dimensional culture that permit cell growth while promoting function and tissue organization should emulate this prototypical hydrogel⁴¹ on multiple length scales (**Figure 1.3**).

The ECM's backbone – a complex architecture of structural, fibrous proteins such as fibronectin, collagen, and laminin – provides the matrix's mechanical properties. Cells sense these mechanics through binding events between integrins on the cell surface and binding motifs of the ECM proteins. Hydrated proteoglycans fill the interstitial voids of this backbone, sequestering soluble biomolecules: growth factors, small integrin-binding glycoproteins (SIBLINGS), and matricellular proteins. Cells dynamically restructure the microenvironment to release signaling molecules, allow migration, or accommodate cell function *via* ECM-cleaving proteins, such as metalloproteinases (MMPs), and the deposition of ECM components, both of which are regulated by integrin-mediated signaling pathways.⁴² This remodeling is necessary for proper tissue homeostasis and becomes more pronounced in pathological and developing states. Although ECM composition varies significantly from tissue to tissue within the organism, understanding its general composition and how remodeling functions in development and wound

healing points to important design criteria for 3D cell culture platforms. For a complete review of ECM remodeling see Daley et al. (2008).⁴²

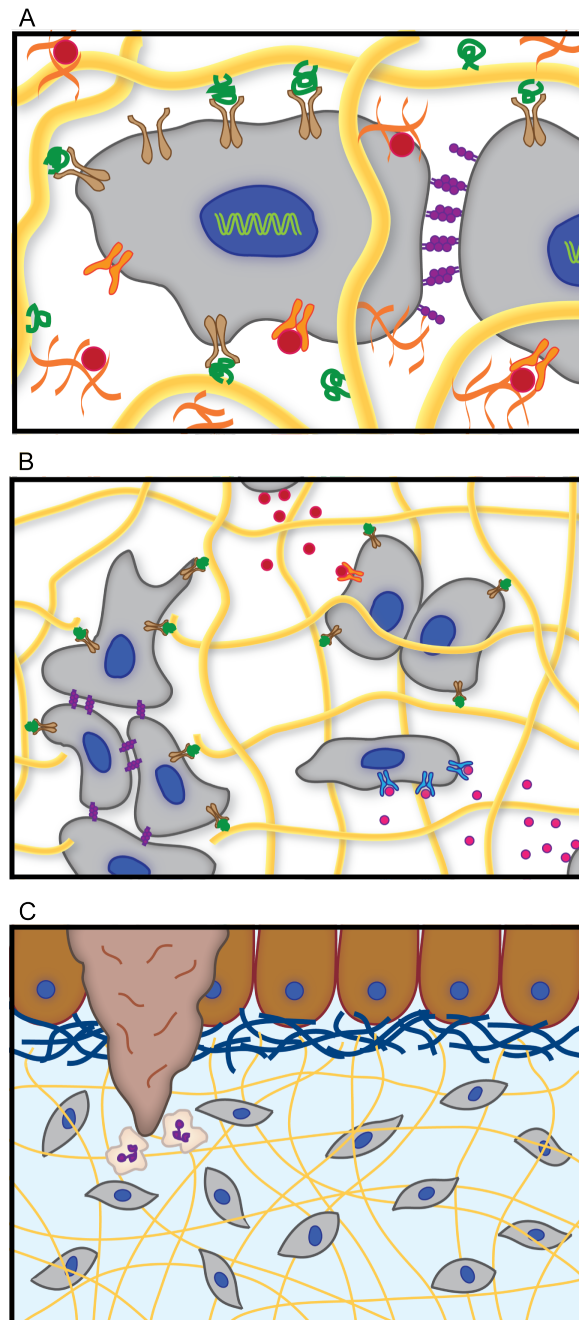


Figure 1.3 The native extracellular matrix. The native ECM is the prototypical hydrogel that regulates cell function on many length scales. (A) Integrin-binding with ECM proteins (green ligands and tan receptors), growth factor sequestration within proteoglycans (red), and cell-cell contact via cadherins (purple) occur on the scale of tens of nanometers to microns. (B) Migration, which is critical in tissue regeneration, cancer metastasis, and wound healing, initiates on the scale of tens to hundreds of microns. Paracrine signaling that directs differentiation (pink

growth factors) and proliferation (red growth factors) is also mediated on this length scale. (C) Tissue homeostasis, development, and wound healing are regulated over hundreds of microns to centimeters. Here, we illustrate neutrophils being recruited to the site of a wound in the epithelium.

1.1.5 Design criteria

Developing bioactive hydrogels for 3D cell culture is an archetypal engineering problem, requiring control of physical and chemical properties on length scales from microns to centimeters and time scales from seconds to weeks. In order to develop a functional ECM mimic, the gel's mechanical properties, adhesive ligand and growth factor presentation, transport and degradation kinetics must be tuned to the given culture's needs *a priori* in a cytocompatible, reliable, and cost effective fashion.^{21,43} Furthermore, these gels' chemistries and their degradation products cannot have a deleterious effect on encapsulated cells.

Traditionally, a scaffold's mechanical and chemical properties are set during encapsulation with little user- or cell-defined control post-fabrication. In order to truly mimic the ECM, it is necessary to develop materials whose mechanical and chemical properties can be tuned on the time and length scale of cell development, exogenously by the user, or endogenously by the cells. Although scaffolds are designed to mimic the native ECM, the prime culture conditions are not precisely known *a priori*, so the expression of one or more facets of the gel can be altered to approach the proper conditions for a desired cellular response. Ultimately, the goal is to rationally engineer biomaterial scaffolds that meld the benefits of synthetic and natural gels to satisfy the required needs of a given culture system in a robust scaffold.

1.1.6 Bridging the gap

Recent work in scaffold engineering demonstrates that 3D synthetic microenvironments can be designed to promote cell viability and direct cell adhesion,⁴⁴ differentiation,⁴⁵ proliferation,⁴⁶ and migration⁴⁷ through the controlled presentation of mechanical and biochemical cues. Such instructive materials are bridging the gap between promoting and permissive gels by incorporating biomimetic signals into synthetic materials that elicit desired cell-gel interactions. These scaffolds can be tailored to the specific cell culture requirements and design criteria and are providing novel and well-defined ECM mimics for controlled hypothesis testing in cell biology and regenerative medicine.³⁵

In vivo, the ECM provides a milieu of binding ligands for cell adhesion that connect a cell's cytoskeleton to the cellular microenvironment.⁴⁸ These ligands encourage integrin-binding events that communicate the mechanics of the ECM to the cell and direct cell fate through intracellular signaling pathways.⁴⁹ Thus, integrin-binding events play a critical role not only in cell adhesion, but also in most cellular processes.⁵⁰ In the simplest case, these binding ligands are recapitulated in synthetic hydrogels by physically entrapping ECM proteins, such as collagen, laminin, or fibronectin, into the network. These large proteins provide binding domains for integrin adhesion and have been shown to improve cell viability and function.⁵¹ However, entrapped proteins can denature, aggregate, introduce multiple binding motifs, and are often heterogeneously distributed throughout the gel, all of which confound their effects.

Protein engineering has evolved such that we can identify active peptide sequences from desired proteins and incorporate them into synthetic hydrogels.⁵² This allows the controlled placement of specific binding domains onto an otherwise bioinert background²³ to study the interactions between adhesive peptide sequences, such as RGD and IKVAV, and cell function.

In PEG scaffolds the incorporation of pendant RGD – the known binding domain of fibronectin – has been shown to increase viability and adhesion of encapsulated cells.⁵³⁻⁵⁵ Further, studies with RGD tethered to synthetic gels have indicated ideal clustering and ligand density for cell spreading⁵⁶ and migration.⁵⁷ Novel polymerization mechanisms, such as photoinitiated thiol-acrylate and thiol-ene chemistries,⁵⁸⁻⁶⁰ are now allowing facile incorporation of peptides within routinely used synthetic gels.

Natively, the presentation of such binding domains is regulated spatially and temporally. For example, during chondrogenesis fibronectin is downregulated within 7-12 days of hMSCs differentiating to chondrocytes by upregulating the production of matrix metalloproteinase 13 (MMP-13), which cleaves fibronectin.⁶¹ To mimic this temporal control, an RGD peptide sequence that was susceptible to MMP-13 cleavage was built into a PEG gel so that hMSCs could remove RGD, the fibronectin analog, as they would naturally. This successfully upregulated chondrogenesis in the synthetic environment as the removal of fibronectin does *in vivo*.⁴⁵ This is not a singular example of temporal presentation, and it is becoming increasingly important to design sophisticated gel niches that afford temporal regulation of such instructive cues.

Similar concepts can be extended to other functional peptide sequences. In the native ECM, the delivery of chemokines, such as growth factors, to specific locations at specific times is mediated by controlled storage and release.⁶² Like ECM proteins, growth factors can simply be entrapped within hydrogel scaffolds and released upon network degradation, such that the release is independent on diffusion and degradation rates.⁶³ To replicate the natural harboring of growth factors within the proteoglycans of the ECM, hydrogels have been synthesized that incorporate heparin to associate proteins with the network that can subsequently be released.⁶⁴

Improvements to this system have been made by covalently linking protein specific ligands to the gel's backbone.⁶⁵ This work points to the need for gels that contain binding ligands that selectively associate desired growth factors, present them in a more physiologically relevant context, and release them based on cellular uptake. Furthermore, controlling the local concentration of tethered peptide ligands creates spatial gradients in chemokine availability. *In vivo*, multiple soluble factors act synergistically or antagonistically to render sophisticated signaling regimes that direct tissue development and homeostasis.¹² To more closely recapitulate these signaling domains, multiple functionalities need to be incorporated within the gel that sequester and present several, orthogonal cues at desired time points.

Cell mediated release of growth factors has been achieved by encapsulating selected proteins within gels that have MMP cleavable sequences in the backbone.⁶⁶ Specifically, Michael addition has been used to construct a network of end-functionalized PEG and thiol-labeled MMP cleavable peptide sequences. Incorporating vascular endothelial growth factor (VEGF) into this network induced vascularization as cells exposed VEGF by cleaving the MMP susceptible peptide sequences.⁶⁶ This cell-mediated release is a better mimic of native growth factor sequestration and can be coupled with peptide binding systems for a more dynamic system.

As biochemical techniques and new small molecule targets, such as micro RNAs (miRNA), small interfering RNAs (siRNA), and RNA aptamers, are better understood, the approaches that are used to deliver large soluble factors will need to be extended to present small molecules that can assist in the precise regulation of gene expression within a 3D environment.

While these approaches mimic biochemical aspects of the ECM, synthetic hydrogels often fail to capture the biophysical structure of the cellular microenvironment (e.g., the fibrillar

structure of collagen and the potential for cellular remodeling of the ECM). To recreate the native restructuring of the cellular microenvironment, it is often necessary to engineer degradation into synthetic ECM analogs so that viable cells can deposit their own ECM,³⁹ migrate,⁶⁷ and undergo morphogenesis.⁶⁸ Synthetic hydrogels have been designed to hydrolytically degrade by incorporating poly(lactic acid)⁶⁹ or poly(caprolactone)⁷⁰ units into the network backbone. In these scaffolds the initial number of hydrolytic bonds present dictates the rate of degradation, but in general, the rate is on a slower time scale than normal cellular processes. Michael addition and photoinitiated reactions of end-functionalized PEG and thiol-labeled MMP cleavable peptide sequences can also be used to create synthetic hydrogels whose degradation is cellularly driven⁷¹ and on a much shorter time scale. Increased production of MMPs allows cells to remodel this synthetic environment, migrate, and deposit their own ECM much like they do *in vivo*. Such systems that possess dynamic feedback between the microenvironment's structure and cell behavior will be extremely useful to study migration, tumor morphogenesis, and cancer metastasis.

Even with degradable synthetic hydrogels, the networks' subcellular processes porosities can pose a barrier for cell migration, proliferation, and differentiation as well as for the proper distribution of soluble factors. These networks often do not possess the fibrillar network structure of the ECM protein backbone. To address this, scaffolds need to be devised that couple robust self-assembly⁷² or nanofabrication techniques with degradable synthetic hydrogels to better recreate critical aspects of the biomechanical structure of the native ECM.

1.1.7 Current directions

While advances in polymer chemistry are driving the evolution of sophisticated synthetic-biologic gels, 3D culture of mammalian cells in such microenvironments is not without challenges. First, oxygen availability requires special notice, since cells are less than 100 μm from a high-oxygen source in metabolically active tissue.⁷³ Second, moving to the third dimension exaggerates the heterogeneities present in the synthetic cellular microenvironment, compared to 2D surfaces. In 3D scaffolds, gradients and defects can occur in material properties, proteins can become diffusion limited leading to heterogeneous distributions, and oxygen and nutrient gradients arise as the culture medium diffuses through the gel. Third, regulating the distribution of soluble growth factors, which influence cellular differentiation and tissue homeostasis, becomes more complicated within 3D networks as the distribution depends on the bulk concentration in the media, diffusion within the gel, and cellular uptake. Finally, the standard techniques for imaging and analyzing cell function and protein distribution are more involved in the 3D environment. When working in a 3D network, cells have limited accessibility for immunostaining or DNA. RNA extraction and secreted proteins can be difficult to extract from the gels. Cell imaging is often complex as light scattering, refraction, and attenuation occur in a 3D composite, cell-laden gel.

These challenges point to the need for sophisticated techniques, as well as sophisticated hydrogel environments, to combine the ability for real-time biological analyses with real-time manipulation of the material environment. The native ECM is far from static; therefore, to facilitate complex cellular behavior ECM mimics must also be dynamic. To use these systems for hypothesis testing, it is important to possess user-defined control over the spatiotemporal presentation of integrin-binding ligands, growth factor release, and biomechanical properties (**Figure 1.4**). The biomaterials field has provided the basis for dynamic scaffold fabrication and

emerging work is offering user-defined control. As an example, click chemistries are being exploited to encapsulate cells and attach adhesive ligands to the network post-fabrication⁷⁴ while photolabile chemistries are being used to spatially and temporally regulate the gel's mechanical and biochemical properties.⁷⁵ Coupling these and other cytocompatible, bioorthogonal chemistries will provide a template for testing cell-ECM interactions and mechanotransduction in a defined, three-dimensional synthetic environment *ex vivo*. Finally, approaches to release cells, proteins, and other biological molecules from their 3D material environments need to be built into these platforms so that sophisticated biological assays can provide better insight into the role of matrix interactions on cell function.

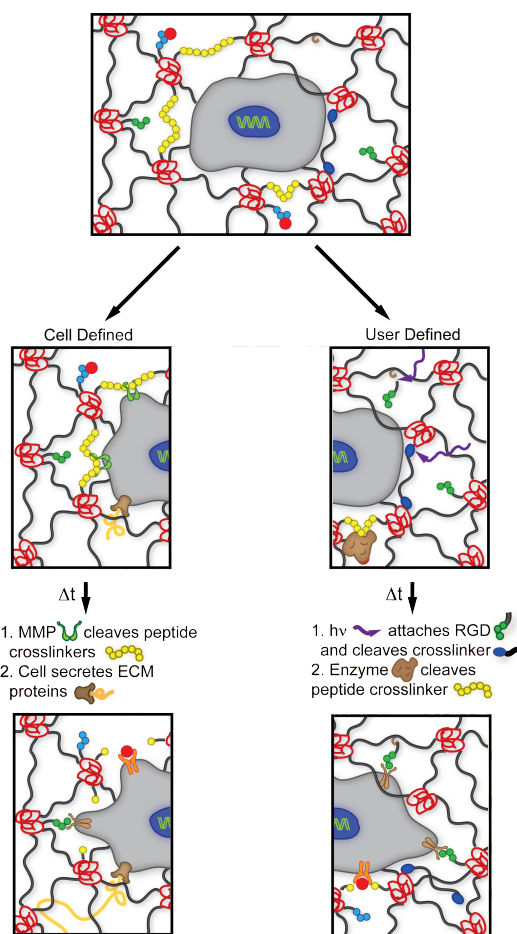


Figure 1.4 Synthetic-biologic hydrogels. Synthetic biologic hydrogels that incorporate several well-defined and orthogonal chemistries serve as robust ECM mimics for 3D cell culture.

Depending on the application, it may be advantageous to incorporate cell- or user-defined regulation of the material properties to emulate the native dynamic environment. However, in many cases, synthetic hydrogels that incorporate both cell- and user-defined chemistries will be necessary. Here, we illustrate a cell cleaving MMP degradable crosslinks (yellow circles) that allow it to access sequestered growth factors (red) and integrin-binding sites, such as RGD (green circles). Ultimately, this cleavage allows cell motility and the deposition of ECM proteins (orange fiber). User-defined chemistries, such as photodegradable crosslinks (blue ellipses) and post-gelation attachment of RGD to the network backbone, afford facile control of the dynamic biochemical and biophysical properties of the gel, thereby directing cell attachment and motility. Further, exogenous application of enzymes (brown) can allow user-defined release of sequestered growth factors.

When employing synthetic hydrogels as ECM mimics, it is necessary to understand the cell's native environment – how the cells interact with, remodel, and migrate through the ECM. To garner biologically relevant conclusions from *in vitro* cell culture, critical matrix factors must be recapitulated in a 3D environment. In cases of tissue development, it may be advantageous to allow cells to dictate changes in their own environment much like they do *in vivo*; however, user-defined control of the mechanical and biochemical properties can be advantageous to test complex hypotheses about the effect of specific cell-ECM interactions in 3D tissue models (**Figure 1.4**). The path to designing the ideal ECM mimic is dependent on the culture at hand, but will likely require multiple, orthogonal chemistries. For instance, photolabile chemistries can be used to erode regions of a gel and the newly exposed surfaces can subsequently be painted with adhesive ligands to encourage cell adhesion and migration. More complex scaffolds, formed of interpenetrating networks of cell- and user-controlled chemistries, will arise. Ultimately, there is no single network that will mimic the complex ECM of every tissue type, but rationally incorporating bioinspired cues into synthetic gels that can provide robust and diverse scaffolds for many cell culture systems.

1.2 Poly(ethylene glycol) hydrogels for cell culture

Synthetic hydrogels are a widely studied class of biomaterials for cell culture and biomedical applications owing to their tissue-like properties, e.g., high water content, elasticity, and transport of biomolecules, and their formation under mild, cytocompatible conditions.^{20,76,77} Traditionally, synthetic hydrogels are formed by chemically crosslinking bioinert polymers to form reticulated and water-swollen networks. The chemical makeup of such gels is defined by the polymer components and polymerization mechanism; therefore, these hydrogels can be formed with predictable and reproducible properties. Further, the material properties can easily be tuned by changing the polymer fraction and the chemistry of the hydrogel.

Research has focused on the synthesis and application of synthetic hydrogels formed from an array of polymer building blocks, including poly(ethylene glycol) (PEG), poly(*N*-isopropylacrylamide) (PNIPAm), and poly(vinyl alcohol) (PVA). Amongst these chemistries, PEG is the most common building block for defined, synthetic hydrogels for cell culture on account of its hydrophilicity and resistance to protein adsorption. As such, cells have minimal non-specific interactions with PEG-based hydrogels, which renders PEG as a blank slate, permissive culture systems on or within which to study cell biology, pathophysiology, and tissue regeneration.

Cytocompatible, PEG-based hydrogels have been formed through the chemical crosslinking of several multi-functional PEG polymers. Specifically, tetrafunctional (meth)acrylate terminated linear PEGs^{36,78} and vinyl sulfone⁷¹ or norbornene⁷⁹ terminated four-arm PEGs have been used as crosslinkers to form synthetic hydrogels. There are different polymerization mechanisms that can be employed to form crosslinked networks for these macromers. For the (meth)acrylate terminated PEGs, insoluble networks are most commonly formed *via* free-radical initiated chain polymerization. Chain polymerization results when an

initiating species generates a reactive center, e.g., radical, anion, or cation, to which monomer molecules add successively, with the regeneration of the reactive center and a sequential elongation of the polymer chain with each addition.⁸⁰ When chain polymerization is conducted in the presence of multifunctional ($f \geq 3$) macromolecular monomers, growing chains become chemically linked by the multifunctional crosslinks creating the hydrogel network. Here, functionality refers to the number of bonds a monomer can form with other reactive species during the polymerization, *i.e.*, an acrylate group is difunctional in a chain polymerization and monofunctional in a step polymerization. Alternatively, vinyl sulfone or norbornene terminated PEGs often form insoluble networks *via* step polymerization. In this reaction scheme, monomers react through a one-to-one addition of complementary reactive groups, e.g., azides to alkynes, vinyl sulfones to thiols, and norbornene to thiols. If the average functionality of the complementary macromolecular monomers is greater than 2 in the precursor solution, an insoluble network will form as the sequential reactions build up a larger and larger molecular weight species and ultimately an infinite molecular weight gel.⁸⁰

Crosslinked hydrogels for biomedical applications have been formed traditionally through the free-radical initiated chain polymerization of PEG-based, telechelic monomers.³⁶ In this manner, cell culture templates and drug delivery vehicles have been fabricated rapidly with tunable material properties and have been functionalized with adhesion peptides and degradation sites.⁴⁷ However, radical initiated chain polymerizations are limited in that they are inhibited by oxygen,⁸¹ proceed with complex kinetics,⁸² can be damaging to nucleic acids and proteins,^{83,84} and inherently introduce inhomogeneities into the network structure as dense regions of kinetic chains are linked by hydrophilic polymers (**Figure 1.5**).^{85,86} These inhomogeneities in the network structure compromise the material integrity as stress is focused on weak portions of the

gel, reducing the macroscopic integrity of the hydrogel.⁸⁷ Furthermore, hydrogels formed by chain polymerization degrade with heterogeneous by-products.

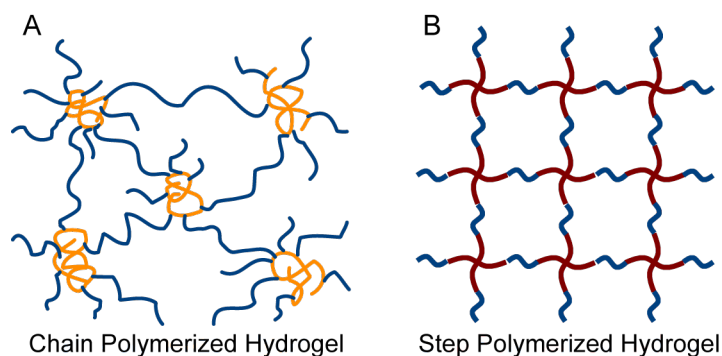


Figure 1.5 Chain and step polymerized hydrogels. (A) Hydrogels formed by a radical initiated chain polymerization are comprised of networks with heterogeneous structure of dense kinetic chains (yellow) connected by crosslinking polymers (blue). (B) Hydrogels formed by step polymerization, in this case of a tetrafunctional monomer (red) with a difunctional monomer (blue), form a more homogeneous network with increased cooperativity between elastically active network strands.

Recent work has focused on the formation of crosslinked hydrogels with ideal, homogeneous microstructures to improve network cooperativity and increase mechanical integrity (Figure 1.5).^{87,88} This has been achieved through the step polymerization of complementary, end-terminated polymers. Originally, Hubbell *et al.* demonstrated the formation of step polymerized hydrogels by crosslinking thiol and electron-poor, vinyl functionalized PEG-based monomers for drug delivery and cell encapsulation.^{71,89} This paradigm has been extended to fabricate gels through the copper-catalyzed, Huisgen azide-alkyne coupling of functionalized PEG-based co-monomers,^{88,90,91} the coupling of propylamine terminated PEG with succinimidyl glutarate terminated PEG,⁸⁷ and the photoinitiated thiol-ene coupling of norbornene functionalized PEG with di-thiol peptides.⁷⁹ Uniquely, Deforest *et al.* demonstrated the formation of step polymerized hydrogels through the copper-free strain promoted azide alkyne cycloaddition (SPAAC), forming hydrogels in a bio-orthogonal and cytocompatible manner.⁷⁴ Seminal mechanical analyses of step polymerized gels have found that these networks possess

increased tensile extension^{88,92} as compared to chain polymerized analogs, while SANS data have demonstrated that these networks, although still not perfectly ideal, possess fewer heterogeneities in the network structure.

Despite the prevalence of hydrogels in the biomedical and materials sciences, the manner by which the crosslinking mechanism and resultant microarchitecture of the hydrogel influences the macroscopic properties, e.g., strength, toughness, and degradation, is still not fully elucidated. A better understanding of the structure-function relationship in hydrogel performance would enable improved rational design of materials for targeted applications.

1.3 Hydrogel material properties

Beyond the chemical composition and reaction mechanism that forms the hydrogel, several other hydrogel properties are important, such as modulus, swelling ratio, mesh size, and degradability. As illustrated by seminal studies in the field of polymer chemistry and polymer physics,⁹³ nearly all material properties of a particular hydrogel chemistry can be related to the number density of elastically active network chains or the crosslinking density, ρ_x - the number of elastically active chains in a given volume, of the material. The volumetric swelling ratio, Q - the ratio of swollen gel volume to dry volume - scales as $Q \sim \rho_x^{-3/5}$ for highly swollen materials.^{93,94} The storage modulus of hydrogels, often measured in a shear geometry and reported as the shear storage modulus G' , is related to ρ_x based on rubber elasticity theory⁹⁵:

$$G' = RT\rho_x Q^{-1/3}$$

where R is the universal gas constant and T is the temperature. Thus, $G' \sim \rho_x^{6/5}$, which has been experimentally verified for PEG hydrogels.^{96,97} The mesh size of the hydrogel, ξ , which dictates the diffusivity of molecules through the material, is related to ρ_x through the Flory-Rehner

equation and rubber elasticity theory, $\xi \sim \rho_x^{-4/5}$.^{95,98} Therefore, by tuning the precursor solution and gelation conditions, it is possible to modulate initial hydrogel properties; however, this offers little control over property evolution in time.

Degradation is commonly employed in hydrogel systems to modulate crosslinking density locally and in real-time in order to tune material properties. Classically, hydrolytically and enzymatically labile moieties were polymerized into the network backbone, which would cleave upon exposure to appropriate environmental stimuli breaking elastically active network strands in the gel and, ultimately, causing mass loss.⁹⁹ In this thesis, degradation refers to the cleavage of individual bonds within the hydrogel backbone, and mass loss refers to the removal of material from the network. Reverse gelation refers to the point when a sufficient fraction of network bonds have been cleaved locally, such that an infinite molecular weight gel no longer exists and instead the network transitions to highly branched, soluble polymer chains. To understand how degradation relates to changes in crosslinking density and material properties, statistical-kinetic models of hydrogel degradation have been developed.¹⁰⁰⁻¹⁰² In brief, these statistical-kinetic models are based on an understanding of the kinetics of the degradation reaction, which is then used to calculate the probability that a given bond is cleaved using a mean-field approach. Given the probability of cleavage of a given bond, network connectivity and statistics can be combined to predict the loss of a given species from the network and, finally, to predict reverse gelation in these systems. While these approaches offer predictable and precise control over material properties in time, there is little user-defined control over property evolution, and there remains a need for chemistries that enable experimenter control degradation and property evolution.

1.4 Photoreactions for dynamic control of hydrogel properties

Light is an unprecedented chemical reagent as it enables the user to dictate where and when reaction is to occur, as well as the extent of reaction through controlled delivery of light.¹⁰³ Photoreactions have long been employed for hydrogel fabrication with the advantage that photoinitiated polymerization of hydrogels offers control over the spatial and temporal evolution of material properties. Further, photopolymerizations can be executed with both chain³⁹ and step⁷⁹ polymerized hydrogels and formed *in vivo* for biomedical applications. In these systems, the macromolecular monomer precursor solution contains a photoactive initiator species, e.g., Irgacure 2959, Irgacure 651, or lithium phenyl-2,4,6-trimethylbenzoylphosphinate (LAP), that cleaves into an active center, often a radical, which initiates the polymerization for network formation. The kinetics of photoinitiation, on which the rate of polymerization depends, is given as follows:

$$R_i = \frac{2.303[PI]\varphi\varepsilon f I_0 \lambda}{N_A h c}$$

where [PI] is the concentration of photoinitiator; φ is the quantum yield of the photoinitiator; ε is the molar absorptivity of the photoinitiator at the wavelength of the initiating light; f is the efficiency of the photoinitiator; I_0 is the intensity of incident irradiation; λ is the wavelength of irradiation; N_A is Avogadro's Number; h is the Planck Constant; and c is the speed of light. Thus, the rate of initiation, as is true in all photochemical reactions, depends on the photoactive molecule concentration, the molar absorptivity of the photoactive molecule, the photophysical properties of the photoactive species, and the intensity of incident irradiation. As such, these reactions can become limited by attenuation of light, as the molecule inherently absorbs the wavelength of interest, and create subsequent gradients in reaction rates.

To extend the utility of photoinitiated reactions beyond network formation, research has focused on the patterning of biochemical functionality into hydrogels for cell culture applications using photochemical reactions. Biochemical functionality can be introduced easily by incorporating small molecule peptides, short chains of amino acid residues linked together by amide bonds that recapitulate binding functionality of proteins, into the polymer backbone. While peptides are most commonly incorporated into hydrogels during formation,¹⁰⁴ West *et al.* demonstrated that classic photopolymerization techniques can be exploited to dynamically introduce biochemical functionality into a PEG diacrylate hydrogel network.^{44,105} Here, a functionalized peptide, Acryl-PEG-RGD, and a photoinitiator, Irgacure 2959, were swollen into the hydrogel and focused laser light was exploited to initiate reaction locally and concomitantly gel functionalization (**Figure 1.6a**). Shoichet *et al.* developed an alternative approach to dynamically pattern hydrogels using light post-fabrication.¹⁰⁶ In this approach, caged thiols were exposed by light in defined regions of the gel with two-photon laser irradiation and maleimide-terminated RGD was subsequently attached to the free thiols (**Figure 1.6b**). Anseth *et al.* exploited photoinitiated thiol-ene photopolymerizations to immobilize thiol-functionalized peptides in PEG based hydrogels.^{74,79,107} In this work, thiol-functionalized peptides and photoinitiators were swelled into the gels and reacted to pendant vinyl groups *via* collimated or focused light exposure (**Figure 1.6c**). Studies have also extended these paradigms to pattern full proteins into hydrogels using photochemical techniques (**Figure 1.6d**).¹⁰⁸

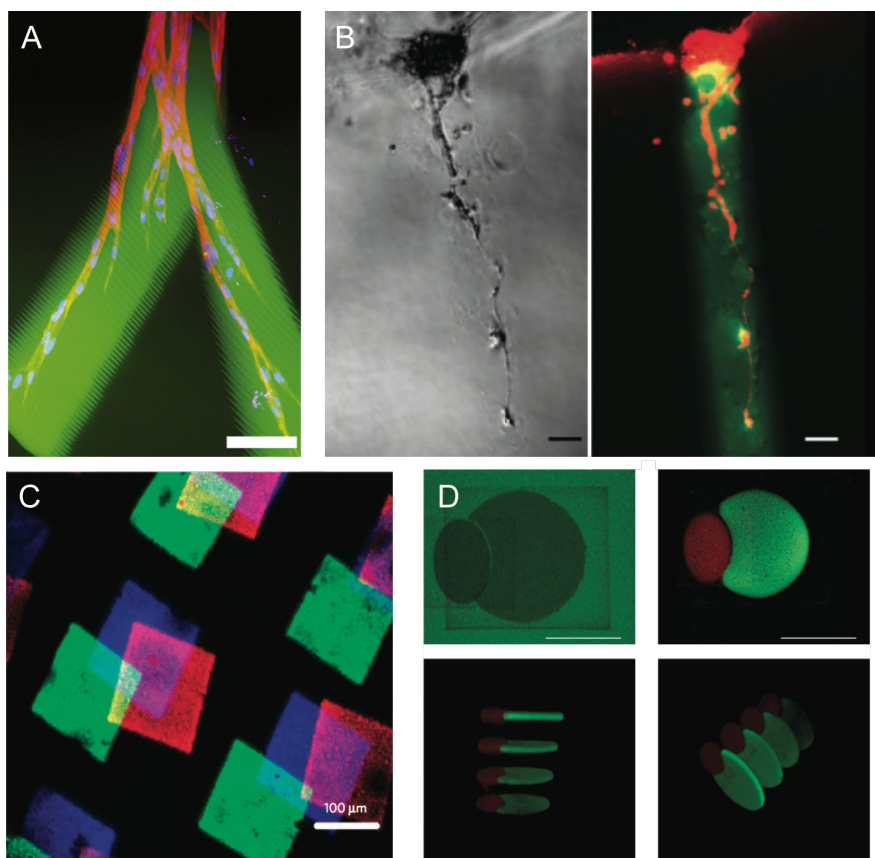


Figure 1.6 Photochemical patterning in hydrogels. (a) Fluorescently-labeled, acrylated RGD was swollen into a preformed PEGDA gel and selectively coupled within the network *via* photopolymerization. In this manner, fibroblast migration was confined to regions of a gel that was patterned with RGD (blue = cell nuclei; red = cell actin; green = RGD).⁴⁴ (b) Photodeprotection of thiols was employed to selectively couple maleimide-functionalized peptides to hydrogel. Here, the outgrowth of dorsal root ganglia cells was confined to adhesively patterned regions of the gel (green = patterned peptide; red = dorsal root ganglia cells).¹⁰⁶ (c) A similar approach coupled fluorescently-labeled peptides to a hydrogel network through photoinitiated thiol-ene chemistry. This afforded the sequential addition of multiple biochemical signals with spatial and temporal control.⁷⁴ (d) Recent work has demonstrated the photoaddition of multiple full-length proteins in three-dimensional hydrogels using photodeprotection of thiols and maleimide-functionalized molecules that capture proteins orthogonally.¹⁰⁸ Scale bars = 100 μm .

Recent work has focused on using similar photoreaction modalities to alter the biophysical parameters of hydrogels, such as modulus, swelling content, and diffusivity, dynamically in time. As described above, the physical parameters of a hydrogel all relate to the crosslinking density of that material. Therefore, efforts have focused on tuning gel connectivity

with light to achieve spatial and temporal control over hydrogel properties. Similar to the work with photopatterned peptides, West *et al.* have employed photoinitiated radical polymerization to increase the crosslinking density, and thus modulus, locally in PEG diacrylate hydrogels.¹⁰⁵ PEG diacrylate and photoinitiator were swollen into the hydrogel and subsequently reacted to pendant acrylate functionalities on the network backbone to locally increase network connectivity and modulus while decreasing diffusivity. In a similar approach, Burdick *et al.* employed hyaluronic acid based hydrogels that contained pendant acrylate functionalities that were subsequently photopolymerized to locally increase network connectivity (**Figure 1.7**).¹⁰⁹⁻¹¹¹

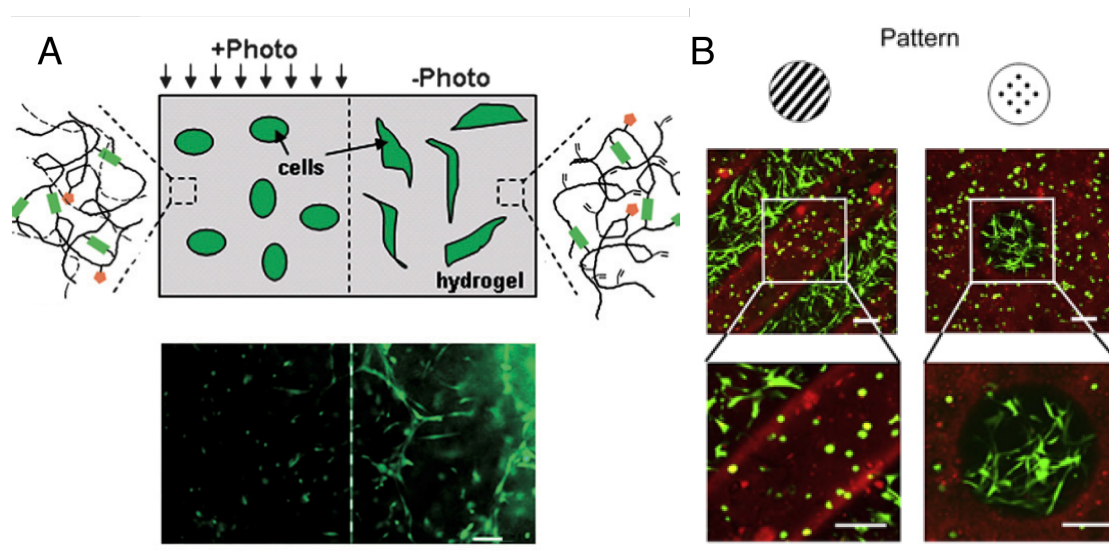


Figure 1.7 Photochemical patterning of hydrogel mechanics. (a) Sequential crosslinking reactions have been employed to photochemically alter the mechanics of a hydrogel. Here, a Michael-addition between dithiol peptides and methacrylated-hyaluronic acid is used to form a gel, which can undergo secondary photochemical crosslinking through unreacted methacrylate groups. In this experiment, cell spreading was prohibited in regions where the gel density was increased *via* photopolymerization.¹⁰⁹ (b) Further, this technique was extended to spatially pattern the mechanics of a hydrogel for cell culture, whereby cell spreading was similarly restricted to regions of lower gel density (red = photocrosslinked gel; green = cells).¹¹⁰ Scale bars, 100 μm .

These examples and others demonstrate that increasing network connectivity can be achieved *via* photopatterning techniques, but as discussed above there is also an interest in

decreasing network connectivity with time. This has traditionally been achieved through degradation of bonds within the network backbone that decreases network connectivity and can ultimately lead to mass loss and reverse gelation. Degradation is most often achieved through the use of hydrolytically or enzymatically susceptible bonds within the network backbone.^{23,36,47,57,68,69,79,112-120} However, these techniques do not take advantage of the spatial and temporal control that is facilitated by the use of photochemical reactions and limit the user's control over physical properties of hydrogels.

The use of light to degrade hydrogel materials *in situ* and in a controlled manner was first introduced by Russell *et al.* and Leblanc *et al.* through the photoreversible dimerization of nitrocinnamate- or anthracene-terminated polymers.^{121,122} In these systems, dimerization forms bonds with 365 nm light, which can subsequently be degraded with 254 nm light; however, the 254 nm light is cytotoxic, constraining the use of these materials to non-biologic applications, and complete network erosion was not observed. More recently, systems have been introduced that generate photodegradable hydrogels capable of undergoing reverse gelation in response to cytocompatible irradiation conditions.^{75,90,91,123} These systems exploit the cytocompatible photocleavage of *o*-nitrobenzyl ether (NBE) moieties to break elastically active network chains in the hydrogel backbone to alter connectivity and network properties in a controlled fashion. Unlike previously studied photolabile functionalities, the NBE moieties degrade in response to cytocompatible irradiation, e.g., one-photon: $\lambda \sim 320\text{-}436$ nm and two-photon: $\lambda \sim 740$ nm. When the moiety absorbs appropriate photons, it can enter a photochemically-excited state and undergo an irreversible rearrangement to form an nitroso- and an acid- terminated byproduct (**Figure 1.8**).¹²⁴

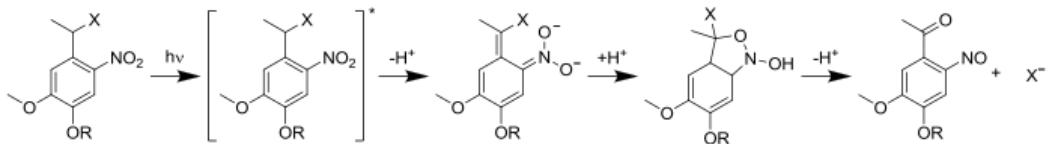


Figure 1.8 Proposed mechanism of *o*-nitrobenzyl ether photocleavage. When an *o*-nitrobenzyl ether moiety is photoexcited, it forms an intermediate five-member ring *via* proton exchange that can result in molecular scission. This results in the release of X, which is typically terminated in a carboxylic acid or amine functionality. Figure adapted from Li *et al.*¹²⁴

Further, this molecule has been used in biologic applications to cleave peptides from solid supports,¹²⁵⁻¹²⁷ to active caged molecules,¹²⁸ and to control cell adhesion dynamically.^{129,130}

Work with NBE moiety based photodegradable hydrogels has investigated the cellular response to dynamic changes in gel geometry and modulus.^{75,123,131}

1.5 Research summary

This thesis aims to develop photodegradable hydrogels based on *o*-nitrobenzyl ether (NBE) functionalized PEG polymers *via* chain and step polymerization to understand how network connectivity and material properties can be tuned with light, as well as to control the physical and biochemical nature of the cellular microenvironment with 3D control and in real-time (**Figure 1.9**). Toward this goal, Chapter II describes the four main objectives of this thesis work: develop a fundamental and quantifiable understanding of light-induced property changes in photodegradable hydrogels, apply these alterations in gel structure to investigate the cellular response to dynamic mechanical signals, exploit these materials to release trophic factors to cells with spatial and temporal control, and engineer unique materials for the culture and capture of mammalian cells that enable subsequent cell release. In Chapter III, a detailed protocol of the synthesis of NBE functionalized monomers and polymers is presented along with a description of hydrogel fabrication *via* chain polymerization, characterization, and mammalian cell culture

with PEG based photodegradable hydrogels. In Chapter IV, a statistical-kinetic model of photodegradation is developed to describe quantitative changes in network connectivity and material properties based on irradiation, demonstrating the physical understanding of photodegradation and the control that this affords. In Chapter V, chemically similar, chain polymerized and step polymerized photodegradable hydrogels are fabricated to investigate the effects of initial network connectivity on mechanical integrity and photodegradation. The statistical-kinetic model of photodegradation is applied to both systems, demonstrating an understanding of the physical mechanisms that result in degradation and reverse gelation for the disparate systems. Chapters VI-VIII illustrate applications of chain polymerized, photodegradable hydrogels to investigate human mesenchymal stem cell (hMSC) response to dynamic changes in the physical nature of the cellular microenvironment. Specifically, gradients in elasticity in the z-dimension are introduced to study cell spreading and morphology as a function of network density (Chapter VI); two-photon irradiation induced erosion is employed to study the dynamic cell response to changes in local adhesivity of hydrogel surfaces (Chapter VII); and dynamic changes in substrate elasticity is used to study the differentiation plasticity of hMSCs in response to mechanical signals (Chapter VIII). Chapter IX exploits the rapid erosion of step polymerized, photodegradable hydrogels to release proteins during cell culture. Namely, microspheres are fabricated to release nanoliter volumes of trophic factors in the presence of cells with spatial and temporal control (Chapter IX). Chapters X-XI demonstrate the ability to engineer unique materials based on the quantitative understanding of light-induced property changes in photoresponsive hydrogels. In Chapter X, enzyme-responsive, photodegradable gels are exploited as three-dimensional culture templates for the defined culture, recovery, and analysis of stem cell populations (Chapter X). In Chapter XI, the characterization and

understanding of photodegradation is exploited to generate thin film hydrogels for the selective capture and release of circulating tumor cells as a cancer diagnostic tool. Finally, Chapter XII summarizes the progress in the development and application of photoresponsive hydrogels from this thesis work and presents future avenues for the utilization of these materials in biomedical applications.

Spatiotemporal control of the cell microenvironment

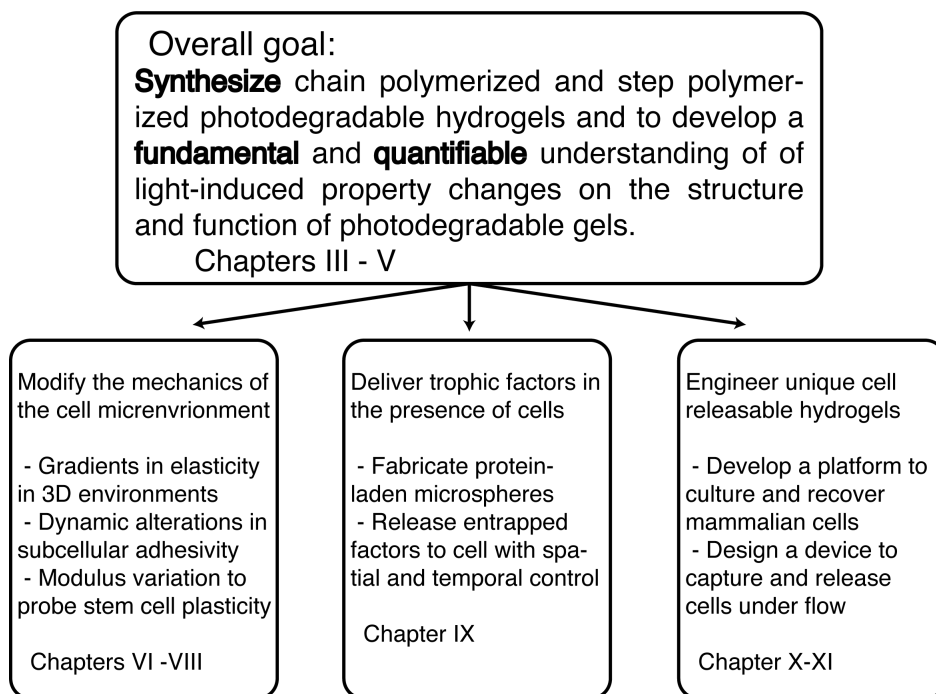


Figure 1.9 Photodegradable hydrogels for spatiotemporal control of the cell microenvironment thesis organization. This thesis focuses on the development of photodegradable hydrogels that enable user-defined control over the mechanics and biochemical nature of the cell microenvironment. The general approach is to develop a fundamental and quantifiable understanding of light-induced property changes on the structure and function of photodegradable gels through characterization and modeling. Using this knowledge, photodegradable hydrogels will be employed to probe the cellular response to dynamic mechanical signals, to direct and assay cell function through the spatiotemporally controlled release of trophic factors, and to engineer unique materials for the culture and capture of mammalian cells that enable subsequent cell release.

1.6 References

1. Jaiswal, N., Haynesworth, S., Caplan, A. & Bruder, S. Osteogenic differentiation of

- purified, culture-expanded human mesenchymal stem cells in vitro. *J Cell Biochem* **64**, 295–312 (1997).
2. Schnaper, H. *et al.* Type-Iv Collagenase(S) and Timps Modulate Endothelial-Cell Morphogenesis in-Vitro. *J. Cell. Physiol.* **156**, 235–246 (1993).
 3. Engler, A. J., Sen, S., Sweeney, H. L. & Discher, D. E. Matrix elasticity directs stem cell lineage specification. *Cell* **126**, 677–689 (2006).
 4. Engler, A. J., Rehfeldt, F., Sen, S. & Discher, D. E. Microtissue elasticity: Measurements by atomic force microscopy and its influence on cell differentiation. *Method Cell Biol* **83**, 521 (2007).
 5. Singhvi, R. *et al.* Engineering Cell-Shape and Function. *Science* **264**, 696–698 (1994).
 6. Chen, C. S. Geometric Control of Cell Life and Death. *Science* **276**, 1425–1428 (1997).
 7. Petersen, O. W., Rønnov-Jessen, L., Howlett, A. R. & Bissell, M. J. Interaction with basement membrane serves to rapidly distinguish growth and differentiation pattern of normal and malignant human breast epithelial cells. *P Natl Acad Sci Usa* **89**, 9064–9068 (1992).
 8. Tanaka, H. *et al.* Chondrogenic differentiation of murine embryonic stem cells: Effects of culture conditions and dexamethasone. *J Cell Biochem* **93**, 454–462 (2004).
 9. Birgersdotter, A., Sandberg, R. & Ernberg, I. Gene expression perturbation in vitro - A growing case for three-dimensional (3D) culture systems. *Semin Cancer Biol* **15**, 405–412 (2005).
 10. Zhang, S., Zhao, X. & Spirio, L. PuraMatrix: Self-assembling peptide nanofiber scaffolds. *Scaffolding in tissue engineering* 217–238 (2005).
 11. Gieni, R. S. & Hendzel, M. J. Mechanotransduction from the ECM to the genome: Are the pieces now in place? *J Cell Biochem* **104**, 1964–1987 (2008).
 12. Ashe, H. & Briscoe, J. The interpretation of morphogen gradients. *Development* **133**, 385–394 (2006).
 13. Le Beyec, J. *et al.* Cell shape regulates global histone acetylation in human mammary epithelial cells. *Exp Cell Res* **313**, 3066–3075 (2007).
 14. Kilian, K. A., Bugarija, B., Lahn, B. T. & Mrksich, M. Geometric cues for directing the differentiation of mesenchymal stem cells. *P Natl Acad Sci Usa* **107**, 4872–4877 (2010).
 15. Shea, L., Smiley, E., Bonadio, J. & Mooney, D. DNA delivery from polymer matrices for tissue engineering. *Nat Biotechnol* **17**, 551–554 (1999).

16. Levenberg, S. *et al.* Differentiation of human embryonic stem cells on three-dimensional polymer scaffolds. *P Natl Acad Sci Usa* **100**, 12741–12746 (2003).
17. Yim, E. & Leong, K. Proliferation and differentiation of human embryonic germ cell derivatives in bioactive polymeric fibrous scaffold. *J Biomat Sci-Polym E* **16**, 1193–1217 (2005).
18. Semino, C., Merok, J., Crane, G., Panagiotakos, G. & Zhang, S. Functional differentiation of hepatocyte-like spheroid structures from putative liver progenitor cells in three-dimensional peptide scaffolds. *Differentiation* **71**, 262–270 (2003).
19. Silva, G. A. *et al.* Selective differentiation of neural progenitor cells by high-epitope density nanofibers. *Science* **303**, 1352–1355 (2004).
20. Peppas, N., Hilt, J., Khademhosseini, A. & Langer, R. Hydrogels in biology and medicine: From molecular principles to bionanotechnology. *Adv Mater* **18**, 1345–1360 (2006).
21. Saha, K., Pollock, J. F., Schaffer, D. V. & Healy, K. E. Designing synthetic materials to control stem cell phenotype. *Curr Opin Chem Biol* **11**, 381–387 (2007).
22. Nguyen, K. T. & West, J. L. Photopolymerizable hydrogels for tissue engineering applications. *Biomaterials* **23**, 4307–4314 (2002).
23. Lutolf, M. P. & Hubbell, J. A. Synthetic biomaterials as instructive extracellular microenvironments for morphogenesis in tissue engineering. *Nat Biotechnol* **23**, 47–55 (2005).
24. Lee, K. Y. & Mooney, D. J. Hydrogels for Tissue Engineering. *Chem Rev* **101**, 1869–1880 (2001).
25. Slaughter, B. V., Khurshid, S. S., Fisher, O. Z., Khademhosseini, A. & Peppas, N. A. Hydrogels in Regenerative Medicine. *Adv Mater* **21**, 3307–3329 (2009).
26. Butcher, J. & Nerem, R. Porcine aortic valve interstitial cells in three-dimensional culture: Comparison of phenotype with aortic smooth muscle cells. *J Heart Valve Dis* **13**, 478–485 (2004).
27. Eyrich, D. *et al.* Long-term stable fibrin gels for cartilage engineering. *Biomaterials* **28**, 55–65 (2007).
28. Masters, K., Shah, D., Walker, G., Leinwand, L. & Anseth, K. Designing scaffolds for valvular interstitial cells: Cell adhesion and function on naturally derived materials. *J Biomed Mater Res A* **71A**, 172–180 (2004).

29. Chung, C. & Burdick, J. A. Influence of three-dimensional hyaluronic Acid microenvironments on mesenchymal stem cell chondrogenesis. *Tissue engineering Part A* **15**, 243–254 (2009).
30. Azab, A. *et al.* Crosslinked chitosan implants as potential degradable devices for brachytherapy: In vitro and in vivo analysis. *J Control Release* **111**, 281–289 (2006).
31. Barralet, J. *et al.* Comparison of bone marrow cell growth on 2D and 3D alginate hydrogels. *J Mater Sci-Mater M* **16**, 515–519 (2005).
32. Huebsch, N. *et al.* Harnessing traction-mediated manipulation of the cell/matrix interface to control stem-cell fate. *Nat Mater* **9**, 518–526 (2010).
33. Augst, A. *et al.* Effects of chondrogenic and osteogenic regulatory factors on composite constructs grown using human mesenchymal stem cells, silk scaffolds and bioreactors. *Journal of The Royal Society Interface* **5**, 929–939 (2008).
34. Dawson, E., Mapili, G., Erickson, K., Taqvi, S. & Roy, K. Biomaterials for stem cell differentiation. *Adv Drug Deliv Rev* **60**, 215–228 (2008).
35. Cushing, M. C. & Anseth, K. S. Hydrogel cell cultures. *Science* **316**, 1133–1134 (2007).
36. Sawhney, A. S., Pathak, C. P. & Hubbell, J. A. Bioerodible hydrogels based on photopolymerized poly(ethylene glycol)-co-poly(.alpha.-hydroxy acid) diacrylate macromers. *Macromolecules* **26**, 581–587 (1993).
37. Martens, P. & Anseth, K. Characterization of hydrogels formed from acrylate modified poly(vinyl alcohol) macromers. *Polymer* **41**, 7715–7722 (2000).
38. Chirila, T. *et al.* Poly(2-Hydroxyethyl Methacrylate) Sponges as Implant Materials - In vivo and In vitro Evaluation of Cellular Invasion. *Biomaterials* **14**, 26–38 (1993).
39. Bryant, S. J. & Anseth, K. S. Hydrogel properties influence ECM production by chondrocytes photoencapsulated in poly(ethylene glycol) hydrogels. *J Biomed Mater Res A* **59**, 63–72 (2002).
40. Shu, X. Z., Ahmad, S., Liu, Y. & Prestwich, G. D. Synthesis and evaluation of injectable, in situ crosslinkable synthetic extracellular matrices for tissue engineering. *J Biomed Mater Res A* **79A**, 902–912 (2006).
41. West, J. L. Bioactive hydrogels: Mimicking the ECM with synthetic materials. *Scaffolding in tissue engineering* (2005).
42. Daley, W. P., Peters, S. B. & Larsen, M. Extracellular matrix dynamics in development and regenerative medicine. *J Cell Sci* **121**, 255–264 (2008).

43. Griffith, L. G. & Naughton, G. Tissue Engineering--Current Challenges and Expanding Opportunities. *Science* **295**, 1009–1014 (2002).
44. Lee, S.-H., Moon, J. J. & West, J. L. Three-dimensional micropatterning of bioactive hydrogels via two-photon laser scanning photolithography for guided 3D cell migration. *Biomaterials* **29**, 2962–2968 (2008).
45. Salinas, C. N. & Anseth, K. S. The enhancement of chondrogenic differentiation of human mesenchymal stem cells by enzymatically regulated RGD functionalities. *Biomaterials* **29**, 2370–2377 (2008).
46. Mann, B. & West, J. Cell adhesion peptides alter smooth muscle cell adhesion, proliferation, migration, and matrix protein synthesis on modified surfaces and in polymer scaffolds. *J Biomed Mater Res A* **60**, 86–93 (2002).
47. West, J. & Hubbell, J. Polymeric biomaterials with degradation sites for proteases involved in cell migration. *Macromolecules* **32**, 241–244 (1999).
48. Wang, N., Butler, J. & Ingber, D. Mechanotransduction Across the Cell-Surface and Through the Cytoskeleton. *Science* **260**, 1124–1127 (1993).
49. Giancotti, F. & Ruoslahti, E. Integrin signaling. *Science* **285**, 1028–1032 (1999).
50. Howe, A., Aplin, A., Alahari, S. & Juliano, R. Integrin signaling and cell growth control. *Curr Opin Cell Biol* **10**, 220–231 (1998).
51. Weber, L. M., Hayda, K. N. & Anseth, K. S. Cell-Matrix Interactions Improve beta-Cell Survival and Insulin Secretion in Three-Dimensional Culture. *Tissue engineering Part A* **14**, 1959–1968 (2008).
52. Ruoslahti, E. RGD and other recognition sequences for integrins. *Annu Rev Cell Dev Bi* **12**, 697–715 (1996).
53. Nuttelman, C., Tripodi, M. & Anseth, K. Synthetic hydrogel niches that promote hMSC viability. *Matrix Biol* **24**, 208–218 (2005).
54. Park, K., Na, K. & Chung, H. Enhancement of the adhesion of fibroblasts by peptide containing an Arg-Gly-Asp sequence with poly(ethylene glycol) into a thermo-reversible hydrogel as a synthetic extracellular matrix. *Biotechnol Lett* **27**, 227–231 (2005).
55. Patel, P., Gobin, A., West, J. & Patrick, C. Poly(ethylene glycol) hydrogel system supports preadipocyte viability, adhesion, and proliferation. *Tissue Eng* **11**, 1498–1505 (2005).
56. Massia, S. & Hubbell, J. An Rgd Spacing of 440nm Is Sufficient for Integrin Alpha-v-Beta-3-Mediated Fibroblast Spreading and 140nm for Focal Contact and Stress Fiber

- Formation. *J Cell Biol* **114**, 1089–1100 (1991).
57. Gobin, A. & West, J. Cell migration through defined, synthetic extracellular matrix analogues. *Faseb J* **16**, 751 (2002).
 58. Khire, V. S., Benoit, D. S. W., Anseth, K. S. & Bowman, C. N. Ultrathin gradient films using thiol-ene polymerizations. *J Polym Sci Pol Chem* **44**, 7027–7039 (2006).
 59. Rydholm, A. E., Held, N. L., Benoit, D. S. W., Bowman, C. N. & Anseth, K. S. Modifying network chemistry in thiol-acrylate photopolymers through postpolymerization functionalization to control cell-material interactions. *J Biomed Mater Res A* **86A**, 23–30 (2008).
 60. Salinas, C. N. & Anseth, K. S. Mixed mode thiol-acrylate photopolymerizations for the synthesis of PEG-peptide hydrogels. *Macromolecules* **41**, 6019–6026 (2008).
 61. Sekiya, I., Vuoristo, J., Larson, B. & Prockop, D. In vitro cartilage formation by human adult stem cells from bone marrow stroma defines the sequence of cellular and molecular events during chondrogenesis. *P Natl Acad Sci Usa* **99**, 4397–4402 (2002).
 62. Ramirez, F. & Rifkin, D. Cell signaling events: a view from the matrix. *Matrix Biol* **22**, 101–107 (2003).
 63. Chen, R. & Mooney, D. Polymeric growth factor delivery strategies for tissue engineering. *Pharm Res-Dord* **20**, 1103–1112 (2003).
 64. Yamaguchi, N. & Kiick, K. Polysaccharide-poly(ethylene glycol) star copolymer as a scaffold for the production of bioactive hydrogels. *Biomacromolecules* **6**, 1921–1930 (2005).
 65. Willerth, S. M. *et al.* Rationally designed peptides for controlled release of nerve growth factor from fibrin matrices. *J Biomed Mater Res A* **80A**, 13–23 (2007).
 66. Zisch, A. *et al.* Cell-demanded release of VEGF from synthetic, biointeractive cell-ingrowth matrices for vascularized tissue growth. *Faseb J* **17**, 2260 (2003).
 67. Raeber, G. P., Lutolf, M. P. & Hubbell, J. A. Mechanisms of 3-D migration and matrix remodeling of fibroblasts within artificial ECMs. *Acta Biomater* **3**, 615–629 (2007).
 68. Mahoney, M. & Anseth, K. Three-dimensional growth and function of neural tissue in degradable polyethylene glycol hydrogels. *Biomaterials* **27**, 2265–2274 (2006).
 69. Metters, A., Anseth, K. & Bowman, C. Fundamental studies of a novel, biodegradable PEG-b-PLA hydrogel. *Polymer* **41**, 3993–4004 (2000).
 70. Nuttelman, C. R., Kloxin, A. M. & Anseth, K. S. Temporal changes in peg hydrogel

- structure influence human mesenchymal stem cell proliferation and matrix mineralization. *Adv. Exp. Med. Biol.* **585**, 135–149 (2006).
71. Lutolf, M. *et al.* Synthetic matrix metalloproteinase-sensitive hydrogels for the conduction of tissue regeneration: Engineering cell-invasion characteristics. *P Natl Acad Sci Usa* **100**, 5413–5418 (2003).
 72. Hartgerink, J. D., Beniash, E. & Stupp, S. I. Self-Assembly and Mineralization of Peptide-Amphiphile Nanofibers. *Science* **294**, 1684–1688 (2001).
 73. Pålsson, B. & Bhatia, S. N. *Tissue engineering*. (Pearson Prentice Hall: Upper Saddle River, NJ, 2004).
 74. Deforest, C. A., Polizzotti, B. D. & Anseth, K. S. Sequential click reactions for synthesizing and patterning three-dimensional cell microenvironments. *Nat Mater* **8**, 659–664 (2009).
 75. Kloxin, A. M., Kasko, A. M., Salinas, C. N. & Anseth, K. S. Photodegradable hydrogels for dynamic tuning of physical and chemical properties. *Science* **324**, 59–63 (2009).
 76. Langer, R. & Tirrell, D. A. Designing materials for biology and medicine. *Nature* **428**, 487–492 (2004).
 77. Ratner, B. & Bryant, S. Biomaterials: Where we have been and where we are going. *Annu Rev Biomed Eng* **6**, 41–75 (2004).
 78. Martens, P., Bryant, S. & Anseth, K. Tailoring the degradation of hydrogels formed from multivinyl poly(ethylene glycol) and poly(vinyl alcohol) macromers for cartilage tissue engineering. *Biomacromolecules* **4**, 283–292 (2003).
 79. Fairbanks, B. D. *et al.* A Versatile Synthetic Extracellular Matrix Mimic via Thiol-Norbornene Photopolymerization. *Adv Mater* **21**, 5005–5010 (2009).
 80. Odian, G. *Principles of Polymerization*. (John Wiley & Sons, Inc.: Hoboken, NJ, 2004).
 81. Hoyle, C. E. & Bowman, C. N. Thiol-Ene Click Chemistry. *Angew Chem Int Edit* **49**, 1540–1573 (2010).
 82. Anseth, K.S., Wang, C. & Bowman, C. Reaction Behavior and Kinetic Constants for Photopolymerizations of Multi(Meth)Acrylate Monomers. *Polymer* **35**, 3243–3250 (1994).
 83. Quick, D. J. & Anseth, K. S. DNA delivery from photocrosslinked PEG hydrogels: encapsulation efficiency, release profiles, and DNA quality. *Journal of controlled release* **96**, 341–351 (2004).
 84. McCall, J. D., Lin, C.-C. & Anseth, K. S. Affinity peptides protect transforming growth

- factor beta during encapsulation in poly(ethylene glycol) hydrogels. *Biomacromolecules* **12**, 1051–1057 (2011).
85. Lin-Gibson, S., Jones, R., Washburn, N. & Horkay, F. Structure-property relationships of photopolymerizable poly(ethylene glycol) dimethacrylate hydrogels. *Macromolecules* **38**, 2897–2902 (2005).
 86. Matsunaga, T., Sakai, T., Akagi, Y., Chung, U.-I. & Shibayama, M. Structure Characterization of Tetra-PEG Gel by Small-Angle Neutron Scattering. *Macromolecules* **42**, 1344–1351 (2009).
 87. Sakai, T. *et al.* Design and fabrication of a high-strength hydrogel with ideally homogeneous network structure from tetrahedron-like macromonomers. *Macromolecules* **41**, 5379–5384 (2008).
 88. Malkoch, M. *et al.* Synthesis of well-defined hydrogel networks using Click chemistry. *Chem Commun* 2774–2776 (2006).
 89. Elbert, D., Pratt, AB, Lutolf, M., Halstenberg, S. & Hubbell, J. Protein delivery from materials formed by self-selective conjugate addition reactions. *J Control Release* **76**, 11–25 (2001).
 90. Johnson, J. A., Finn, M. G., Koberstein, J. T. & Turro, N. J. Synthesis of photocleavable linear macromonomers by ATRP and star macromonomers by a tandem ATRP-click reaction: Precursors to photodegradable model networks. *Macromolecules* **40**, 3589–3598 (2007).
 91. Johnson, J. A., Baskin, J. M., Bertozzi, C. R., Koberstein, J. T. & Turro, N. J. Copper-free click chemistry for the in situ crosslinking of photodegradable star polymers. *Chem Commun* 3064–3066 (2008).
 92. Yang, T. *et al.* Characterization of Well-Defined Poly(ethylene glycol) Hydrogels Prepared by Thiol-ene Chemistry. *J Polym Sci Pol Chem* **49**, 4044–4054 (2011).
 93. Flory, P. J. *Principles of Polymer Chemistry*. (Cornell University Press: Ithaca, NY, 1953).
 94. Bryant, S.J. & Anseth, K.S. Photopolymerization of hydrogel scaffolds. *Scaffolding in Tissue Engineering* 1–21 (2006).
 95. Anseth, K.S., Bowman, C.N. & BrannonPeppas, L. Mechanical properties of hydrogels and their experimental determination. *Biomaterials* **17**, 1647–1657 (1996).
 96. Metters, A., Bowman, C. & Anseth, K.S. Verification of scaling laws for degrading PLA-b-PEG-b-PLA hydrogels. *Aiche J* **47**, 1432–1437 (2001).
 97. Mason, M., Metters, A., Bowman, C. & Anseth, K. Predicting controlled-release

- behavior of degradable PLA-b-PEG-b-PLA hydrogels. *Macromolecules* **34**, 4630–4635 (2001).
98. Flory, P. & Rehner, J. Statistical mechanics of cross-linked polymer networks I Rubberlike elasticity. *J Chem Phys* **11**, 512–520 (1943).
 99. Nicodemus, G. D. & Bryant, S. J. Cell encapsulation in biodegradable hydrogels for tissue engineering applications. *Tissue Engineering Part B: Reviews* **14**, 149–165 (2008).
 100. Metters, A., Bowman, C. & Anseth, K. A statistical kinetic model for the bulk degradation of PLA-b-PEG-b-PLA hydrogel networks. *J Phys Chem B* **104**, 7043–7049 (2000).
 101. Reddy, S., Anseth, K. & Bowman, C. Modeling of network degradation in mixed step-chain growth polymerizations. *Polymer* **46**, 4212–4222 (2005).
 102. Rydholm, A. E., Reddy, S. K., Anseth, K. S. & Bowman, C. N. Development and Characterization of Degradable Thiol-Allyl Ether Photopolymers. *Polymer* **48**, 4589–4600 (2007).
 103. Johnson, J. A., Turro, N. J., Koberstein, J. T. & Mark, J. E. Some hydrogels having novel molecular structures. *Prog Polym Sci* **35**, 332–337 (2010).
 104. Burdick, J. A. & Anseth, K. S. Photoencapsulation of osteoblasts in injectable RGD-modified PEG hydrogels for bone tissue engineering. *Biomaterials* **23**, 4315–4323 (2002).
 105. Hahn, M. S., Miller, J. S. & West, J. L. Three-Dimensional Biochemical and Biomechanical Patterning of Hydrogels for Guiding Cell Behavior. *Adv Mater* **18**, 2679–2684 (2006).
 106. Luo, Y. & Shoichet, M. S. A photolabile hydrogel for guided three-dimensional cell growth and migration. *Nat Mater* **3**, 249–253 (2004).
 107. Polizzotti, B. D., Fairbanks, B. D. & Anseth, K. S. Three-dimensional biochemical patterning of click-based composite hydrogels via thiolene photopolymerization. *Biomacromolecules* **9**, 1084–1087 (2008).
 108. Wylie, R. G. *et al.* Spatially controlled simultaneous patterning of multiple growth factors in three-dimensional hydrogels. *Nat Mater* **10**, 799–806 (2011).
 109. Khetan, S., Katz, J. S. & Burdick, J. A. Sequential crosslinking to control cellular spreading in 3-dimensional hydrogels. *Soft Matter* **5**, 1601–1606 (2009).
 110. Khetan, S. & Burdick, J. A. Patterning network structure to spatially control cellular

- remodeling and stem cell fate within 3-dimensional hydrogels. *Biomaterials* **31**, 8228–8234 (2010).
111. Guvendiren, M. & Burdick, J. A. Stiffening hydrogels to probe short- and long-term cellular responses to dynamic mechanics. *Nat Commun* **3**, – (2012).
 112. Anseth, K. S. *et al.* In situ forming degradable networks and their application in tissue engineering and drug delivery. *Journal of Controlled Release* **78**, 199–209 (2002).
 113. Rydholm, A. E., Reddy, S. K., Anseth, K. S. & Bowman, C. N. Controlling network structure in degradable thiol-acrylate biomaterials to tune mass loss behavior. *Biomacromolecules* **7**, 2827–2836 (2006).
 114. Bryant, S. & Anseth, K. Controlling the spatial distribution of ECM components in degradable PEG hydrogels for tissue engineering cartilage. *J Biomed Mater Res A* **64A**, 70–79 (2003).
 115. Benoit, D. S. W., Durney, A. R. & Anseth, K. S. Manipulations in hydrogel degradation behavior enhance osteoblast function and mineralized tissue formation. *Tissue Eng* **12**, 1663–1673 (2006).
 116. Lutolf, M., Raeber, G., Zisch, A., Tirelli, N. & Hubbell, J. Cell-responsive synthetic hydrogels. *Adv Mater* **15**, 888 (2003).
 117. Anderson, S. B., Lin, C.-C., Kuntzler, D. V. & Anseth, K. S. The performance of human mesenchymal stem cells encapsulated in cell-degradable polymer-peptide hydrogels. *Biomaterials* **32**, 3564–3574 (2011).
 118. Rice, M. A., Sanchez-Adams, J. & Anseth, K. S. Exogenously Triggered, Enzymatic Degradation of Photopolymerized Hydrogels with Polycaprolactone Subunits: Experimental Observation and Modeling of Mass Loss Behavior. *Biomacromolecules* **7**, 1968–1975 (2006).
 119. Jo, Y. S. *et al.* Biomimetic PEG hydrogels crosslinked with minimal plasmin-sensitive tri-amino acid peptides. *J Biomed Mater Res A* **93A**, 870–877 (2010).
 120. Patterson, J. & Hubbell, J. A. Enhanced proteolytic degradation of molecularly engineered PEG hydrogels in response to MMP-1 and MMP-2. *Biomaterials* **31**, 7836–7845 (2010).
 121. Andreopoulos, F. *et al.* Photoscissable hydrogel synthesis via rapid photopolymerization of novel PEG-based polymers in the absence of photoinitiators. *J Am Chem Soc* **118**, 6235–6240 (1996).
 122. Zheng, Y. *et al.* PEG-based hydrogel synthesis via the photodimerization of anthracene groups. *Macromolecules* **35**, 5228–5234 (2002).

123. Frey, M. T. & Wang, Y.-L. A photo-modulatable material for probing cellular responses to substrate rigidity. *Soft Matter* **5**, 1918–1924 (2009).
124. Zhao, Y. *et al.* New caged coumarin fluorophores with extraordinary uncaging cross sections suitable for biological imaging applications. *J Am Chem Soc* **126**, 4653–4663 (2004).
125. Holmes, C. & Jones, D. Reagents for Combinatorial Organic-Synthesis - Development of a New O-Nitrobenzyl Photolabile Linker for Solid-Phase Synthesis. *J Org Chem* **60**, 2318–2319 (1995).
126. Holmes, C. Model studies for new o-nitrobenzyl photolabile linkers: Substituent effects on the rates of photochemical cleavage. *J Org Chem* **62**, 2370–2380 (1997).
127. Whitehouse, D., Savinov, S. & Austin, D. An improved synthesis and selective coupling of a hydroxy based photolabile linker for solid phase organic synthesis. *Tetrahedron Lett* **38**, 7851–7852 (1997).
128. Deiters, A. Principles and Applications of the Photochemical Control of Cellular Processes. *Chembiochem* **11**, 47–53 (2010).
129. Ohmuro-Matsuyama, Y. & Tatsu, Y. Photocontrolled cell adhesion on a surface functionalized with a caged arginine-glycine-aspartate peptide. *Angew Chem Int Edit* **47**, 7527–7529 (2008).
130. Kaneko, S. *et al.* Photocontrol of cell adhesion on amino-bearing surfaces by reversible conjugation of poly(ethylene glycol) via a photocleavable linker. *Phys Chem Chem Phys* **13**, 4051–4059 (2011).
131. Kloxin, A. M., Benton, J. A. & Anseth, K. S. In situ elasticity modulation with dynamic substrates to direct cell phenotype. *Biomaterials* **31**, 1–8 (2010).

CHAPTER II

THESIS OBJECTIVES

2.1 Overview

Hydrogels are increasingly employed as materials in microfabricated devices,¹ as vehicles for drug delivery,^{2,3} as well as mimics of the extracellular matrix for defined cell culture.^{4,5} For proper culture of mammalian cells, sophisticated control over hydrogel properties in both three-dimensional (3D) space and time is often required to understand the complex and dynamic relationship between the biochemical and mechanical properties of the extracellular matrix and cell function.⁶ Specifically, four-dimensional (4D, 3D space and time) control of hydrogel properties is hypothesized to facilitate proper morphogenesis of tissue structures *in vitro* and *in vivo* and to enable investigation of dynamic physiology and pathophysiology. Several hydrogel systems have been developed that afford dynamic control over material properties in the presence of cells through hydrolytic^{7,8} or enzymatic⁹⁻¹¹ degradation. In these systems, property control is either pre-defined or cellularly dictated, which limits full 4D control of gel properties. As such, advancements and improvements in cell culture matrices are needed to present both physical and biochemical signals dynamically to understand which signals are critical to recapitulate for regenerative medicine applications and to better understand biological systems.

Photoresponsive materials have recently emerged that exploit the unique properties of light as a chemical reagent to initiate property changes wherever and whenever light is delivered.¹²⁻¹⁵ Specifically, photochemical reactions have enabled the fabrication of materials in the presence of cells with spatial and temporal control¹¹ and subsequent modification.¹⁶ Thus, the overall goal of this thesis research is to develop and characterize photoresponsive hydrogels whose properties can be tuned with light and to employ this platform to investigate the influence of dynamic signals from the extracellular matrix on cell function.

Specifically, this thesis focuses on the fabrication of photoresponsive hydrogels from a macromolecular precursor that contains *o*-nitrobenzyl ether moieties, which can undergo an irreversible cleavage upon exposure to appropriate wavelengths of light. We hypothesize that these hydrogel materials will enable well-defined and precise control over hydrogel properties exogenously in both 3D space and time. Further, we hypothesize that these hydrogels will allow dynamic changes in the extracellular environment on which cells are cultured and enable unique experiments to investigate how cells respond to spatiotemporally varying signals in their microenvironment. The approach of this thesis is to develop a fundamental and quantifiable understanding of how light-induced changes control the structure and function of hydrogel cell culture matrices through both experimental characterization and modeling. From this detailed understanding, we then seek to make predictable and defined changes in the cellular microenvironment to gain unique insight as to how cells sense these extracellular changes and how this influences some of their key functional properties.

With this approach in mind and to test these hypotheses, the specific objectives of this thesis research are to

- 1. Synthesize both chain and step polymerized hydrogels using a divinyl, poly(ethylene glycol)-based, photodegradable crosslinker. Experimentally measure light-induced property changes and compare these data to a statistical-kinetic model of photodegradation;**
- 2. Explore the relationship between dynamic changes in material mechanics and human mesenchymal stem cell function in both 2D and 3D culture;**
- 3. Exploit the rapidly eroding, step polymerized, photodegradable hydrogels to deliver trophic factors to cells during culture; and**
- 4. Harness the well-defined and spatially precise degradation of photodegradable hydrogels for the selective culture or capture and subsequent release of individual mammalian cells.**

The *in vivo* cellular microenvironment is a complex and dynamic milieu of physical and chemical signals, e.g., cell-matrix interactions, cell-cell junctions, and growth factor gradients, that ultimately direct cell functions, such as proliferation, migration, differentiation, and extracellular matrix remodeling.⁴ To enable biologically-relevant assessment of cell physiology and pathophysiology *in vitro*, it is critical that cell culture systems recapitulate this dynamic presentation of cues that occurs in the native extracellular matrix. Especially enabling are materials that allow user-defined, real-time changes in the physical and chemical properties of a cell culture platform in both 3D space and time to study precisely the influence of individual cues on cell function.

Toward the development of materials with real-time, user-defined and quantifiable changes in properties, photodegradable hydrogels and their precursors are synthesized (Objective 1, Chapter III and V). A diacrylate, PEG-based, photodegradable crosslinking monomer, which

includes the photolabile moiety *o*-nitrobenzyl ether, is synthesized from which photodegradable hydrogels are created *via* redox-initiated free radical polymerization or Michael-addition polymerization. To fully characterize and understand the photo- and polymer physics that enable degradation of these networks, photodegradable hydrogels are irradiated with UV or visible light and a statistical-kinetic model of photodegradation is developed to compare with experimental results (Chapter IV).

Spatial and temporal control over the physical structure of chain polymerized hydrogels is demonstrated with both one-photon and two-photon irradiation and employed to investigate cellular responses to dynamic changes in the mechanics and geometry of the extracellular matrix (Objective 2, Chapters VI-VIII). To achieve this, we exploit the quantifiable changes in photodegradable gels afforded by the characterization in Chapters III-V to introduce defined signals during cell culture. The ability to generate gradients in modulus in the *z*-dimension of photodegradable hydrogels is used to investigate the influence of polymer density on 3D cell spreading and morphology (Chapter VI). Focused, two-photon irradiation of photodegradable hydrogels is employed to study cytoskeletal remodeling in response to dynamic changes in cell adhesion at the subcellular scale (Chapter VII). Dynamic alterations to substrate modulus are utilized to investigate mechanotransduction and differentiation plasticity of human mesenchymal stem cells in 2D (Chapter VIII).

The rapid erosion of step polymerized, photodegradable hydrogels is demonstrated and employed to release trophic factors on-demand and with spatiotemporal control to modulate the biochemical cellular microenvironment (Objective 3, Chapters IX). The step polymerized hydrogel formulation is processed uniquely into microspheres to entrap factors that can subsequently be released to cells at defined locations and points in time (Chapter IX). This

methodology is employed to both stimulate cell function through the release of TGF- β 1 and assay cell function through the release of Annexin V. Further, the release of factors is presented in both 2D and 3D cultures with full spatial control. Future work is exploring the use of these photodegradable microspheres to direct chemotaxis with released chemokines and neural precursor differentiation with released growth factors.

Based on a better understanding and characterization of photodegradable hydrogels, we engineer systems for the selective culture or capture of mammalian cells that enable their subsequent release (Objective 4, Chapter X-XI). Specifically, a step polymerized hydrogel is rationally engineered that is both enzymatically and photolytically degradable to enable three-dimensional culture and recovery of adult stem cells and neuronal precursor cells (Chapter X). Uniquely, this culture platform enables capture and further analyses of cells that is difficult, if not impossible, to achieve in traditional, synthetic, three-dimensional culture platforms. See comment above.. Similarly, a microfluidic system is developed from the chain polymerized, photodegradable gels for the selective capture and release of mammalian cells (Objective 4, Chapter XI). Thin-films of antibody-functionalized, photodegradable hydrogel are photopolymerized in microfluidic channels, which enables cell suspensions to flow over the surface of the gel and be captured selectively based on antibody-surface receptor interactions. Since the gel is photodegradable, the attached cells can be released individually or collectively as groups, owing to the spatial control over gel degradation afforded by light exposure. Finally, future directions and broader implications of these studies are discussed (Chapter XII).

2.2 References

1. Weibel, D. B., DiLuzio, W. R. & Whitesides, G. M. Microfabrication meets microbiology. *Nat Rev Microbiol* **5**, 209–218 (2007).

2. Langer, R. & Peppas, N. Advances in biomaterials, drug delivery, and bionanotechnology. *Aiche J* **49**, 2990–3006 (2003).
3. Liechty, W. B., Kryscio, D. R., Slaughter, B. V. & Peppas, N. A. Polymers for drug delivery systems. *Annu Rev Chem Biomol Eng* **1**, 149–173 (2010).
4. Lutolf, M. P. & Hubbell, J. A. Synthetic biomaterials as instructive extracellular microenvironments for morphogenesis in tissue engineering. *Nat Biotechnol* **23**, 47–55 (2005).
5. Tibbitt, M. W. & Anseth, K. S. Hydrogels as Extracellular Matrix Mimics for 3D Cell Culture. *Biotechnol Bioeng* **103**, 655–663 (2009).
6. Stevens, M. M. & George, J. H. Exploring and Engineering the Cell Surface Interface. *Science* **310**, 1135–1138 (2005).
7. Metters, A. & Hubbell, J. Network formation and degradation behavior of hydrogels formed by Michael-type addition reactions. *Biomacromolecules* **6**, 290–301 (2005).
8. Nicodemus, G. D. & Bryant, S. J. Cell encapsulation in biodegradable hydrogels for tissue engineering applications. *Tissue Engineering Part B: Reviews* **14**, 149–165 (2008).
9. Lutolf, M., Raeber, G., Zisch, A., Tirelli, N. & Hubbell, J. Cell-responsive synthetic hydrogels. *Adv Mater* **15**, 888 (2003).
10. Rice, M. A., Sanchez-Adams, J. & Anseth, K. S. Exogenously Triggered, Enzymatic Degradation of Photopolymerized Hydrogels with Polycaprolactone Subunits: Experimental Observation and Modeling of Mass Loss Behavior. *Biomacromolecules* **7**, 1968–1975 (2006).
11. Fairbanks, B. D. *et al.* A Versatile Synthetic Extracellular Matrix Mimic via Thiol-Norbornene Photopolymerization. *Adv Mater* **21**, 5005–5010 (2009).
12. Johnson, J. A., Finn, M. G., Koberstein, J. T. & Turro, N. J. Synthesis of photocleavable linear macromonomers by ATRP and star macromonomers by a tandem ATRP-click reaction: Precursors to photodegradable model networks. *Macromolecules* **40**, 3589–3598 (2007).
13. Johnson, J. A., Baskin, J. M., Bertozzi, C. R., Koberstein, J. T. & Turro, N. J. Copper-free click chemistry for the in situ crosslinking of photodegradable star polymers. *Chem Commun* 3064–3066 (2008).
14. Kloxin, A. M., Kasko, A. M., Salinas, C. N. & Anseth, K. S. Photodegradable hydrogels for dynamic tuning of physical and chemical properties. *Science* **324**, 59–63 (2009).

15. Frey, M. T. & Wang, Y.-L. A photo-modulatable material for probing cellular responses to substrate rigidity. *Soft Matter* **5**, 1918–1924 (2009).
16. Deforest, C. A., Polizzotti, B. D. & Anseth, K. S. Sequential click reactions for synthesizing and patterning three-dimensional cell microenvironments. *Nat Mater* **8**, 659–664 (2009).

CHAPTER III

SYNTHESIS OF PHOTODEGRADABLE HYDROGELS AS DYNAMICALLY TUNABLE MATERIALS FOR 2D AND 3D CELL CULTURE

As published in *Nature Protocols*, **5**, 1867-1887 (2010)

3.1 Abstract

We describe a facile procedure to create photolabile, poly(ethylene glycol)-based (PEG) hydrogels and manipulate material properties *in situ*. The cytocompatible chemistry and degradation process enable dynamic, tunable changes during 2D or 3D cell culture. The materials are created by synthesizing an *o*-nitrobenzyl ether-based photodegradable monomer that can be coupled to primary amines. Here, we provide coupling procedures to PEG-*bis*-amine to form a photodegradable crosslinker or to the fibronectin-derived peptide RGDS to form a photoreleasable tether. Hydrogels are synthesized with the photodegradable crosslinker in the presence or absence of cells. Cell-material interactions can be probed in 2D and 3D, and by spatiotemporally controlling the gel microenvironment, unique experiments can be performed to monitor cell response to changes in their niche. Degradation can be readily achieved with cytocompatible wavelengths with low intensity flood irradiation (365 to 420 nm) in minutes or with high-intensity laser irradiation (405 nm) in seconds.

3.2 Introduction

3.2.1 Background

Physiological processes are guided by interactions between cells and their extracellular matrix, and this understanding has led to a growing interest in the development of material systems for improved 3D cell culture. In particular, hydrogel systems based on both protein components (e.g., collagen and Matrigel) and highly-tunable synthetic chemistries (e.g., PEG) have evolved to address some of these needs¹⁻³. However, as advances in real-time tracking of dynamic cellular functions have emerged⁴⁻⁶, complementary approaches to alter the surrounding extracellular environment in a user-defined and highly-controlled fashion are extremely limited. Such materials systems would have the potential to significantly improve our understanding of how cells receive information from their microenvironment and the role that these dynamic processes may play in biological questions ranging from directing stem cell differentiation^{4, 5} to understanding cancer metastasis^{6, 7}. To realize this need for dynamically tunable culture systems, we recently developed an approach for *in situ* hydrogel property manipulation with light, allowing intimate control of a cell's microenvironment in both time and space⁸. These photoactive hydrogels afford unique user-defined manipulation of the biochemical and biomechanical nature of the extracellular microenvironment. The application of these photochemically tunable 3D cell culture materials is of growing interest to a diverse audience of scientists and engineers^{9, 10}. The goal of this manuscript is to provide facile protocols that make synthesis of these photolabile gels and related degradation techniques simple and accessible. This contribution includes a step-by-step protocol for synthesis of the photolabile group and photolabile monomer, which can be easily coupled to any primary amine-containing molecule. Subsequently, we provide the sequential protocol for synthesis of a photodegradable, PEG-based crosslinking monomer and photoreleasable peptide tether, allowing the synthesis and

manipulation of hydrogel crosslinking density/modulus or peptide presentation, respectively, during 2D and 3D cell culture. Lastly, we provide detailed gel synthesis and degradation protocols, focusing on the manipulation of gel structure with photolithography or focused 405 nm light and subsequent verification of structural changes with a confocal microscope. While protocols for synthesizing the photolabile group for solid phase peptide synthesis or functional group (un)caging are available in the literature¹¹⁻¹³, these protocols do not cover the details of synthesizing and degrading photolabile monomers and gels in the presence of cells. This manuscript provides a universal protocol for synthesizing photolabile gels from the ground up, and our goal is to facilitate the translation of these systems for a broad range of cell culture applications.

3.2.2 Development of the protocol

This synthetic protocol for synthesis and degradation of photolabile hydrogels under cytocompatible conditions was developed for precisely controlling the presentation of biophysical or biochemical cues within a cell's microenvironment⁸. The photolabile group, ethyl 4-(4-(1-hydroxyethyl)-2-methoxy-5-nitrophenoxy)butanoic acid, was selected as the degradable unit because of its previous use in live cell cultures.¹⁴ Further, this moiety degrades in response to long-wave UV light (≥ 365 nm), visible (up to 420 nm), and two-photon irradiation, all of which are cytocompatible^{12, 15}. Similar nitrobenzyl photolabile molecules have been used in a number of different applications.^{11, 16} These applications are growing and include the (un)caging of proteins¹⁷, reactive groups within hydrogels^{18, 19}, or adhesive ligands on culture plates^{20, 21} to promote cell signaling, process extension, or control cell attachment, respectively; controlled degradation of hydrophobic, step-growth polymer networks^{22, 23}; release of PEG from surfaces to

modulate cell attachment²⁴; and *in situ* tuning of poly(acrylamide) gel modulus during 2D cell culture²⁵. Recent work from our group⁸ demonstrates how this photolabile group can be incorporated within water-soluble macromolecular monomers to create a versatile platform that allows manipulation of the gel's physical or biochemical properties in 2D²⁶ and 3D^{8, 27}. To generate these photolabile hydrogels, a reactive monomer was synthesized from the *o*-nitrobenzylether-based photolabile group and coupled to PEG-*bis*-amine to create a photodegradable crosslinking monomer or to a cell adhesion peptide sequence, RGDS, to create photoreleasable pendant functional groups⁸. Using either the photodegradable crosslinker or the bifunctional monomer, an adaptable culture system can be fabricated that offers simultaneous manipulation and monitoring of cell-material interactions in either two or three dimensions.

3.2.3 Applications of the method

To date, these synthetic approaches have been used to create photolabile hydrogels based on poly(ethylene glycol) with or without pendant peptide functionalities. However, the chemistry is quite diverse and could be easily coupled with other macromolecules to make densely or loosely crosslinked networks, neutral or polyelectrolyte gels, or even more hydrophobic or hydrophilic material systems, to achieve a broad range of properties. Beyond peptides, functional gels containing other small molecules, proteins, or biological signals could be readily envisioned. Further, by varying the polymerization mechanism, materials could be designed with controlled structures, surface functionalization, or gradient properties. Because care was taken in the design of the monomer chemistry to insure cytocompatibility, we focus our discussion on how this protocol can be used for the creation of photodegradable or photoreleasing hydrogels for cell culture and discuss how it might be exploited to answer a

diverse array of biological questions.

As cell culture systems, the photodegradable hydrogels presented in this protocol can be used for the real-time manipulation and monitoring of single and/or multiple cells. We have applied these photolabile hydrogels to *(i)* probe the influence of microenvironment modulus and dynamic changes in stiffness on cell differentiation, *(ii)* investigate how matrix density influences cell morphology and process extension, and *(iii)* examine how the temporal presentation of ligands in a stem cell niche influences cell differentiation. There is a growing appreciation of the role of a cell's microenvironmental context in dictating how cells respond to biological cues (e.g., soluble growth factors). For example, substrate modulus has been shown to influence cell differentiation^{28, 29} and migration³⁰, but in general, these materials have had static properties and less is known about how a cell would respond to dynamic changes^{25, 31, 32} in its microenvironment. Photodegradable hydrogels afford spatiotemporal control of modulus during 2D and 3D cell culture (Figure 3.1a) and present the opportunity to conduct unique experiments. For example, valve fibroblasts were shown to activate into a wound healing phenotype on high modulus substrates, and subsequently, deactivate if the substrate modulus was lowered via photodegradation to make it soft.²⁶ This finding provides unique insight into the broader issue of fibrosis, and demonstrates how these novel material systems allow a better understanding of factors (e.g., matrix stiffness) that may be used to reverse myofibroblast activation and potentially disease progression.

The ability to spatially and temporally regulate the hydrogel's crosslinking density and modulus allows one to explore many basic questions, including how cell morphology changes in response to the local polymer density or how cells sense local changes or gradients in modulus and migrate. Such information could be beneficial to those seeking to expand or direct the

differentiation of stem cells, understand mechanisms of migration or metastasis, or even regenerate tissues. For example, human mesenchymal stem cell morphology and spreading have been controlled in 3D via controlled gel photodegradation and spatially-specific crosslinking density manipulation²⁷. This strategy could be expanded to examine the effect of crosslinking density and modulus on more complex cell functions such as differentiation, process extension and signaling, and migration in 3D. Additionally, advanced patterning techniques can be used to degrade micron-scale voids or channels around, between, or under cells for directing cell process extension, migration, or detachment (Figure 3.1b), and the resulting cell response can be imaged in real time. Triggering and monitoring a change in a specific cell-material interaction is particularly important for understanding and controlling signals within the stem cell niche (e.g., the role of structure and modulus in directing cell fate via mechanotransduction).

Cell adhesion within the microenvironment might also be probed by controlled peptide presentation using photoreleasable tethers for introduction, as well as removal of biochemical cues (Figure 3.1a). In particular, hMSC adhesion and chondrogenic differentiation were regulated within degradable PEG hydrogels when RGDS was temporally released at an appropriate time during 3D culture⁸. Such approaches can prove quite valuable for *in situ* regulation of cell adhesion in 2D or 3D. In general, we believe that these photolabile hydrogels will prove especially useful for testing hypotheses about the role of the cell environment in directing cell function. In addition to controlled presentation of peptides, this protocol can be used to create hydrogels that precisely release entrapped proteins via photodegradation³³ or cleavage of a photoreleasable tether, as has been done previously with hydrolytically³⁴ or enzymatically³⁵ materials. The advantage here is the spatiotemporal control afforded by light-based degradation, which can be used to screen the effect of different release rates on biological

function *in vitro* or tuning release rates *in situ*.

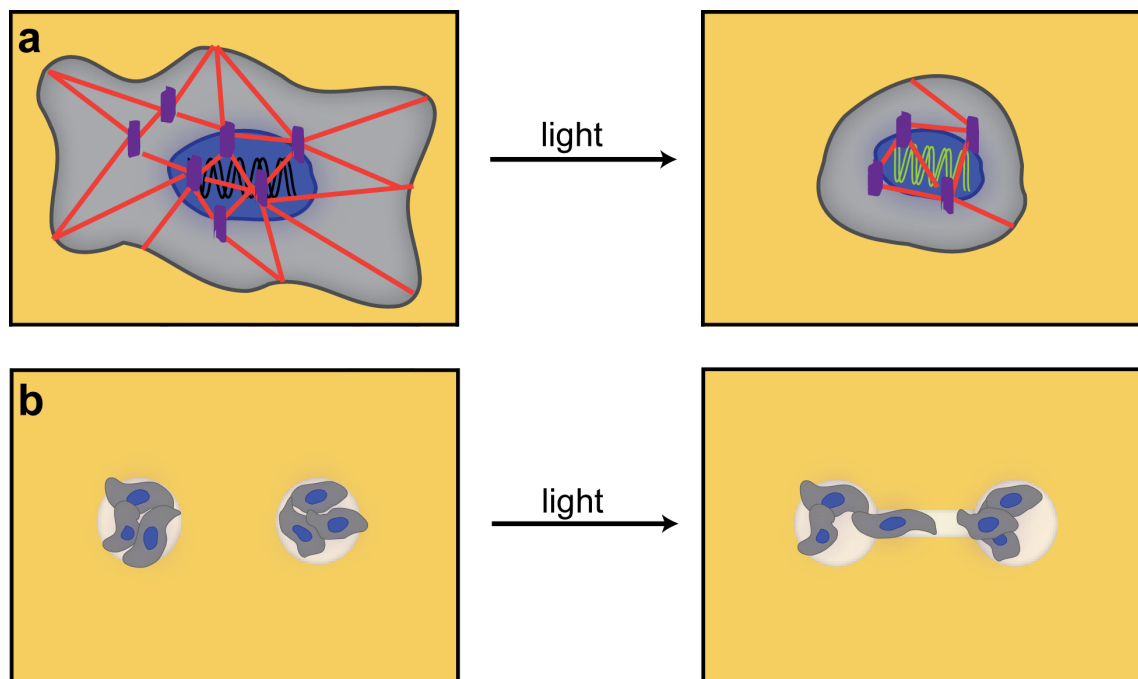


Figure 3.1 Photolabile hydrogels for cell culture. Recent work has emphasized the importance of cues from the extracellular matrix in directing cell function. Namely, the elasticity, adhesive context, geometry, and biochemical nature of the cellular microenvironment have been shown to direct cell migration, differentiation, and fate. Photolabile hydrogels are a dynamic class of cell culture materials that can be exploited to precisely and predictably alter the cellular microenvironment in both space and time. By incorporating photolabile functionalities into the gels, the user can tune dynamically the elasticity/polymer density, biochemical nature, or geometry of the cell culture platform in real time with light. **(a)** Dynamic changes in the adhesive context influence cell morphology and cytoskeletal organization. Here, light-induced changes in polymer density or ligand concentration are employed to control cell spreading and cytoskeletal organization. **(b)** Cells can be seeded within wells of photoactive hydrogels and subsequent changes to the geometry of the cellular microenvironment can be introduced with light. Here, a channel is introduced between two wells, encouraging cells to migrate out of their niche. These patterning strategies can be extended easily to tune the cellular microenvironment around encapsulated cells or to connect encapsulated cells in 3D cell culture.

4.2.4 Comparison with other methods

The protocol used for synthesis of the photolabile molecule is based on protocols originally developed by Holmes¹² and Akerblom *et al.*¹³ This photolabile molecule was then acrylated and used to form a photodegradable crosslinker and photoreleasable tether, which are

then readily polymerized to form light degradable materials. Complementary synthetic approaches to the formation of the photodegradable acrylate monomer and the photodegradable crosslinker were recently presented by Wong *et al.* with increased yield for the photodegradable acrylate³⁶.

For dynamic cell culture, some examples exist where cells are cultured on 2D surfaces and the underlying properties are manipulated. For example, electroresponsive substrates for controlled adhesive ligand presentation³⁷ and thermoresponsive substrates for controlled swelling^{38, 39} have been used to temporally regulate cell adhesion and release in pre-defined geometries. For property regulation in three-dimensions, fewer materials allow the tuning of properties in the presence of cells. Some recent advances include temporally controlled cell spreading and morphology in 3D by the addition of crosslinks with photopatterning³¹ or the removal of crosslinks with ion concentration^{32, 40}. These approaches provide alternative methods for externally-triggered manipulation of the cell microenvironment and offer varying levels of control.

For spatiotemporal property control, several photoresponsive polymer networks and gels have been developed. These systems include organic-solvent-based, photodegradable polymer networks for controlled degradation products^{22, 23}, DNA-based polymer networks with photoreactive amino acids for increasing crosslinking and modulus with light⁴¹, photoreversible hydrogels for controlled protein release with low-wavelength UV light^{42, 43}, and alginate-based hydrogels with photolabile group caged reactive groups for the spatiotemporal controlled addition of peptides^{18, 19}. While interest and effort has grown in the development of photolabile materials, few photodegradable systems have been demonstrated for property manipulation *during* cell culture. Part of this relates to the challenges of developing material systems that are

compatible with cell encapsulation and subsequent degradation mechanisms that can also be performed in the presence of cells. With respect to the latter, Frey and Wang recently demonstrated real-time modulus control by irradiation of polyacrylamide-based photodegradable hydrogels to study how real-time modulus changes influenced 3T3 cell morphology and migration in 2D²⁵. Simultaneously, acrylate-based photodegradable monomers were developed and demonstrated for both cell encapsulation and controlled degradation of the physical or chemical structure of the cell microenvironment. These materials allow for real-time property control in 2D and 3D cell culture and are the materials presented in this protocol. In addition to cell culture, Wong *et al.* recently have demonstrated use of these photodegradable monomers and a new coumarin-based photodegradable monomer for positive and negative feature generation with single- and two-photon irradiation³⁶.

3.3 Experimental

3.3.1 Monomer synthesis

In this protocol, several monomers are synthesized as precursors for making photolabile hydrogels. These monomers include (i) a base photodegradable acrylate monomer that can be coupled to primary amine containing molecules, (ii) a crosslinking macromolecular monomer for making photodegradable hydrogels, and (iii) an asymmetric monomer with a photolabile tether for releasing peptides or other molecules of interest from non-degradable gels. The synthesis and characterization of each of these will be covered.

3.3.1a Photodegradable acrylate

The base photolabile group is first synthesized, or can be purchased (EMD NovaBiochem, hydroxyethyl photolinker). The synthetic route presented here for the photolabile

group⁸ is based on several other protocols¹²⁻¹⁴ and is described in detail within this contribution for the synthesis of large, bench-scale batches. To create the photodegradable acrylate (PDA) monomer, the photolabile group is acrylated and purified to yield a small molecule monomer that cleaves in response to light and can be coupled to primary amine containing molecules, such as peptides, proteins, and PEG-*bis*-amine, for incorporating them within a hydrogel, or more generally within other polymer network. The acrylate functionality could be replaced with a methacrylate or other reactive functionality for the creation of monomers with different polymerization rates or reaction mechanisms.

3.3.1b Photodegradable crosslinker

The photodegradable crosslinking monomer is synthesized using the base PDA and PEG-*bis*-amine ($M_n \sim 3400$ g/mol, PEG3400). The carboxylic acid on the PDA is activated and coupled to the primary amine end groups of PEG-*bis*-amine using solid phase peptide synthesis (SPPS) chemistry. The resulting crosslinker is purified and can be used to create hydrogels for 2D or 3D cell culture whose modulus can be tuned or the gel eroded via light-controlled degradation. While PEG3400 is used here to create hydrogels for 2D and 3D cell culture, this crosslinker synthesis strategy could be used to create other photodegradable macromers (macromolecular monomers). For example, the PDA could be reacted with PEG-*bis*-amine of varying molecular weight or functionality (e.g., multi-arm PEG) or with other synthetic or natural-based polymers with pendant amine groups to create an array of crosslinking monomers.

3.3.1c Photoreleasable tether

The photoreleasable tether monomer is synthesized using the PDA and a peptide bound to a solid phase support (e.g., on resin). The adhesion peptide RGDS is synthesized on resin using standard SPPS techniques. The PDA is coupled to the terminal amine of the peptide on

resin following SPPS procedures. Cleavage of the peptide from resin is short (< 2 h) to avoid cleavage of the ester bond within the PDA. The resulting peptide is purified and can be used for controlling peptide presentation and cell adhesion to a non-degradable hydrogel during 2D or 3D culture. While only synthesis of the fibronectin mimic RGDS is presented here, this tether strategy could be used for controlled release of other peptides, therapeutics, or proteins with light.

3.3.2 Hydrogel synthesis

Photoactive hydrogels can be formed from the photodegradable crosslinker or the photoreleasable tether via redox-initiated free radical chain polymerization (Figure 3.2a). To fabricate photodegradable hydrogels, a macromer solution of the photodegradable crosslinker PEGdiPDA, PEG monoacrylate, and ammonium persulfate are prepared and aliquoted into individual tubes for each gel sample. To fabricate photoreleasable hydrogels, a base macromer solution of the non-degradable crosslinker PEG diacrylate (PEGDA), photoreleasable tether, and ammonium persulfate are prepared and aliquoted into individual tubes for each gel sample. Addition of tetraethylmethylenediamine (TEMED) initiates free radical chain polymerization of the macromer solution, and this polymerizing solution can be pipetted into defined molds to fabricate insoluble hydrogels of specified geometries. The initial biomechanical and biochemical properties of the photoactive hydrogels can be tuned by changing the initial composition of the macromer solution. For example, increasing the concentration of the crosslinker in the macromer solution will lead to an increase in the elasticity of the subsequently formed gel, and acrylated or methacrylated signaling peptides can be incorporated into the macromer solution to introduce biochemical signals. Further, the concentrations of ammonium persulfate and TEMED can be modified to control the time required for the macromer solution to reach complete

gelation. Other initiation schemes, such as thermal initiation or photoinitiation, can also be used, and we present the redox-initiation as a simple and robust approach for hydrogel fabrication. In general, this protocol provides the basis to fabricate photodegradable or photoreleasable hydrogels with tunable mechanical or biochemical properties, which can be formed with sample dimensions and geometries of choice.

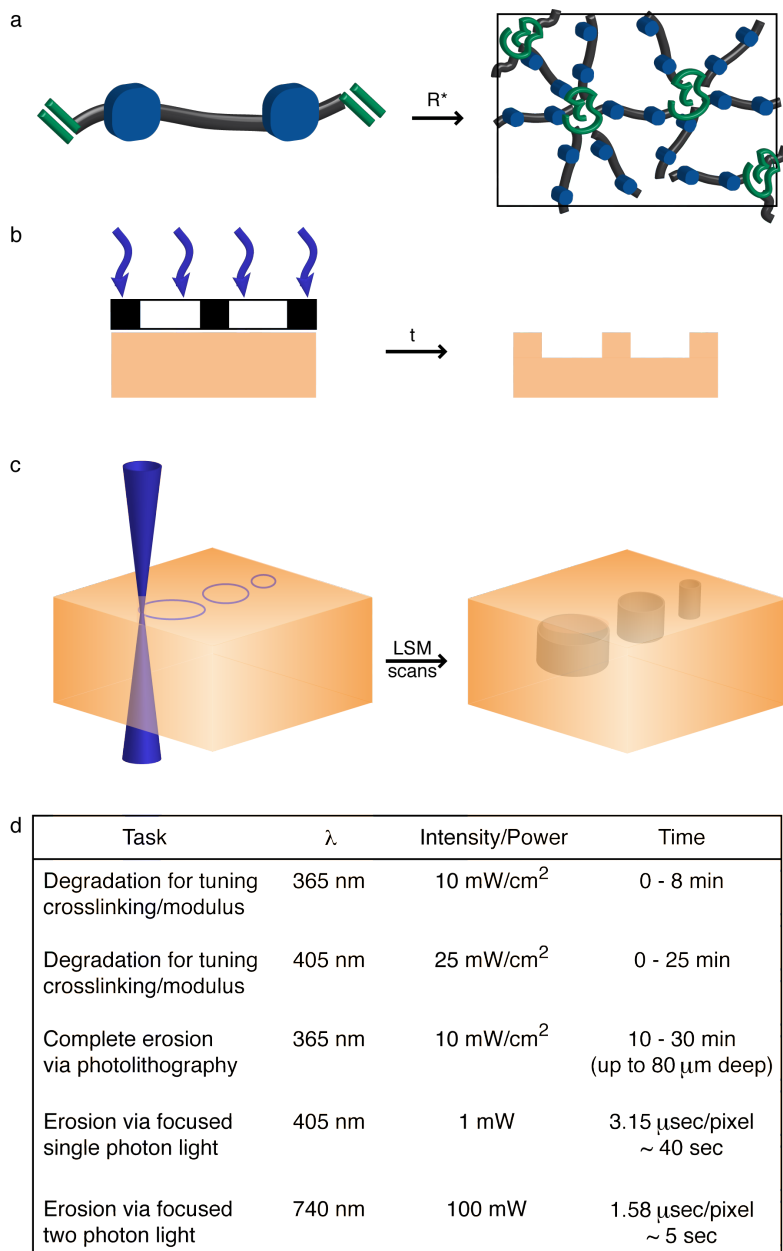


Figure 3.2 Photodegradable hydrogel synthesis and patterning. (a) Photodegradable hydrogels are formed by redox initiated, free radical chain polymerization of PEGdiPDA

crosslinking molecules, rapidly forming an insoluble hydrogel. The resultant network structure is comprised of polyacrylate kinetic chains (green) connected by PEG-based crosslinks (black) with photocleavable *o*-nitrobenzylether moieties (blue) in the backbone. **(b)** Chrome masks (black and white layer) can be placed at the surface of photodegradable gels (orange) to selectively occlude incident light (purple). With sufficient irradiation time (*t*) features are formed at the surface of PEGdiPDA gels, where the depth of feature formation depends on the duration of exposure. This photolithographic degradation can be used to generate features in the surface of a gel with minutes of irradiation time. **(c)** The focal point of a laser can be used to pattern features *within* PEGdiPDA hydrogels. Here, a laser scanning microscope (LSM) with a 405 nm laser is used to draw regions of interest (ROI) in the material. The laser focal point is rastered through the ROI and into the z-dimension to completely erode 3D features within the hydrogel in seconds. Both of these patterning strategies can be translated for spatiotemporally controlled presentation of biochemical ligands with gels containing the photoreleasable tether. **(d)** An overview of irradiation parameters for degradation and complete erosion of photodegradable hydrogels. Ultimately, these patterning approaches allow the rapid, *in situ* creation of micron-scale features in the presence or absence of cells in 2D and 3D.

3.3.3 Cell encapsulation

Cells can be encapsulated with either photolabile hydrogel formulation: *(i)* photodegradable hydrogel formed with the photodegradable crosslinking monomer or *(ii)* photoreleasing tether hydrogel formed with the photoreleasable tether monomer and a non-degradable PEG crosslinker. In this protocol, we show the case of encapsulation with the photodegradable hydrogel (option *(i)*). The base photodegradable hydrogel formulation described in the previous section is prepared, and fibronectin is added to promote cell adhesion within the gel. While we demonstrate the entrapment of fibronectin, other large extracellular matrix proteins, such as laminin, can be added and entrapped within the hydrogel to promote specific cell interactions (e.g., selective integrin binding). With this monomer solution, cells are encapsulated based on other protocols in the literature⁴⁴ but using a redox initiation system instead of a light-based initiation system: cells are isolated and counted, and an aliquot of cells for achieving the desired cell density within the gel (2×10^6 cells/mL here) is centrifuged, resuspended in the monomer solution, and polymerized within a mold. After polymerization (~

5 min), the cell-gel construct is placed in excess media, and the media is refreshed repeatedly over 24 h to remove any unreacted monomer and initiator. This procedure has been used to encapsulate several different cell lines and primary cells in our lab, including PC12s (pheochromocytoma cells, model cell line for neuronal differentiation), HT1080s (fibrosarcoma cells, model cell line for tumor metastasis), NIH 3T3s (fibroblast cell line), and human mesenchymal stem cells (bone marrow derived primary cells). The protocol easily can be adapted for use with other cell types, cell seeding densities, and gel formulations.

3.3.4 Photodegradation of hydrogels

A major benefit of using photolabile hydrogels is that the incorporation of the *o*-nitrobenzylether moiety provides a phototunable handle through which the biomechanical or biochemical nature of the gel can be tuned with light. Since the user possesses both temporal and spatial control over light delivery, he/she can control spatiotemporally the mechanics or biochemistry of the hydrogel. In this protocol, we present the use of standard photolithography and confocal laser scanning microscopy (LSM) to pattern surface elasticity gradients, surface features, and bulk features within photodegradable hydrogels. The techniques described herein can be easily translated to pattern similar gradients or regions of defined biochemical signals with photoreleasable hydrogels. Furthermore, these degradation techniques are fully cytocompatible and can be performed in the presence of cells in the same manner described below with extra care taken when handling the samples to maintain sterility and cell viability.

3.3.4a Photolithography

Standard photolithography is a powerful technique employed to photopattern features in the x-y plane at the surface of photodegradable hydrogels with spatial resolution on the scale of 10 μm when using chrome masks (Figure 3.2b). Features can be transferred into the z-

dimension, and the depth of feature formation depends on the irradiation conditions (intensity and wavelength) and the exposure time. When patterning photodegradable or photoreleasable hydrogels with standard photolithography, there are three critical aspects: (i) light source, (ii) patterning mask, and (iii) exposure time. In this protocol, we describe the use of standard photolithography with a 365 nm light source to generate gradients in elasticity and features at the surface of photodegradable hydrogels. To form the gradient, an opaque mask is passed over the gel surface at a controlled rate during irradiation, and to form patterned features, a chrome mask with opaque squares is used. The parameters described herein can be tuned depending on the experimental situation; however, we advocate using 365 nm light and chrome masks for the best results. Exposure times can be tuned readily to generate surface gradients of varying steepness or features of variable depths.

3.3.4b Single-photon confocal microscope

Laser scanning confocal microscopy (LSM) with 405 nm light can also be employed to pattern the surface of photodegradable hydrogels or to fabricate features within the bulk of photodegradable gels (Figure 3.2c). LSM patterning offers micron-scale resolution in the x-y plane and z-dimension and readily tunable feature geometry. LSM patterning easily can be adapted to any confocal microscope with a 405 nm light source and region of interest (ROI) software. The user draws the desired geometry in the ROI software and subsequently irradiates the selected regions with the 405 nm light source. In this protocol, we employ a 30 mW, 405 nm laser at 50% transmission (power measured at the sample to be ~ 1 mW) with a pixel dwell time of 3.15 μ sec; however, these irradiation conditions can be tuned for other microscopes and/or needs. Furthermore, LSM pattern formation offers simultaneous imaging of changes in gel structure and cell response to changes in gel structure. Since the sample is already on the

confocal stage, the irradiation parameters can be changed to excite fluorophores attached to the gel backbone (e.g., methacrylated rhodamine, 543 nm) to image changes in gel structure or cell labeling fluorophores (e.g., GFP, 488 nm) to image cellular responses.

3.3.4c Degradation parameter overview

Typical irradiation parameters and associated gel degradation times are given for each of these degradation strategies in Figure 3.2d. While these are typical parameters used, nuances exist for degradation with 405 nm focused, single photon irradiation. For example, an increased “dose” of light is received with larger x-y features (e.g., a 50- μm versus a 5- μm diameter x-y circle), owing to overlapping regions of out of focus light, and results in increased non-specific z-direction degradation and patterned feature depth. These degradation parameter subtleties should be considered when planning advanced patterning experiments. If precise z-direction degradation is required within a gel (< 10 μm non-specific z-degradation), a focused, two photon irradiation source might be preferred⁸.

3.4 Materials

3.4.1 Reagents

CAUTION Most of the reagents listed below are hazardous (e.g., toxic, corrosive, flammable, irritant, lachrymator, sensitizer) and appropriate care as prescribed by the MSDS should be taken when handling them. All monomer synthesis steps should be performed within a chemical fume hood.

3.4.1a Monomer synthesis

Acetovanillone (Acros Organics, 102421000)

N,N-Dimethylformamide (Mallinckrodt, 492908)

Ethyl 4-bromobutyrate (Sigma-Aldrich, 167118-50G)

Potassium carbonate (anhydrous, Fisher, P208500)

Deionized water (DI water, 18 M Ω -cm, Barnstead NANOpure II)

Nitric acid (Mallinckrodt, 2704-46)

Ice

Ethanol (EtOH, absolute, Sigma-Aldrich, E7023 or similar)

Sodium borohydride (Sigma-Aldrich, 452882) **CAUTION** This reagent reacts violently with water and produces hydrogen gas. It should be handled with extreme caution in a fume hood.

Trifluoroacetic acid (TFA, Sigma-Aldrich, T62200) **CAUTION** This reagent is very corrosive and should be handled with extreme caution in a fume hood.

Deuterated chloroform (CDCl₃, Cambridge Isotope Laboratory, DLM-7-100)

Deuterated dimethylsulfoxide ((CD₃)₂SO, Cambridge Isotope Laboratory, DLM-10-50)

Dichloromethane (DCM, anhydrous, Acros, AC348465000)

Triethylamine (TEA, Sigma-Aldrich, T0886)

Acryloyl chloride (AC, Sigma-Aldrich, A24109) **CAUTION** This reagent is very corrosive and a lachrymator and should be handled with extreme caution in a fume hood.

Alumina (adsorption, Fisher, A540500)

Sodium bicarbonate (Fisher, S233500)

Hydrochloric acid (HCl, Mallinckrodt, H613-45)

Sodium chloride (NaCl, Fisher, S271-3)

Acetone (Mallinckrodt, 244016)

N-methylpyrrolidone (NMP, Applied Biosystems, 400580)

2-(1H-benzotriazole-1-yl)-1,1,3,3-tetramethyluronium hexafluorophosphate (HBTU, Anaspec, 21001)

1-hydroxybenzotriazole (HOBt, Anaspec, 21003; may be no longer available but can be purchased through Fisher Scientific, NC9342953)

N,N-diisopropylethylamine (DIEA, Anaspec, 27221)

Poly(ethylene glycol)-*bis*-amine (average molecular weight (M_n) ~ 3400 g/mol; Laysan Bio, NH2-PEG-NH2-3400-5g)

Ethyl ether (Fisher, E1384)

Amino acids for peptide synthesizer (Anaspec): glycine (G, 20128), arginine (R, 20312), aspartic acid (D, 20008), and serine (S, 20136)

DCM (standard, Mallinckrodt, 488108)

Tiisopropylsilane (TIPS, Sigma-Aldrich, 233781)

TFA (spectrophotometric grade, Sigma-Aldrich, 302031; use with HPLC solvents)

Acetonitrile (HPLC grade, Sigma-Aldrich, 34851)

α -cyano-4-hydroxycinnamic acid (Sigma-Aldrich, C8982-10X10)

3.4.1b Gel synthesis

Hydrogen peroxide (Fisher, H325100) **CAUTION** These two reagents (hydrogen peroxide and sulfuric acid) react strongly, producing heat and hydrogen gas. Extreme caution should be taken when mixing, and no flammables should be present in the fume hood.

Sulfuric acid (Fisher, A298212)

3-acryloxypropyltrimethoxysilane (Gelest, SIA0200)

Poly(ethylene glycol) diacrylate (PEGDA, synthesized per [45]; can also be purchased from Laysan Bio, ACRL-PEG-ACRL)

Poly(ethylene glycol) monoacrylate (PEGA, Monomer-Polymer & Dajac Labs, Inc, 9357)

Ammonium persulfate (AP, Acros, AC401165000)

Tetramethylene diamine (TEMED, Sigma-Aldrich, T9281-50mL)

PolyFluor™ 570 (Methacryloxyethyl Thiocarbonyl Rhodamine B) (MeRho, Polysciences, Inc., 23591)

Fibronectin (FN, Becton Dickinson, 354008)

Sterile Dulbecco's phosphate buffered saline (PBS, Invitrogen, 14190144)

Human mesenchymal stem cells (hMSCs, isolated from bone marrow)⁴⁶

hMSC growth media⁴⁶

LIVE/DEAD Cytotoxicity Assay (Invitrogen, L-3224)

3.4.2 Equipment

Round-bottomed flasks, one-necked

Beakers

Erlenmeyer flasks

Buchner funnels

Filter flasks

Addition funnel with gas purge

Keck clips

Magnetic stir bars

Rubber septa

Gas adapter

Thermometer

Temperature-controlled hotplate (e.g., IKA RCT Basic Safety Control Magnetic Stirrer, Fisher, 14-261-100)

Crystallization dish for reaction water/ice bath

Mortar and pestle

Spatulas

Scoopulas

Glass pipettes with rubber bulbs

Pipetteman with non-sterile and sterile plastic tips (P2, P20, P200, and P1000)

Glass funnel

Solid addition funnel

Refrigerator

Freezer (-20°C and -80°C)

Vacuum oven

Scintillation vials with caps (20 mL, Sigma-Aldrich, V7130-500EA; ½ dram, Fisher, 03-340-1A)

Metal cannula (18-gauge)

Separatory funnels

Filter paper (Whatman qualitative circles)

Glass frit filter (medium)

Rotary evaporator and water bath (e.g., Yamato RE47 and Yamato BM100)

Schlenk line and argon source

Desiccator

UV-visible (UV-vis) spectrophotometer (Lambda 40 UV/VIS Spectrophotometer, PerkinElmer)

NMR (Varian Inova 500 MHz NMR Spectrometer)

Quartz cuvettes

Centrifuge (e.g., Thermo Electron Corporation Centra CL3R)

Centrifuge tubes (50 mL)

Dialysis tubing (SpectraPor 7, molecular weight cutoff ~ 1000 g/mol, Spectrum Labs, 132105)

Lyophilizer

Peptide synthesizer (433A Peptide Synthesizer, Applied Biosystems)

Glass reaction vial for peptide coupling (Fisher, CG-1861-13)

Vortexer

High performance liquid chromatograph (HPLC, e.g., Waters Delta Prep 4000)

Matrix-assisted laser desorption/ionization-mass spectrometer (MALDI-MS, PerSeptive Biosystems)

Staining chamber

Non-reactive plastic chamber

Rubber gasket/spacer (254- μm thick (0.01"), McMaster-Carr, 87315K62; 500 μm -thick, McMaster-Carr, 3788T21)

Glass microscope slides (25 mm x 75 mm, Corning, 2947-3x1; 50 mm x 75 mm, Corning, 2947-75x50)

Glass cover slips (22 mm x 22 mm, #2, Fisher, 12-546-1)

Binder clips

6-well tissue culture plate

Tissue culture plates (100 mm, Corning, 430167)

Sterile syringes and needles (3, 5, and 10 mL syringes; 18 gauge needles)

Sterile filters

Eppendorf tubes (0.7 mL, ISC BioExpress, C-3268; 1.7 mL, ISC BioExpress, C-3269)

Razor blade

UV-visible light source (mercury arc lamp, Novacure 1000 (or equivalent), EXFO)

Band pass filters (365 nm, EXFO, 019-01006; 400-500 nm, EXFO, 019-01008; 320-500 nm, EXFO, 019-01011; 405 nm, MELLES GRIOT, 03FIM002),

Liquid-filled light guide (5 mm x 1000 mm, EXFO, 805-00002)

Collimating lens (Large lens with adjustable aperture (shown here), EXFO, 810-00014; Small lens, EXFO, 810-00017)

Ring stand with two clamps

Radiometer (International Light, Model IL1400A)

Syringe pump (e.g., Harvard Apparatus 44)

Foam board

Chrome photomask (PhotoSciences, Inc.)

Optical microscope (e.g., Nikon Eclipse TE2000-S)

Confocal microscope with region of interest (ROI) scanning capability and high numerical aperture objective (N.A. > 0.75) (e.g., Zeiss LSM 710)

3.4.3 Equipment setup

Glassware: All glassware used in described reactions are washed with soap and water, rinsed with water, cleaned in a base bath, rinsed with water, neutralized in an acid bath, rinsed with water and DI water, air dried, rinsed with acetone, blown dry with air, and dried in an 80°C oven for at least 1 h to overnight.

HPLC: Peptide purification was performed on a C18 preparatory column using a gradient of 5:95 acetonitrile:water to 95:5 with 0.1% TFA over 70 min at 20 mL/min. Peptide elution was monitored with UV absorbance at 220 nm and 280 nm.

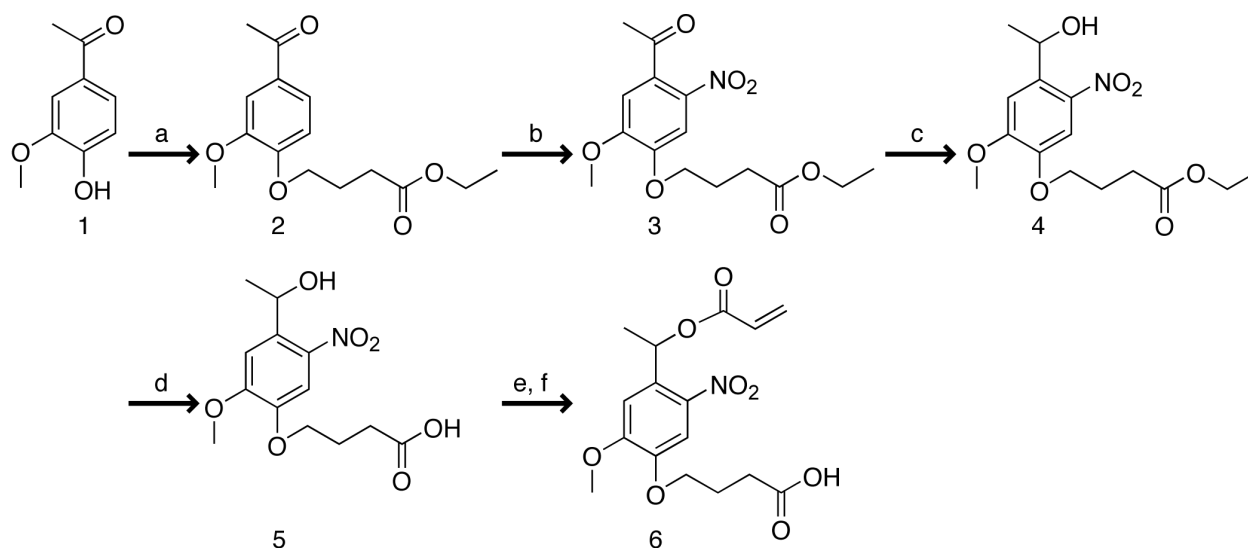


Figure 3.3 Photodegradable acrylate monomer synthetic scheme. Synthetic route for preparing photodegradable acrylate. Reagents and conditions: **(a)** DMF, ethyl-4-bromobutyrate, Ar, K_2CO_3 ; **(b)** HNO_3 , $\sim 5\text{ }^\circ\text{C} \rightarrow \sim 32\text{ }^\circ\text{C}$; **(c)** EtOH, Ar, $NaBH_4$, $38\text{ }^\circ\text{C}$; **(d)** DI H_2O , TFA, $\sim 90\text{ }^\circ\text{C}$; **(e)** Ar, DCM, TEA, AC, $0\text{ }^\circ\text{C} \rightarrow \text{room temperature}$; **(f)** acetone, DI H_2O .

3.5 Procedure

3.5.1 Monomer synthesis

1. *Photodegradable acrylate: synthesis of photolabile group (a, Steps 1-3).* The sequential reactions for synthesis of the photodegradable acrylate monomer are shown in **Fig. 3** and are covered in Steps 1-34. Add acetovanillone (1) (30 g, 180.5 mmol), DMF (150 mL), and ethyl 4-bromobutyrate (31 mL, 217 mmol) to a single-necked round-bottomed flask (500 mL) equipped with a gas adapter and magnetic stirrer. While stirring, purge the vessel with argon gas (10 min). Add potassium carbonate (37.4 g, 271 mmol), forming a suspension. Stir at room temperature overnight under argon.
2. In a large beaker or Erlenmeyer flask (2000 mL) with magnetic stir bar, add DI water (1500 mL). While stirring, pour the reaction mixture into the DI water to dissolve remaining potassium carbonate and precipitate product. Stir at room temperature for 2 h.

Stop stirring, and cool to 4°C for 4 h to overnight to fully precipitate the product.

3. Filter solution through a Buchner funnel with qualitative filter paper using a filter flask under vacuum. Pull air through the white powder product to dry (1-2 h). Transfer powder to a glass dish or weigh boat, and finish drying in a vacuum oven at 40°C overnight. Verify product (2) purity with ^1H NMR in CDCl_3 . Typical reaction yield is 97%.
4. *Photodegradable acrylate: synthesis of photolabile group (b, Steps 4-12)*. Split the product from Step 3 in half (2x 25 g), and nitrate each portion in a separate reaction as described below.
5. For each portion, add nitric acid (70 mL) to a single-necked round-bottomed flask (1000 mL) with magnetic stir bar and thermometer. Cool the flask on ice until the nitric acid is less than 5°C.

CRITICAL STEP Heat transfer between the reaction vessel and the ice bath is important for maintaining the prescribed reaction temperature. Use of a round bottom flask that is at least 10 times the reaction volume.

6. Grind the powder product from step 3 (24.5 g, 87 mmol) with a mortar and pestle to break apart any large clumps of powder. Add the powder in small portions (~ 3 spatula scoops). Allow each portion to dissolve in the nitric acid before adding the next portion (~ 5 min between each addition for a total addition time of ~ 1 h).

CRITICAL STEP Nitration of multiple positions of the aromatic ring can create an explosive material. Do not attempt to nitrate more than 50 g of material at a time. In addition, reaction yields have been best with 25 g batches as it is easier to maintain the reaction temperature at this scale.

7. Once all powder has been added, remove the ice bath, and heat the open reaction vessel with a water bath to 32°C. Check the reaction temperature every 5 min. When the reaction temperature reaches 33-35°C, place it back on ice until the mixture is cooled below 20°C. When the reaction temperature is below 20°C, return it to the 35°C water bath. Repeat this process until the total time of the reaction in the water bath is 1 h. The reaction should be yellow to orange/red.

CRITICAL STEP The reaction temperature is critical for nitration of the ortho position of the aromatic ring. Do not leave the reaction for more than 5 min without checking its temperature. If the reaction temperature is too low (never reaches 30°C), then the reaction will be incomplete. If the reaction temperature exceeds 35°C-40°C, then multiple positions will be nitrated on the ring, which makes purification difficult and is dangerous due to the explosive nature of trinitro aromatic compounds.

8. Add the reaction mixture drop-wise to chilled DI water (1050 mL at 4°C) on ice in a large beaker (2000 mL) with magnetic stir bar, stirring vigorously. To prevent further reaction during this time, keep the reaction mixture on ice during the precipitation.

PAUSE POINT Dissolution of the nitric acid into water occurs slowly. Due to the density of the nitric acid, the reaction mixture can sink to the bottom of the beaker with precipitation subsequently occurring around the stir bar. Slowly add the reaction mixture to the DI water. If significant clumping begins, stop adding the reaction mixture for 30 min while the nitric acid phase dissipates; keep the reaction mixture on ice during this time.

9. Stir the precipitate mixture for 1 h at room temperature. The precipitate should be yellow to orange. Place the precipitate mixture at 4°C overnight.
10. Filter the precipitate mixture through a medium glass frit filter on a filter flask while

pulling vacuum. Rinse recovered product on filter with cold DI water (4°C). Pull air through the filter for several hours to dry the product.

11. Re-crystallize the product from ethanol. Bring absolute EtOH (~ 700 mL) to a boil in an Erlenmeyer flask. Add powder product to a beaker (1000 mL) with magnetic stir bar, and add boiling EtOH while stirring until powder dissolves (usually less than 500 mL of EtOH). If any brown clumps remain, carefully gravity filter (qualitative filter paper on glass funnel) the solution while hot to remove these insoluble impurities. Turn off the heat, stop the magnetic stirring, and let the solution and hot plate together cool to room temperature. Some crystal formation may be observed here. **TROUBLESHOOTING?**
12. Place re-crystallization solution at 4°C overnight for complete crystallization. Filter the suspension through a medium glass frit filter and pull air through the filter to dry the yellow fine powder product (~ 1 h). Verify product (3) purity with ¹H NMR in CDCl₃. Typical reaction yield is 60%.

CRITICAL STEP If little crystallization is observed, then too much EtOH may have been added; evaporate the EtOH using a rotary evaporator, and repeat the re-crystallization. In addition, if NMR shows impure an product (e.g., nitration of different ring positions), repeat re-crystallization (Steps 11-12). **TROUBLESHOOTING?**

13. *Photodegradable acrylate: synthesis of photolabile group (c, Steps 13-16).* Add absolute EtOH (515 mL) and the nitrated product (30.9 g, 95 mmol) to a single-neck round-bottomed flask (1000 mL) with magnetic stir bar, gas adapter for argon purge, and water bath. Purge the reaction for 10 min with argon. Heat the reaction to 38°C using the water bath to improve dissolution of the powder in EtOH.
14. Add sodium borohydride (2.25 g, 59 mmol) in portions to the reaction solution (adding a

portion every 5 min over 1 h). Bubbles of gas should be observed forming in the reaction solution. Stir at 38°C overnight. Reaction turns a deep orange/red.

CRITICAL STEP Hydrogen gas is evolved during this reaction. The argon purge should be vented through a Schlenk line. Do not have open flames in the fume hood and avoid significantly larger batches.

15. Add DI water to a large beaker or Erlenmeyer flask (5000 mL) with magnetic stir bar. Slowly pour the reaction solution into the beaker. Light yellow precipitate should form. After 30 min, place precipitate suspension at 4°C overnight.
16. Filter suspension to recover product. Dry in vacuum oven at 40°C overnight. Verify product (4) purity with ¹H NMR in (CD₃)₂SO. Typical reaction yield is 60%.
17. *Photodegradable acrylate: synthesis of photolabile group (d, Steps 17-19)*. Grind product from Step 16 to a fine powder (18 g, 55 mmol). Add finely ground powder and DI water (450 mL) to an Erlenmeyer flask with magnetic stir bar on a hot plate. Add TFA (45 mL), and heat suspension to ~ 90°C, heating the reaction mixture but not boiling. **CAUTION** Use care and proper personal protective equipment when handling TFA. It is corrosive and causes severe burns.
18. Add additional TFA after 8 h (22.5 mL), and react overnight. Add additional TFA (22.5 mL), and react for 4 h, until brightening of the reaction mixture is not observed upon TFA addition. A light yellow powder in suspension should remain.
19. Cool to room temperature. Filter with a medium glass frit filter, and rinse with a small amount of chilled DI water (4°C). Dry in vacuum oven at 40°C overnight. Verify product (5) purity with ¹H NMR in (CD₃)₂SO. Typical reaction yield is 63%.

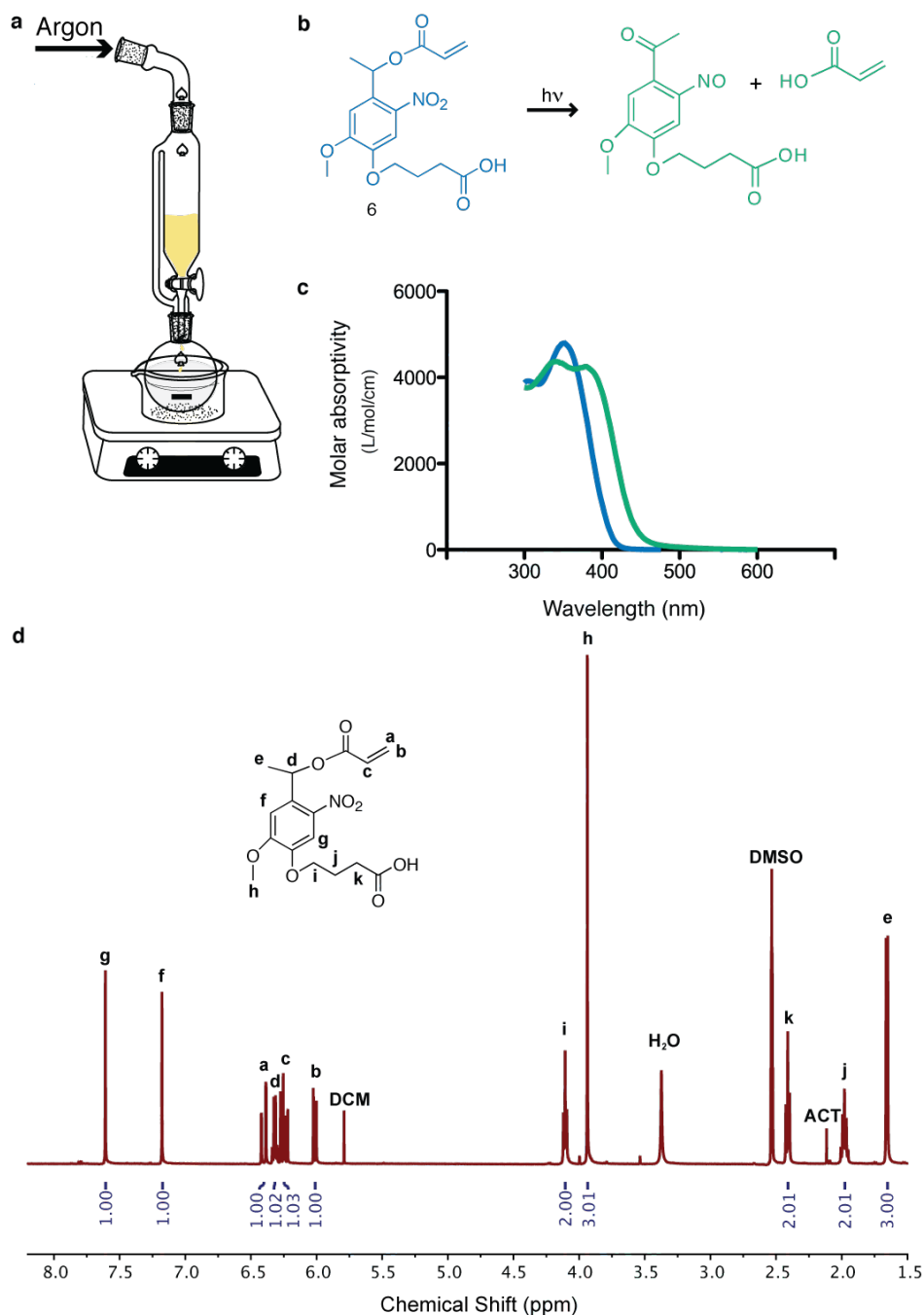


Figure 3.4 Photodegradable acrylate. (a) The reaction set-up for the acrylation of the photolabile group. The photolabile group is added to a round-bottomed flask with DCM and a stir bar and chilled to $0\text{ }^\circ\text{C}$ in an ice bath. TEA is added to the round-bottomed flask while AC is mixed with DCM in an addition funnel under Ar purge. The AC/DCM is added dropwise to the round-bottomed flask. (b) In response to light, the photodegradable acrylate (blue) undergoes irreversible cleavage, producing the cleaved photolabile group and acrylic acid (green). (c) The molar absorptivities of photodegradable acrylate (blue) and the cleaved photolabile group (green) from 300 to 600 nm. (d) ^1H NMR shifts for the photodegradable acrylate monomer for synthetic verification.

20. *Photodegradable acrylate: acrylation of the photolabile group (e and f, Steps 20-34).*

Add the photolabile group (4 g, 13 mmol, from Step 19 or purchased) to a single-neck round-bottomed flask (250 mL) with magnetic stir bar, addition funnel with gas purge, and septum (**Fig. 4**).

21. Using two 18-gauge needles (one for gas inlet from a Schlenk line and one as gas outlet to the fume hood), purge the reaction vessel with argon (~ 10 min).

22. Remove the argon inlet from the reaction vessel septum. Use argon administered from a Schlenk line to transfer anhydrous DCM (~ 155 mL) air-free to the addition funnel through an 18-gauge metal cannula inserted into the reaction vessel septum.

23. Return the argon purge to the addition funnel, and use the addition funnel to add DCM (~ 120 mL) to the round bottom flask.

24. Gently lift the addition funnel off of the round bottom flask and inject TEA (7.45 mL, 53 mmol). Quickly replace the addition funnel on the round bottom flask. The photolabile group should completely dissolve. Continue argon purge.

25. Inject AC through the addition funnel septum (3.26 mL, 43 mmol) into the remaining DCM.

26. Place the round bottom flask in an ice bath (~ 15 min). Add the AC/DCM solution dropwise to the round bottom flask (~ 1 drop every 5 s).

CRITICAL STEP As the volume of solution in the addition funnel changes, the stopcock position may need to be adjusted to maintain the proper drop rate. If reaction solution begins to turn brown or if flask appears cloudy in the vapor phase, slow down the drop rate.

27. React at room temperature overnight. Triethylamine salts, white crystals, may form in the reaction. Reaction mixture should be orange/brown.

28. Concentrate the reaction mixture by evaporating the DCM on a rotary evaporator (do not heat above 35°C), precipitating triethylamine salts.
29. Filter reaction mixture over alumina in a Buchner funnel with qualitative filter paper to remove triethylamine and triethylamine salts. Lightly rinse filtrate with additional DCM.
30. Add filtered reaction solution (100 mL) to a separatory funnel and wash (1:1) sequentially with sodium bicarbonate solution (5 w/v% aqueous) to remove any unreacted photolabile group, dilute HCl (0.1 M aqueous) to remove any remaining triethylamine, and brine (10 w/v% NaCl aqueous) to remove water. After each wash, allow layers to fully separate (~ 30 min); the DCM phase with product is the dense, lower layer. Brine can be added to water phase to improve separation. Add the intermediate product solution to a single-neck round-bottomed flask (500 or 1000 mL).
31. Evaporate the DCM using a rotary evaporator. Make an acetone:water mixture (50:50, 400 mL total), and add to round bottom flask with magnetic stir bar to dissolve product. Stir this mixture overnight at room temperature; the reaction mixture should become translucent.
32. Evaporate the acetone from the reaction solution using a rotary evaporator (do not heat above 45°C). The orange liquid product will begin to separate from the remaining aqueous solution.
33. Add the aqueous solution to a separatory funnel and extract the product with DCM (4x 100 mL), using brine to improve separation of the DCM and water phases.
34. Concentrate the product solution by rotary evaporation (~ 100 mL). Wash this solution (1:1) sequentially with dilute HCl (0.1 M aqueous) and brine. Dry the product solution over magnesium sulfate (~ 30 min or less), filter, and evaporate the solvent. Verify

photodegradable acrylate monomer (6, **Fig. 4b**) product absorbance with a UV-vis spectrophotometer (**Fig. 4c**) and purity with ^1H NMR in $(\text{CD}_3)_2\text{SO}$ (**Fig. 4d**). Typical reaction yield is 53%.

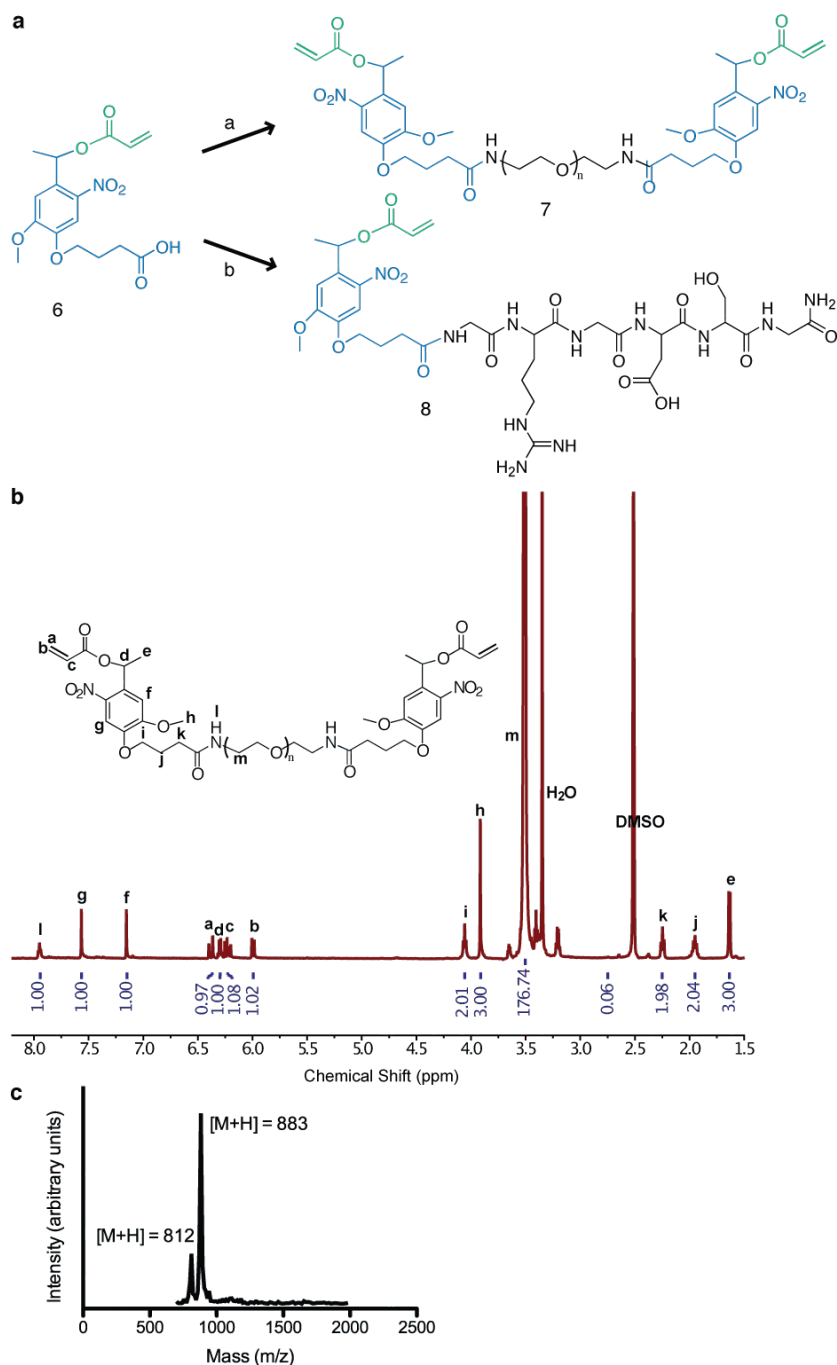


Figure 3.5 Macromolecular synthetic schemes. (a) Synthetic route for preparing the photodegradable crosslinker (a) and photoreleasable tether (b). (a) NMP, HBTU, HOBt, DIEA, and PEG-*bis*-amine. (b) NMP, HBTU, HOBt, DIEA, and RGDS peptide. **(b)** ^1H NMR shifts for

the photodegradable crosslinker for synthetic verification. (c) MALDI-TOF spectrum for the photoreleasable tether for synthetic verification.

35. *Photodegradable crosslinker.* Add PDA (2.08 g, 5.9 mmol, from Step 34) to a scintillation vial with NMP (10 mL). Vortex and lightly heat with a heat gun to dissolve. Add HBTU (2.45 g, 6.5 mmol) and HOBt (0.87 g, 6.5 mmol) to the vial and rinse down with NMP (5 mL). Repeat vortexing and heating to begin dissolution.
36. Add PEG-*bis*-amine (2.5 g, 0.73 mmol) to a scintillation vial with NMP (15 mL). Vortex and lightly heat with a heat gun to dissolve.
37. Add PDA, HBTU, and HOBt in NMP from Step 35 to a single-neck round-bottomed flask with magnetic stir bar and gas adapter. Rinse scintillation vial with small amount of NMP (~ 5 mL) to insure all is added. Add DIEA (2.05 mL, 11.8 mmol) and stir reaction solution, noting color change from orange to red/brown indicating activation of the PDA carboxylic acid (5 min). Add PEG-*bis*-amine in NMP, rinsing scintillation vial with NMP (~ 5 mL), and purge the reaction with argon (**Fig. 5a**, top).
38. Stir the reaction overnight. Precipitate in ice cold ethyl ether using eight 50 mL centrifuge tubes, each containing 40 mL of ether and evenly split reaction solution added dropwise. Vortex solution, balance weights, and centrifuge (5 min at 4°C with 1000 g). Decant off ether and repeat ether wash two times. Place centrifuge tubes under vacuum overnight to remove any remaining ether. Some NMP will remain with the precipitate, making it a soft solid.
39. Dissolve the product in DI water (100 mL), vortexing and stirring to break apart any clumps. A cloudy orange suspension will be formed. Centrifuge this mixture (4x 30 min at 4°C with 1400 g) to sediment out the precipitated HBTU/HOBt by-products. Decant

off the translucent yellow/orange product solution. Dialyze the solution against DI water (5 L) for 3 days at room temperature, refreshing the DI water 3x per day. Additional precipitate may sediment over this time to the bottom of the dialysis tubing.

TROUBLESHOOTING?

40. Recover the clear, dialyzed product solution, freeze, and lyophilize (~ 2-3 days). Verify product purity (7) with ^1H NMR in $(\text{CD}_3)_2\text{SO}$ (modification of PEG with PDA ~ 85-90%) (**Fig. 5b**). Typical reaction yield is 70%.
41. *Photodegradable tether*. Using a peptide synthesizer or following standard SPPS procedures,⁴⁷ synthesize GRGDSG on resin. Do not cap the final amine terminus of the peptide.

PAUSE POINT Peptide on resin can be stored at -20°C for a few days prior to PDA coupling.

42. In a small peptide reaction vessel or a scintillation vial, swell resin in DCM (10 mL) for 30 min.
43. Rinse with DCM (3x 5 mL). Rinse with NMP (3x 5 mL). Remove NMP.
44. Add the PDA (0.353 g, 1 mmol, from Step 34), HBTU (0.417 g, 1.1 mmol), HOBT (0.149 g, 1.1 mmol), and NMP (~ 2 mL) to a scintillation vial. Intermittently vortex and gently heat to dissolve. Add DIEA (0.348 mL, 2 mmol). Vortex and allow to activate for 5 min; a color change should be observed. Add the reaction mixture to the reaction vial containing the resin. Rinse the scintillation vial several times with NMP to insure that all of the solution is added such that the total amount of NMP does not exceed 10 mL (**Fig. 5a**, bottom).
45. Stir the reaction overnight at room temperature. Remove the reaction solution, retaining the resin. Wash the resin with NMP (3x 5 mL) and DCM (3x 5 mL)

46. Using the ninhydrin assay,⁴⁷ verify that all amines on the resin have been reacted. If amines are still present, repeat Steps 43-46.

47. Add 95% TFA, 2.5% TIPS, and 2.5% DI water to the vial containing the resin and react for 1 h to cleave the peptide.

CRITICAL STEP This cleavage time is shorter than typically prescribed for peptide cleavage (> 2 h) and is used to maintain the ester bond of the PDA. This cleavage time may need to be adjusted for different peptide sequences, as amino acid deprotection times vary.

48. The cleavage solution was removed from the resin and precipitated in ice cold ethyl ether in two 50 mL centrifuge tubes. The precipitate was pelleted by centrifugation (5 min at 4°C with 1000 g), and ether decanted. The peptide was washed twice with cold ethyl ether and desiccated overnight under vacuum.

49. The peptide was purified by HPLC using a gradient of 5:95 acetonitrile:water to 95:5 with 0.1% TFA over 70 min at 20 mL/min on a C18 preparatory column. Peptide elution was monitored with UV absorbance at 220 nm and 280 nm. Product elution was observed at ~ 35 min, where the collected effluent is a translucent yellow indicating the presence of the PDA.

50. An aliquot of the purified product solution was mixed with the matrix molecule α -cyano-4-hydroxycinnamic acid, and peptide purity was verified by MALDI-MS. The MALDI laser can photolytically cleave the PDA, so a small amount of photodegraded peptide may also be observed in the MALDI-MS trace (**Fig. 5c**).

51. The purified peptide (8) solution was frozen in 50 mL centrifuge tubes and lyophilized (2-3 days). Typical reaction yield is ~ 50%.

3.5.2 Hydrogel synthesis

52. *Acrylation of glass cover slips.* Clean glass cover slips (22 mm x 22 mm) in a solution of 75 mL of hydrogen peroxide and 75 mL of sulfuric acid for ~ 1 h. **CAUTION** This solution of hydrogen peroxide and sulfuric acid is extremely reactive and should be prepared in an empty chemical fume hood free of solvents and flammables.
53. Rinse the cover slips well with DI H₂O to remove the cleansing solution. Place the cover slips on a Kimwipe and rinse the first side with acetone. Let the acetone evaporate for ~ 10 min; flip the cover slips and rinse the other side with acetone.
54. While the second dose of acetone evaporates, place two 20 mL scintillation vials in a Teflon chamber with a screw-on lid. Fill two ½ dram scintillation vials with 60 µL of acryloxytrimethoxysilane each and place them within the 20 mL scintillation vials in the Teflon chamber. Once the acetone has evaporated, place the cover slips in the Teflon chamber standing vertically on a microscope slide holder.
55. Purge the Teflon chamber with argon for ~ 5 min. Seal the chamber and place it in an oven at 60 °C for 3 – 12 h.
56. *Synthesis of photodegradable and photoreleasable gels.* Prepare sterile stock solutions of PEGdiPDA (20 w/w% in DI H₂O), PEGDA (20 w/w% in DI H₂O), PEGA (40 w/w% in DI H₂O), photodegradable tether (100 mM in DI H₂O), ammonium persulfate (AP, 2 M in DI H₂O), and TEMED (2 M in DI H₂O). If you will be fabricating photodegradable gels for cell encapsulation, prepare a stock of fibronectin (1 mg/mL in PBS), or if you will be imaging the gels, prepare a stock of methacrylated rhodamine (MeRho, 300 nM sterile filtered).

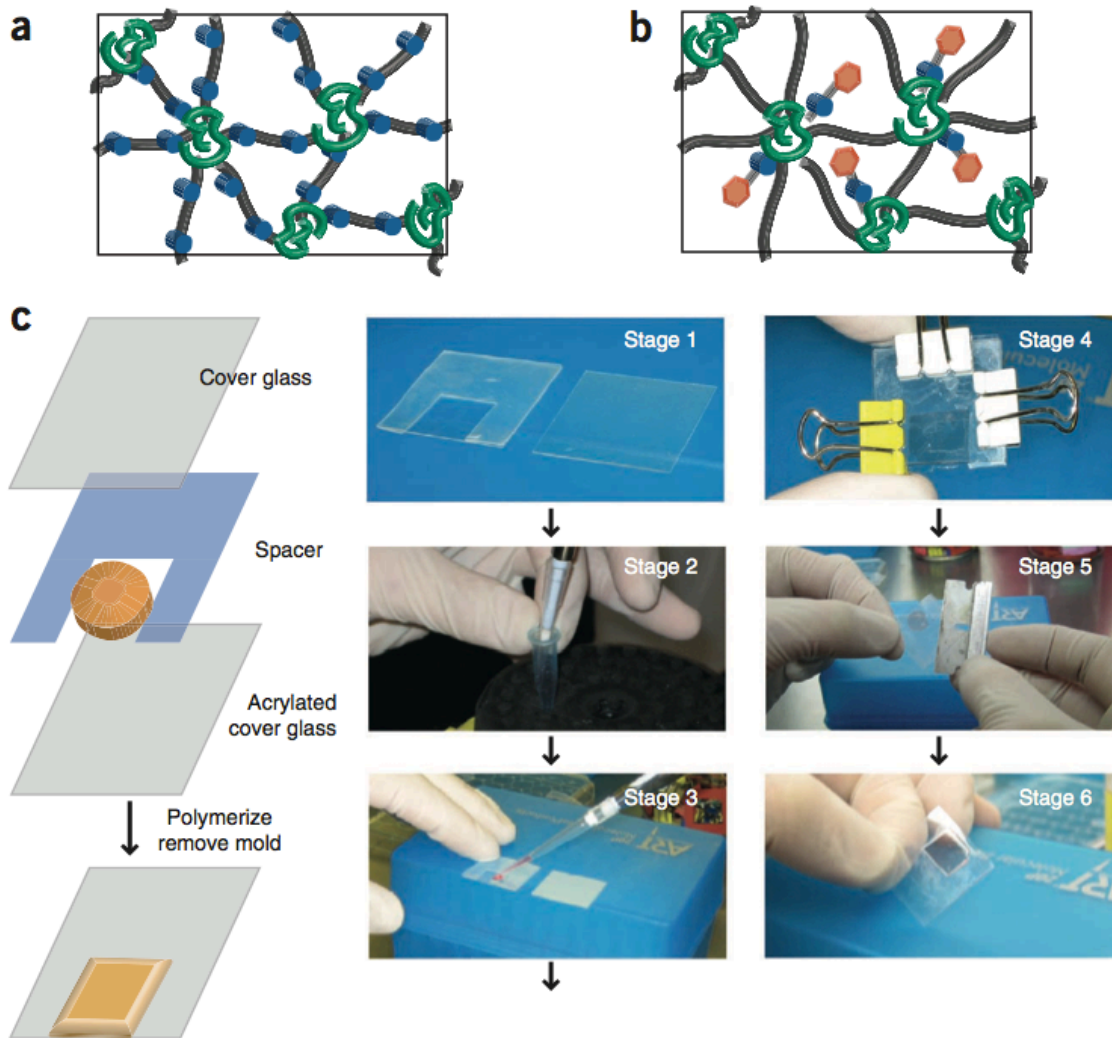


Figure 3.6 Hydrogel synthesis. (a) A schematic of the network structure of photodegradable hydrogels formed via free-radical chain polymerization of the photodegradable crosslinker: polyacrylate kinetic chains (green coils), PEG-based crosslinks (black lines), and photolabile moieties (blue circles). (b) A schematic of the network structure of photoreleasing hydrogels formed via free-radical chain co-polymerization of the non-degradable crosslinker with the photoreleasable tether: polyacrylate kinetic chains (green coils), PEG-based crosslinks (black lines), photolabile moieties (blue circles), and pendant peptides (orange hexagons). (c) Photolabile hydrogels are formed between an acrylated cover glass and a non-acrylated cover glass in a silicon mold (spacer). The silicon mold is placed on the acrylated cover glass (1) and set-up next to the non-acrylated cover glass. The macromer solution is initiated by adding TEMED to the solution while mixing (2), and this solution is quickly pipetted onto the acrylated cover glass (3) in the void of the mold. The non-acrylated cover glass is used to cover the solution, and the sandwich is clamped shut with binder clips (4). After ~ 5 min, the sandwich is opened with a razor blade (5), and the formed gel (6) is placed in PBS.

57. To prepare 40 μL photodegradable hydrogels, sufficient to fill a 1 cm x 1 cm x 254 μm geometry, combine 16.4 μL of the PEGdiPDA stock solution, 6.8 μL of the PEGA solution, and 10.8 μL PBS for each gel (**Fig. 6a**). Add 4 μL of the AP solution for each gel to the macromer solution and aliquot the macromer solution into 38 μL volumes into individual 0.7 mL Eppendorf tubes for each gel to be made. If you plan to fluorescently image with these gels (e.g., for patterning), substitute 7.5 μL of the PBS with MeRho solution (for a final concentration of 300 nM), and if you plan to seed cells on or encapsulate cells within these gels, substitute 5.3 μL of the PBS with fibronectin solution. If you plan to both image and encapsulate or seed substitute the PBS with 5.3 μL of fibronectin solution and 5.8 μL of MeRho solution.

CRITICAL STEP Once the AP has been added to the macromer solution, it should be used within ~ 30 min. Further, at this point, the initial properties of the gel (e.g., crosslinking density and biofunctionality) can be tuned by altering the concentrations of the components in the macromer solution, entrapping other proteins than fibronectin, or incorporating other acrylated/methacrylated moieties. If the amount of PEGdiPDA is altered, the final concentrations of AP and TEMED will need to be adjusted since the *o*-nitrobenzylether moiety is an effective radical scavenger. As the concentration of PEGdiPDA is increased, the concentration of AP and TEMED should be increased in order to achieve gelation, and as the concentration of PEGdiPDA is decreased, the concentration of AP and TEMED should be decreased so that the solution does not gel too rapidly. As adjustments are made, the changes in volumes should be supplemented with PBS to maintain the total volume at 40 μL per gel.

TROUBLESHOOTING?

58. To prepare 40 μL photoreleasable gels, combine 16.4 μL of the PEGDA solution, 6.8 μL

of the PEGA solution, 4 μL of the photodegradable tether solution, and 5.4 μL of PBS for each gel (**Fig. 6b**). Add 2 μL of the AP solution for each gel to the macromer solution and aliquot the macromer solution into 39 μL volumes into individual 0.7 mL Eppendorf tubes for each gel to be made.

CRITICAL STEP Once the AP has been added to the macromer solution, it should be used within ~ 30 min. Further, at this point the initial properties of the gel, e.g., crosslinking density and biofunctionality, can be tuned by altering the concentrations of the components in the macromer solution, entrapping other proteins than fibronectin, or incorporating other acrylated/methacrylated moieties. If the amount of photodegradable tether is altered, the final concentrations of AP and TEMED will need to be adjusted since the *o*-nitrobenzylether moiety is an effective radical scavenger. As the concentration of photodegradable tether is increased the concentration of AP and TEMED should be increased in order to achieve gelation and as the concentration of photodegradable tether is decreased the concentration of AP and TEMED should be decreased so that the solution does not gel too rapidly. As adjustments are made, the changes in volumes should be supplemented with PBS to maintain the total volume at 40 μL per gel. **TROUBLESHOOTING?**

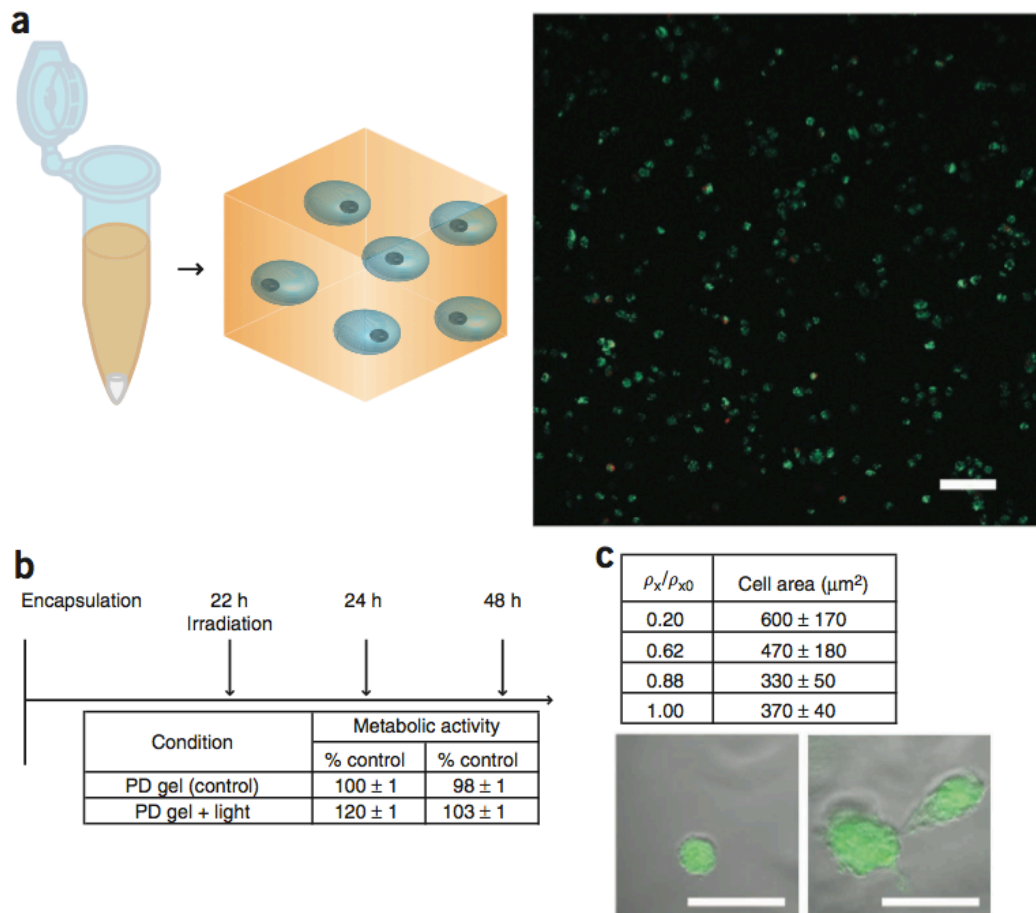


Figure 3.7 Cell encapsulation within photodegradable hydrogels. (a) Cells are encapsulated within photolabile hydrogels by resuspending a cell pellet in the macromer solution just before the addition of TEMED. Cell viability is verified after polymerization using a LIVE/DEAD Cytotoxicity Assay and confocal imaging. Here hMSCs exhibit good viability within the photodegradable hydrogel after encapsulation (live cells stained green, dead cells stained red, day 1, confocal z-projection). Scale bar, 100 μm . (b) Cell function after irradiation and gel degradation can be assessed by measuring metabolic activity with the alamarBlue assay. Metabolic activity of hMSCs encapsulated in a photodegradable gel increases slightly on irradiation and degradation (8 min of 10 mW/cm^2 at 365 nm), compared with photodegradable gels without irradiation (control) ($P < 0.001$), but the two conditions are similar ~ 24 h after irradiation (48 h in 3D culture). (c) Irradiation of the hydrogels for up to 8 min (10 mW/cm^2 at 365 nm) creates z-gradient in degradation and gel cross-linking density (ρ_x). Cells were imaged on day 4 in culture after irradiation for 8 min on day 1. This 3D gradient in cross-linking density can be used to study how gel density influences cell function in 3D culture. hMSCs labeled with CellTracker Green are observed spreading in lower cross-linking density regions of the gel (right, confocal slice overlaid with bright field) as compared with regions with high cross-linking density (left), and increasing cell area in response to this z-direction gradient is observed and quantified with image analysis (table, ρ_x normalized to its initial, nondegraded value, ρ_{x0}). Scale bars, 50 μm .

59. Prepare an acrylated cover slip with a 254 μm silicon gasket (**Fig. 6c-1**), a non-acrylated cover slip, three small binder clips, and a P200 pipette set to 40 μL with a tip.
60. Whether making photodegradable or photoreleasable gels, take one of the 0.7 mL Eppendorf tubes with an aliquot of macromer solution. While mixing the macromer solution vigorously, add 2 μL of TEMED for photodegradable crosslinker gels and 1 μL of TEMED for photoreleasable tether gels (**Fig. 6c-2**). Take the solution to the prepared cover slip mold and pipette the 40 μL solution into the center of the void in the silicon gasket (**Fig. 6c-3**). Cover the solution with the non-acrylated cover slip, close the mold, and clamp with the binder clips (**Fig. 6c-4**).

CRITICAL STEP Once the TEMED is added, the macromer solution will begin to gel within ~ 30 s, so the transfer to the prepared mold should be rapid.

61. Allow the solution to gel in the mold for ~ 5 min. Upon gelation, open the mold carefully with a razor blade (**Fig. 6c-5**) and place the formed gel (**Fig. 6c-6**) into ~ 4 mL of PBS (or enough to fully cover the gel) to allow unreacted monomer and initiator to diffuse out. Refresh the PBS after ~ 30 min.

PAUSE POINT The gels should remain attached to the cover slip for 10-14 days and can be used for degradation or cell seeding at any time. To maintain sterility, keep the gel submerged in sterile PBS in an incubator for the duration of the gel's use.

62. *Cell encapsulation.* All operations described in this section are performed using sterile technique. The base monomer solution was prepared as described in Step 57, and fibronectin was added (225 nM) to promote cell adhesion within the hydrogel. A rectangular mold was prepared from two glass microscope slides and a 254- μm -thick medical-grade silicon rubber gasket.

63. Media was aspirated from hMSCs on 100-mm dishes. The plated cells were rinsed with PBS (5 mL per plate) to remove any remaining media and incubated with 1x trypsin (4 mL per plate for ~ 6 min at 37°C) to detach the cells from the plate. The trypsin was quenched with fresh media (2 mL per plate); the detached cells were collected; and an aliquot of cells (2x 10 µl) was counted with a hemacytometer while the collected cells were pelleted by centrifugation (5 min at room temperature with 200 g).

64. The cells were re-suspended in a small amount of media (~ 1 mL), and an aliquot was taken to achieve a cell density of 2×10^6 cells/mL in the monomer solution. This aliquot of cells was pelleted by centrifugation (5 min at room temperature with 200 g) in an Eppendorf tube (1.7 mL), media removed, and re-suspended in the monomer solution (**Fig. 6d**).

CRITICAL STEP Take care to gently triturate cells in the monomer solution to break apart any cell clusters and suspend cells individually within the gel for probing cell-material interactions.

65. Following Step 60, TEMED was added to the monomer-cell solution while vortexing, and the polymerizing solution quickly pipetted into the glass mold.

CRITICAL STEP Since redox initiation is used, the polymerization begins as soon as TEMED is added, and molding gels within this time constraint (< 1 min before gelation) may take practice.

66. After 5 min of polymerization, the mold was submerged in media and opened with a sterile razor blade. The top glass slide was removed, and the gel was cut into 3 pieces (three ~ 25 mm x 25 mm pieces). Each piece was transferred to a well of a 6-well plate (5 mL media per well) using sterile metal spatulas. The media was aspirated from the plates and replaced with fresh media after 30 min, 4 h, and 24 h to ensure that all

unreacted monomer and initiation components were removed.

67. Culture plates were incubated at 37°C, and media was refreshed every 2-3 days. Cell viability was checked using the LIVE/DEAD Cytotoxicity assay.

3.5.5 Hydrogel degradation and patterning

68. *Hydrogel degradation with photolithography: gradient formation.* Set-up a 365 nm light source, such as an EFOS/EXFO NovaCure or OmniCure, with a liquid filled light guide and collimating lens (**Fig. 7**). Tune the intensity such that the intensity is 10 mW/cm² at the sample height. Collimate the light spot with the collimating lens so that the intensity is even over the sample (**Fig. 7a**).

69. Put a gel between two glass slides (50 mm x 75 mm) spaced by a 500 µm rubber gasket and fill the void with PBS or serum-free, phenol-red-free media. Place the chamber under the light source such that the sample is directly below the center of the light spot.

CRITICAL POINT If cells are attached to the surface of the gel, special care should be taken when transferring the gel between liquids.

70. Attach an opaque rectangle, such as a piece of foam board (**Fig. 7b**), to the drive shaft of a syringe pump, such that the foam board will move with the drive shaft. Align the edge of the foam board to be flush with one edge of the gel so that all of the gel is initially exposed to the light source.

71. Set the syringe pump diameter to 1.1283 mm such that an infuse rate of 1 µL/min will be equal to movement of 1 mm/min. Start the syringe pump at the same time as the light source shutter is opened. Irradiate the sample for 8 min; this will insure that 8 mm of the gel is covered by the end of the irradiation and that a gradient in degradation will be created over the first 8 mm of the gel.

72. Submerge the gel in PBS or media to allow the degradation products to diffuse out of the gel. After ~ 30 min refresh the PBS or media.

73. *Hydrogel degradation with photolithography: pattern formation.* Set up a 365 nm light source, such as an EFOS NovaCure or OmniCure, with a liquid filled light guide and collimating lens (**Fig. 7**). Tune the intensity such that the intensity is 10 mW/cm^2 at the sample height. Collimate the light spot with the collimating lens so that the intensity is even over the sample (**Fig. 7a**).

74. Place a gel on a glass slides (25 mm x 75 mm) and pipette ~ 150 μL of PBS or serum-free, phenol-red-free media onto the gel surface. Place three cover slips on either side of the gel to support the chrome mask. Place the sample directly below the center of the light spot.

CRITICAL POINT If cells are attached to the surface of the gel, special care should be taken when transferring the gel between liquids.

75. Rest a chrome mask with the desired pattern on the stacks of cover slips adjacent to the sample such that the pattern is covering the surface of the gel.

76. Turn the light source on and irradiate the sample for at least 8 min to create features at the surface of the gel.

PAUSE POINT The length of irradiation dictates the depth of feature formation as described in [27], thus the user should tune the exposure time based on the desired depth of feature formation.

77. Submerge the gel in PBS or media to allow the degradation products to diffuse out of the gel. After ~ 30 min, refresh the PBS or media.

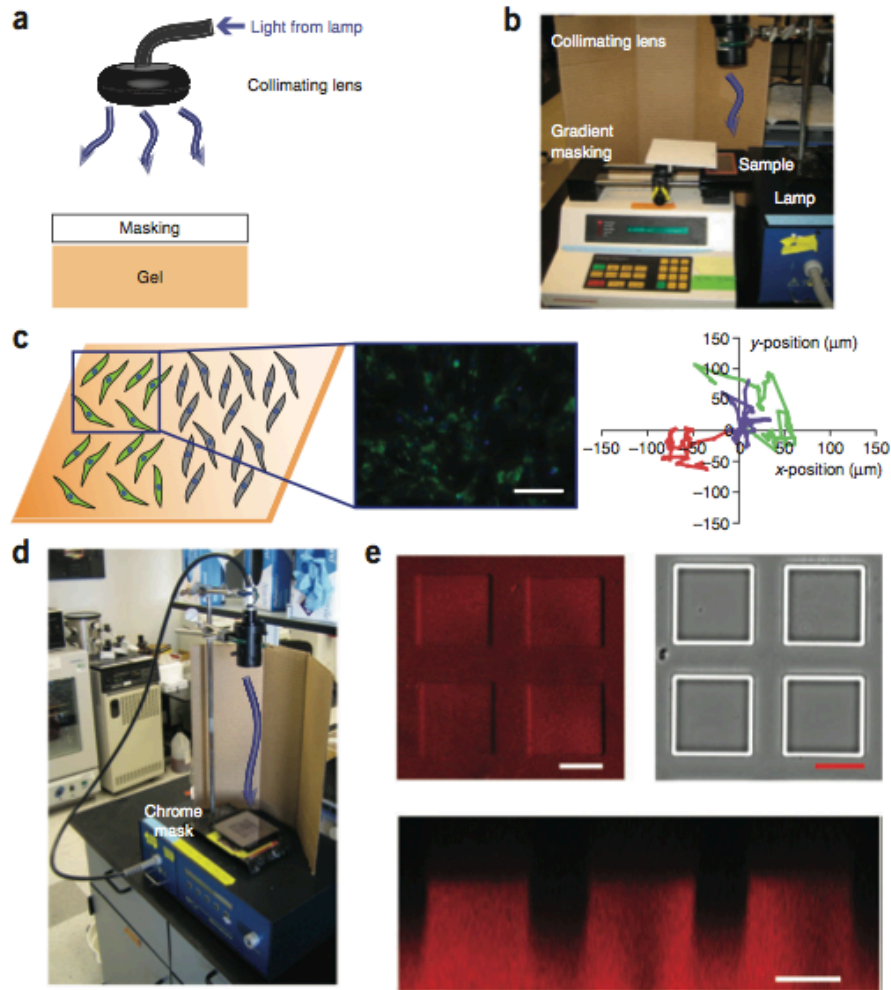


Figure 3.8 Photopatterning with photolithography. (a) To pattern photolabile hydrogels with standard photolithography, a mask is placed between a collimated light source and the gel surface. For proper pattern transfer, it is important that the light be well collimated with a collimating lens and that the mask be appropriately placed above the hydrogel surface. (b) Photopatterning can be used to form gradients in elasticity or biochemical signals in photolabile hydrogels via gradient masking. Briefly, the sample is placed in a PBS/media filled chamber, and a syringe pump is used to slowly cover the sample so that the sample receives a gradient of light, which induces a gradient in photocleavage. (c) Photopatterning can also be employed to generate features at the surface of photolabile hydrogels using a chrome mask. To ensure pattern transfer, use a well-collimated light source and rest the chrome mask just above the gel surface on glass slides or cover glass. Here, we used a mask with square features to pattern positive square pillars at the surface of photodegradable hydrogels. Features are shown in a confocal surface image (upper left), brightfield image (upper right), and confocal cross section image (bottom).

78. *Hydrogel degradation with confocal microscopy.* Place a gel between two glass slides (25 mm x 75 mm) separated by 500 μm rubber gasket and fill the void with PBS or

serum-free, phenol-red-free media (**Fig. 8a-1**).

79. Place the chamber with the sample on the stage of a confocal microscope with a 405 nm light source (**Fig. 8a-2**). Find the surface of the gel by imaging the first plane that fluoresces with MeRho or by looking for dust particles or surface aberrations.
80. Using the region of interest software (ROI) that accompanies the microscope, draw ROIs into the gel (**Fig. 2c** and **8b&c**). To transfer these patterns into the third dimension, generate a z-stack of the desired size with 1- μm slices/intervals.

CRITICAL STEP Due to the nature of the confocal process, there is out of plane irradiation causing a loss in the resolution of the pattern. This problem exacerbates with increasing feature size (**Fig. 8b**, fluorescent cross-section) and the user should take this into account when generating features with the ROI software.

81. Irradiate these samples with a 30 mW, 405 nm laser at 50% transmission (~ 1 mW measured at sample) with a pixel dwell time of 3.15 μs (total time to scan 512 x 512 pixel² frames in 1- μm intervals over a 50- μm stack is ~ 40 s).
82. When the pattern is formed, the sample can be imaged using transmitted light or with fluorescent confocal microscopy on the same stage.
83. Upon completion of patterning and imaging, the sample should be removed from the confocal microscope and submerged in PBS or media.

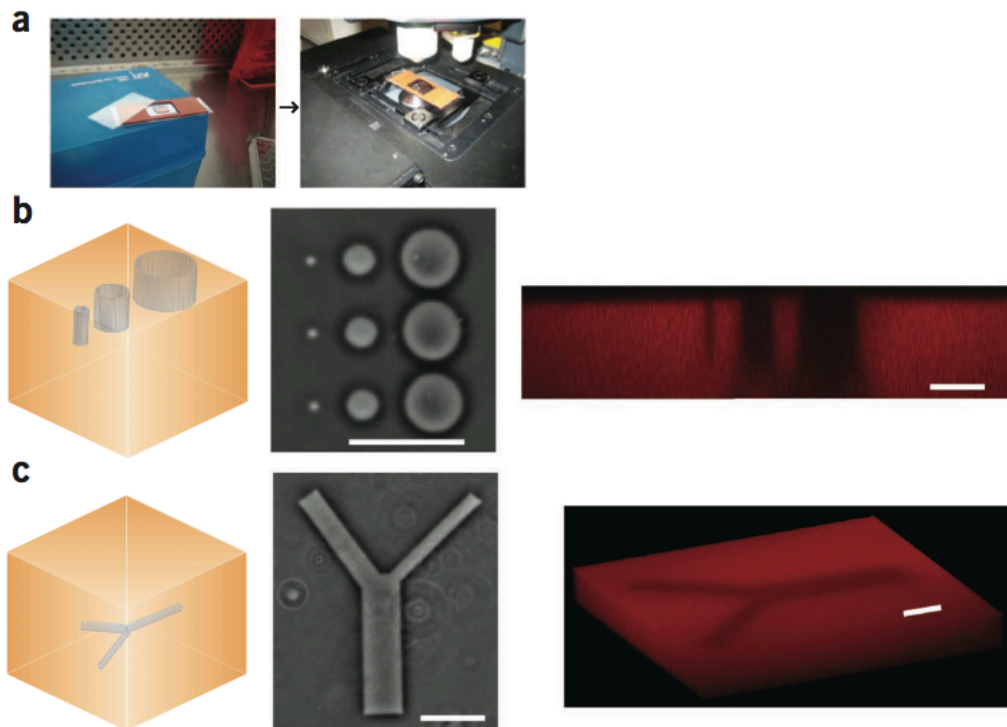


Figure 3.9 3D photopatterning with a confocal microscope. Focused, 405 nm laser light can be used on a confocal microscope to completely erode features within photodegradable hydrogels. **(a)** To maintain sterility the prepared gel is sealed within a liquid filled chamber that fits onto the stage of a confocal microscope. ROI software is used to raster the focal point of the 405 nm laser through defined geometries within photolabile hydrogels. **(b)** Here, cylindrical wells (5, 25, and 50 μm diameter, left to right) are degraded into the surface of a photodegradable gel and imaged in brightfield (middle, scale bar 100 μm) and confocal fluorescence (right, y-cross section, scale bar 50 μm). Such surface features can be used for cell aggregation, studying cell connectivity and migration, and manipulation of cell adhesion. **(c)** Further, channels can be created *within* photodegradable hydrogels on size scales relevant to mammalian cells to study 3D migration and connectivity. Here, we show a bifurcating channel patterned 50 μm below the gel surface as imaged in brightfield (middle, scale bar 100 μm) and confocal fluorescence (right, z-cross section, scale bar 50 μm). Note that there is non-specific degradation in the z-dimension owing to overlapping regions of out-of-focus light.

3.5.4 Timing

Steps 1-3, Synthesis of photolabile group (reaction a), 24 h

Steps 4-12, Synthesis of photolabile group (reaction b), 48 h

Steps 13-16, Synthesis of photolabile group (reaction c), 36 h

Steps 17-19, Synthesis of photolabile group (reaction d), 36 h

Steps 20-24, Synthesis of photodegradable acrylate (reaction e and f), 48 h

Steps 35-38, Synthesis of photodegradable crosslinker (reaction), 48 h

Step 39, Synthesis of photodegradable crosslinker (dialysis), 3 days

Step 40, Synthesis of photodegradable crosslinker (lyophilization), 3 days

Step 41, Synthesis of photoreleasable tether (peptide synthesis), 24 h

Steps 42-46, Synthesis of photoreleasable tether (coupling reaction), 24 h

Steps 47-48, Synthesis of photoreleasable tether (cleavage), 24 h

Steps 49-50, Synthesis of photoreleasable tether (HPLC purification), 24 h

Step 51, Synthesis of photoreleasable tether (lyophilization), 3 days

Steps 52-55, Hydrogel synthesis (acrylation of cover slips), 5-24 h

Steps 56-60, Hydrogel synthesis (hydrogel fabrication), 3 h

Step 61, Hydrogel synthesis (hydrogel rinsing and swelling), 12-24 h

Steps 62-67, Cell encapsulation and viability verification, 24 h

Steps 68-72, Hydrogel degradation (surface gradient formation), 90 min

Steps 73-77, Hydrogel degradation (surface feature formation), 2 h

Steps 78-83, Hydrogel degradation (confocal photopatterning), 3 h

3.5.5 Troubleshooting

Step	Problem	Possible reason	Solution
11	Fine white powder emerges upon mixing of the product with boiling EtOH	Reaction temperature was too low, and incomplete nitration occurred.	Re-start the procedure at Step 4.
12	Multiple re-crystallizations do not lead to pure product	Reaction became too hot and lead to over half of the product being nitrated in the wrong position or multiple positions on the benzyl ring.	Product can be purified by other methods, such as column chromatography, or procedure can be re-started at Step 4.

39	By-product precipitate does not completely settle during centrifugation	Particle size is small and/or remaining NMP in combination with PEG is forming a stable suspension.	Leave at least half of the volume of the dialysis tubing empty and allow dialysis to proceed for longer until solution is translucent.
57 or 58	Gelation occurs before the solution can be pipetted into the mold	Initiator (AP & TEMED) concentrations are too high in the final macromer solution.	Decrease the final concentration of AP & TEMED in the macromer solution while maintaining a 2:1 ratio, respectively.
57 or 58	Gelation fails to occur after 5 min.	Initiator (AP & TEMED) concentrations are too low in the final macromer solution.	Increase the final concentration of AP & TEMED in the macromer solution while maintaining a 2:1 ratio, respectively.

3.6 NMR reference spectra

3.6.1 Synthesis of photolabile group (reaction a)

White solid, ^1H NMR (500 MHz, CDCl_3) δ 7.6 (d, 1H), δ 7.58 (s, 1H), δ 6.92 (d, 1H), δ 4.2 (tm, 4H), δ 3.95 (s, 3H), δ 3.6 (s, 3H), δ 2.58 (t, 2H), δ 2.2 (m, 2H), and δ 1.3 (t, 3H).

3.6.2 Synthesis of photolabile group (reaction b)

Yellow solid, ^1H NMR (500 MHz, CDCl_3) δ 7.62 (s, 1H), δ 6.75 (s, 1H), δ 4.18 (tm, 4H), δ 3.95 (s, 3H), δ 2.55 (t, 2H), δ 2.5 (s, 3H), δ 2.2 (m, 2H), and δ 1.25 (t, 3H).

3.6.3 Synthesis of photolabile group (reaction c)

Yellow solid, ^1H NMR (500 MHz, $(\text{CD}_3)_2\text{SO}$) δ 7.55 (s, 1H), δ 7.4 (s, 1H), δ 5.55 (s, 1H), δ 5.3 (m, 1H), δ 4.1 (tm, 4H), δ 3.95 (s, 3H), δ 2.5 (t, 2H), δ 2.0 (m, 2H), δ 1.4 (d, 3H), and δ 1.2 (t, H).

3.6.4 Photolabile group (reaction d)

Yellow solid, ^1H NMR (500 MHz, $(\text{CD}_3)_2\text{SO}$) δ 12.2 (s, 1H), δ 7.6 (s, 1H), δ 7.4 (s, 1H), δ 5.5 (s, 1H), δ 5.3 (m, 1H), δ 4.1 (t, 2H), δ 3.9 (s, 3H), δ 2.4 (t, 2H), δ 2.0 (m, 2H), and δ 1.4 (d, 3H).

3.6.5 Photodegradable acrylate (reaction e and f)

Orange liquid to crystalline solid (crystallizes upon storage at 4°C), ¹H NMR (500 MHz, (CD₃)₂SO) δ 12.2 (s, 1H), δ 7.6 (s, 1H), δ 7.2 (s, 1H), δ 6.4 (d, 1H), δ 6.35 (m, 1H), δ 6.25 (m, 1H), δ 6.05 (d, 1H), δ 4.1 (t, 2H), δ 3.9 (s, 3H), δ 2.4 (t, 2H), δ 2.0 (m, 2H), and δ 1.4 (d, 3H).

3.6.6 Photodegradable crosslinker

Light yellow powder, ¹H NMR (500 MHz, (CD₃)₂SO) δ 8.0 (t, 1H), δ 7.6 (s, 1H), δ 7.2 (s, 1H), δ 6.4 (d, 1H), δ 6.35 (m, 1H), δ 6.25 (m, 1H), δ 6.05 (d, 1H), δ 4.1 (t, 2H), δ 3.9 (s, 3H), δ 3.5 (m, ~304H), δ 2.75 (t, 2H), δ 2.4 (t, 2H), δ 2.0 (m, 2H), and δ 1.4 (d, 3H).

3.7 References

1. Lutolf, M.P. & Hubbell, J.A. Synthetic biomaterials as instructive extracellular microenvironments for morphogenesis in tissue engineering. *Nat. Biotechnol.* **23**, 47-55 (2005).
2. Liu, S.Q. et al. Synthetic hydrogels for controlled stem cell differentiation. *Soft Matter* **6**, 67-81 (2010).
3. Tibbitt, M.W. & Anseth, K.S. Hydrogels as Extracellular Matrix Mimics for 3D Cell Culture. *Biotechnol. Bioeng.* **103**, 655-663 (2009).
4. Guilak, F. et al. Control of Stem Cell Fate by Physical Interactions with the Extracellular Matrix. *Cell Stem Cell* **5**, 17-26 (2009).
5. Hwang, N.S., Varghese, S. & Elisseeff, J. Controlled differentiation of stem cells. *Adv. Drug Deliv. Rev.* **60**, 199-214 (2008).
6. Wolf, K. et al. Multi-step pericellular proteolysis controls the transition from individual to collective cancer cell invasion. *Nat. Cell Biol.* **9**, 893-U839 (2007).
7. Tayalia, P., Mendonca, C.R., Baldacchini, T., Mooney, D.J. & Mazur, E. 3D Cell-Migration Studies using Two-Photon Engineered Polymer Scaffolds. *Adv. Mater.* **20**, 4494-4498 (2008).
8. Kloxin, A.M., Kasko, A.M., Salinas, C.N. & Anseth, K.S. Photodegradable Hydrogels for Dynamic Tuning of Physical and Chemical Properties. *Science* **324**, 59-63 (2009).

9. Jay, S.M. & Saltzman, W.M. Shining light on a new class of hydrogels. *Nat. Biotechnol.* **27**, 543-544 (2009).
10. Lutolf, M.P. Spotlight on hydrogels. *Nat. Mater.* **8**, 451-453 (2009).
11. Yu, H.T., Li, J.B., Wu, D.D., Qiu, Z.J. & Zhang, Y. Chemistry and biological applications of photo-labile organic molecules. *Chem. Soc. Rev.* **39**, 464-473 (2010).
12. Holmes, C.P. Model studies for new o-nitrobenzyl photolabile linkers: Substituent effects on the rates of photochemical cleavage. *Journal Of Organic Chemistry* **62**, 2370-2380 (1997).
13. Akerblom, E.B., Nygren, A.S. & Agback, K.H. Six new photolabile linkers for solid-phase synthesis. 1. Methods of preparation. *Mol. Divers.* **3**, 137-148 (1998).
14. Zhao, Y.R. et al. New caged coumarin fluorophores with extraordinary uncaging cross sections suitable for biological imaging applications. *Journal Of The American Chemical Society* **126**, 4653-4663 (2004).
15. Alvarez, M. et al. Single-Photon and Two-Photon Induced Photocleavage for Monolayers of an Alkyltriethoxysilane with a Photoprotected Carboxylic Ester. *Adv. Mater.* **20**, 4563-4567 (2008).
16. Pelliccioli, A.P. & Wirz, J. Photoremovable protecting groups: reaction mechanisms and applications. *Photochem. Photobiol. Sci.* **1**, 441-458 (2002).
17. Deiters, A. Principles and Applications of the Photochemical Control of Cellular Processes. *ChemBioChem* **11**, 47-53 (2010).
18. Luo, Y. & Shoichet, M.S. A photolabile hydrogel for guided three-dimensional cell growth and migration. *Nat. Mater.* **3**, 249-253 (2004).
19. Wosnick, J.H. & Shoichet, M.S. Three-dimensional chemical Patterning of transparent hydrogels. *Chem. Mat.* **20**, 55-60 (2008).
20. Ohmuro-Matsuyama, Y. & Tatsu, Y. Photocontrolled cell adhesion on a surface functionalized with a caged arginine-glycine-aspartate peptide. *Angew. Chem.-Int. Edit.* **47**, 7527-7529 (2008).
21. Nakanishi, J. et al. Spatiotemporal control of cell adhesion on a self-assembled monolayer having a photocleavable protecting group. *Anal. Chim. Acta* **578**, 100-104 (2006).
22. Johnson, J.A., Finn, M.G., Koberstein, J.T. & Turro, N.J. Synthesis of photocleavable linear macromonomers by ATRP and star macromonomers by a tandem ATRP-Click reaction: precursors to photodegradable model networks. *Macromolecules* **40**, 3589-3598 (2007).

23. Johnson, J.A., Baskin, J.M., Bertozzi, C.R., Koberstein, J.T. & Turro, N.J. Copper-free click chemistry for the in situ crosslinking of photodegradable star polymers. *Chemical Communications*, 3064-3066 (2008).
24. Kikuchi, Y. et al. Grafting Poly(ethylene glycol) to a Glass Surface via a Photocleavable Linker for Light-induced Cell Micropatterning and Cell Proliferation Control. *Chem. Lett.* **37**, 1062-1063 (2008).
25. Frey, M.T. & Wang, Y.L. A photo-modulatable material for probing cellular responses to substrate rigidity. *Soft Matter* **5**, 1918-1924 (2009).
26. Kloxin, A.M., Benton, J.A. & Anseth, K.S. In situ elasticity modulation with dynamic substrates to direct cell phenotype. *Biomaterials* **31**, 1-8 (2010).
27. Kloxin, A.M., Tibbitt, M.W., Kasko, A.M., Fairbairn, J.F. & Anseth, K.S. Tunable hydrogels for external manipulation of cellular microenvironments through controlled photodegradation. *Adv. Mater.* **22**, 61-66 (2010).
28. Engler, A.J., Sen, S., Sweeney, H.L. & Discher, D.E. Matrix elasticity directs stem cell lineage specification. *Cell* **126**, 677-689 (2006).
29. Chowdhury, F. et al. Material properties of the cell dictate stress-induced spreading and differentiation in embryonic stem cells. *Nat. Mater.* **9**, 82-88 (2010).
30. Wong, J.Y., Velasco, A., Rajagopalan, P. & Pham, Q. Directed movement of vascular smooth muscle cells on gradient-compliant hydrogels. *Langmuir* **19**, 1908-1913 (2003).
31. Khetan, S., Katz, J.S. & Burdick, J.A. Sequential crosslinking to control cellular spreading in 3-dimensional hydrogels. *Soft Matter* **5**, 1601-1606 (2009).
32. Gillette, B.M., Jensen, J.A., Wang, M.X., Tchao, J. & Sia, S.K. Dynamic Hydrogels: Switching of 3D Microenvironments Using Two-Component Naturally Derived Extracellular Matrices. *Adv. Mater.* **22**, 686 (2010).
33. Murayama, S. & Kato, M. Photocontrol of Biological Activities of Protein by Means of a Hydrogel. *Analytical Chemistry* **82**, 2186-2191 (2010).
34. Benoit, D.S.W., Nuttelman, C.R., Collins, S.D. & Anseth, K.S. Synthesis and characterization of a fluvastatin-releasing hydrogel delivery system to modulate hMSC differentiation and function for bone regeneration. *Biomaterials* **27**, 6102-6110 (2006).
35. Salinas, C.N. & Anseth, K.S. The enhancement of chondrogenic differentiation of human mesenchymal stem cells by enzymatically regulated RGD functionalities. *Biomaterials* **29**, 2370 (2008).

36. Wong, D.Y., Griffin, D.R., Reed, J. & Kasko, A.M. Photodegradable Hydrogels to Generate Positive and Negative Features over Multiple Length Scales. *Macromolecules* **43**, 2824-2831 (2010).
37. Yeo, W.S. & Mrksich, M. Electroactive self-assembled monolayers that permit orthogonal control over the adhesion of cells to patterned substrates. *Langmuir* **22**, 10816-10820 (2006).
38. Yamato, M. et al. Temperature-responsive cell culture surfaces for regenerative medicine with cell sheet engineering. *Prog. Polym. Sci.* **32**, 1123-1133 (2007).
39. Williams, C. et al. Aligned Cell Sheets Grown on Thermo-Responsive Substrates with Microcontact Printed Protein Patterns. *Adv. Mater.* **21**, 2161 (2009).
40. Mohammed, J.S. & Murphy, W.L. Bioinspired Design of Dynamic Materials. *Adv. Mater.* **21**, 2361-2374 (2009).
41. Nowatzki, P.J., Franck, C., Maskarinec, S.A., Ravichandran, G. & Tirrell, D.A. Mechanically tunable thin films of photosensitive artificial proteins: Preparation and characterization by nanoindentation. *Macromolecules* **41**, 1839-1845 (2008).
42. Andreopoulos, F.M. & Persaud, I. Delivery of basic fibroblast growth factor (bFGF) from photoresponsive hydrogel scaffolds. *Biomaterials* **27**, 2468-2476 (2006).
43. Trenor, S.R., Shultz, A.R., Love, B.J. & Long, T.E. Coumarins in polymers: From light harvesting to photo-cross-linkable tissue scaffolds. *Chem. Rev.* **104**, 3059-3077 (2004).
44. Nuttelman, C.R., Tripodi, M.C. & Anseth, K.S. In vitro osteogenic differentiation of human mesenchymal stem cells photoencapsulated in PEG hydrogels. *J. Biomed. Mater. Res. Part A* **68A**, 773-782 (2004).
45. Salinas, C.N. & Anseth, K.S. The influence of the RGD peptide motif and its contextual presentation in PEG gels on human mesenchymal stem cell viability. *J. Tissue Eng. Regen. Med.* **2**, 296-304 (2008).
46. Salinas, C.N., Cole, B.B., Kasko, A.M. & Anseth, K.S. Chondrogenic differentiation potential of human mesenchymal stem cells photoencapsulated within poly(ethylene glycol)-arginine-glycine-aspartic acid-serine thiol-methacrylate mixed-mode networks. *Tissue Eng.* **13**, 1025-1034 (2007).
47. Chan, W.C. & White, P.D. (eds.) Fmoc Solid Phase Peptide Synthesis. (Oxford University Press, Inc., New York; 2000).

CHAPTER IV

MODELING CONTROLLED PHOTODEGRADATION IN OPTICALLY THICK HYDROGELS

Under review at *Journal of Polymer Science Part A: Polymer Chemistry*, Fall 2012

4.1 Abstract

There is a growing interest in developing dynamically responsive hydrogels whose material properties are modulated by environmental cues, including with light. These photoresponsive hydrogels afford spatiotemporal control of material properties through an array of photoaddition and photodegradation reactions. For photoresponsive hydrogels to be utilized most effectively in a broad range of applications, the photoreaction behavior should be well understood, enabling the design of dynamic materials with uniform or anisotropic material properties. Here, a general statistical-kinetic model has been developed to describe controlled photodegradation in hydrogel polymer networks containing photolabile crosslinks. The heterogeneous reaction rates that necessarily accompany photochemical reactions were described by solving a system of partial differential equations that quantify the photoreaction kinetics in the material. The kinetics were coupled with statistical descriptions of network structure in chain polymerized hydrogels to model material property changes and mass loss that occur during the photodegradation process. Finally, the physical relevance of the model was demonstrated by

comparing model predictions with experimental data of mass loss and material property changes in photodegradable, PEG-based hydrogels.

4.2 Introduction

Hydrogels comprise a class of hydrophilic, crosslinked polymers that are useful in a broad range of applications owing to their facile synthesis, biocompatibility, tailorability for transport of both low and high molecular weight molecules, as well as robust physical properties.¹ Currently, there is an interest in developing dynamically responsive hydrogels whose material properties can be modulated in time by environmental cues, enabling complex spatial and temporal control of the chemistry and structure of the gels. Responsive hydrogel networks are being exploited to engineer improved drug delivery vehicles,² cell culture scaffolds for regenerative medicine,^{3,4} biosensors,⁵ and actuators in microfluidic devices.⁶ Within this paradigm, researchers have developed a unique class of *photo*responsive hydrogels that provide the experimenter with spatiotemporal control over the chemical and physical properties of the gels through photoaddition and photodegradation reactions.⁷⁻¹⁵

Degradation reactions are employed to modulate physical properties of hydrogels in time and is achieved most typically through the incorporation of hydrolytically or enzymatically degradable moieties within the hydrogel network backbone.¹⁶ Cleavage of the degradable moieties breaks elastically active strands within the network, forms soluble degradation products, and, ultimately, causes erosion of the gel. As a general characterization, each bond that is degraded within the network leads to a decrease in the local crosslinking density with a concomitant decrease in modulus and an increase in water swelling. Once a sufficient fraction of local crosslinks is degraded, erosion occurs within the network resulting in mass loss and

changes in the geometry of the gel. Throughout this article, the terms degradation and erosion arise frequently; degradation refers to the reaction that cleaves an individual covalent bond, while erosion refers to the local depletion of mass from the network caused by degradation.^{17,18}

Hydrolytically and enzymatically degradable hydrogels are both effective in a broad range of applications,¹⁹ but they are limited in that the degradation kinetics are governed by the initial chemistry and offer little control over material property evolution post-fabrication. As an alternative approach and one that enables new opportunities for dynamic material property control, photodegradable hydrogels have been engineered that contain photolabile bonds within the network crosslinks, which can be cleaved upon absorbance of light. This unique approach to hydrogel fabrication allows the experimenter to modulate the physical properties of the gel in both space and time exogenously through controlled irradiation. On the molecular level, hydrogels are rendered photodegradable by incorporating specific photocleavable moieties (*e.g.*, nitrobenzyl ether or coumarin) into the macromolecular precursors that comprise the gel network. After formation, these photoactive moieties reside in the network backbone and can be cleaved irreversibly when photons of the appropriate wavelength are absorbed. Through this process, light is employed to degrade bonds within the material, leading to changes in the gel's modulus and swelling ratio, and, ultimately, to erode the gel. Such systems afford opportunities for innovative experiments to better understand how hydrogel degradation influences desired material properties, as well as offering unprecedented spatiotemporal control of the network structure in real-time.

Several photodegradable hydrogels have been developed^{7,8} and employed as cell culture platforms,^{9-13,20,21} drug delivery vehicles,^{15,22,23} and photolithographic materials.¹⁴ Initially, Turro and coworkers synthesized photodegradable polymer networks via click-chemistry

demonstrating the utility of light to tune material properties.^{7,8} Anseth and coworkers and Wang and coworkers extended this paradigm to demonstrate that light can be used to tune the modulus of photolabile hydrogels in real time to control fibroblast activation²¹ or migration¹¹, as well as mesenchymal stem cell morphology.^{12,20} Further, Kasko and coworkers utilized photodegradable hydrogels as photolithographic materials.²⁴ A separate class of photodegradable gels has been developed that are comprised of photolabile bonds, which are reversible with low wavelength UV light ($\lambda = 254$ nm), and these gels have been applied for drug delivery.^{25,26} In each of these investigations, thorough characterization of the material in use allowed the experimenters to describe the light induced changes to the hydrogel's properties via controlled light presentation.

However, for photoresponsive hydrogels to be utilized most effectively in a broad range of applications, the degradation behavior should be described *a priori*. A general class of statistical-kinetic models for degradation in hydrolytically and enzymatically degradable hydrogels has been developed that integrates cleavage kinetics with network structural information to predict material property changes during degradation.^{17,18,27,28} The goal of the current investigation is to develop a generalized and comprehensive, statistical-kinetic model of hydrogel photodegradation to provide a method to describe and predict light induced changes in the properties of photodegradable hydrogels. In this manner, the concomitant alterations in material properties caused by irradiation can be better understood, predicted, and manipulated to accelerate the design of unique cell culture scaffolds, delivery vehicles, high performance elastomers, and more complex photoresponsive hydrogels.

4.3 Materials and Methods

All chemical reagents were purchased from Sigma Aldrich except as otherwise noted.

4.3.1 Synthesis of nitrobenzyl ether photolabile moiety

The photolabile moiety, ethyl 4-(4-(1-hydroxyethyl)-2-methoxy-5-nitrophenoxy)butanoic acid was prepared as previously described.²⁹ In short, acetovanillone (200 mmol) and ethyl 4-bromobutyrate (240 mmol) were dissolved in 150 ml of dimethyl formamide and then potassium carbonate (300 mmol) was added. The reaction was stirred overnight, precipitated in water, and filtered to recover the ketone product. The ketone product (100 mmol) was nitrated using nitric acid (75 mL) that was added to the ketone at 0°C and reacted for 1 h off ice, ensuring that the temperature of the reaction remained below 35°C for the duration of the reaction. The nitrated product was precipitated in water, filtered, recrystallized from ethanol, and desiccated overnight. The nitrated ketone product (50 mmol) was reduced to an alcohol in ethanol (100 mL) by reacting with sodium borohydride (31 mmol) at 40°C. The reaction was stirred until the product dissolved completely; quenched with methanol (~ 1 mL); and precipitated in water, filtered, and desiccated overnight. The nitrated alcohol (50 mmol) was then reacted with potassium hydroxide (75 mmol) in a THF and water blend to deprotect the carboxylic acid. Upon completion, the reaction mixture was cooled, filtered, washed with water, and desiccated to recover the nitrobenzyl ether photolabile moiety. Product purity was confirmed by proton nuclear magnetic resonance (¹H NMR, Varian Inova 400 NMR Spectrometer).

4.3.2 Acrylation of nitrobenzyl ether photolabile moiety

The photolabile moiety was acrylated as previously described.²⁹ The photolabile moiety (20 mmol) was suspended in anhydrous dichloromethane (180 mL) and stirred in a round bottom flask with triethylamine (82 mmol). Acryloyl chloride (66 mmol) in anhydrous dichloromethane (54 mL) was added dropwise at 0°C. The reaction mixture was stirred overnight at room

temperature and then washed with sodium bicarbonate (5 w/v% aq.), dilute hydrochloric acid (1 v/v% aq.), and deionized water. Excess dichloromethane was evaporated and the liquid product was dissolved in a 50:50 acetone:water solution (~ 500 mL). This solution was stirred overnight at room temperature and filtered to remove insoluble impurities. The product was extracted with dichloromethane and washed with dilute hydrochloric acid (1 v/v% aq.) and deionized water, dried over sodium sulfate, and the remaining dichloromethane was evaporated to leave behind the acrylated photolabile moiety (PDA). Product purity was confirmed by proton nuclear magnetic resonance (^1H NMR, Varian Inova 400 NMR Spectrometer).

4.3.3 Synthesis of photolabile crosslinker

The photolabile crosslinker was synthesized and purified as previously described.²⁹ The acrylated photolabile moiety (PDA, 8 mmol) was dissolved in anhydrous *N*-methyl-2-pyrrolidone (150 mmol). The standard solid-state peptide synthesis coupling agent HATU (Anaspec, 8.8 mmol) was added with diisopropylethylamine (14 mmol) and stirred for 5 minutes before PEG bisamine (Laysan Bio.; 1 mmol) in minimal NMP (~100 mmol) was added to the reaction. Upon complete dissolution of the reactants, the mixture was stirred overnight, precipitated in diethyl ether at 0°C, and centrifuged to collect the product. The precipitate was desiccated under vacuum, redissolved in deionized water, dialyzed (SpectraPor 7, MWCO 1000 g/mol), and lyophilized to recover the photolabile crosslinker (PEGdiPDA). Product purity was confirmed by proton nuclear magnetic resonance (^1H NMR, Varian Inova 400 NMR Spectrometer).

4.3.4 Synthesis of photolabile hydrogels

Stock solutions of the redox initiator ammonium persulfate (AP), base catalyst tetramethylethylenediamine (TEMED), co-monomer PEGA, and photolabile crosslinker (PEGdiPDA) were formed in water at 2 M, 2M, 40 wt%, and 20 wt%, respectively. Solutions were prepared from these stocks to produce a total of 15 wt% total polymer in water and 0.2 M AP. In experiments where imaging was necessary, a methacrylated rhodamine (300 μ M) was added to the pre-hydrogel solution. The pre-hydrogel solution was vortexed while TEMED (0.1 M) was added and quickly transferred to the gel-forming mold. The liquid solution was polymerized for 5 minutes, which corresponds to complete polymerization as determined by rheometry. Gels were polymerized between rubber gaskets at varying thickness from 100 μ m to 1500 μ m or on a parallel plate rheometer (TA, Ares) with a thickness of 50 μ m.

4.3.5 Measurement of molar absorptivities

The molar absorptivities of the *o*-nitrobenzyl ether (NBE) and the nitrobenzyl cleavage product (NBP) were calculated using a UV-visible spectrophotometer (Lambda 40 UV/Vis Spectrometer, Perkin Elmer) in a mixture of DI water and dimethyl sulfoxide (DMSO). The molar absorptivity of NBE was measured prior to irradiation. The sample was then irradiated ($\lambda = 365$ nm; $I_0 = 10$ mW/cm²) and the molar absorptivity of NBP was measured.

4.3.6 Measurement of quantum yield via photorheometry

To determine the kinetic constants of photolysis in PEGdiPDA hydrogels, thin films ($z = 50$ μ m) were polymerized *in situ* on a parallel plate photorheometer (TA, Ares). After complete polymerization, the hydrogel was surrounded by water to maintain hydration and then photodegraded ($\lambda = 365$ nm or 405 nm; $I_0 = 10$ mW/cm² or 25 mW/cm², respectively). The shear

component of the gel's storage modulus (G') was measured as a function of irradiation time, t . A characteristic kinetic constant for photolysis, k , was determined by linear regression of this data ($0.5 \leq G'/G'_0 \leq 1$) based on gel mechanical theories, degradation kinetics, and photolysis kinetics.^{10,20,29} The following was used to calculate k :

$$\ln\left(\frac{G'}{G'_0}\right) = -2kt$$

where t is the irradiation time; G'_0 is the initial shear component of the gel's storage modulus; and the factor of 2 arises from the structure of the monomer containing two photolabile linkers.

The quantum yield, φ , can be calculated from the characteristic kinetic constant as

$$\varphi = 10^6 \frac{kN_A hc}{\epsilon \lambda I_0}$$

where N_A is Avagadro's constant; h is Planck's constant; c is the speed of light; ϵ is the molar absorptivity of the NBE at the wavelength of irradiation; λ is the wavelength of irradiation; and I_0 is the irradiation intensity.³⁰

4.3.7 Measurement of quantum yield via NMR

To confirm the quantum yield measurements for 365 nm irradiation, the quantum yield was also determined by NMR analysis of degradation of the NBE moiety. Characteristic ring peaks in the NBE shift dramatically upon degradation, which can be quantified to track the kinetics of degradation as a function of time. Dilute PEGdiPDA solutions were irradiated ($\lambda = 365$ nm; $I_0 = 10$ mW/cm²) for 1, 2, 3, 5, 10, 20, and 30 minutes each. A characteristic kinetic constant for photolysis, k , was determined by linear regression of the intact NBE concentration versus time. The following was used to calculate k :

$$\ln\left(\frac{C}{C_0}\right) = -kt$$

where C is the concentration of NBE moieties; C_0 is the initial concentration of NBE moieties; and t is the irradiation time. As before, the quantum yield, φ , can be calculated from the characteristic kinetic constant as

$$\varphi = 10^6 \frac{kN_A hc}{\epsilon \lambda I_0}$$

where N_A is Avagadro's constant; h is Planck's constant; c is the speed of light; ϵ is the molar absorptivity of the NBE at the wavelength of irradiation; λ is the wavelength of irradiation; and I_0 is the irradiation intensity. For practical purposes solution NMR studies of the degradation rate were employed to model degradation rates in the gel network, but as the PEGdiPDA molecule resides in a highly swollen polymer network mobility constraints should not strongly influence the quantum yield and solution studies should approximate in gel reaction kinetics.

4.3.8 Fractional mass loss of PEGdiPDA hydrogels

Data for the fractional mass loss of PEGdiDPA hydrogels exposed to 365 nm irradiation (Fig. 5a) was reported previously in ref. 20, and new results at 405 nm irradiation are added to this data. For fractional mass loss, PEGdiPDA hydrogels ($[NBE] = 0.04$ or 0.058 M; $z = 1500$ μm) were exposed to collimated surface irradiation ($\lambda = 365$ or 405 nm; $I_0 = 20.0 \pm 1.0$ or 25.0 ± 1.0 mW cm^{-2} , respectively). At each time point, three gels were removed from the light and lyophilized and weighed. Fractional mass loss was calculated as the normalized mass at each time point.²⁰

4.3.9 Channel patterning in PEGdiPDA hydrogels

Data for the channel patterning in PEGdiPDA hydrogels (Fig. 5c) was reported previously in ref. 20. Briefly, channels were generated in PEGdiPDA hydrogels ($[NBE] = 0.04$ M; $z = 500$ μm) via photolithography ($\lambda = 365$ nm; $I_0 = 10.0 \pm 0.5$ mW cm^{-2} ; 400 μm wide black lines separated by 400 μm wide transparent lines; Mask Aligner, Optical Associates Inc., Model J500) for different times (5 – 30 min) to form channels within the gel through photoerosion. Irradiation was conducted with the gel just below the photomask and surrounded by PBS to facilitate dissolution of erosion products into a surrounding sink during degradation. Channels were measured quantitatively via profilometry (Style Profiler, Dektak 6M) and visually confirmed via confocal LSM (Zeiss 710 NLO LSM) on cross-sections of the gel.²⁰

4.3.10 Surface gradient patterning in PEGdiPDA hydrogels

Data for the gradient in the elastic modulus (Young's modulus, E) along the surface of PEGdiPDA (Fig. 5d) was reported previously in ref. 20. Briefly, the gradient was generated by exposing the surface of a PEGdiPDA hydrogel ($[NBE] = 0.04$ M; $z \sim 200$ μm) to collimated irradiation ($\lambda = 365$ nm; $I_0 = 10.0 \pm 0.5$ mW cm^{-2}) in a gradient fashion. The gradient of light was achieved by continuously occluding the hydrogel surface with an opaque substrate from the initial side (0 mm) to the final side (9 mm) linearly over the course of 5 minutes. The surface gradient was then measured with AFM (PicoPlusTM scanning probe microscope; Molecular Imaging, Inc.; pyramidal silicon nitride tip with force constant 0.12 N/m, radius = 10 nm, height = 2.5-3.5 nm, and angle of pyramid = 35°) and fitting data to a Hertz model with $\nu \sim 0.2$ for the surface of PEG hydrogel.²⁰

4.3.11 Model calculations

The model was written and executed in MATLAB (Mathworks) with a spatial step size, Δz , of 100 nm and a temporal step size, Δt , of 10 ms. At each temporal node, the z-dependent light intensity profile was solved by Euler integration of the Beer-Lambert law (Eq. 1) over the whole spatial grid. Then, the extents of cleavage of *o*-nitrobenzyl ether and generation of the cleavage product were calculated through Euler integration of Eqs. 2 & 3, utilizing the light intensity profile for the current temporal node, to update the concentration profiles for the photoactive species. This iterative numerical method was repeated to generate the spatiotemporally varying light intensity and concentration profiles through the depth of the gel at each discrete time step. The fidelity of the numerical method was verified in the manner of Miller *et al.*³¹ by comparing calculations to analytic solutions from Wegscheider.^{32,33}

4.4 Model Development

4.4.1 Modeling Light Intensity and Photoactive Species Profiles

A statistical-kinetic model of photodegradation was developed that combines the kinetics of photocleavage reactions with statistical, mean-field descriptions of network connectivity to calculate mass loss in chain polymerized, photodegradable networks. The photodegradation process relies on photochemical reactions whose rates are heterogeneous in both space and time,³³ making descriptions of light-induced material property changes difficult. This hallmark of photochemical reactions occurs because the local reaction rate is proportional to the product of the local concentration of the photoactive species and the local intensity of light.³³ Since photons must be absorbed for reaction to occur, light intensity becomes optically attenuated in photoresponsive networks, causing intensity to be a function of position. Furthermore, the

products of most photodegradation reactions possess different molar extinction coefficients than the reactants while erosion of the material removes absorbers from the light path. Both of these phenomena alter the absorptivity of the light path as the reaction progresses, modulating the light intensity profile and, thus, the reaction rate with time. In this manner, optical attenuation produces both spatial and temporal variation in the light intensity profiles, local photodegradation rates, and species concentration profiles.

To model these heterogeneities, one needs to solve a system of coupled partial differential equations that describes the local light intensity and local photoactive species concentrations as functions of both space and time. The Beer-Lambert law was employed to quantify the spatiotemporally varying light intensity profile.

$$\frac{\partial I(z,t)}{\partial z} = -2.3I(z,t) \sum_i \varepsilon_i [C_i](z,t) \quad \text{Eq. 1}$$

Here, $I(z,t)$ is the local irradiation intensity (W cm^{-2}) at a given depth in the gel, z , and a given time, t ; ε_i is the molar absorptivity ($\text{L mol}^{-1} \text{cm}^{-1}$) of the i -th photoactive species in the system for the wavelength of degradation; and $[C_i]$ is the local concentration (mol L^{-1}) of the i -th photoactive species in the system. The incident irradiation was assumed to be constant throughout the time course of degradation so that

$$I(0, t) = I_0$$

The photocleavage reaction was modeled with first-order kinetics such that the local rate of photoreaction and concentration of photoactive species, $[C_i](z,t)$, is described by

$$\frac{\partial [C_i](z,t)}{\partial t} = -\frac{\varphi \varepsilon_i \lambda}{N_A h c} [C_i](z,t) I(z,t) \quad \text{Eq. 2}$$

In this equation, φ is the quantum yield (unitless) for the cleavage reaction of i -th photoactive species for the wavelength of irradiation; ε_i is the molar absorptivity ($\text{L mol}^{-1} \text{cm}^{-1}$) of i -th photoactive species for the wavelength of irradiation; N_A is Avagadro's number (mol^{-1}); h is the

Planck constant ($m^2 \text{ kg s}^{-1}$); c is the speed of light ($m \text{ s}^{-1}$); and λ is the wavelength of irradiation (m). For every cleavage event there is a one-to-one generation of cleavage product(s) described by

$$\frac{\partial [C_j](z,t)}{\partial t} = \frac{\varphi \varepsilon_i \lambda}{N_A h c} [C_i](z,t) I(z,t) \quad \text{Eq. 3}$$

Here, $[C_j](z,t)$ is the concentration (mol L^{-1}) of the j -th cleavage product corresponding to the i -th photoactive species. The rate of generation of the cleavage product(s) is equal and opposite to the consumption of the photoactive species. Note that the molar absorptivity of the cleavage products must be taken into account in Eq. 1 as they can contribute significantly to the attenuation of light. It was assumed that all photoactive species concentrations were initially uniform throughout the material and that all photoactive species were initially intact, so that

$$[C_i](z,0) = C_{i,0}$$

$$[C_j](z,0) = 0$$

Eqs. 1-3 and the corresponding boundary conditions comprise a set of coupled partial differential equations that describe the kinetics of photodegradation as a function of both space and time.^{8,31,33} To calculate the light intensity and concentration profiles at each point in space and time, finite element methods were employed to solve this system of coupled equations numerically. Previous studies in optically thick films have presented models of non-uniform photochemical reactions in both bleaching photopolymerizations and photorelease of small molecules.^{21,22,31,33} These analyses similarly accounted for the complex dynamics between light attenuation and photochemical reactions by solving a similar series of partial differential equations that describe the attenuation of light and the kinetics of photoreactions. This work uniquely extends this framework to model material property changes and mass loss in chain polymerized photodegradable hydrogels.^{10,11}

4.4.2 PEGdiPDA photodegradable hydrogels

The purpose of this work is to describe a general framework to model photodegradation in swollen hydrogels using a minimum number of measurable parameters that describe the system of interest. In this manner, the methodology can be extended to a range of photodegradable hydrogels or non-swollen networks for which the governing physical parameters can be determined. In this work, a general photodegradation model is developed and applied to describe the degradation and erosion behavior for a specific photodegradable hydrogel, originally presented by Kloxin *et al.*^{10,12,20,29} Further, model predictions are compared to experimental results to demonstrate the physical relevance of the model.

Poly(ethylene glycol) diphotodegradable acrylate (PEGdiPDA) hydrogels were formed through a redox-initiated, free-radical chain polymerization of the crosslinker, PEGdiPDA, with PEGA (poly(ethylene glycol) monoacrylate) under aqueous conditions (Figure 1a). The incorporation of an *o*-nitrobenzyl ether (NBE) into the crosslinking molecule PEGdiPDA renders the hydrogels photodegradable, as the NBE is susceptible to irreversible cleavage in response to one-photon ($\lambda \sim 320\text{-}436\text{nm}$) or two-photon ($\lambda \sim 740\text{nm}$) irradiation.^{25,26,29}

For the PEGdiPDA hydrogel system, there are only two photoactive species, NBE and the single nitrobenzyl cleavage product NBP. The molar absorptivity of each of these compounds was quantified previously over the range of irradiation wavelengths (Figure 1c).^{17,18,27-29} Eq. 2 governed the rate of photocleavage and concentration profile of the single photolabile moiety, NBE. As the NBE species was cleaved, there was a one-to-one generation of the cleavage product, NBP, governed by Eq. 3. It was assumed that the NBE species concentration was initially uniform throughout the hydrogel and that all NBE moieties were initially intact, so that

$$[\text{NBE}](z, 0) = [\text{NBE}]_0$$

$$[\text{NBP}](z, 0) = 0$$

4.4.3 Statistical model of degradation and erosion in the gel

To extend this kinetic modeling to predict mass loss and erosion from PEGdiPDA gels, light intensity profiles (Eq. 1) and reaction kinetics (Eqs. 2 & 3) were employed to quantify the concentration of intact NBE species at any point in space and time. The concentration of intact NBE moieties was then combined with statistical descriptions of network connectivity to model the crosslinking density, mass loss, and erosion in the gel during the degradation process. Since this work focuses on modeling degradation in PEGdiPDA networks that are formed from the chain polymerization of telechelic monomers, the appropriate statistical descriptions of chain polymerized hydrogels are employed.^{17,18,27,29} However, the general approach is broad, and the model presented here can be extended to describe photodegradable gels that are formed by step-growth or mixed-mode polymerizations by incorporating the appropriate statistical descriptions of these networks, described elsewhere.^{18,28,29}

To predict network property evolution in PEGdiPDA hydrogels, the spatially and temporally varying concentration profile of intact NBE, $[\text{NBE}](z, t)$, calculated by the iterative numerical method, was combined with a statistical description of chain polymerized network connectivity. This approach relied on a mean-field approximation and fundamental probability statements that correlate cleavage of NBE moieties with the degradation of crosslinks in the gel, release of network fragments, and, ultimately, erosion of the material. The probability that a given NBE moiety has been cleaved, $P(z, t)$, was related to the local fraction of intact NBE species

$$P(z, t) = 1 - \frac{[\text{NBE}](z, t)}{[\text{NBE}]_0(z, t)} \quad \text{Eq. 4}$$

where $[\text{NBE}]_0$ is the initial concentration of NBE in the network. Mass loss was approximated in this model by calculating the probability that specific species were released, which is no longer bound to the gel backbone, based on the probability of NBE cleavage (Eq. 4) and a mathematical description of the hydrogel network structure. While a wide range of different molecular weight species can be released from the gel during mass loss, it was approximated that the dominant mass loss would be from three main erosion products, following the work of Metters *et al.* and Reddy *et al.*^{17,18,29} The three dominant erosion products, for which release was explicitly modeled were (i) free PEGdiPDA crosslinks, (ii) poly(acrylate) kinetic chains, and (iii) poly(acrylate) kinetic chains with pendant PEGdiPDA crosslinks (Figure 1d).

As Metters *et al.* demonstrated, it is convenient to calculate the state of the crosslinks to model the release of the erosion products from these chain polymerized hydrogels.^{10,17,20,29} Each PEGdiPDA crosslink can exist in one of three states: (1) an intact crosslink, in which both NBE moieties are intact, (2) a crosslink dangling from a poly(acrylate) kinetic chain, in which one NBE moiety is cleaved and the other intact, and (3) free crosslink, in which both NBE moieties have been cleaved. The fraction of PEGdiPDA crosslinks in each of these three states was calculated from the probability that a given NBE moiety has been cleaved, $P(z, t)$.

(1) Fraction of intact crosslinks

$$f_1(z, t) = (1 - P(z, t))^2 \quad \text{Eq. 5}$$

(2) Fraction of dangling crosslinks

$$f_2(z, t) = 2P(z, t)(1 - P(z, t)) \quad \text{Eq. 6}$$

(3) Fraction of free crosslinks

$$f_3(z, t) = P(z, t)^2 \quad \text{Eq. 7}$$

Note that $f_1(z,t)$ can be used to calculate the crosslinking density (ρ_x) as a function of space and time directly: $\rho_x(z,t) = f_1(z,t) \cdot \rho_{x,0}$.

The fractional populations of PEGdiPDA crosslinks, Eqs 5-7, were combined with the connectivity of the network to predict mass loss from the network. For chain-growth hydrogels, the key connectivity parameter is the average number, N , of crosslinks per kinetic chain. It is important to note that crosslinks can exist as loops or dangling ends in the initial gel formation and N only accounts for the number of fully intact crosslinks per kinetic chain. For a poly(acrylate) kinetic chain to be released directly from the network as a type (ii) or (iii) erosion product, all of the crosslinks connected to it must exist in state (2) or (3), i.e., none of the crosslinks attached to the kinetic chain remain intact.^{17,18,30}

As mentioned above, this assumes that larger molecular weight species, such as a PEGdiPDA molecule with two kinetic chains at both ends, were not released from the material. While these other species can have high molecular weights and contribute significantly to mass loss when released, release only occurs appreciably at late time points in the degradation, and their release is captured by the reverse gelation condition, described below. Therefore, under these assumptions, a kinetic chain connected to N crosslinks has a fractional probability of being released from the network, $F_{kc,N}(z,t)$:

$$F_{kc,N}(z,t) = (f_2(z,t) + f_3(z,t))^N = (2P(z,t)(1 - P(z,t) + P(z,t)^2))^N \quad \text{Eq. 8}$$

Once $F_{kc,N}(z,t)$ is known, the fraction of PEGdiPDA crosslinks released, $F_{xl}(z,t)$, was calculated by summing the fraction of free crosslinks, $f_3(z,t)$, with the fraction of dangling crosslinks that are released with kinetic chains, $F_{kc,N}(z,t) \cdot f_2(z,t)/2$. Therefore, $F_{xl}(z,t)$ can be calculated as:

$$F_{xl}(z,t) = F_{kc,N}(z,t) \frac{f_2(z,t)}{2} + f_3(z,t) = F_{kc,N}(z,t)P(z,t)(1 - P(z,t)) + P(z,t)^2 \quad \text{Eq. 9}$$

Given the fractions of the eroded products, $F_{kc,N}(z,t)$ and $F_{xl}(z,t)$, as functions of space and time, the fractional mass loss for the corresponding locale was calculated by summing the products of the weight fraction of the gel in each of the eroded species by the fraction of each species that is released.

$$ML(z, t) = (W_{kc}F_{kc,N}(z, t) + W_{xl}F_{xl}(z, t)) \quad \text{Eq. 10}$$

Here, W_{kc} and W_{xl} represent the weight fraction of the gel in the kinetic chains and the PEGdiPDA crosslinks, respectively.

As photodegradation proceeds, individual NBE moieties cleave, degrading PEGdiPDA crosslinks, and, ultimately, causing the release of erosion products and mass loss of the gel. This process eventually reaches a limit, the reverse gelation point, where the network components no longer form an infinite molecular weight gel locally. The reverse gelation point is reached when a sufficient fraction of NBE moieties are cleaved, P_c , and the local network is then transformed into highly branched soluble polymer chains. At this point, the local network is entirely soluble and the fractional mass loss is assumed to approach 1, $ML(z,t) = 1$. A recursive approach, originally developed by Miller and Macosko,^{20,34,35} was used to determine the critical fraction of cleaved NBE moieties that leads to reverse gelation.¹⁸ In this work a monodisperse N was assumed such that all kinetic chains were attached to exactly N PEGdiPDA crosslinks. In reality, a distribution of N crosslinks per kinetic chain exists, and while this can be investigated in future work, previous work in similar systems has shown a modest effect of the distribution of N on the mass loss profile.¹⁸ From this approach, the critical fraction of intact NBE moieties, P_c , at which reverse gelation occurs is given by:

$$P_c = 1 - \frac{1}{\sqrt{N-1}} \quad \text{Eq. 11}$$

Therefore, the function describing the local fractional mass loss is described by Eq. 10 when $P > P_c$ and is equal to unity once $P \leq P_c$. The average number of crosslinks per kinetic chain, N , is employed as the sole fitting parameter in the model by comparing model prediction to experimental measurements of the reverse gelation point.

The kinetic description of photodegradation, Eqs 1-4, was solved numerically to calculate $P(z,t)$, and at each time point, $P(z,t)$ was combined with Eqs. 5-11 to determine $ML(z,t)$. $ML(z,t)$ was summed over the spatial nodes to determine the total fractional mass loss of the gel, $ML(t)$.

$$ML(t) = \frac{\sum_{i=1}^{N_z} ML(i,t)}{N_z} \quad \text{Eq. 12}$$

where N_z is the number of spatial nodes in the system.

4.5 Results and Discussion

A statistical-kinetic model characterizing photodegradation of hydrogel networks (Eqs. 1-12) is developed based solely on physical parameters of the system. This approach combined model equations that describe heterogeneous photochemical reactions with a mean-field, statistical description of network connectivity for hydrogels formed via chain polymerization of telechelic polymers. In this manner, the methodology could be extended to a broad range of photodegradable hydrogels for which statistical descriptions of network connectivity are known, including polymeric hydrogel networks formed via chain-growth, step-growth, or mixed-mode polymerizations.^{18,28}

Further, the general form of the model can be applied to photodegradable hydrogels that are based on any photolytic molecule for which the molar absorptivities, ϵ_i , and quantum yields, ϕ_i , can be measured for the irradiation wavelengths of interest. In this work, application of the photodegradation model focused on hydrogels formed from the chain co-polymerization of a

PEGdiPDA crosslinker, originally developed by Kloxin *et al.*¹⁰ These gels photodegrade on account of the *o*-nitrobenzyl ether (NBE) moieties in the PEGdiPDA crosslinkers, which undergo an irreversible cleavage to the by-product, NBP, in response to single-photon irradiation ($\lambda = 320\text{-}436$ nm).

The photophysical parameters for NBE and NBP were measured for the irradiation wavelengths of interest, with a specific focus on 365, 405, and 436 nm irradiation, bands readily available with a mercury arc lamp. The molar absorptivities of NBE, ϵ_{NBE} , and NBP, ϵ_{NBP} , were calculated previously for 320 – 436 nm light (Figure 1c).²⁹ At 365 nm, $\epsilon_{\text{NBE}} = 4300 \text{ L mol}^{-1} \text{ cm}^{-1}$ while $\epsilon_{\text{NBP}} = 4200 \text{ L mol}^{-1} \text{ cm}^{-1}$, indicating minimal bleaching upon photoreaction. At 405nm, $\epsilon_{\text{NBE}} = 720 \text{ L mol}^{-1} \text{ cm}^{-1}$ while $\epsilon_{\text{NBP}} = 3300 \text{ L mol}^{-1} \text{ cm}^{-1}$, indicating a red shift in the absorptivity of the NBE upon photoreaction. At 436nm, $\epsilon_{\text{NBE}} = 16 \text{ L mol}^{-1} \text{ cm}^{-1}$ while $\epsilon_{\text{NBP}} = 800 \text{ L mol}^{-1} \text{ cm}^{-1}$, similarly red shifting upon cleavage. The quantum yields for NBE photocleavage were found experimentally to be $\phi_{\text{NBE}} = 0.027$ and $\phi_{\text{NBE}} = 0.017$ for 365 and 405 nm and 436 nm irradiation, respectively. The quantum yield at 436 nm was found previously as $\phi_{\text{NBE}} = 0.23$.²²

PEGdiPDA hydrogels were fabricated via redox-initiated, free-radical chain polymerization at two disparate macromer concentrations, 10 mol% PEGdiPDA:90 mol% PEGA and 25 mol% PEGdiPDA:75 mol% PEGA of a total 15 wt% polymer gel (Figure 1a). These gels possessed concentrations of NBE, $[\text{NBE}]$, of 0.040 M and 0.058 M, respectively, and were assumed to possess an average number of crosslinks per kinetic chain, N , of 20 as fit to the reverse gelation point and based on previous work with similar degradable hydrogels.³⁶ Gels were polymerized with a thickness, z , ranging from 100 μm to 1500 μm and, subsequently, irradiated with a collimated light source incident on the surface of the gel (Figure 1b) leading to attenuation and spatially varying degradation rates in the z -dimension.

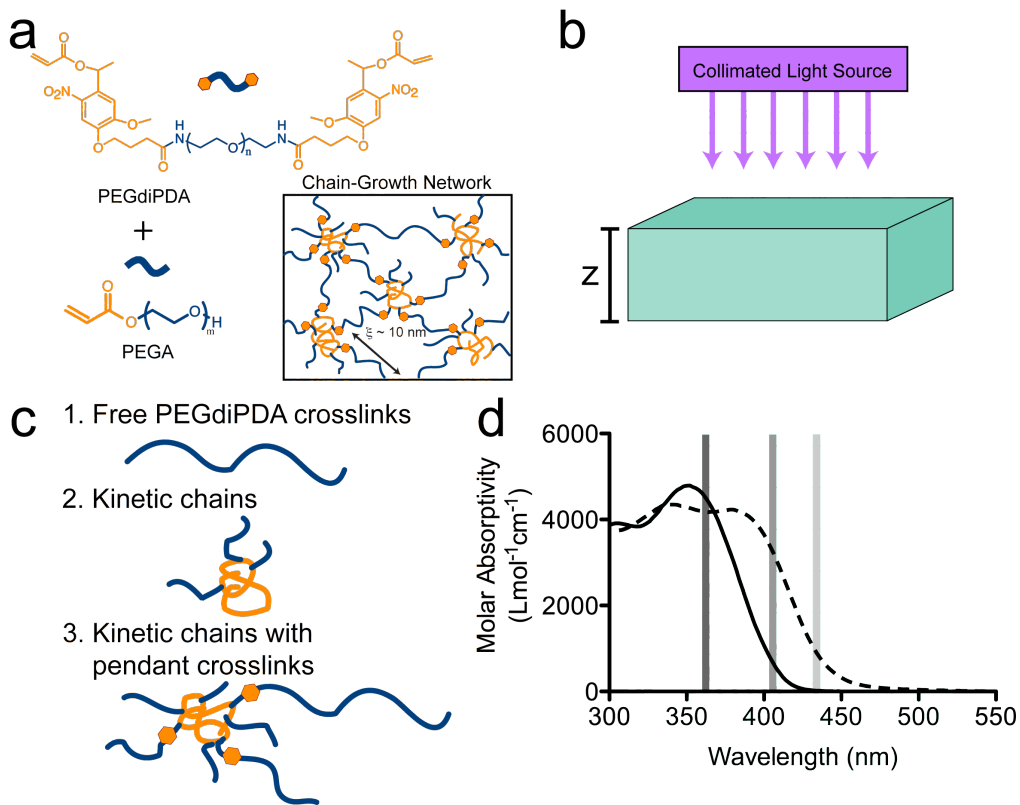


Figure 4.1 Photodegradable hydrogel system. (a) Photodegradable PEG based hydrogels were formed through redox-initiated free radical polymerization of the photodegradable crosslinker (PEGdiPDA) with a co-monomer (PEGA). (b) Upon exposure to collimated irradiation, these gels degrade as the photolabile *o*-nitrobenzyl ether (NBE) cleaves leading to mass loss and, ultimately, erosion. (c) Mass loss results from the release of cleavage products from the network that predominantly fall into three categories: i. free PEGdiPDA crosslinks, ii. kinetic chains, and iii. kinetic chains with pendant crosslinks. Once a sufficient fraction of NBE moieties are cleaved in a local region, the gel undergoes reverse gelation where the polymers no longer form an infinite molecular weight network and the local material erodes from the gel. (d) Photodegradation can be achieved at wavelengths where NBE absorbs light (solid line). In this work, 365 nm, 405 nm, and 436 nm were employed for degradation. The mechanism of mass loss of the gels was dictated by the total absorptivity of the degradable hydrogels, which depends on the molar absorptivity of NBE (solid line), the molar absorptivity of the cleavage product (NBP; dashed line), the concentrations of photoactive species, the thickness of the gel, and the wavelength of irradiation. Molar absorptivity data previously reported in ref. 29.

The governing equations of the photodegradation model (Eqs. 1-14) were solved numerically to predict the spatially and temporally varying profiles for the irradiation intensity, concentration of NBE, crosslinking density, and fractional mass loss for these PEGdiPDA hydrogels. The light intensity profiles followed a distinct decay that is indicative of attenuation

in the material, which depends on the absorptivity of the particular hydrogel formulation (Figure 2). The absorptivity of the material is related directly to the thickness of the gel, the concentration of the photoactive species, and the molar absorptivity of the photoactive species at the irradiation wavelength as described by the Beer-Lambert Law (Eq. 1). For discussion, the initial absorbance is defined as $A = \epsilon_{\text{NBE}} \cdot [\text{NBE}] \cdot z$. Predicted light attenuation profiles at $t = 0$ for $\lambda = 365 \text{ nm}$, $I_0 = 10 \text{ mW/cm}^2$ irradiation in PEGdiDPA hydrogels ($[\text{NBE}] = 0.04 \text{ M}$) with $z = 10, 100, 1000 \text{ }\mu\text{m}$ demonstrated that the fractional penetration depth of the light is dependent on the thickness of the gel (Figure 2a). The light intensity was nearly uniform through the depth of a $10 \text{ }\mu\text{m}$ gel ($A = 0.17$), while only a small volume near the surface of a $1000 \text{ }\mu\text{m}$ ($A = 17$) gel receives significant light at $t = 0$.

Similarly, varying the concentration of NBE within the PEGdiPDA gels ($z = 100 \text{ }\mu\text{m}$) modulated the light attenuation profile ($\lambda = 365 \text{ nm}$; $I_0 = 10 \text{ mW/cm}^2$) through the gel (Figure 2b). At a low concentration, ($[\text{NBE}] = 0.004 \text{ M}$; $A = 0.17$), light is able to penetrate through the full depth of the gel with only a small amount of attenuation, as the lower concentration of NBE decreases the absorptivity of the gel. As the concentration of NBE, and thus the absorptivity, increases, less light is able to penetrate the full thickness of the gel, creating a steeper gradient in light intensity throughout the depth of the gel.

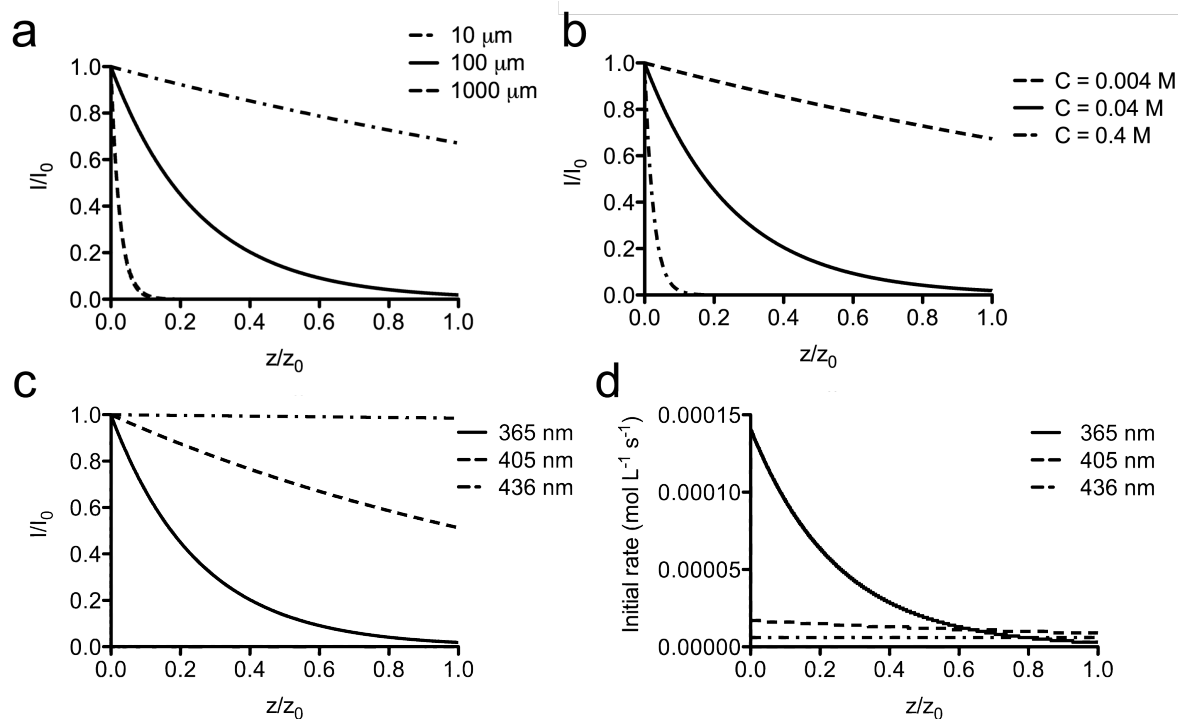


Figure 4.2 Model predictions of light intensity profiles and kinetic rates. The incident irradiation is attenuated in the hydrogel on account of the absorbing NBE within the PEGdiPDA hydrogels. **(a)** Increased thickness of the hydrogel ($[\text{NBE}] = 0.04 \text{ M}$; $\lambda = 365 \text{ nm}$; $I_0 = 10 \text{ mW cm}^{-2}$) leads to decreased penetration depth of the light through the gel ($z = 10 \mu\text{m}$, dash-dot line; $z = 100 \mu\text{m}$, solid line; $z = 1000 \mu\text{m}$, dashed line). **(b)** Similarly, increased concentration of the NBE moieties in the gel ($z = 100 \mu\text{m}$; $\lambda = 365 \text{ nm}$; $I_0 = 10 \text{ mW cm}^{-2}$) leads to decreased penetration depth of the light through the gel ($[\text{NBE}] = 0.004 \text{ M}$, dashed line; $[\text{NBE}] = 0.04 \text{ M}$, solid line; $[\text{NBE}] = 0.4 \text{ M}$, dash-dot line). **(c)** The penetration depth of the light in the gel is also dependent on the wavelength of incident irradiation ($[\text{NBE}] = 0.04 \text{ M}$; $z = 100 \mu\text{m}$; $I_0 = 10 \text{ mW cm}^{-2}$). Here, 365 nm irradiation (solid line) is strongly attenuated owing to the high molar absorptivity of NBE at 365 nm ($\epsilon_{\text{NBE}} = 4300 \text{ L mol}^{-1} \text{ cm}^{-1}$). 405 nm irradiation (dashed line) leads to increased penetration depth ($\epsilon_{\text{NBE}} = 720 \text{ L mol}^{-1} \text{ cm}^{-1}$) while 436 nm irradiation (dash-dot line) is nearly uniform through the depth of the gel ($\epsilon_{\text{NBE}} = 16 \text{ L mol}^{-1} \text{ cm}^{-1}$). **(d)** The initial photocleavage rate as a function of depth is dependent on the local light intensity and the wavelength of irradiation, through changes in absorbance and quantum yield. ($[\text{NBE}] = 0.04 \text{ M}$; $I_0 = 10 \text{ mW cm}^{-2}$; $z = 100 \mu\text{m}$; $\lambda = 365 \text{ nm}$, solid line; $\lambda = 405 \text{ nm}$, dashed line; $\lambda = 436 \text{ nm}$, dash-dot line)

Irradiating the gel at different wavelengths of light further modified the penetration of light through the gel in a manner that correlates with the absorptivity of the material (Figure 2c).

The molar extinction coefficient of NBE (Figure 1c) at the different wavelengths of interest

governed the total absorbance of the PEGdiPDA hydrogels ($[NBE] = 0.04 \text{ M}$; $z = 100 \text{ }\mu\text{m}$). Since 436 nm is only weakly absorbed by NBE moieties ($\epsilon_{NBE} = 16 \text{ L mol}^{-1} \text{ cm}^{-1}$), incident irradiation at this wavelength penetrates the full depth of the gel uniformly ($A = 0.0064$). However, as the molar absorptivity of NBE increases at lower wavelengths of light, the incident irradiation becomes attenuated more strongly as evidenced by the model light intensity profiles for 405 nm ($\epsilon_{NBE} = 720 \text{ L mol}^{-1} \text{ cm}^{-1}$; $A = 0.29$) and 365 nm ($\epsilon_{NBE} = 4300 \text{ L mol}^{-1} \text{ cm}^{-1}$; $A = 1.7$). In general, the uniformity of light through the sample is governed by the initial absorbance of the material such that $A \leq 0.1$ allows relatively uniform light penetration, whereas $A \geq 10$ caused light to be confined primarily to a thin surface region.

Since the photocleavage rate is directly proportional to the local light intensity (Eq. 2), the initial cleavage rate profiles ($t = 0$) were defined by the attenuated light intensity profiles. In this manner, the rate profiles can be tuned by modulating the absorptivity of the material by altering the thickness of the material (z) or the concentration of the photoactive species ($[NBE]$). Tuning the wavelength of irradiation also modulates the rate profile as the gel absorbance strongly depends on the wavelength of light; however, the quantum yield is also a function of wavelength and an important parameter in determining the ultimate rate of photocleavage (Eq. 2). Thus, varying the wavelength of light modifies both the uniformity and magnitude of the degradation rate profiles (Figure 2d). For 436 nm irradiation, the rate profile was nearly uniform throughout the depth of the PEGdiPDA gel ($[NBE] = 0.04 \text{ M}$; $z = 100 \text{ }\mu\text{m}$) on account of the small absorbance ($A = 0.0064$), but the initial rate at the surface ($t = 0$; $z = 0$) was only $5.6 \times 10^{-6} \text{ mol L}^{-1} \text{ s}^{-1}$. In comparison, for 365 nm irradiation ($[NBE] = 0.04 \text{ M}$; $z = 100 \text{ }\mu\text{m}$) there was significant heterogeneity in the initial rate profile through the gel owing to the high absorbance ($A = 1.7$), but the initial rate at the surface is much higher, $1.4 \times 10^{-4} \text{ mol L}^{-1} \text{ s}^{-1}$.

As explained in the model development, the absorptivity of the photodegradable gel changes as the photodegradation proceeds on account of cleavage of NBE to NBP, each possessing different molar absorptivities, and mass loss that occurs at later time points. Therefore, it is necessary to track the evolution of both the light intensity profiles and intact photoactive species concentration profiles in time to better understand the evolution of material properties (Figure 3). Here, two conditions were investigated, one that primarily involved surface erosion of a gel ($[NBE] = 0.23 \text{ M}$; $z = 100 \text{ }\mu\text{m}$; $\lambda = 365 \text{ nm}$; $I_0 = 10 \text{ mW/cm}^2$; $A = 10$) and one that led to a more uniform, bulk degradation of the gel ($[NBE] = 0.0056 \text{ M}$; $z = 25 \text{ }\mu\text{m}$; $\lambda = 405 \text{ nm}$; $I_0 = 10 \text{ mW/cm}^2$; $A = 0.01$). Surface erosion occurs when light is confined to the surface of the gel, concentrating the photocleavage and, thus, the mass loss to this local region (Figure 3a,b). As time progressed the light was able to move through the gel in a wave-like fashion, owing to mass loss at the surface that removes light attenuating material from the light path. Reverse gelation of the material occurs when $[NBE]/[NBE]_0 \leq .23$, and it was assumed that the erosion products rapidly diffused out of the light path, which is typically reasonable for highly swollen hydrogels. When mass loss occurs, light is able to penetrate further into the gel, resulting in a continual sloughing away of the surface of the gel. The assumption of rapid diffusion of erosion products breaks down for systems in which the degradation occurs more rapidly than the diffusion time scales.

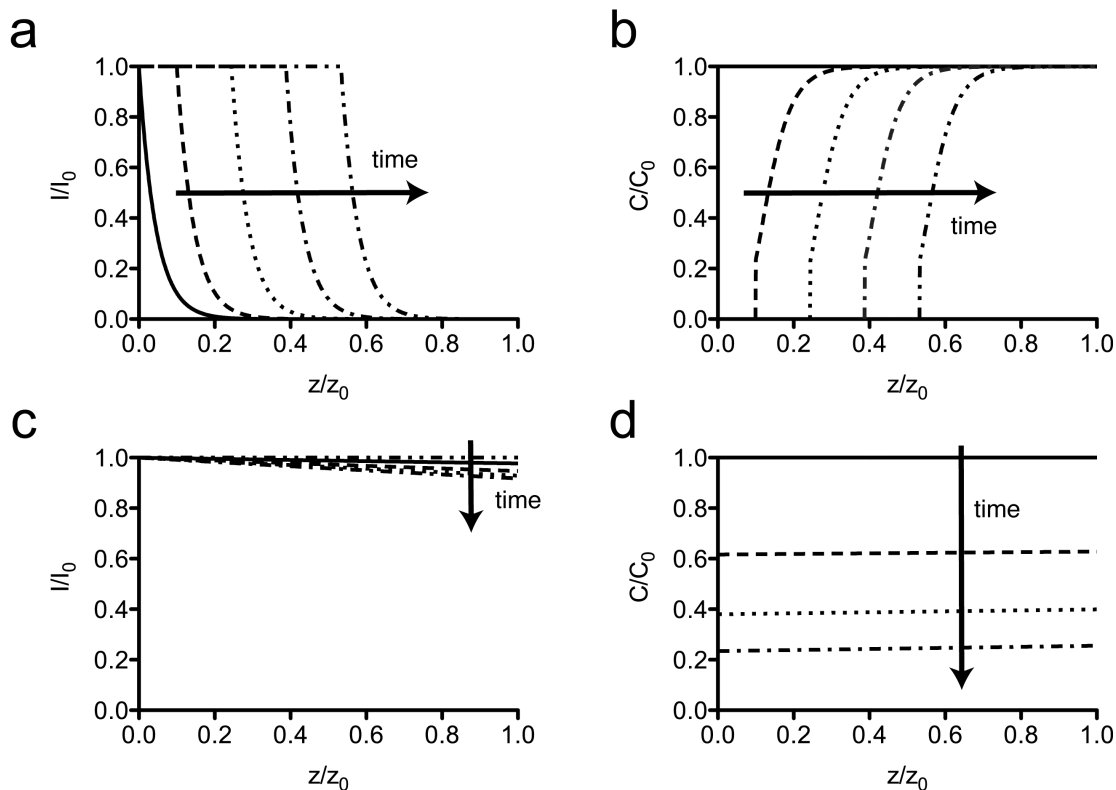


Figure 4.3 Model predictions of surface and bulk erosion of photodegradable hydrogels. Surface erosion and bulk degradation are both observed *in silico* for photodegradable hydrogels depending on the total absorbance of the material. **(a)** PEGdiPDA hydrogels with high absorbance ($A = 10$; $[NBE] = 0.23$ M; $z = 100$ μm) severely attenuate the incident irradiation ($\lambda = 365$ nm; $I_0 = 10$ mW cm^{-2}), which leads to a front of light moving through the depth of the material as degradation proceeds. (arrows indicate the direction of increasing time; $t = 0$ min, solid line; $t = 22.5$ min, dashed line; $t = 45$ min, dotted line; $t = 67.5$ min, dash-dot line; $t = 90$ min, dash-double dot line) **(b)** Photodegradation erodes the surface of the material, where light remains at a high intensity. Erosion is indicated by $C/C_0 = 0$. In this surface erosion case, the strongly coupled equations (Eqs. 1 - 3) lead to a propagation of light and mass loss through the depth of the gel with time. ($t = 0$ min, solid line; $t = 22.5$ min, dashed line; $t = 45$ min, dotted line; $t = 67.5$ min, dash-dot line; $t = 90$ min, dash-double dot line) **(c)** PEGdiPDA hydrogels with low absorbance ($A = 0.01$; $[NBE] = 0.0056$ M; $z = 25$ μm) allow incident irradiation ($\lambda = 405$ nm; $I_0 = 25$ mW cm^{-2}) to penetrate through the full depth of the gel uniformly, which results in bulk degradation of the material. ($t = 0$ min, solid line; $t = 7.5$ min, dashed line; $t = 15$ min, dotted line; $t = 22.5$ min, dash-dot line; $t = 30$ min, dash-double dot line) **(d)** As light penetrates the material uniformly, the reaction rate is uniform through the depth of the gel, which results in an even decrease in $[NBE]$ through the depth of the gel, which is indicative of bulk degradation. At late time points, the whole material erodes. ($t = 0$ min, solid line; $t = 7.5$ min, dashed line; $t = 15$ min, dotted line; $t = 22.5$ min, dash-dot line; $t = 30$ min, dash-double dot line) For all model calculations $N = 20$.

In contrast, bulk degradation occurs whenever the light is more uniformly distributed through the depth of the material ($A \leq 0.1$), leading to a similar photocleavage rate throughout

the depth of the gel. As time progresses, the light intensity profile is altered slightly as the NBP degradation product absorbs light at 405 nm more strongly than the intact NBE (Figure 3c). Concomitantly, the concentration profile was altered by a near uniform decrease in intact NBE units ($[NBE]/[NBE]_0$) with depth until the reverse gelation point is reached and the entire gel solubilizes (Figure 3d).

Photodegradation of physically relevant gels often resides in a complex regime that is a blend of the surface erosion and bulk degradation phenomena. Pure bulk degradation only occurs in materials that can be approximated as optically thin films, i.e., $A \leq 0.1$. Typical photodegradable hydrogels are 100-1000 μm thick and contain 1-10 wt% photodegradable polymer, which corresponds to $A \sim 0.1-10$. In such systems, much of the incident light is confined to the surface of the gel owing to attenuation, but a fraction of the light is able to penetrate through the full thickness of the gel, causing non-negligible cleavage of crosslinks (Figure 4a). This results in a surface-eroding wave moving through the gel preceded by a degradation gradient (Figure 4b). Such complex degradation processes are more difficult to conceptualize and model, but can also lead to particularly interesting, anisotropic materials.

Once the degradation profiles and mass loss behavior are better understood and quantified, this experimental space can be an attractive degradation regime and exploited to generate materials with gradients in crosslinking density through the z-dimension of the material (Figure 4c). Crosslinking density controls many important material properties, including both the volumetric swelling ratio, $Q \sim \rho_x^{-3/5}$, and Young's modulus, $E \sim \rho_x^{6/5}$, for PEG hydrogels (Figure 4d).³⁷ As such, gradients in crosslinking density created through photodegradable materials can provide a simple method to fabricate materials with anisotropic properties, which can be difficult to fabricate by traditional methods.

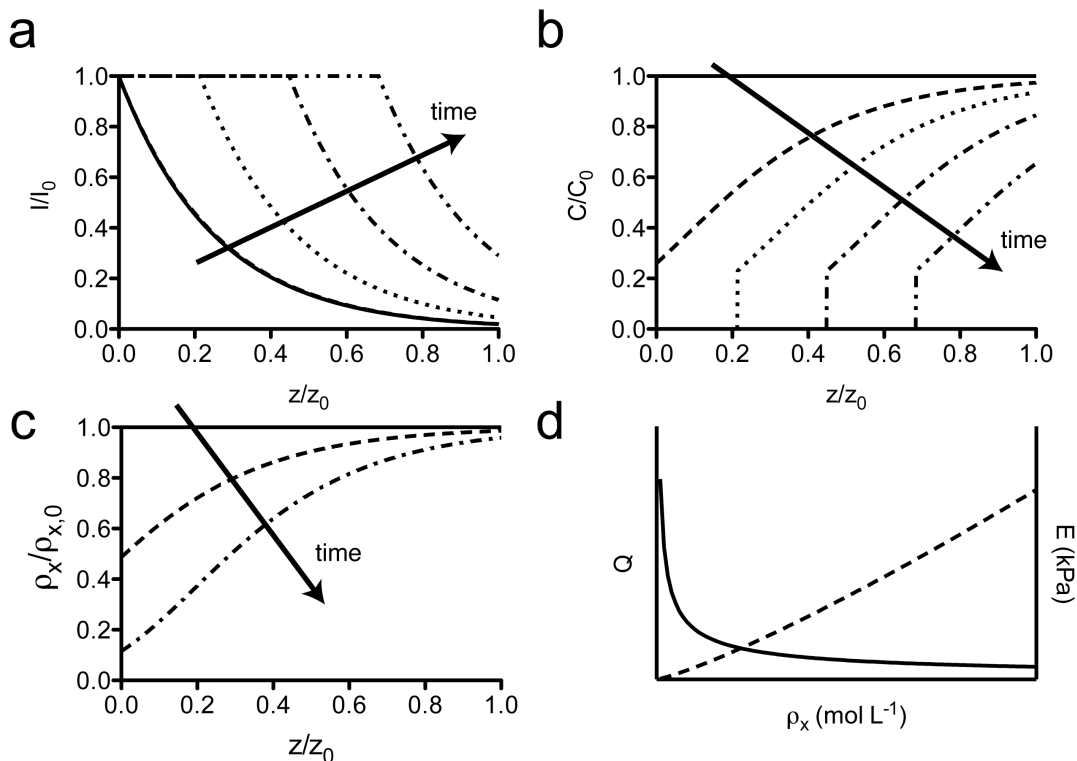


Figure 4.4 Model predictions of photodegradation in PEGdiPDA hydrogels. For PEGdiPDA hydrogels with intermediate absorbance ($A \sim 0.1 - 10$), degradation is observed to be a mixture of surface erosion and bulk degradation. **(a)** In these materials, light is mostly confined to the surface volume of the gel, while a portion of the light is able to penetrate the full thickness, leading to non-negligible cleavage of NBE moieties. **(b)** As time progresses the light front moves through the gel surface, eroding the material while anisotropically patterning the full depth of the gel. (arrows indicate the direction of increasing time; $t = 0$ min, solid line; $t = 7.5$ min, dashed line; $t = 15$ min, dotted line; $t = 22.5$ min, dash-dot line; $t = 30$ min, dash-double dot line) **(c)** The anisotropic patterning caused by this phenomenon is predicted to generate materials with gradients in crosslinking density as a function of depth. ($t = 0$ min, solid line; $t = 2$ min, dashed line; $t = 6$ min, dashed-dot line) **(d)** Since the volumetric swelling ratio, Q , and Young's modulus, E , of PEG hydrogels depend on the crosslinking density, ρ_x , anisotropies in crosslinking density are readily generated to create spatially varying materials, that can be difficult to synthesize through traditional fabrication routes. For all model calculations, $N = 20$; $[NBE] = 0.04$ M; $z = 100$ μm ; $\lambda = 365$ nm; $I_0 = 10$ mW cm^{-2} ; $A = 1.7$.

From a modeling perspective, the generation of materials with anisotropic materials is not trivial. Since the photodegradation process alters the crosslinking density, ρ_x , and ultimately, swelling ratio, Q , the hydrogel geometry and concentration of photoactive species within the gel can change as a function of time. For this work, it was assumed that swelling does not influence

the concentration of photoactive species during the degradation process, as the initial equilibrium water content of the gels is relatively high (i.e., 85-95% water). However, degradation-induced swelling may introduce dimensional changes into the material. For example, if Q were to increase from 10 to 20 in a bulk degrading hydrogel with isotropic swelling (a large swelling change that one would observe only at late stages of degradation), the sample thickness would change by a factor of 1.26. This version of the photodegradation model does not account for dimensional changes in the material, but future investigations could account for this by incorporating floating boundary conditions that account for dynamic swelling during degradation.

The PEGdiPDA chain polymerized hydrogels developed in previous studies and modeled in this work ($[NBE] = 0.04$ or 0.058 M; $z = 100 - 1500$ μm ; $A \approx 0.3 - 39$) fall primarily in the range of intermediate degradation (a mixture of surface erosion and bulk degradation) with $\lambda = 365$ and 405 nm. To demonstrate the physical relevance of this model and the ability that it offers to predict complex degradation and mass loss profiles, the model was applied to described mass loss and erosion of previously studied PEGdiPDA gels. Specifically, the mass loss profiles of thick gels ($z = 1500$ μm ; $[NBE] = 0.04$ or 0.06 M; $A \approx 26 - 39$) exposed to 365 nm irradiation at 20 mW/cm^2 were modeled and compared to experimental erosion profiles (Figure 5a).²⁰ The model predicted the linear mass loss profile as a function of time in both cases, as expected from surface erosion driven degradation that was expected for these gels. Similar mass loss experiments were conducted with PEGdiPDA hydrogels exposed to 405 nm irradiation at 25 mW/cm^2 ($z = 500$ μm ; $[NBE] = 0.04$; $A \approx 1.4$; Figure 5b). The model predicted the experimental trends and data well, yet there are some deviations to note in these experiments. Part of this deviation could be caused by an inaccurate determination of N , the average number of crosslinks

per kinetic chain, or the assumption that mass diffused out of the path of the light instantly upon reverse gelation. For experiments where the timescale of diffusion, τ_D , is much less than the timescale of degradation, τ_{PD} , this is a fair assumption. However not all experiments are in this regime, as $\tau_D/\tau_{PD} \sim 0.1 - 1$ for a 100 μm diffusion distance for these gels assuming a diffusion coefficient on the order of $10^{-6} \text{ cm}^2/\text{s}$, which is reasonable for small molecules in water. To improve on this possible error, future iterations of mass loss models in photodegradable hydrogels might focus on better modeling diffusion of degradation and erosion products.

The surface erosion phenomenon was further modeled PEGdiPDA hydrogels ($[\text{NBE}] = 0.04 \text{ M}$; $z = 250 \mu\text{m}$; $A = 0.7 - 4.3$) in which channels were formed using a photomask with 365 nm irradiation at $I_0 = 10 \text{ mW}/\text{cm}^2$.²⁰ Similar to the fractional mass loss, the model predicted the progression of channel depth as a function of time, except for some small deviation at short time scales (Figure 5c). However, there is also a degradation gradient that evolves behind the channel growth, as predicted by the mixed-mode degradation. This gradient was indicative of the complex surface erosion and bulk degradation properties of these gels and has been exploited to generate functional materials with gradients in elasticity in both the z -dimension²⁰ and the x - y dimension.^{20,21} The photodegradation model was employed to predict an x - y gradient (Figure 5d) generated with this material in a previous study.²⁰

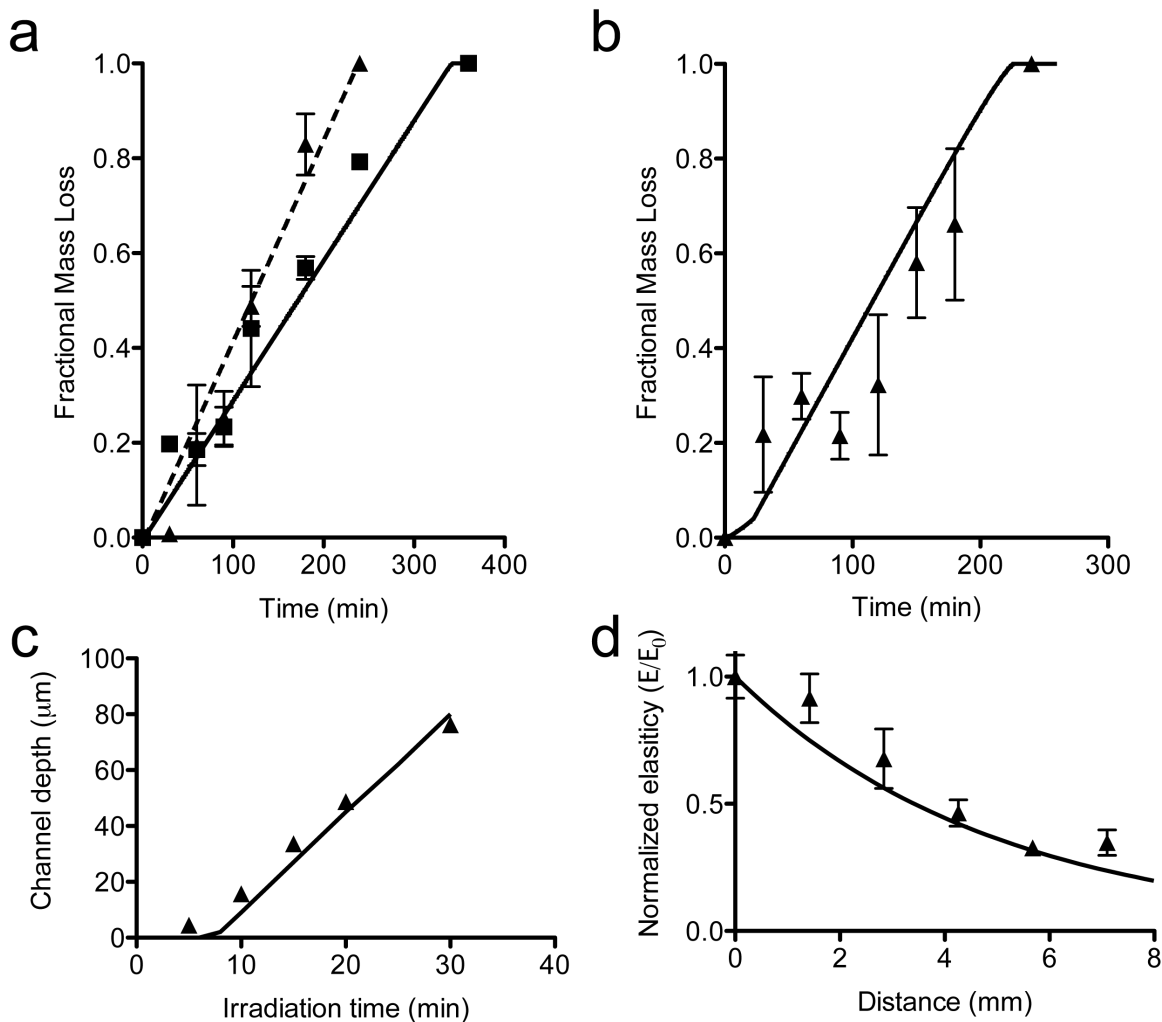


Figure 4.5 Model predictions compared to experimental degradation of PEGdiPDA hydrogels. The photodegradation model was employed to predict mass loss and material property changes in chain polymerized, PEGdiPDA hydrogels. **(a)** Fractional mass loss for two formulations ($[\text{NBE}] = 0.04 \text{ M}$; $z = 1500 \mu\text{m}$; triangles – experimental, previously reported data found in ref. 20; dashed line – prediction and $[\text{NBE}] = 0.058 \text{ M}$; $z = 1500 \mu\text{m}$; squares – experimental, previously reported data found in ref. 20; solid line – prediction) in response to irradiation ($\lambda = 365 \text{ nm}$; $I_0 = 20 \text{ mW/cm}^2$) was predicted by the statistical-kinetic mass loss model. **(b)** Fractional mass loss for PEGdiPDA hydrogels ($[\text{NBE}] = 0.04 \text{ M}$) in response to irradiation ($\lambda = 405 \text{ nm}$ at $I_0 = 25 \text{ mW/cm}^2$) also compared well with predictions. (triangles – experimental; solid line – prediction) **(c)** The depth of channels patterned into the surface of PEGdiPDA hydrogels ($[\text{NBE}] = 0.04 \text{ M}$; $\lambda = 365 \text{ nm}$; $I_0 = 10 \text{ mW/cm}^2$) was predicted, except at short irradiation times. (triangles – experimental, previously reported data found in ref. 20; solid line – prediction) **(d)** A gradient in surface elasticity generated by photomasking was also predicted by the statistical-kinetic model. (triangles – experimental, previously reported data found in ref. 21; solid line – prediction, line connects discrete model predictions) For all model calculations, $N = 20$.

In all, the model of photodegradation presented herein should facilitate and improve the design of hydrogel compositions for desired applications. With this model, physically relevant gels can be designed that preferentially bulk degrade or undergo surface erosion based on material composition. Furthermore, complex, anisotropic materials can be predicted and subsequently engineered using the insight gained from the mass loss models. In this manner, the model of photodegradation is an enabling tool in the design and use of photoresponsive hydrogels.

4.6 Conclusions

A statistical-kinetic model of photodegradation was presented that predicts photodegradation rates and concomitant changes in material properties as functions of space and time for photolabile hydrogels. The model accounted for the complexity of photodegradation caused by the inherent heterogeneity of the photoreaction as a result of light attenuation within the material. The initial absorbance of the material was used to predict whether the system would undergo bulk degradation and mass loss or surface erosion based on the uniformity or non-uniformity of light in each case. The model methodology is general and can be applied to a broad range of photoresponsive hydrogels whose material properties are connected to photoreactions within the material. In this work, kinetic modeling that combined the Beer-Lambert Law and kinetic expressions to describe the photocleavage reaction was combined with statistical descriptions of mass loss in chain polymerized networks, which facilitated the prediction of material property changes in a model PEGdiPDA hydrogel system. In all cases, the predictions compared well with experimental data. In all, a method for modeling photodegradation has been

presented that will prove useful in the design and fabrication of photoresponsive networks for cell culture experiments, anisotropic material synthesis, and drug delivery vehicles.

4.7 References:

1. Peppas, N., Hilt, J., Khademhosseini, A. & Langer, R. Hydrogels in biology and medicine: From molecular principles to bionanotechnology. *Adv Mater* **18**, 1345–1360 (2006).
2. Liechty, W. B., Kryscio, D. R., Slaughter, B. V. & Peppas, N. A. Polymers for drug delivery systems. *Annu Rev Chem Biomol Eng* **1**, 149–173 (2010).
3. Tibbitt, M. W. & Anseth, K. S. Hydrogels as Extracellular Matrix Mimics for 3D Cell Culture. *Biotechnol Bioeng* **103**, 655–663 (2009).
4. Lutolf, M. P. & Hubbell, J. A. Synthetic biomaterials as instructive extracellular microenvironments for morphogenesis in tissue engineering. *Nat Biotechnol* **23**, 47–55 (2005).
5. Hilt, J. Z., Gupta, A. K., Bashir, R. & Peppas, N. A. Ultrasensitive Biomems Sensors Based on Microcantilevers Patterned with Environmentally Responsive Hydrogels. *Biomedical Microdevices* **5**, 177–184 (2003).
6. Dong, L. & Jiang, H. Autonomous microfluidics with stimuli-responsive hydrogels. *Soft Matter* **3**, 1223 (2007).
7. Johnson, J. A., Finn, M. G., Koberstein, J. T. & Turro, N. J. Synthesis of photocleavable linear macromonomers by ATRP and star macromonomers by a tandem ATRP-click reaction: Precursors to photodegradable model networks. *Macromolecules* **40**, 3589–3598 (2007).
8. Johnson, J. A., Baskin, J. M., Bertozzi, C. R., Koberstein, J. T. & Turro, N. J. Copper-free click chemistry for the in situ crosslinking of photodegradable star polymers. *Chem Commun* 3064–3066 (2008).doi:10.1039/b803043j
9. Luo, Y. & Shoichet, M. S. A photolabile hydrogel for guided three-dimensional cell growth and migration. *Nat Mater* **3**, 249–253 (2004).
10. Kloxin, A. M., Kasko, A. M., Salinas, C. N. & Anseth, K. S. Photodegradable hydrogels for dynamic tuning of physical and chemical properties. *Science* **324**, 59–63 (2009).
11. Frey, M. T. & Wang, Y.-L. A photo-modulatable material for probing cellular responses to substrate rigidity. *Soft Matter* **5**, 1918–1924 (2009).

12. Tibbitt, M. W., Kloxin, A. M., Dyamenahalli, K. U. & Anseth, K. S. Controlled two-photon photodegradation of PEG hydrogels to study and manipulate subcellular interactions on soft materials. *Soft Matter* **6**, 5100–5108 (2010).
13. Deforest, C. A. & Anseth, K. S. Cytocompatible click-based hydrogels with dynamically tunable properties through orthogonal photoconjugation and photocleavage reactions. *Nat Chem* **3**, 925–931 (2011).
14. Wong, D. Y., Griffin, D. R., Reed, J. & Kasko, A. M. Photodegradable Hydrogels to Generate Positive and Negative Features over Multiple Length Scales. *Macromolecules* **43**, 2824–2831 (2010).
15. Peng, K. *et al.* Dextran based photodegradable hydrogels formed via a Michael addition. *Soft Matter* **7**, 4881–4887 (2011).
16. Nicodemus, G. D. & Bryant, S. J. Cell encapsulation in biodegradable hydrogels for tissue engineering applications. *Tissue Engineering Part B: Reviews* **14**, 149–165 (2008).
17. Metters, A., Bowman, C. & Anseth, K. A statistical kinetic model for the bulk degradation of PLA-b-PEG-b-PLA hydrogel networks. *J Phys Chem B* **104**, 7043–7049 (2000).
18. Reddy, S., Anseth, K. & Bowman, C. Modeling of network degradation in mixed step-chain growth polymerizations. *Polymer* **46**, 4212–4222 (2005).
19. Slaughter, B. V., Khurshid, S. S., Fisher, O. Z., Khademhosseini, A. & Peppas, N. A. Hydrogels in Regenerative Medicine. *Adv Mater* **21**, 3307–3329 (2009).
20. Kloxin, A. M., Tibbitt, M. W., Kasko, A. M., Fairbairn, J. A. & Anseth, K. S. Tunable Hydrogels for External Manipulation of Cellular Microenvironments through Controlled Photodegradation. *Adv Mater* **22**, 61–66 (2010).
21. Kloxin, A. M., Benton, J. A. & Anseth, K. S. In situ elasticity modulation with dynamic substrates to direct cell phenotype. *Biomaterials* **31**, 1–8 (2010).
22. Griffin, D. R., Patterson, J. T. & Kasko, A. M. Photodegradation as a mechanism for controlled drug delivery. *Biotechnol Bioeng* **107**, 1012–1019 (2010).
23. Tibbitt, M. W., Han, B. W., Kloxin, A. M. & Anseth, K. S. Synthesis and application of photodegradable microspheres for spatiotemporal control of protein delivery. *J Biomed Mater Res A* **100**, 1647–1654 (2012).
24. Wong, D. Y., Griffin, D. R., Reed, J. & Kasko, A. M. Photodegradably hydrogels to generate positive and negative features over multiple length scales. *Macromolecules* **43**, 2824–2831 (2010).
25. Andreopoulos, F. M. & Persaud, I. Delivery of basic fibroblast growth factor (bFGF) from photoresponsive hydrogel scaffolds. *Biomaterials* **27**, 2468–2476 (2006).

26. Trenor, S., Shultz, A., Love, B. & Long, T. Coumarins in polymers: From light harvesting to photo-cross-linkable tissue scaffolds. *Chem Rev* **104**, 3059–3077 (2004).
27. Martens, P., Metters, A., Anseth, K. & Bowman, C. A generalized bulk-degradation model for hydrogel networks formed from multivinyl cross-linking molecules. *J Phys Chem B* **105**, 5131–5138 (2001).
28. Rydholm, A. E., Reddy, S. K., Anseth, K. S. & Bowman, C. N. Development and Characterization of Degradable Thiol-Allyl Ether Photopolymers. *Polymer* **48**, 4589–4600 (2007).
29. Kloxin, A. M., Tibbitt, M. W. & Anseth, K. S. Synthesis of photodegradable hydrogels as dynamically tunable cell culture platforms. *Nat Protoc* **5**, 1867–1887 (2010).
30. Odian, G. *Principles of Polymerization*. (John Wiley & Sons, Inc.: Hoboken, NJ, 2004).
31. Miller, G., Gou, L., Narayanan, V. & Scranton, A. Modeling of photobleaching for the photoinitiation of thick polymerization systems. *J Polym Sci Pol Chem* **40**, 793–808 (2002).
32. Wegscheider, R. *Z. Physical Chemistry* **103**, 273–306 (1923).
33. Terrones, G. & Pearlstein, A. Effects of optical attenuation and consumption of a photobleaching initiator on local initiation rates in photopolymerizations. *Macromolecules* **34**, 3195–3204 (2001).
34. Macosko, C. W. & Miller, D. R. A new derivation of average molecular weights of nonlinear polymers. *Macromolecules* **9**, 199–206 (1976).
35. Miller, D. R. & Macosko, C. W. A new derivation of post gel properties of network polymers. *Macromolecules* **9**, 206–211 (1976).
36. Nuttelman, C. R., Kloxin, A. M. & Anseth, K. S. Temporal changes in peg hydrogel structure influence human mesenchymal stem cell proliferation and matrix mineralization. *Adv. Exp. Med. Biol.* **585**, 135–149 (2006).
37. Bryant, S. Photopolymerization of hydrogel scaffolds. *Scaffolding in Tissue Engineering* 1–21 (2006).

CHAPTER V

MECHANICAL PROPERTIES AND DEGRADATION OF CHAIN AND STEP POLYMERIZED PHOTODEGRADABLE HYDROGELS

Submitted to *Macromolecular Rapid Communications*, Fall 2012

5.1 Introduction

Covalently crosslinked hydrogels are applied as cell culture templates,^{1,2} absorbent materials, non-fouling coatings,³ contact lenses,⁴ and drug delivery vehicles.⁵ Owing to high water content, reasonable transport of small molecules, and robust mechanical properties, covalently crosslinked hydrogels are particularly attractive materials for a broad array of biological and cellular applications. These reticulated polymer networks are formed by chemical crosslinking of hydrophilic macromolecules, such as synthetically derived poly(ethylene glycol) (PEG) or poly(vinyl alcohol) and naturally derived hyaluronic acid, gelatin, or alginate, often mildly and in the presence of cells.⁶ Despite the prevalence of hydrogels in the biomedical sciences, the manner by which the crosslinking mechanism and resultant microarchitecture of the hydrogel influences the macroscopic properties, e.g., strength, toughness, and degradation, is still not fully elucidated. A better understanding of the structure-function relationship in hydrogel performance would enable improved rational design of materials for a range of targeted applications.

Crosslinked, synthetic hydrogels have been formed traditionally through a free-radical initiated chain polymerization of telechelic monomers (e.g., diacrylated PEG or 2-hydroxy ethyl methacrylate copolymerized with diethylene glycol dimethacrylate).⁷ In this manner, hydrogels have been fabricated rapidly with tunable material properties⁸ and have been functionalized with adhesion peptides and degradation sites.⁹ However, radical initiated chain polymerizations are limited in that they are inhibited by oxygen,¹⁰ proceed with complex kinetics,¹¹ can be damaging to nucleic acids and proteins,^{12,13} and inherently introduce inhomogeneities into the network structure.^{14,15} These inhomogeneities compromise the material properties as stress is focused on weak portions of the gel, reducing the macroscopic integrity of the hydrogel.¹⁵ Furthermore, hydrogels formed by chain polymerization degrade with heterogeneous by-products.

Recent work has focused on the formation of crosslinked hydrogels with ideal, homogeneous microstructures to improve network cooperativity and increase hydrogel mechanical integrity.¹⁵⁻¹⁸ This has been achieved through the step polymerization of complementary, end-terminated co-monomers. Originally, Hubbell and coworkers demonstrated the formation of step polymerized hydrogels by crosslinking thiol and electron-poor, vinyl functionalized PEG-based monomers for drug delivery and cell encapsulation.^{19,20} This paradigm has been extended to fabricate gels utilizing several different step growth reactions and associated functional groups, including the copper-catalyzed, Huisgen azide-alkyne coupling of functionalized PEG-based co-monomers,^{16,21,22} the coupling of propylamine terminated PEG with succinimidyl glutarate terminated PEG,¹⁵ and the photoinitiated thiol-ene coupling of norbornene functionalized PEG with di-thiol peptides.²³ Uniquely, Deforest et al. demonstrated the formation of step polymerized hydrogels through the copper-free, strain promoted azide alkyne cycloaddition (SPAAC), forming hydrogels in a bio-orthogonal and cytocompatible

manner.²⁴ Seminal mechanical analyses of step polymerized gels have found that these networks possess increased tensile extension^{16,18} as compared to chain polymerized analogs, while SANS data have demonstrated that these networks, although still not perfectly ideal, possess fewer heterogeneities in the network microstructure.¹⁷ While differences between chain and step polymerization mechanisms and resultant hydrogels are clear, there is little literature on the direct comparison of mechanics and degradation between chain polymerized and step polymerized hydrogels. One can gain valuable insight of the structure-function relationship of hydrogels through direct comparisons between chain and step polymerized hydrogels with similar chemical structures, but profoundly different network connectivities, which will enable the rational design and application of unique hydrogel-based materials.

Furthermore, there is a growing interest in controlling the material properties of both step and chain polymerized hydrogels dynamically and in a user-defined fashion using cleavable chemistries whose degradation can be triggered exogenously. Toward this end, recent work has presented a class of photodegradable hydrogels whose physical and chemical properties can be modified by light post-fabrication with full spatial and temporal control.^{21,25-29} In this manner, photodegradable hydrogels are appropriate for a myriad of applications in the biomedical and materials sciences. Within the tissue engineering field there is a particular interest in designing cytocompatible, photodegradable hydrogels that allow the experimenter to control the extracellular microenvironment in the presence of cells in 3D and in real time.²⁹⁻³³ Meanwhile, the drug delivery community is exploiting photodegradable hydrogels to release factors at specific locations and at specific times.^{34,35} For photodegradable hydrogels to be utilized most effectively in the broad range of applications, a precise and predictable understanding of how irradiation *and* network structure influence degradation-induced changes in material properties is

required. In addition, photodegradation suggests unique opportunities to perform experiments that might provide a better understanding as to how network structure influences material properties during temporally regulated changes to the hydrogel structure.

This work presents the synthesis and characterization of hydrogel networks that are formed by both chain and step polymerization of a single photodegradable PEG based macromolecular precursor as model systems to understand differences in both mechanical properties and degradation between the resultant network structures. The formation and associated material properties of both hydrogels are investigated and compared. Furthermore, the photolabile linker in the hydrogel is employed to compare and contrast the photodegradation-induced changes in the two gels. A previously developed statistical-kinetic model of photodegradation is adapted and expanded to describe the degradation of step growth networks. This model accurately describes degradation differences between hydrogels formed by chain or step growth mechanisms, elucidating aspects of the structure-function relationship in hydrogel photodegradation. In all, the material chemistry enables a more robust understanding of how network connectivity and gel architecture influence properties and degradation, and this fundamental understanding should translate into an improved design of hydrogel cells carriers and drug delivery vehicles for biomedical applications.

5.2 Materials and Methods

All reagents were purchased from Sigma-Aldrich and used as received except as otherwise noted.

5.2.1 Synthesis of gel forming monomers

A photolabile, acrylate functionalized monomer, poly(ethylene glycol) diphotodegradable acrylate (PEGdiPDA), was synthesized according to previous published protocols.^{25,27} Briefly, an acrylated, *o*-nitrobenzyl ether was synthesized and coupled to poly(ethylene glycol) bisamine ($M_n \sim 3400$ Da; Laysan Bio Inc.) to generate a photoresponsive monomer that is capable of forming both chain and step polymerized networks. A four-arm poly(ethylene glycol) ($M_n \sim 10$ kDa; JenKem Technology USA) functionalized with thiol end groups (PEG4SH) was synthesized according to previously published protocol.³⁶

5.2.2 Fabrication of chain polymerized hydrogels

Chain polymerized hydrogels were fabricated by co-polymerizing PEGdiPDA with monoacrylated poly(ethylene glycol) ($M_n \sim 400$ Da, PEGA; Monomer-Polymer Dajac Labs) via redox-initiated, free-radical chain polymerization. Stock solutions of the gel forming precursors were prepared: 49 mM PEGdiPDA in PBS, 1 M PEGA in PBS, 2M ammonium persulfate (APS) in PBS, and 2M tetramethylethylenediamine (TEMED) in PBS. PEGdiPDA and PEGA were combined in PBS at final solution concentrations of 17 mM and 0.2 M, respectively. To initiate polymerization, APS and then TEMED were added to the solution while vortexing at final solution concentrations of 0.2 M and 0.1 M, respectively. The solution was reacted for 7 min to achieve complete polymerization, upon which the gels were swelled in PBS. Gels were formed *in situ* on a parallel-plate shear rheometer (TA Instruments Ares 4400) or between glass slides separated by 0.5 – 1.5 mm thick silicon rubber gaskets.

5.2.3 Fabrication of step polymerized hydrogels

Step polymerized hydrogels were fabricated by co-polymerizing PEGdiPDA with thiol-functionalized, four-arm poly(ethylene glycol) (PEG4SH) via base-catalyzed, Michael-addition. Stock solutions of the gel forming precursors were prepared: 49 mM PEGdiPDA in PBS pH 8.0, 10 mM PEG4SH in PBS pH 8.0, and 1 M triethanolamine (TEOHA) in PBS pH 8.0. PEGdiPDA and PEG4SH were combined in PBS pH 8.0 at final solution concentrations of 11 mM and 5.5 mM, respectively. To accelerate polymerization, TEOHA was added to the solution while vortexing at a final solution concentration of 0.3 M.²⁰ The solution was reacted for 25 min to achieve complete polymerization, upon which the gels were swelled in PBS. Gels were formed *in situ* on a parallel-plate shear rheometer (TA Instruments Ares 4400) or between glass slides separated by 0.5 – 1.5 mm thick silicon rubber gaskets.

5.2.4 Modulus measurements of hydrogels

In situ polymerization was quantified with time sweep tests on gelling solutions in a parallel-plate shear rheometer (TA Instruments Ares 4400; 8.0 mm diameter and 0.05 mm height). Time sweep tests were conducted at 10 rad/s with 10% strain, which was determined to be in the linear viscoelastic regime for both chain and step polymerized hydrogels. Polymerization was followed until the shear storage modulus (G') reached a plateau. The shear storage moduli of swollen chain and step polymerized hydrogels were measured with the parallel-plate shear rheometer. Swollen hydrogel disks (~ 8 mm diameter, ~ 0.5 mm thickness; exact geometry for each gel was obtained with digital calipers prior to analysis) were placed on the shear rheometer while strain and frequency sweeps were conducted to determine the equilibrium swollen, shear storage modulus for each sample.

5.2.5 Tensile testing of hydrogels

Tensile testing of chain and step polymerized hydrogels was performed in uniaxial extension with a materials tester (MTS Synergie 100) with a 10 N load head. Swollen hydrogels were cut into ~ 5 mm x ~ 25 mm rectangles, and the width, length, and thickness of each sample was measured with digital calipers prior to analysis. Each sample was fixed on the materials tester by compression clamps at the top and bottom of the sample (~ 10 mm from each end of the gel) and the local environment was kept humidified during the analyses. The initial separation distance was measured with digital calipers and a constant strain rate of 0.15 mm/mm/min was applied to the sample to failure. The load, stress, strain, and elongation values recorded were used to calculate the true stress and strain from the measured dimensions of each sample. The percent strain at failure was calculated as the final extension divided by the initial separation distance multiplied by 100, and the toughness was calculated by numerically integrating for the area under the stress-strain curve.

5.2.6 Degradation of hydrogels

The kinetics of the photodegradation reaction in both chain and step polymerized hydrogels was quantified by irradiating ($\lambda = 365$ nm; $I_0 = 20$ mW/cm²) *in situ* polymerized gels on a parallel-plate shear rheometer (TA Instruments Ares 4400) and following the modulus evolution as a function of irradiation time. The normalized modulus G'/G'_0 is proportional to the normalized number density of elastically active network strands ν/ν_0 , where ν is the number density of elastically active network strands, for each gel system. As irradiation cleaves bonds within the NBE moiety in the PEGdiPDA molecule, elastically active network strands are broken and based on polymer physics and photoreaction kinetics:

$$\frac{G'}{G'_0} = \frac{\nu}{\nu_0} = \exp(-kt)$$

where

$$k = \frac{\phi \varepsilon I_0}{N_A h \nu} = k_{eff} I_0$$

Here, ϕ is the quantum yield of the NBE moiety; ε is the molar absorptivity of the NBE moiety at the wavelength of irradiation ($\varepsilon = 4300 \text{ L mol}^{-1} \text{ cm}^{-1}$ for $\lambda = 365 \text{ nm}$); I_0 is the incident irradiation intensity (W cm^{-2}); N_A is Avagadro's number; h is the Planck constant; ν is the frequency at the wavelength of irradiation; k_{eff} is the effective rate constant by gathering all variables except for I_0 . A linear fit of $\ln(G'/G'_0)$, as measured by the rheometry experiments, as a function of irradiation time was employed to calculate k and, thus, k_{eff} for both chain and step polymerized hydrogels.

5.2.7 Degradation with collimated light

Collimated light was delivered from an Omnicure S1000 with an internal 365 nm filter through a liquid filled light guide and collimating lens. (All irradiation equipment was purchased from EXFO). Irradiation intensities for all degradation experiments were measured with a calibrated radiometer (Model IL1400A, International Light, Inc., Newburyport, MA), and attenuation of light by the rheometer or photomasks was accounted for by increasing the incident light intensity so that the transmitted light was at the desired intensity.

5.2.8 Erosion of channels into hydrogel surfaces

Photopatterns (400 μm wide black lines spaced by 400 μm) were originally drawn in Adobe Illustrator and printed on Mylar (Advance Reproductions, North Andover, MA). The

photopatterns were attached to glass slides with double-sided tape. Swollen chain and step polymerized gels (10 mm x 10 mm x 1 mm) were aligned under the channel patterns and surrounded by PBS to maintain hydration and facilitate dissolution of degraded products during patterning. The gels were then exposed to collimated 365 nm light at 10 mW/cm² for up to 30 min (Omniculture S1000 with 365 nm filter, liquid filled light guide, and collimating lens, EXFO). Depths of the patterned channels were verified with a profilometer (Stylus Profiler, Dektak 6M).

5.2.9 Model predictions

A statistical-kinetic model of photodegradation³⁷ in chain polymerized networks was applied to model the erosion depth as a function of time for the chain polymerized hydrogels in this work. This model was extended to describe photodegradation in step growth networks by altering the statistical assumptions of network connectivity to account for the differences in network structure in the step polymerized hydrogels in this work. Furthermore, as the time scale of erosion is much faster for step polymerized hydrogels than chain polymerized an additional dissolution assumption was included. Briefly, this states that eroded products at the surface of the gel do not instantly diffuse out of the light path, but diffuse through the PBS solution in the light path to a solution sink at the original surface of the gel. By including this simple assumption, the statistical-kinetic model was able to describe the erosion depth as a function of irradiation time in both chain and step polymerized hydrogels.

5.2.10 Statistics

All data is reported as mean \pm sem and significance was determined by one-tailed or two-tailed t-tests ($p < 0.05$), as appropriate and dependent on the null hypothesis being one mean is

greater or less than the other as compared the null hypothesis being the means are equivalent, respectively.

5.3 Results and Discussion

5.3.1 Formation of chain and step polymerized photodegradable hydrogels

Photodegradable hydrogels were synthesized via chain and step polymerization (**Figure 5.1a**). Chain polymerized (CP) hydrogels were formed by reacting the tetrafunctional PEGdiPDA with a difunctional co-monomer, PEGA, under redox-initiated free-radical chain polymerization. Step polymerized (SP) hydrogels were formed by reacting the difunctional PEGdiPDA with a tetrafunctional co-monomer, PEG4SH, through a base-catalyzed Michael-addition. In each case, the network formation occurred through the chemical bonding of the acrylate-functionalized PEGdiPDA. In the chain polymerization each acrylate is difunctional allowing the PEGdiPDA to serve as a tetrafunctional crosslinker, whereas in the step polymerization each acrylate is monofunctional extending the elastically active chains between the tetrafunctional PEG4SH crosslinkers.

Previous studies have shown that the network microstructure of PEG gels formed by chain polymerization is comprised of dense polyacrylate kinetic chains connected by PEG crosslinks.¹⁴ These heterogeneities exist on the length scale of the PEG crosslinker, while further heterogeneities form as radical initiation stochastically leads to regions of increased crosslinking density on the micron scale. In contrast, PEG hydrogels formed by step polymerizations have been shown to possess fewer heterogeneities on all length scales.¹⁵ These heterogeneities are limited generally to cyclization and dangling ends. In this manner, the chain polymerization

(CP) of PEGdiPDA formed a heterogeneous network structure,¹⁴ while the step polymerization (SP) formed a more ideal network structure (**Figure 5.1a**).¹⁷

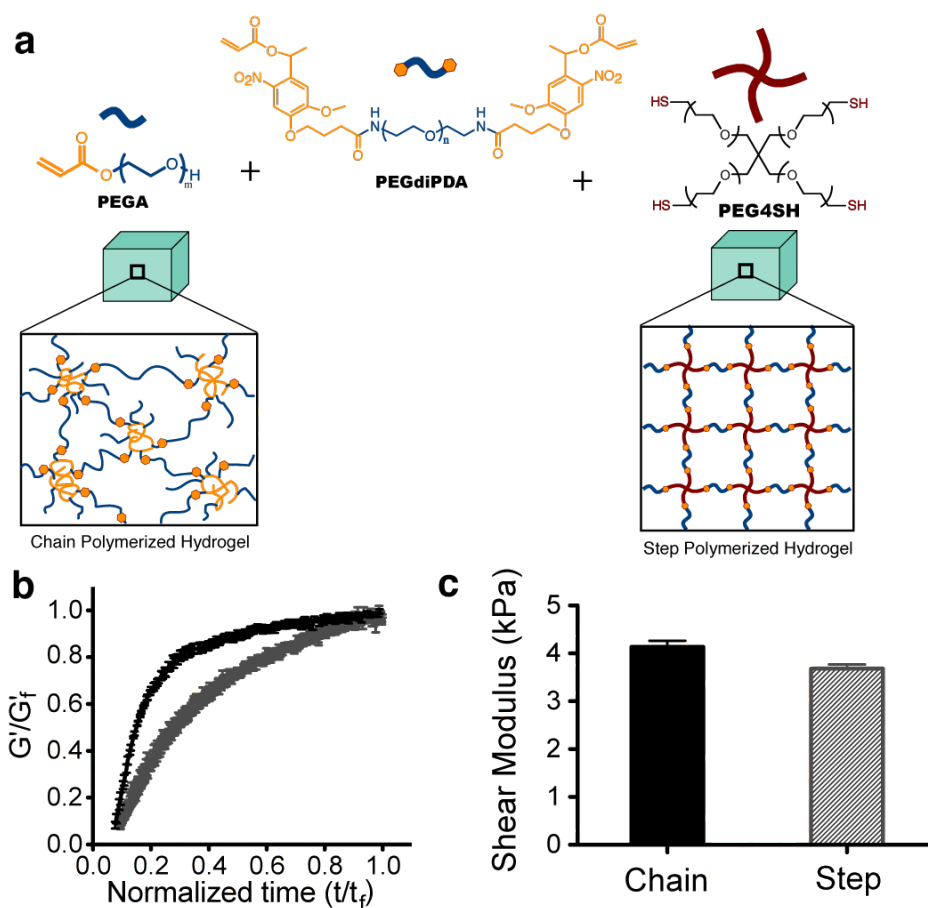


Figure 5.1 Fabrication of chain and step polymerized photodegradable hydrogels. **(a)** Chain polymerized and step polymerized hydrogels were formed with the same photolabile monomer, PEGdiPDA. Chain polymerized hydrogels (CP gels) were fabricated through the copolymerization of PEGdiPDA with PEGA via free-radical polymerization, resulting in a heterogeneous network structure. Step polymerized hydrogels (SP gels) were fabricated through the copolymerization of PEGdiPDA with PEG4SH via Michael-addition polymerization. **(b)** Chain polymerized and step polymerized hydrogels form in minutes, $t_f = 370 \pm 1$ s for CP gels and $t_f = 1470 \pm 60$ s for SP gels. **(c)** Chain polymerized and step polymerized hydrogels form with similar shear storage moduli, $G'_f = 4140 \pm 130$ Pa for CP gels and $G'_f = 3680 \pm 90$ Pa for SP gels.

Hydrogels were formed for each gel system *in situ* on a parallel plate rheometer (TA ARES) to quantify the evolution of shear storage modulus (G') as a function of polymerization time (**Figure 5.1b**). For the CP hydrogel, the time to complete polymerization, defined by the

plateau in the storage modulus, was 370 ± 1 seconds. The time to complete polymerization for the SP hydrogel was 1470 ± 60 seconds. The final shear storage moduli for the chain and step systems were 4140 ± 130 Pa and 3680 ± 90 Pa, respectively (**Figure 5.1c**). In either case, the total polymerization time can be tuned by altering the initial macromer concentration and the initiator concentrations (ammonium persulfate/TEMED for the chain polymerization and triethanolamine/pH for the step polymerization). (data not shown) For this work, the focus remained on these two specific formulations as they generated hydrogels with similar final shear storage moduli and crosslinking densities, while possessing disparate network architectures. In this manner, we were able to compare other material properties that should depend on network cooperativity and connectivity, independent of crosslinking density.

5.3.2 Mechanical analysis of chain and step polymerized hydrogels

It has been suggested that the increased homogeneity and network cooperativity of SP hydrogels results in an increase in mechanical integrity, specifically tensile strain to break, as compared to CP hydrogels.¹⁶ To compare the tensile properties of the chain and step polymerized PEG hydrogels studied in this work, dynamic mechanical analysis was conducted on both gels. The percent strain to failure of CP gels was 33 ± 4 % whereas the percent strain to failure for SP gels was 129 ± 11 %. The analyses further indicated that, despite similar storage moduli, the SP gels possessed significantly increased tensile toughness compared to CP gels (4130 ± 370 Pa and 1250 ± 300 Pa, respectively) owing to the cooperativity of elastically active network strands in the microstructure (**Figure 5.2**).

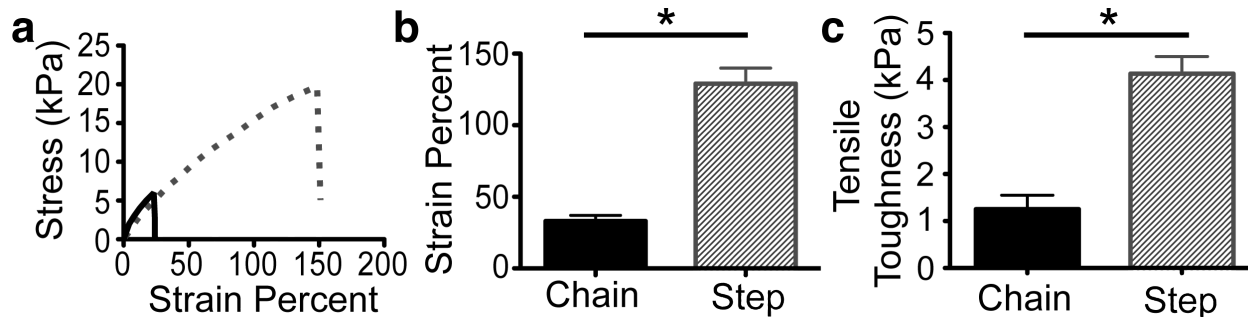


Figure 5.2 Mechanical analysis of chain and step polymerized hydrogels. (a) Uniaxial extension of CP and SP gels was conducted to measure the percent strain to failure and modulus of toughness from the stress-strain curves. Solid black line is a representative stress-strain curve for the CP gels. Dotted grey line is a representative stress-strain curve for the SP gels. (b) The average percent strain to failure was significantly higher for SP (grey) gels as compared to CP (black) gels, $129 \pm 11\%$ compared to $33 \pm 4\%$. (c) The SP (grey) gels also demonstrated a significantly increased tensile toughness as compared to CP (black) gels, 4130 ± 370 Pa compared to 1250 ± 300 Pa.

From both the tensile analyses, it was observed that mechanical integrity, *i.e.*, ductility and toughness, is significantly improved for hydrogels formed by step polymerization as compared to chain polymerization. These differences in material properties are conferred by the network structure, specifically the increased network cooperativity and decreased heterogeneity in the SP hydrogel, and suggest that applications that require more ductile or tough materials should employ SP hydrogels. In addition to mechanical integrity, network connectivity directly relates to the diffusion of macromolecules through the hydrogel network as ideal networks should facilitate more uniform diffusion as compared to heterogeneous structures. Finally, mechanical stresses are translated anisotropically in heterogeneous networks, which may be important for mechanical stimulation or differentiation of mammalian cells.

5.3.3 Photodegradation of chain and step polymerized hydrogels

The CP and SP gels were formed from the same photolabile monomer, PEGdiPDA, rendering them both photodegradable. The degradation is facilitated by the *o*-nitrobenzyl ether

(NBE) moieties that reside within the PEGdiPDA monomer (**Figure 1a**) and undergo an irreversible cleavage in the presence of light (one-photon: $\lambda = 320\text{-}436\text{ nm}$ and two-photon: $\lambda = 740\text{ nm}$).²⁷ On account of this property, light was able to cleave bonds within the materials, resulting in the breakage of elastically active network strands and, ultimately, erosion of the gel with light exposure (**Figure 5.3a,b**). Prior to erosion, photodegradation led to an exponential decrease in the shear storage modulus (**Figure 5.3c**), which was governed by the inherent rate of photocleavage of the NBE moiety, k_{eff} . As both gels contained the same NBE moiety in the network backbone, it was predicted that the initial cleavage rate of elastically active strands, measured as a decrease in shear storage modulus, would be the same for both the CP and SP gels. The cleavage rate, k_{eff} , for the CP gel was $0.0140 \pm 0.0012\text{ s}^{-1}$ and the cleavage rate for the SP gel was $0.0142 \pm 0.0012\text{ s}^{-1}$. These effective cleavage rates were not statistically different and were in agreement with previously reported cleavage rates for similar NBE moieties.^{25,29,32,37,38}

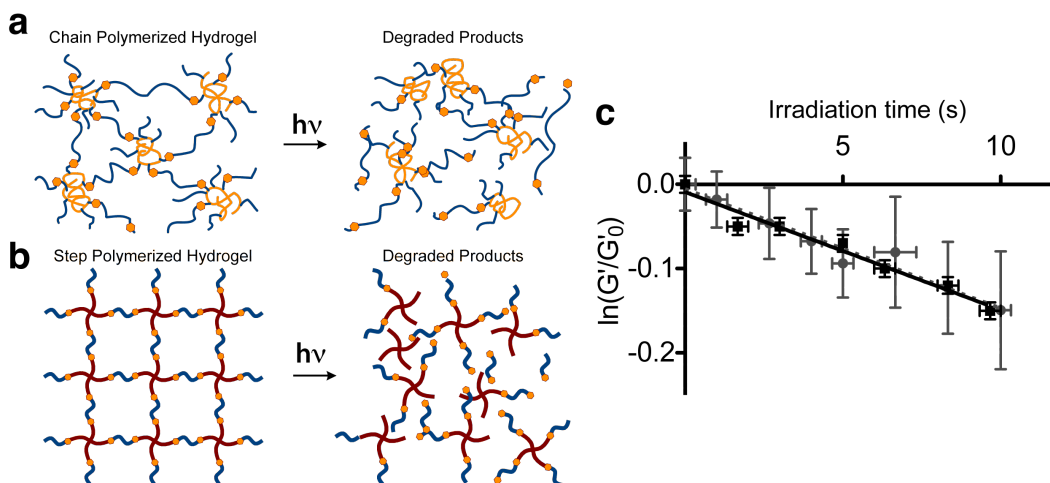


Figure 5.3 Photodegradation of chain and step polymerized hydrogels. (a) and (b) The *o*-nitrobenzyl ether moieties (orange ring structures) in PEGdiPDA undergo an irreversible cleavage in response to irradiation (one-photon: $\lambda \sim 320\text{-}436\text{ nm}$, two-photon: $\lambda \sim 740\text{ nm}$), breaking elastically active network strands in the hydrogel backbone. In this manner, light can be employed to degrade and, ultimately, erode the CP and SP hydrogels. (c) Owing to the inclusion of the same photolabile monomer into the network backbone, the initial effective cleavage kinetic constant, defined as the opposite of the slope of $\ln(G/G_0)$ as a function of irradiation time divided by the incident irradiation intensity, was similar for the CP (black) and SP (grey) gels.

To investigate how network structure influences mass loss and erosion rates of the CP and SP gels, physical channels were eroded into the surfaces of both gels. While rheometry results indicated that the inherent rate of photodegradation is independent of network structure, the erosion rates for the CP and SP gels diverged even at short timescales (**Figure 5.4a**). Statistical-kinetic models of photodegradation and erosion in chain polymerized³⁷ and step polymerized hydrogels were applied to describe the depth of channel formation as a function of time to elucidate how network connectivity leads to dramatic differences in pattern formation rate. In both cases, the simple statistical-kinetic model captured the observed erosion behavior (**Figure 5.4a**), which indicates that the statistical-kinetic model includes the relevant physics of erosion in CP and SP photodegradable gels. These results demonstrate that lower network connectivity, observed in SP gels, leads to a faster erosion rate. For these experiments, the assumption of dissolution of erosion by-products was accounted for in the rapidly degrading step polymerized gels.

In both of these models, the critical parameter that dictates the erosion rate is the critical fraction of cleaved NBE species, P_{rg} , that results in reverse gelation. Here, reverse gelation refers to the critical extent of bonds cleaved to cause the insoluble gel to erode completely into soluble polymer chains (**Figure 5.3a,b**). The network structure of the SP gels resulted in a $P_{rg} = 0.42$ while the CP gels resulted in a $P_{rg} = 0.77$. A critical time scale, t_c , was defined as the time to reach reverse gelation at the surface of a photodegradable and is a function of P_{rg} :

$$t_c = \frac{-\ln(1-P_{rg})}{k_{eff}I_0} \quad \text{Eq. 1}$$

where, k_{eff} is the effective kinetic constant of cleavage of the NBE moiety; I_0 is the intensity of the incident irradiation. Since the cleavage reaction followed first-order kinetics with the same

effective kinetic constant in both gels and each was exposed to the same incident irradiation, the difference in P_{rg} alone determined the difference in erosion time constants, $t_c = 490$ seconds for CP gels and $t_c = 180$ seconds for SP gels.

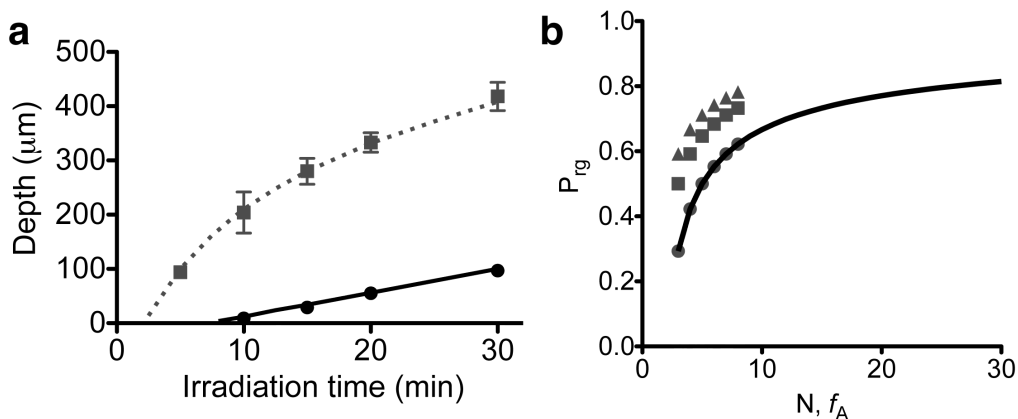


Figure 5.4 Modeling erosion in chain and step polymerized hydrogels. (a) The erosion depth of photopatterned channels as a function of irradiation time was plotted for the CP (black) and SP (grey) photodegradable hydrogels. A statistical-kinetic photodegradation model based on the photocleavage reaction and network connectivity predicted these functions over the 30 minute exposure time. (b) The critical extent of NBE moieties that need to be cleaved to reach reverse gelation governs the rate at which features can be patterned into photodegradable gels. P_{rg} is a function of network connectivity in both CP and SP gels. Here, $P_{rg}(N)$ is plotted for CP gels (solid black line) and $P_{rg}(f_A)$ is plotted for SP gels with $f_B = 2$ (grey circles), $f_B = 3$ (grey squares), and $f_B = 4$ (grey triangles).

The critical erosion time scale, t_c , governed not only the time to erode the surface of the gel, but also the rate at which erosion progresses through the depth of the gel. A critical length scale, z_c , was defined as the inverse of the initial absorbance of the hydrogel:

$$z_c = \frac{1}{2.3\epsilon_i C_i} \quad \text{Eq. 2}$$

where, ϵ_i is the molar absorptivity of the NBE moiety; C_i is the concentration of the NBE moiety.

A rate for which the erosion progressed through the gel was predicted as the critical length scale of photodegradation divided by the critical time scale of photodegradation:

$$\frac{z_c}{t_c} = \frac{-k_{eff} I_0}{2.3\epsilon_i C_i \ln(1-P_{rg})} \quad \text{Eq. 3}$$

Owing to the differences in the concentration of NBE moieties and P_{rg} in the CP and SP gels, the rate of erosion was significantly faster for SP gels as compared to CP gels. The simple scaling analysis predicted an erosion rate of 3.6 $\mu\text{m}/\text{min}$ and 18.4 $\mu\text{m}/\text{min}$ compared to experimental values of $4.4 \pm 0.1 \mu\text{m}/\text{min}$ and $18.6 \pm 2.0 \mu\text{m}/\text{min}$ for the CP and SP gels, respectively.

The above analysis of erosion rates and P_{rg} holds for the specific chain polymerized and step polymerized hydrogels in this manuscript and gels formed with the same connectivity. However, more broadly, the equations hold for the general class of *photodegradable* hydrogels for which the network structure and physical parameters are known. Specifically, step polymerized gels have been formed from PEG monomers with varying functionality leading to different network connectivity.^{18,39} For instance, the crosslinking of an octafunctional, thiol-terminated PEG with a tetrafunctional, vinyl-sulfone terminated PEG would form a network with different connectivity than a tetrafunctional, thiol-terminated PEG and a trifunctional, vinyl-sulfone terminated PEG. Differences in network connectivity are directly related to P_{rg} and, ultimately, the rate of erosion. The reverse gelation point for step polymerized hydrogels, formed from two complementary monomers, has been adapted from classical derivations by Flory and Rehner that describe network formation in step growth polymerizations:^{23,40,41}

$$P_{rg}^{step} = 1 - \frac{1}{\sqrt{r(f_A-1)(f_B-1)}} \quad \text{Eq. 4}$$

where, f_A is the functionality of the A-terminated monomer; f_B is the functionality of the B-terminated monomer; and r is the stoichiometric ratio of A to B. Similarly, the reverse gelation point for chain polymerized hydrogels has been adapted from classical derivations of Macosko and Miller:⁴²⁻⁴⁴

$$P_{rg}^{chain} = 1 - \frac{1}{\sqrt{N-1}} \quad \text{Eq. 5}$$

where, N is the number of crosslinking molecules per polyacrylate kinetic chain, which is determined by the polymerization conditions and monomer formulation. Eqs. 1 & 2 indicate how network connectivity relates to P_{rg} , which can be related to the rate of erosion in photodegradable hydrogels (Eq. 3).

Figure 5.4b illustrates how P_{rg} is related to the monomers or polymerization conditions for both chain and step polymerized hydrogels (r was assumed to be unity for all step polymerization conditions; **Figure 5.4b**). For a multifunctional monomer reacting with a difunctional monomer through step polymerization (**Figure 5.4b**, circles), P_{rg} collapses onto the curve for the chain polymerization. However, chain polymerizations typically result in an N of 10 – 100, while it is difficult to synthesize multifunctional monomers beyond a functionality of 8 for step polymerizations ($f_A \leq 8$). Therefore, to achieve reverse gelation points that are similar to common chain polymerized formulations, one can co-polymerize multifunctional monomers ($f_A = 3-8$) with trifunctional or tetrafunctional complementary monomers (**Figure 5.4b**; squares and triangles, respectively).

The above analysis illustrates how network structure relates to the rates of erosion or feature generation in photodegradable hydrogels. By exploiting the rapid erosion of step polymerized hydrogels formed by the co-polymerization of complementary tetrafunctional and difunctional monomers, photodegrading hydrogels were designed for the controlled release entrapped factors³⁵ and cells,²⁹ as well as geometric patterning of cell culture microwells.⁴⁵ Further, the increased P_{rg} for the CP gels is advantageous to generate materials with broad anisotropic elasticities in the x - y ³⁰ or z -dimensions³¹ as the gel remains intact at a lower crosslinking density than the SP gels.

5.4 Conclusion

Photodegradable hydrogels were fabricated by both chain and step polymerization from the same photolabile monomer, PEGdiPDA. Compared to chain polymerized gels, step polymerized hydrogels possessed increased mechanical integrity, as quantified by ductility and toughness. Increases in mechanical integrity were attributed to increased homogeneity and network connectivity possessed in step polymerized hydrogels as compared to the relatively heterogeneous chain polymerized gels. Light-induced degradation and erosion was demonstrated in both the chain polymerized and step polymerized gels. The inherent kinetic constant of photodegradation was the same in the two systems as both gels possess the same *o*-nitrobenzyl ether moiety in their backbones, while the rate of erosion was much faster in step polymerized hydrogels on account of the network connectivity. Taken together, these studies illustrate the utility of hydrogels polymerized by either chain or step growth polymerization for different applications and provide a quantitative tool for designing and predicting degradation, a critical parameter for regulating cell fate,⁴⁶ tissue regeneration,⁴⁷ or drug release⁵ amongst many other biomedical applications.

5.5 References

1. Lutolf, M. P. & Hubbell, J. A. Synthetic biomaterials as instructive extracellular microenvironments for morphogenesis in tissue engineering. *Nat Biotechnol* **23**, 47–55 (2005).
2. Tibbitt, M. W. & Anseth, K. S. Hydrogels as Extracellular Matrix Mimics for 3D Cell Culture. *Biotechnol Bioeng* **103**, 655–663 (2009).
3. Magin, C. M. *et al.* Antifouling performance of cross-linked hydrogels: refinement of an attachment model. *Biomacromolecules* **12**, 915–922 (2011).
4. Kidane, A., Szabocsik, J. & Park, K. Accelerated study on lysozyme deposition on poly(HEMA) contact lenses. *Biomaterials* **19**, 2051–2055 (1998).

5. Liechty, W. B., Kryscio, D. R., Slaughter, B. V. & Peppas, N. A. Polymers for drug delivery systems. *Annu Rev Chem Biomol Eng* **1**, 149–173 (2010).
6. Peppas, N., Hilt, J., Khademhosseini, A. & Langer, R. Hydrogels in biology and medicine: From molecular principles to bionanotechnology. *Adv Mater* **18**, 1345–1360 (2006).
7. Sawhney, A. S., Pathak, C. P. & Hubbell, J. A. Bioerodible hydrogels based on photopolymerized poly(ethylene glycol)-co-poly(.alpha.-hydroxy acid) diacrylate macromers. *Macromolecules* **26**, 581–587 (1993).
8. Anseth, K., Bowman, C. & BrannonPeppas, L. Mechanical properties of hydrogels and their experimental determination. *Biomaterials* **17**, 1647–1657 (1996).
9. West, J. L. & Hubbell, J. A. Polymeric Biomaterials with Degradation Sites for Proteases Involved in Cell Migration. *Macromolecules* **32**, 241–244 (1999).
10. Hoyle, C. E. & Bowman, C. N. Thiol-Ene Click Chemistry. *Angew Chem Int Edit* **49**, 1540–1573 (2010).
11. Anseth, K., WANG, C. & Bowman, C. Reaction Behavior and Kinetic Constants for Photopolymerizations of Multi(Meth)Acrylate Monomers. *Polymer* **35**, 3243–3250 (1994).
12. Quick, D. J. & Anseth, K. S. DNA delivery from photocrosslinked PEG hydrogels: encapsulation efficiency, release profiles, and DNA quality. *Journal of controlled release : official journal of the Controlled Release Society* **96**, 341–351 (2004).
13. McCall, J. D., Lin, C.-C. & Anseth, K. S. Affinity peptides protect transforming growth factor beta during encapsulation in poly(ethylene glycol) hydrogels. *Biomacromolecules* **12**, 1051–1057 (2011).
14. Lin-Gibson, S., Jones, R., Washburn, N. & Horkay, F. Structure-property relationships of photopolymerizable poly(ethylene glycol) dimethacrylate hydrogels. *Macromolecules* **38**, 2897–2902 (2005).
15. Sakai, T. *et al.* Design and fabrication of a high-strength hydrogel with ideally homogeneous network structure from tetrahedron-like macromonomers. *Macromolecules* **41**, 5379–5384 (2008).
16. Malkoch, M. *et al.* Synthesis of well-defined hydrogel networks using Click chemistry. *Chem Commun* 2774–2776 (2006).doi:10.1039/b603438a
17. Matsunaga, T., Sakai, T., Akagi, Y., Chung, U.-I. & Shibayama, M. Structure Characterization of Tetra-PEG Gel by Small-Angle Neutron Scattering. *Macromolecules* **42**, 1344–1351 (2009).
18. Yang, T. *et al.* Characterization of Well-Defined Poly(ethylene glycol) Hydrogels Prepared by Thiol-ene Chemistry. *J Polym Sci Pol Chem* **49**, 4044–4054 (2011).

19. Elbert, D., Pratt, A.B., Lutolf, M., Halstenberg, S. & Hubbell, J. Protein delivery from materials formed by self-selective conjugate addition reactions. *J Control Release* **76**, 11–25 (2001).
20. Lutolf, M., Raeber, G., Zisch, A., Tirelli, N. & Hubbell, J. Cell-responsive synthetic hydrogels. *Adv Mater* **15**, 888–+ (2003).
21. Johnson, J. A., Baskin, J. M., Bertozzi, C. R., Koberstein, J. T. & Turro, N. J. Copper-free click chemistry for the in situ crosslinking of photodegradable star polymers. *Chem Commun* 3064–3066 (2008).doi:10.1039/b803043j
22. Johnson, J. A., Finn, M. G., Koberstein, J. T. & Turro, N. J. Synthesis of photocleavable linear macromonomers by ATRP and star macromonomers by a tandem ATRP-click reaction: Precursors to photodegradable model networks. *Macromolecules* **40**, 3589–3598 (2007).
23. Fairbanks, B. D. *et al.* A Versatile Synthetic Extracellular Matrix Mimic via Thiol-Norbornene Photopolymerization. *Adv Mater* **21**, 5005–5010 (2009).
24. Deforest, C. A., Polizzotti, B. D. & Anseth, K. S. Sequential click reactions for synthesizing and patterning three-dimensional cell microenvironments. *Nat Mater* **8**, 659–664 (2009).
25. Kloxin, A. M., Kasko, A. M., Salinas, C. N. & Anseth, K. S. Photodegradable hydrogels for dynamic tuning of physical and chemical properties. *Science* **324**, 59–63 (2009).
26. Frey, M. T. & Wang, Y.-L. A photo-modulatable material for probing cellular responses to substrate rigidity. *Soft Matter* **5**, 1918–1924 (2009).
27. Kloxin, A. M., Tibbitt, M. W. & Anseth, K. S. Synthesis of photodegradable hydrogels as dynamically tunable cell culture platforms. *Nat Protoc* **5**, 1867–1887 (2010).
28. Wong, D. Y., Griffin, D. R., Reed, J. & Kasko, A. M. Photodegradable Hydrogels to Generate Positive and Negative Features over Multiple Length Scales. *Macromolecules* **43**, 2824–2831 (2010).
29. Deforest, C. A. & Anseth, K. S. Cytocompatible click-based hydrogels with dynamically tunable properties through orthogonal photoconjugation and photocleavage reactions. *Nat Chem* **3**, 925–931 (2011).
30. Kloxin, A. M., Benton, J. A. & Anseth, K. S. In situ elasticity modulation with dynamic substrates to direct cell phenotype. *Biomaterials* **31**, 1–8 (2010).
31. Kloxin, A. M., Tibbitt, M. W., Kasko, A. M., Fairbairn, J. A. & Anseth, K. S. Tunable Hydrogels for External Manipulation of Cellular Microenvironments through Controlled Photodegradation. *Adv Mater* **22**, 61–66 (2010).
32. Tibbitt, M. W., Kloxin, A. M., Dyamenahalli, K. U. & Anseth, K. S. Controlled two-

- photon photodegradation of PEG hydrogels to study and manipulate subcellular interactions on soft materials. *Soft Matter* **6**, 5100–5108 (2010).
33. Deforest, C. A. & Anseth, K. S. Photoreversible Patterning of Biomolecules within Click-Based Hydrogels. *Angew Chem Int Ed Engl* **51**, 1816–1819 (2012).
 34. Peng, K. *et al.* Dextran based photodegradable hydrogels formed via a Michael addition. *Soft Matter* **7**, 4881–4887 (2011).
 35. Tibbitt, M. W., Han, B. W., Kloxin, A. M. & Anseth, K. S. Synthesis and application of photodegradable microspheres for spatiotemporal control of protein delivery. *J Biomed Mater Res A* **100**, 1647–1654 (2012).
 36. Fairbanks, B. D., Singh, S. P., Bowman, C. N. & Anseth, K. S. Photodegradable, Photoadaptable Hydrogels via Radical-Mediated Disulfide Fragmentation Reaction. *Macromolecules* **44**, 2444–2450 (2011).
 37. Tibbitt, M. W., Kloxin, A. M. & Anseth, K. S. Modeling Photodegradation in Optically Thick Polymer Networks for the Predictable Control of Network Evolution. *Macromolecules* **In Review**.
 38. Griffin, D. R., Patterson, J. T. & Kasko, A. M. Photodegradation as a mechanism for controlled drug delivery. *Biotechnol Bioeng* **107**, 1012–1019 (2010).
 39. Gould, S. T., Darling, N. J. & Anseth, K. S. Small peptide functionalized thiol-ene hydrogels as culture substrates for understanding valvular interstitial cell activation and de novo tissue deposition. *Acta Biomater* (2012).
 40. Flory, P. J. *Principles of Polymer Chemistry*. (Cornell University Press, 1953).
 41. Flory, P. & Rehner, J. Statistical mechanics of cross-linked polymer networks I Rubberlike elasticity. *J Chem Phys* **11**, 512–520 (1943).
 42. Macosko, C. W. & Miller, D. R. A new derivation of average molecular weights of nonlinear polymers. *Macromolecules* **9**, 199–206 (1976).
 43. Miller, D. R. & Macosko, C. W. A new derivation of post gel properties of network polymers. *Macromolecules* **9**, 206–211 (1976).
 44. Reddy, S., Anseth, K. & Bowman, C. Modeling of network degradation in mixed step-chain growth polymerizations. *Polymer* **46**, 4212–4222 (2005).
 45. Kloxin, A. M. *et al.* Responsive culture platform to examine the influence of microenvironmental geometry on cell function in 3D. *Integr. Biol.* **4**, 1540–1549 (2012).
 46. Anderson, S. B., Lin, C.-C., Kuntzler, D. V. & Anseth, K. S. The performance of human mesenchymal stem cells encapsulated in cell-degradable polymer-peptide hydrogels. *Biomaterials* **32**, 3564–3574 (2011).

47. Bryant, S. & Anseth, K. Controlling the spatial distribution of ECM components in degradable PEG hydrogels for tissue engineering cartilage. *J Biomed Mater Res A* **64A**, 70–79 (2003).

CHAPTER VI

TUNABLE HYDROGELS FOR EXTERNAL MANIPULATION OF CELLULAR MICROENVIRONMENTS THROUGH CONTROLLED PHOTODEGRADATION

As published in *Advanced Materials*, **22**, 61-66 (2010)

6.1 Introduction

Hydrogels provide a unique environment for three-dimensional cell culture, but typically, the material properties are fixed upon formation. Given the growing interest in understanding how material microenvironments influence cellular functions, numerous approaches have emerged to control not only the initial biochemical and biophysical properties of gels, but also how these properties change with degradation. While these strategies allow the synthesis of hydrogels with predictable degradation profiles and property changes, a material system that allows external manipulation of the properties of a cell-laden gel at any point in time or space would fill a unique niche. For example, such a cell culture system would allow real-time manipulation of the extracellular microenvironment and simultaneous monitoring of cellular processes in three-dimensional culture. In this contribution, photocleavable linkers were integrated into the crosslinks of a poly(ethylene glycol)-based (PEG) hydrogel, allowing the network structure to be tuned exogeneously and predictably with irradiation under cytocompatible conditions. Such a material system will enable new opportunities to test

hypotheses about how precise variations in the local gel environment direct important cellular functions, such as process extension, migration, and mechanotransduction.

There is a growing interest in the development of hydrogels as a platform for encapsulating cells and their application in fields ranging from tissue engineering to three-dimensional cell culture.¹ As one example, di(meth)acrylated PEG macromolecules can be polymerized via photoinitiation to form a hydrogel in the presence of cells,² and these covalently crosslinked materials have been widely used in numerous tissue engineering applications.³⁻⁵ Beyond simple cell encapsulation, Hahn et al.⁶ reported the chemical patterning of these PEG networks using a two-photon confocal laser scanning microscope (LSM). Using a two-step process, an RGD functionalized PEG network was formed in spatially defined regions within an existing PEG gel. More recently, Tayalia et al.⁷ demonstrated the potential of two-photon initiation to spatially direct polymerization of multifunctional acrylate monomers. Networks with uniform pores ranging from 10 to 100 μm were fabricated, allowing the examination of cell migration as a function of pore size. While control of the initial network structure and chemistry is important for cell culture scaffolds, an equally critical aspect of hydrogel design is temporal regulation of the material properties (i.e., degradation).

Hydrogel property control via degradation is critical, as many dynamic cellular processes require temporal and spatial changes in the material environment. Changes in hydrogel properties, such as crosslinking density and modulus, allow and even dictate changes in cell function such as migration,⁸ process extension,⁹ and differentiation.¹⁰ Degradation of PEG hydrogels is often achieved by incorporating hydrolytically or enzymatically degradable blocks within the gel-forming macromers. Classically, hydrolytically degradable gels have been synthesized from poly(lactic acid)-*b*-PEG-*b*-poly(lactic acid) (PLA-*b*-PEG-*b*-PLA) and

poly(caprolactone)-*b*-PEG-*b*-poly(caprolactone) (PCL-*b*-PEG-*b*-PCL) macromers with vinyl end groups, where the temporal degradation rate is dictated by the initial macromer chemistry.¹¹⁻¹³ While this chemistry leads to hydrogels with predictable changes in their material properties with time, the process occurs uniformly in the bulk and cannot be altered after gel formation. More recently enzymatically degradable gels have been created from PEG macromers containing matrix metalloprotease-degradable (MMP) peptide blocks or through a step-growth reaction of thiol-functionalized oligopeptides with vinyl functionalized PEGs.^{10, 14} In these materials, cells secrete MMPs and locally dictate the degradation rate. This mechanism provides specific advantages for many tissue engineering applications, as the gel degradation does not need to be fixed *a priori*. However, the experimenter cannot easily manipulate the cellular microenvironment, and understanding how the cells are manipulating their local material environment is challenging. Thus, a three-dimensional cell culture system that would allow externally regulated changes in the gel structure and properties in time and space would address a void in current biomaterial scaffolds.

Light-induced reactions have the potential to offer this level of temporal and spatial material property control. Literature demonstrates that hydrogels formed by dimerization of nitrocinnamate groups afford reversible hydrogel formation but require cytotoxic irradiation conditions (254 nm light).^{15,16} To avoid use of this cytotoxic wavelength, researchers have incorporated nitrobenzyl ether derivatives within hydrogels, which cleave upon exposure to 365 nm light for post-gelation modification with pendant functionalities.¹⁷ Recently, we have incorporated this photolabile moiety into PEG-based hydrogels to control gel erosion and the presentation of an adhesion peptide.¹⁸ Here, we demonstrate that this chemistry affords precise and predictable tuning of the gel structure in real-time with low-intensity, long-wavelength UV

light under cytocompatible conditions. Specifically, gradients in crosslinking density are created and utilized to control cell morphology in three-dimensions, and mass loss and gel erosion are controlled and predicted using a photodegradation model. Further, by focusing a single-photon visible light source, the desired properties are manipulated in three-dimensions with micron-scale resolution.

6.2 Results and Discussion

6.2.1 Synthesis of photodegradable, three-dimensional culture platforms

Photodegradable PEG-based hydrogels containing a nitrobenzyl ether photolabile moiety^{19,20} were synthesized by redox-initiated radical chain copolymerization of a diacrylated PEG-based photodegradable crosslinking macromer (PEGdiPDA)¹⁸ with a monoacrylated PEG (PEGA) in water. The molar ratio of PEGdiPDA to PEGA was varied to alter the initial gel crosslinking density (**Figure 6.1**). Upon irradiation, the photocleavable crosslinks degrade, releasing modified PEG and decreasing the crosslinking density until complete dissolution at the reverse gel point.²¹ Depending on the irradiation wavelength and concentration of the photodegradable group in the swollen gel, light can either penetrate uniformly, leading to bulk degradation (**Figure 6.1b**, top), or become attenuated, leading to gradient changes in the crosslinking density (**Figure 6.1b**, middle) or surface erosion (**Figure 6.1b**, bottom). At commonly used wavelengths for cell encapsulation and imaging, the molar extinction coefficients of the photodegradable crosslinker decrease from 7600 L mol⁻¹ cm⁻¹ at 365 nm to 1640 L mol⁻¹ cm⁻¹ at 405 nm to 73 L mol⁻¹ cm⁻¹ at 488 nm. Based on the photolabile moiety's light absorbance and quantum yield, the irradiation wavelength and intensity dictate the degradation rate and are used to predictably tune the hydrogel properties in time and space. In

addition, light can be focused within the hydrogel using a single photon LSM, eroding the gel only near the focal point and allowing subsequent rastering of the focal point within the gel to create three-dimensional structures (**Figure 6.1c**).

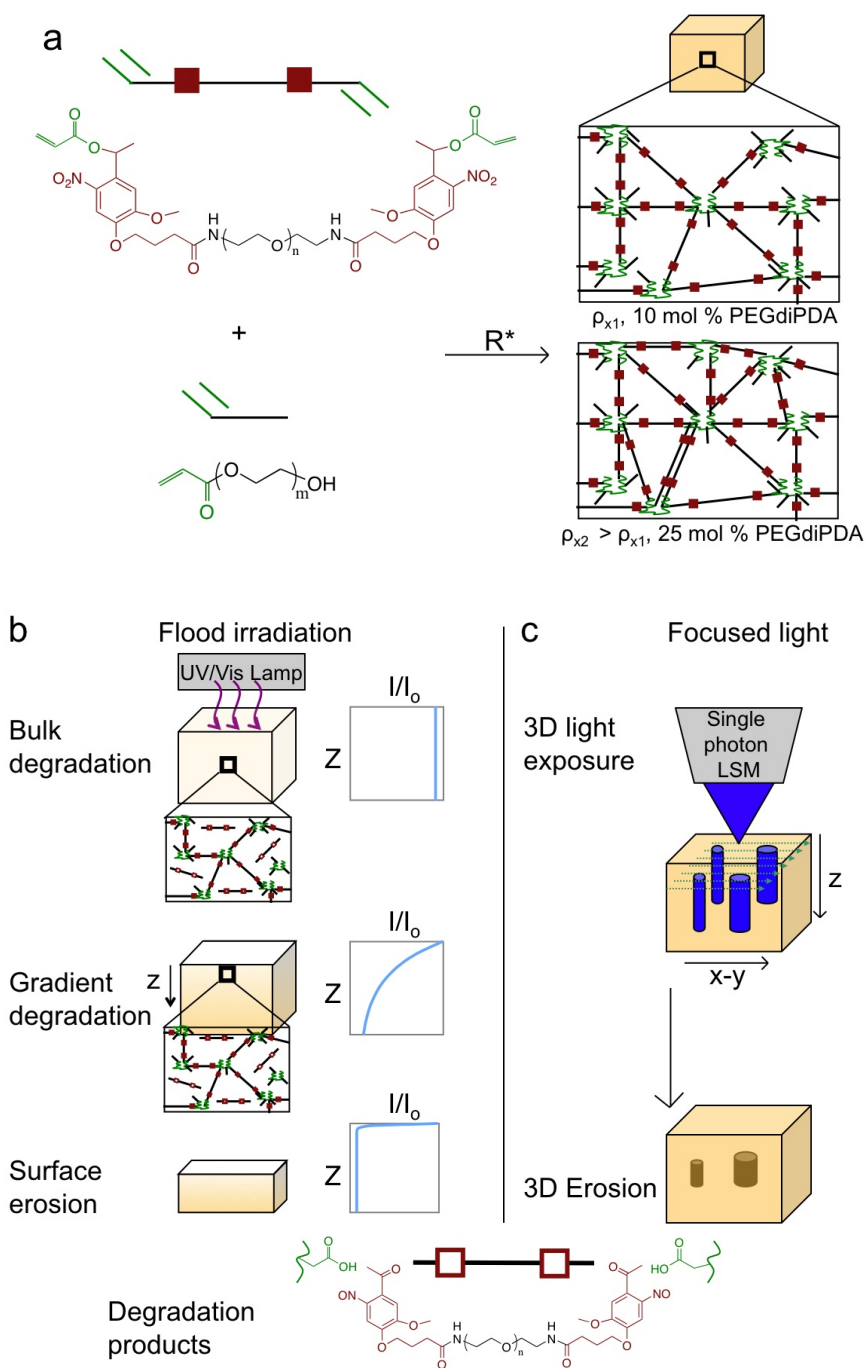


Figure 6.1 Photodegradable hydrogel synthesis and degradation schematics. (a) Photodegradable hydrogels were synthesized by redox-initiated radical chain polymerization of PEGdiPDA (top left) with PEGA (bottom left) (15 wt% total macromer in water). The resulting swollen polymer network consists of polyacrylate chains (green coils) linked by degradable PEG (black lines with red boxes). The initial gel crosslinking density (ρ_x) is varied with crosslinker concentration. (b) Upon irradiation, the photolabile moiety is cleaved (open red boxes), releasing PEG (black) and decreasing the gel crosslinking density. With flood irradiation, light can either penetrate the gel uniformly, causing bulk degradation (top), or be attenuated with absorption by the photolabile group, causing gradient changes in the crosslinking density (middle) or surface erosion (bottom). The intensity profile within the gel is dictated by the irradiation wavelength and the photolabile group concentration. (c) Three-dimensional structures are eroded in a hydrogel using focused light directed by a single photon LSM, where desired shapes are drawn using region of interest software and subsequently scanned with a laser within the hydrogel.

6.2.2 Degradation of three-dimensional, photodegradable hydrogels

To characterize the hydrogel's degradation kinetics, the bulk degradation of optically thin gels was followed with rheometry during irradiation. The hydrogel elasticity (the storage modulus, G') scales with the gel crosslinking density (ρ_x), and, from this, the photolabile group characteristic degradation time constant (t) was calculated (Eqn. 1).

$$\ln\left(\frac{G'}{G_o}\right) = \ln\left(\frac{\rho_x}{\rho_{x_o}}\right) = -\frac{2t}{\tau} \quad (1)$$

Here, G'_o is the initial storage modulus, ρ_{x_o} is the initial crosslinking density, and t is the irradiation time. The factor of 2 is included as cleavage of the photodegradable group on either side of the PEG leads to a decrease in the network's crosslinking density. τ scales inversely with the incident light intensity, I_o , and the photolabile molecule's molar absorptivity (ϵ).^{22,23} The characteristic degradation times for several cytocompatible light conditions²⁴ were determined with rheometry (**Figure 6.2a**). Using these t values, hydrogel photodegradation and changes in commensurate materials properties, such as crosslinking density, over time (**Figure 6.2b**) were predicted.

Spatial property gradients were achieved in the x-y plane or z-direction by controlling the light exposure and intensity, respectively. A surface gradient was created by moving an opaque plate across the sample during irradiation to create a linear gradient in exposure time from 0 min (at 0 mm) to 5 min (at 9 mm). The resulting degradation-induced crosslinking density gradient was measured with AFM and compares well to predictions based on τ (Fig. 2c). A gradient within the gel was fabricated using an optically thick sample, where the photolabile group substantially attenuates the light intensity over the hydrogel thickness. In this example, < 1% of the incident light at the surface is transmitted at a depth of 100 μm . To characterize this gradient with depth, the backbone of the polymer network was covalently labeled with rhodamine. As the gel degrades, PEG is released, along with PEG attached to the fluorescently-labeled polyacrylate backbone chains. As imaged with a confocal LSM, uniform fluorescence is initially observed throughout a cross-section of the gel, while a gradient in fluorescence is observed after 5 minutes of irradiation (**Figure 2d**). Using the measured values for τ (**Figure 2a**, inset) and accounting for spatially varying light intensities via the Beer-Lambert law, the corresponding profiles in the crosslinking density gradient were predicted as a function of exposure time. In general, a large array of biologically relevant property gradients can be generated in this manner, by manipulating irradiation parameters such as wavelength, intensity, and time. For example, varying the steepness and absolute magnitude of crosslinking density gradients in the x-y plane may be useful for studying cell migration on surfaces, while patterning gradients in the z-direction allows the user to investigate the effect of crosslinking density on cell morphology in 3D.

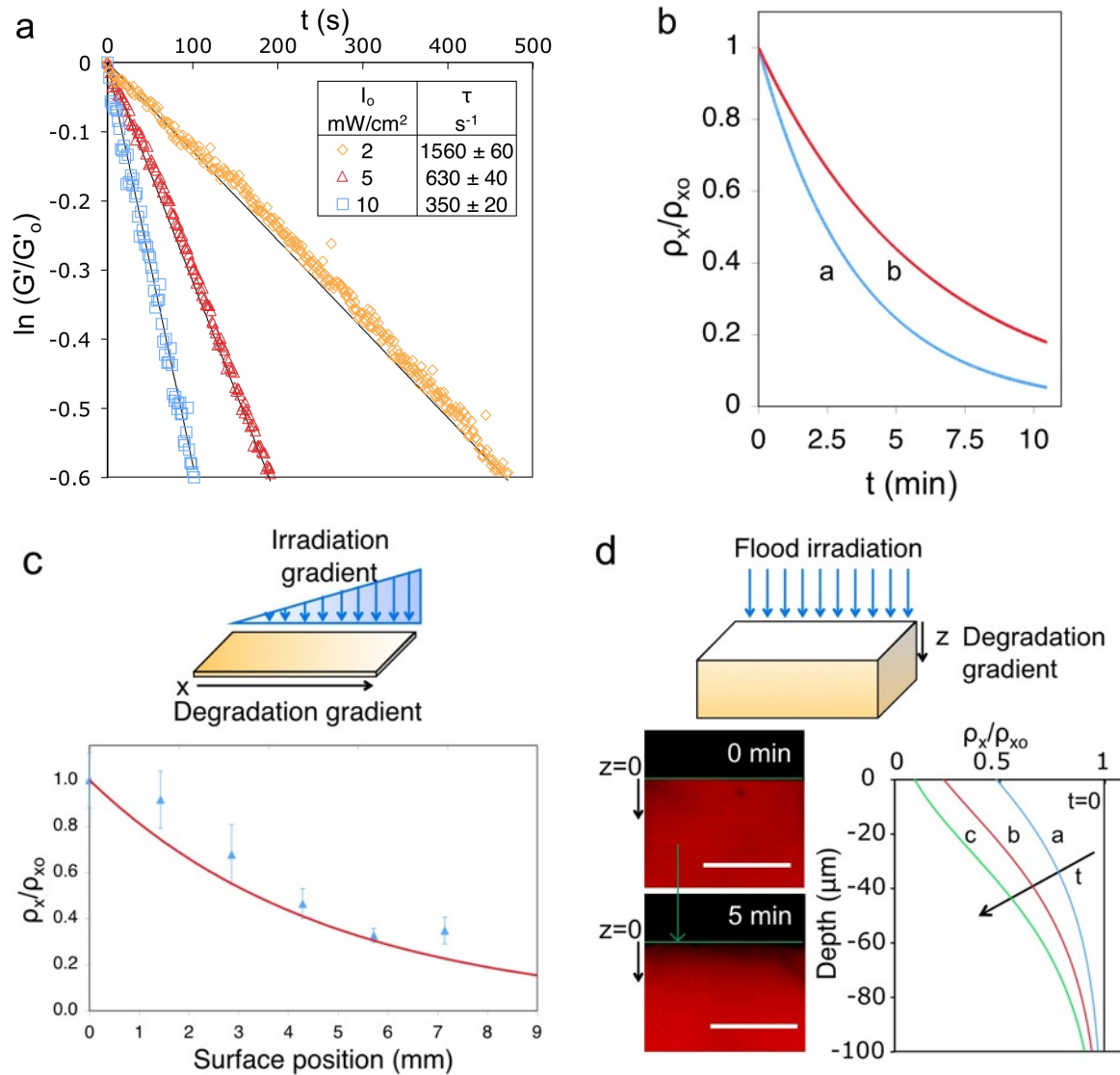


Figure 6.2 Photolysis kinetics and gradient photodegradation. (a) Degradation of these hydrogels was characterized using the more loosely crosslinked gel composition (10 mol % : 90 mol % PEGdiPDA : PEGA). Photodegradation rates were characterized via rheometry, where the natural log of the storage modulus G' normalized to its initial value G'_0 decreases with 365 nm irradiation. Fits of this data yield the characteristic degradation time, τ , which varies with the irradiation intensity (inset) and was used in conjunction with a photodegradation model to predict changes in the hydrogel crosslinking as well as gel mass loss. (b) The experimentally-determined τ values were used to predict the hydrogel's crosslinking density with time during bulk degradation (normalized to initial value, (a) 10 mW cm⁻² and (b) 5 mW cm⁻² at 365 nm). (c) A gradient in the hydrogel's crosslinking density within the top 50 μm of the gel was created with an irradiation gradient across the surface. No degradation occurs on the left, 5 min of degradation occurs on the right, and a continuous and linear gradient of exposure times occurs between these two extremes (365 nm at 10 mW cm⁻²). The resulting crosslinking density gradient was measured with AFM (blue triangles) and compares well to predicted values based on τ (solid curve). (d) Flood irradiating a thick hydrogel with a highly absorbed wavelength

creates a degradation gradient in the z-direction within the hydrogel. This degradation gradient was visualized with a confocal LSM (left), where decreased fluorescence indicates loss of backbone chains. The effect of this degradation gradient on the material properties can be estimated through predicted changes in the crosslinking density (normalized to its initial value) with irradiation: (a) 2.5, (b) 5, and (c) 8 min (right). Scale bars are 100 μm .

Beyond controlling the gel's crosslinking density and subsequent material properties, the ability to direct gel erosion (i.e., complete mass loss) to create voids and channels within a cell-laden material environment would be highly useful. Such three-dimensional cell culture systems would afford the opportunity to spatially and temporally direct process extension, migration, or even cell-cell interactions. However, erosion is dependent on both the degradation kinetics (t) and overall network connectivity. In particular, the time to reach the reverse gel point (complete dissolution), t_{rev} , depends on several factors: (i) the wavelength and intensity of irradiation and hydrogel thickness, which adjust t and the intensity profile within the hydrogel due to light attenuation; (ii) the length of the polyacrylate backbone chains comprising the network; and (iii) the connectivity of the polyacrylate chains dictated by the initial amount of crosslinker.

To examine these effects on the time to reach reverse gelation, thick hydrogels that undergo mass loss via surface erosion when exposed to a highly absorbing wavelength were synthesized. The mass loss profiles were adjusted with the initial crosslinker concentration, where increased crosslinker concentration increases the time to complete degradation. These profiles compare well to model predictions based on τ and the gel connectivity (**Figure 3a**). Further, spatially-specific surface erosion was achieved with photolithography. Channels were degraded into a hydrogel by irradiation with a highly absorbed wavelength through a periodic photomask (400 μm lines). Erosion of the hydrogel increases with irradiation time, as channels of increasing depth are generated (**Figure 3b**). The channel depth was quantified with

profilometry and increased linearly with irradiation time, which compares well to predicted erosion based on τ (**Figure 3c**).

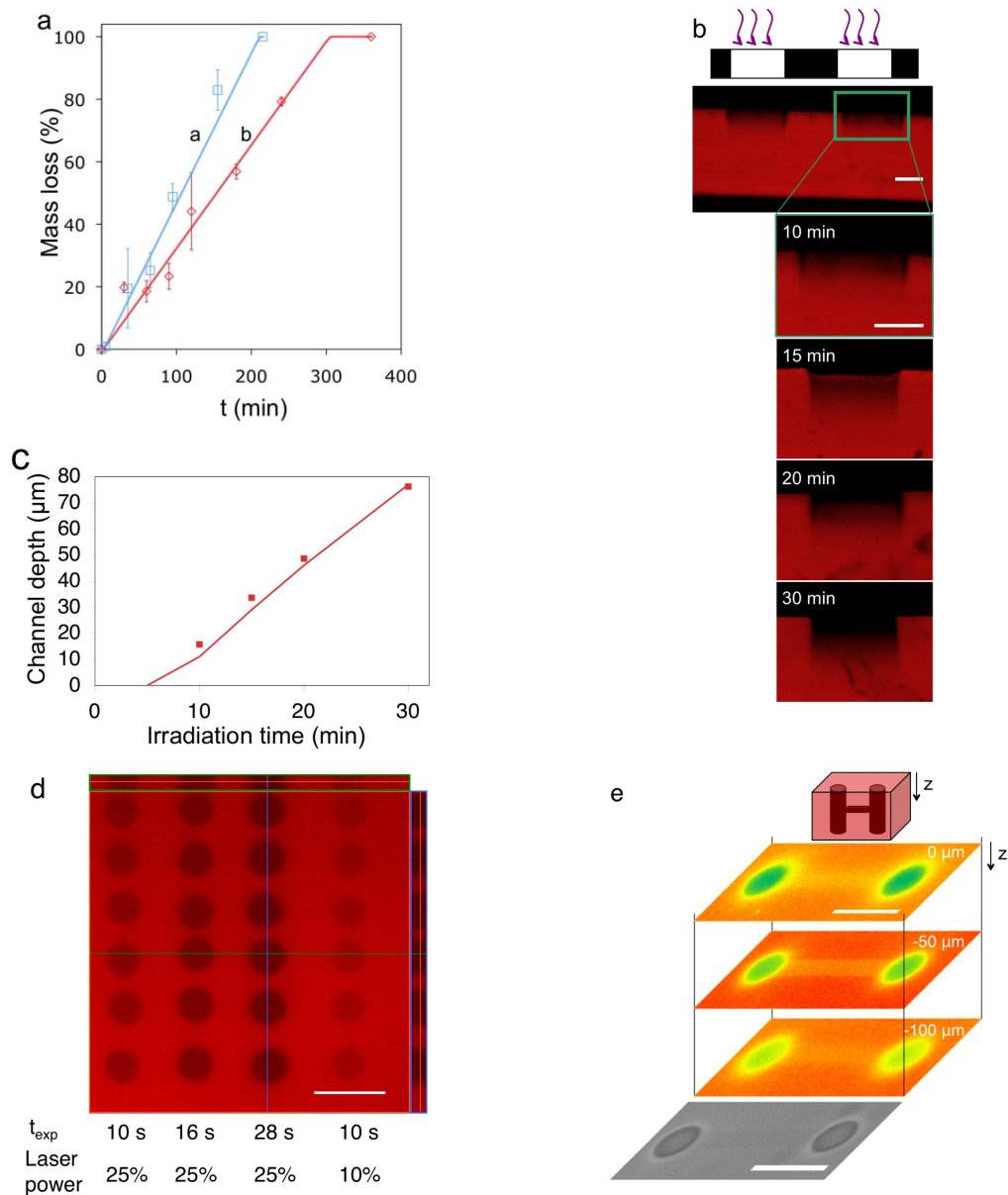


Figure 6.3. Hydrogel spatial erosion. (a) Mass loss profile and time to complete degradation with irradiation (365 nm at 20 mW cm^{-2}) were adjusted with the initial crosslinker concentration and agree well with predictions based on τ (solid lines): 15 wt% total macromer and (a) 10 mol% and (b) 25 mol% photodegradable crosslinker. (b) Photolithography (365 nm at 10 mW cm^{-2} through $400\text{ }\mu\text{m}$ clear lines separated by $400\text{ }\mu\text{m}$ black lines) was used for spatially-specific erosion, creating channels of increasing depth with increasing irradiation, (confocal images of the gel cross-section with irradiation time noted). (c) The observed eroded channel depth

(squares) compares well with channel depths predicted with τ and the photodegradation model (solid line). **(d)** Spatial erosion of cylinders within a hydrogel was achieved using 405 nm laser on a LSM (top-down view of confocal stack with corresponding cross-sections marked by blue and green lines). Each column of cylinders is a different irradiation condition with decreasing scan speed and increasing laser power resulting in increased mass loss (left to right, scan time per plane and laser power (a) 10 s and 25%, (b) 16 s and 25%, (c) 28 s and 25%, and (d) 10 s and 10%). **(e)** Similarly, vertical cylinders were degraded within a hydrogel (scan time 2 s per plane, 25% laser power, 100 μm z-scan) and subsequently connected with a horizontal channel within the hydrogel (scan time 16 s per plane, 1 μm z-scan) (confocal slices false colored to aid in visualization, with red indicating most fluorescence intensity (no degradation) and yellow to green least fluorescence (most degradation and mass loss)). The presence of the structure within the hydrogel was verified in brightfield. All scale bars are 100 μm .

6.2.3 Spatially defined erosion of three-dimensional, photodegradable hydrogels

Upon characterizing τ and t_{rev} for this photodegradable hydrogel system, one can select other irradiating wavelengths of interest, especially those that would allow three-dimensional patterning in real time using common lasers and scanning speeds. While erosion takes several minutes using low intensity 365 nm light, higher intensity focused lasers allow more rapid gel erosion. In particular, region of interest functionality on a LSM (405 nm, 30 mW laser) was used to scan shapes within individual planes in the gel, locally eroding the gel. These shapes were subsequently scanned in the z-direction to create a three-dimensional void. The rate of degradation was dictated by the irradiation dose, which was controlled with the laser scan speed and power. Increased degradation and x-y plane resolution were observed with decreased scan speed (i.e., increased irradiation time) or increased laser power (i.e., increased irradiation intensity, I_0) (**Figure 3d**), where cylinders were degraded in the hydrogel with 5 mm z-scans. Scan times for erosion with the 405 nm laser are consistent with calculated values of τ , where 25 to 10% of the laser power corresponds to a τ of 0.2 to 0.4 ms per plane and a t_{rev} of 50 to 130 s per plane. Experimentally, complete degradation is observed with 10 to 30 s of exposure per plane. This faster erosion is likely due to underestimates of the laser focal point intensity and/or

overlapping regions of out-of-focus light during z-scans. With these t_{rev} predictions, varying scan speeds and z-scan lengths were subsequently utilized to create connected channels within a hydrogel, where vertical cylinders connected by a horizontal channel were degraded within the hydrogel (**Figure 3e**). This three-dimensional erosion with focused light can be predicted and utilized to create structures within a hydrogel, such as a channel connecting two cells. Total patterning of the hydrogel is complete in a few minutes.

6.2.4 Cell response to dynamic changes in gel microenvironment

To examine how precise, predictable changes in the gel microenvironment (i.e., crosslinking density) influence cell morphology, human mesenchymal stem cells (hMSCs) were encapsulated in photodegradable or non-degradable hydrogels. A portion of the photodegradable gels were subsequently flood irradiated on Day 1 to create a z-direction crosslinking density gradient via degradation. The remaining photodegradable hydrogels were cultured without irradiation as a control for non-specific cell-induced degradation, while the non-degradable gels were irradiated as a control for non-specific light-induced degradation. Photodegradation and the corresponding change in crosslinking density lead to an increase in the molecular porosity of the hydrogel, or mesh size, and a decrease in the polymer density surrounding the cells, which have been previously shown to influence numerous cell functions such as cell morphology and spreading,⁹ viability,²⁵ and diffusion of secreted molecules.²⁶ Upon irradiation and degradation on Day 1, no significant change in cell viability was observed (Supplemental Material, **Figure 6.5**), demonstrating the cytocompatibility of the photodegradation reaction and degradation products *in vitro*. In addition, cell spreading was observed over 4 days (**Figure 6.7**) within the upper region of the degraded gel (top 100 μm , **Figure 6.4a**), where the crosslinking density is

lowered due the z-direction degradation gradient (**Figure 6.2d**). No spreading is observed in control gels that were not irradiated over 4 days, which is expected since the polymer density in the non-degraded gels should be too high to allow cell spreading (**Figure 6.4b**, **Figure 6.6**). This change in spreading was quantified, where an average cell area of $706 \pm 77 \mu\text{m}^2$ and $473 \pm 94 \mu\text{m}^2$ were observed with and without irradiation, respectively. Furthermore, cell spreading and area were observed to be greatest in the upper regions of the gel, correlating with the z-direction degradation gradient, while no correlation of cell area with z-position was observed in non-degraded gels (**Figure 6.4d**). These photodegradable gels can be used to further explore the influence of hydrogel structure/polymer density on cell morphology, on other cell functions such as cytoskeletal organization and differentiation, or on ECM elaboration via gradient degradation.

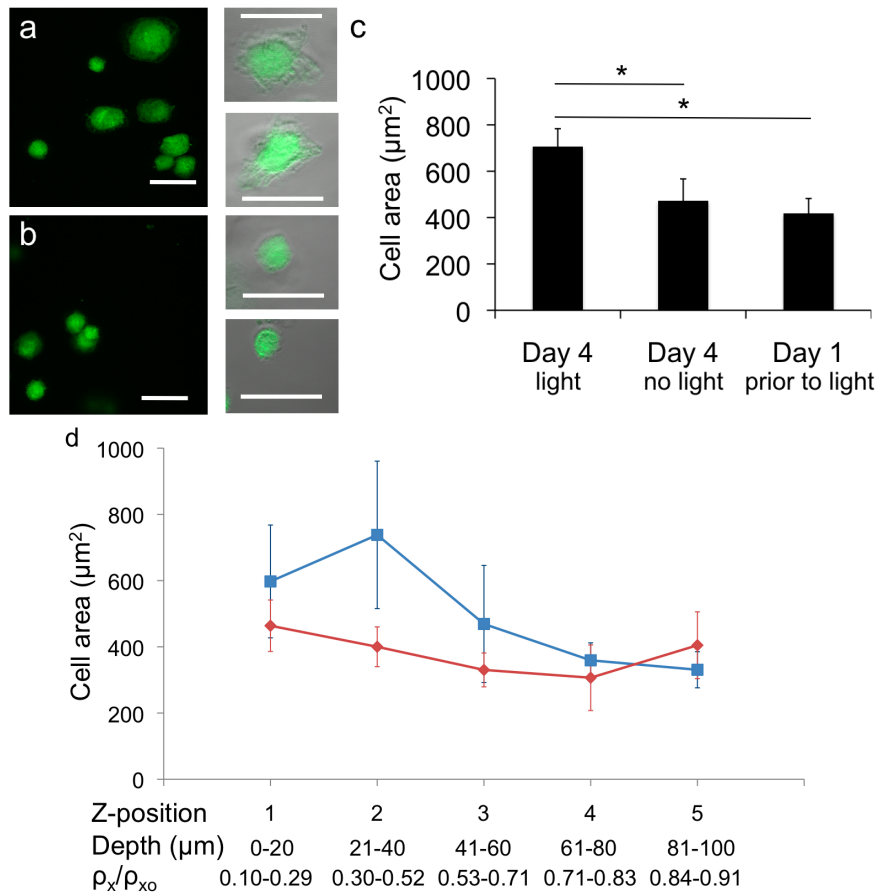


Figure 6.4 Cell area and morphology in gradient degraded hydrogels. hMSCs were encapsulated in photodegradable hydrogels and irradiated (365 nm at 10 mW cm⁻² for 8 min) on Day 1 to create a crosslinking density gradient in the z-direction. **(a)** By Day 4, cell spreading is observed within the upper portion of the irradiated hydrogel (top ~ 100 μm), which possesses a significantly decreased crosslinking density based on predictions shown in Fig. 2, whereas limited spreading is observed in **(b)** degradable gels without irradiation (top down view of confocal LSM stack). Changes in cell morphology were confirmed with brightfield images (right). Scale bars are 50 μm. **(c)** No change in cell area was observed over 4 days without irradiation (Day 1 prior to irradiation, Day 4 no light). In contrast, an increase in cell area was observed with irradiation and degradation (Day 4 light) as compared to these controls (* p < 0.1). **(d)** Spreading in response to the crosslinking density gradient ($\rho_x/\rho_{x_0} = 0.1 - 0.9$, $\rho_{x_0} = 0.006$ M) was examined by splitting the 100-μm thick confocal stack into 20-μm thick confocal projections (top 20 μm of the gel = position 1). On Day 4, increased cell area was observed in the top of the gel as compared to the lower regions in irradiated samples (blue squares), whereas no change in cell area was observed in the z-direction without irradiation (red diamonds, $\rho_x/\rho_{x_0} = 1$ at all positions).

6.3 Conclusion

Photodegradable hydrogels were synthesized, and their degradation kinetics in response to low-intensity irradiation was characterized via rheometry to determine rate constants for predicting changes in crosslinking density and mass loss. These hydrogels were degraded under cytocompatible irradiation conditions to create z- or x-direction property gradients, as well as to predictably erode hydrogels for controlled mass loss at any point in time and in three dimensions. Cell spreading was directed with a z-direction degradation gradient, where encapsulated cell area was greatest in the most highly degraded regions of the gel. These photodegradable gels can be used for culturing cells in three dimensions and allowing real-time, externally-triggered manipulation of the cell microenvironment to examine its dynamic effect on cell function.

6.4 References

1. Drury, J. & Mooney, D. Hydrogels for tissue engineering: scaffold design variables and applications. *Biomaterials* **24**, 4337–4351 (2003).

2. Nuttelman, C. R. *et al.* Macromolecular Monomers for the Synthesis of Hydrogel Niches and Their Application in Cell Encapsulation and Tissue Engineering. *Prog Polym Sci* **33**, 167–179 (2008).
3. Wang, D.-A. *et al.* Multifunctional chondroitin sulphate for cartilage tissue-biomaterial integration. *Nat Mater* **6**, 385–392 (2007).
4. Peppas, N., Hilt, J., Khademhosseini, A. & Langer, R. Hydrogels in biology and medicine: From molecular principles to bionanotechnology. *Adv Mater* **18**, 1345–1360 (2006).
5. Benoit, D. S. W., Nuttelman, C. R., Collins, S. D. & Anseth, K. S. Synthesis and characterization of a fluvastatin-releasing hydrogel delivery system to modulate hMSC differentiation and function for bone regeneration. *Biomaterials* **27**, 6102–6110 (2006).
6. Hahn, M. S., Miller, J. S. & West, J. L. Three-Dimensional Biochemical and Biomechanical Patterning of Hydrogels for Guiding Cell Behavior. *Adv Mater* **18**, 2679–2684 (2006).
7. Tayalia, P., Mendonca, C. R., Baldacchini, T., Mooney, D. J. & Mazur, E. 3D Cell-Migration Studies using Two-Photon Engineered Polymer Scaffolds. *Adv Mater* **20**, 4494–4498 (2008).
8. Raeber, G. P., Lutolf, M. P. & Hubbell, J. A. Mechanisms of 3-D migration and matrix remodeling of fibroblasts within artificial ECMs. *Acta Biomater* **3**, 615–629 (2007).
9. Mahoney, M. & Anseth, K. Three-dimensional growth and function of neural tissue in degradable polyethylene glycol hydrogels. *Biomaterials* **27**, 2265–2274 (2006).
10. Adeloew, C., Segura, T., Hubbell, J. A. & Frey, P. The effect of enzymatically degradable poly(ethylene glycol) hydrogels on smooth muscle cell phenotype. *Biomaterials* **29**, 314–326 (2008).
11. Metters, A., Anseth, K. & Bowman, C. Fundamental studies of a novel, biodegradable PEG-b-PLA hydrogel. *Polymer* **41**, 3993–4004 (2000).
12. Nuttelman, C. R., Kloxin, A. M. & Anseth, K. S. Temporal changes in peg hydrogel structure influence human mesenchymal stem cell proliferation and matrix mineralization. *Adv. Exp. Med. Biol.* **585**, 135–149 (2006).
13. Davis, K. A. & Anseth, K. S. Controlled release from crosslinked degradable networks. *Crit Rev Ther Drug Carrier Syst* **19**, 385–423 (2002).
14. Seliktar, D., Zisch, A. H., Lutolf, M. P., Wrana, J. L. & Hubbell, J. A. MMP-2 sensitive, VEGF-bearing bioactive hydrogels for promotion of vascular healing. *J Biomed Mater Res A* **68**, 704–716 (2004).

15. Andreopoulos, F. *et al.* Photocrosslinkable hydrogel synthesis via rapid photopolymerization of novel PEG-based polymers in the absence of photoinitiators. *J Am Chem Soc* **118**, 6235–6240 (1996).
16. Zheng, Y. *et al.* PEG-based hydrogel synthesis via the photodimerization of anthracene groups. *Macromolecules* **35**, 5228–5234 (2002).
17. Luo, Y. & Shoichet, M. S. A photolabile hydrogel for guided three-dimensional cell growth and migration. *Nat Mater* **3**, 249–253 (2004).
18. Kloxin, A. M., Kasko, A. M., Salinas, C. N. & Anseth, K. S. Photodegradable hydrogels for dynamic tuning of physical and chemical properties. *Science* **324**, 59–63 (2009).
19. Zhao, Y. *et al.* New caged coumarin fluorophores with extraordinary uncaging cross sections suitable for biological imaging applications. *J Am Chem Soc* **126**, 4653–4663 (2004).
20. Holmes, C. Model studies for new o-nitrobenzyl photolabile linkers: Substituent effects on the rates of photochemical cleavage. *J Org Chem* **62**, 2370–2380 (1997).
21. Metters, A., Bowman, C. & Anseth, K. A statistical kinetic model for the bulk degradation of PLA-b-PEG-b-PLA hydrogel networks. *J Phys Chem B* **104**, 7043–7049 (2000).
22. Odian, G. *Principles of Polymerization*. (John Wiley & Sons, Inc.: Hoboken, NJ, 2004).
23. Young, R. & Lovell, P. *Introduction to polymers*. (Chapman & Hall: London, UK, 1991).
24. Bryant, S., Nuttelman, C. & Anseth, K. Cytocompatibility of UV and visible light photoinitiating systems on cultured NIH/3T3 fibroblasts in vitro. *J Biomat Sci-Polym E* **11**, 439–457 (2000).
25. Hudalla, G. A., Eng, T. S. & Murphy, W. L. An approach to modulate degradation and mesenchymal stem cell behavior in poly(ethylene glycol) networks. *Biomacromolecules* **9**, 842–849 (2008).
26. Bryant, S. J., Bender, R. J., Durand, K. L. & Anseth, K. S. Encapsulating chondrocytes in degrading PEG hydrogels with high modulus: engineering gel structural changes to facilitate cartilaginous tissue production. *Biotechnol Bioeng* **86**, 747–755 (2004).

6.5 Supplemental Information

6.5.1 Experimental

6.5.1a Photodegradable Hydrogel Synthesis

The photodegradable crosslinker (PEGdiPDA, $M_n \sim 3400$ g/mol) was synthesized as previously described.¹ PEGdiPDA was copolymerized with PEGA ($M_n \sim 375$ g/mol, Sigma-Aldrich). The total amount of monomer was fixed at 15 wt% in water and two different molar ratios of PEGdiPDA to PEGA were used to vary the initial gel crosslinking density for mass loss studies (10 mol%:90 mol% and 25 mol%:75 mol%). All other hydrogels were prepared with the lower PEGdiPDA monomer ratio (10 mol%:90 mol%). The monomer solution was polymerized via redox-initiated free radical polymerization by adding 0.2 M ammonium persulfate (AP) and subsequently 0.1 M tetraethylmethylenediamine (TEMED) while vortexing. For 3D patterning experiments, a methacrylated rhodamine (300 μ M, methacryloxyethyl thiocarbamoyl rhodamine B, Polysciences) was added to the monomer solution to covalently label the hydrogel backbone chains. The hydrogels were formed *in situ* for rheometry experiments and between glass slides with a spacer (0.5 mm) for all other experiments. The polymerization is complete within 5 min, based on modulus evolution followed by rheometry, and all molded hydrogels were transferred to phosphate buffered saline (PBS) that was refreshed after 30 min to remove any remaining monomer or initiator.

6.5.1b Hydrogel degradation characterization and prediction

Hydrogel degradation rates were characterized with a photorheometer ($\gamma=10\%$ and $\omega=10$ rad/s, linear viscoelastic regime), where a sample is irradiated while monitoring the hydrogel modulus (ARES, TA). Thin hydrogels (0.05 mm) were polymerized *in situ* between an 8 mm

diameter flat quartz plate and a temperature-controlled Peltier flat plate (25°C). Upon complete polymerization, the hydrogel was surrounded with a thin bead of water to prevent dehydration. The hydrogel storage modulus (G') was monitored ($G \approx G'$ when $G' > G''$),² while irradiating the sample with UV or visible light (365 nm at 2, 5, or 10 mW cm⁻², 405 nm at mW cm⁻², Novacure with liquid-filled light guide and collimating lens, EFOS). A characteristic photolabile group degradation time, τ , was determined by linear regression of this data ($0.5 \leq G'/G'_o \leq 1$) based on photolysis kinetics,³ gel degradation kinetics,⁴ and gel mechanical properties.⁴ Equation S1 was used to calculate τ .

$$\ln\left(\frac{G'}{G'_o}\right) = \ln\left(\frac{\rho_x}{\rho_{x_o}}\right) = -\frac{2t}{\tau} \quad (\text{S1})$$

τ is defined by equation S2.

$$\tau = \frac{N_A hc}{\phi \epsilon \lambda I (2.3 \times 10^{-6})} \quad (\text{S2})$$

Where ϕ is the quantum yield of photolysis (events photon⁻¹); N_A is Avogadro's number (photons mol⁻¹); h is Planck's constant (J s); c is the speed of light (m s⁻¹); I is the light intensity (W cm⁻²); t is the irradiation time (s); ϵ is the molar absorptivity (L mol⁻¹ cm⁻¹); and λ is the wavelength (nm). These experimentally determined values of τ were used to calculate the concentration of the photolabile group, C , at each x and t , where I at a depth x within the hydrogel was calculated by the Beer-Lambert law (Eqn. S3)

$$I = I_o \exp(-2.3\epsilon Cx) \quad (\text{S3})$$

The probability that a crosslink is degraded was subsequently calculated (Eqn. S4).

$$P_{\text{deg}} = 1 - \frac{C}{C_o} = 1 - \exp\left(-\frac{t}{\tau}\right) \quad (\text{S4})$$

This probability of crosslink degradation was applied to a statistical-kinetic model for mass loss from PEG diacrylate hydrogels.⁵ These expressions were iteratively solved at each x , allowing for the prediction of hydrogel mass loss and crosslinking density as a function of depth in the gel and irradiation time. In this model, reverse gelation, or gel dissolution, occurs when the local crosslinking density falls below the critical crosslinking density required to connect the chains into an infinite 3D network.⁶ Specifically, this occurs when the weight average number of crosslinks per chain drops below two. At reverse gelation, the local material undergoes a nearly instantaneous solid-to-liquid transition, releasing soluble polymer chains into solution.

6.5.1c Hydrogel gradient degradation

A crosslinking density gradient in the z -direction was created by exposing the hydrogel to uniform intensity, collimated irradiation (i.e., flood irradiation) with 365 nm at 10 mW cm⁻² light for 8 min or less, prior to reverse gelation of the surface as predicted by rheometry. A crosslinking density gradient in the x -direction was created by irradiating the surface of photodegradable hydrogel with a light gradient (365 nm at 10 mW cm⁻² for 0 to 5 min across the surface). This light gradient was achieved by irradiating the hydrogel while continuously covering the hydrogel surface with an opaque plate from one side (0 mm) to the other (9 mm).⁷ The resulting surface modulus gradient, limited to the top ~ 50 μ m of the gel by light attenuation, was measured with AFM⁸ (PicoPlusTM scanning probe microscope, Molecular Imaging, Inc., pyramidal silicon nitride tip with force constant 0.12 N/m, radius=10 nm, height=2.5-3.5 nm, and angle of pyramid=35 $^\circ$), where the elastic modulus (E) at various linear positions across a gel surface was obtained using the Hertz model and $\nu \approx 0.2$ for the surface of a PEG hydrogel.⁹ These

E values were converted to shear modulus G and subsequently crosslinking density using rubber elasticity theory and $\nu \approx 0.5$ for the bulk of a PEG hydrogel.^{2,4}

6.5.1d Hydrogel degradation with photolithography

Photodegradable hydrogels were spatially degraded via photolithography (365 nm at 10 mW cm⁻², 400 μ m wide black lines separated by 400 μ m wide transparent lines, Mask Aligner, Optical Associates Inc., Model J500) for different irradiation times (5 to 30 min) to erode channels with increasing depth. The eroded channels were examined visually by imaging a cross-section of the gel with a confocal LSM and quantitatively with profilometry (Stylus Profiler, Dektak 6M, force=1 mg, radius=12.5 mm, and range=1 mm). Based on τ and the photodegradation model, eroded channel depth was predicted for each irradiation time.

6.6.1e Hydrogel degradation with focused light

Three-dimensional voids were created within photodegradable hydrogels using focused light (405 nm, 30 mW laser, LSM 510, Zeiss). The photodegradable hydrogel within a 35 mm glass bottom Petri dish (MatTek Corporation) was surrounded with PBS and unidirectionally scanned within the in-focus x-y plane with a 405 nm laser using Zeiss region of interest (ROI) software. The x-y scanned shape subsequently was scanned in the z-direction to degrade three-dimensional features within the gel. Arrays of cylinders (50 μ m diameter) were patterned using different LSM parameters for each column of the array (5 μ m stack scanned in 1 μ m intervals, 10 to 25% laser power, scan speed setting=2 to 4 corresponding to 10 to 28 s per plane). In addition, interconnected channels were created (vertical cylinders: 25% power, scan speed=7 corresponding to 2 s per plane, 60 μ m stack scanned in 1 μ m intervals; horizontal channel: 25%

power, scan speed=3 corresponding to 16 s per plane, 1 μm stack). These degraded regions were imaged with a confocal LSM in brightfield and in fluorescence, where the rhodamine-labeled hydrogel fluoresces red and the degraded void is black due to removal of the fluorescently-labeled polymer backbone and crosslinks that comprise the gel.

6.5.1f Encapsulation and spreading cells within gradient degraded hydrogel

Adult human mesenchymal stem cells (hMSCs) (Cambrex Bio Science) were plated at 5,000 cells cm^{-2} in 10 cm diameter tissue culture polystyrene Petri dishes (BD Bioscience). The hMSCs were cultured in stem cell growth media (10% fetal bovine serum, 1 $\mu\text{g}/\text{mL}$ amphotericin B, 50 U/mL penicillin, 50 $\mu\text{g}/\text{mL}$ streptomycin, and 20 $\mu\text{g}/\text{mL}$ gentamicin in DMEM containing low-glucose, Invitrogen). The cells were grown under standard cell culture conditions (37 $^{\circ}\text{C}$ incubator with 5% CO_2), and media was changed twice per week. Cells were grown to confluency and passaged twice prior to encapsulation.

To examine cell morphology, cells were fluorescently labeled with Cell Tracker Green (5 μM , 30 min, Invitrogen) prior to encapsulation; to examine cell viability and cytoskeletal organization, cells were encapsulated without any prior labeling. A photodegradable PEG-based monomer solution, as described earlier, and a non-degradable PEG diacrylate-based (PEGDA, $M_n \sim 4600$ g/mol) monomer solution (10 mol%:90 mol% PEGDA:PEGA, 0.05 M AP, and 0.025 M TEMED) were prepared with fibronectin (100 nM, BD Biosciences). Each solution was mixed with cells for an encapsulation concentration of 2×10^6 cells mL^{-1} and polymerized for 5 min between glass slides with a spacer (0.25 mm). Upon complete polymerization, the hydrogels constructs were transferred to fresh growth media, which was refreshed after 30 min, 12 h, and subsequently twice per week. On Day 1, a portion of the photodegradable cell-gel

constructs were flood irradiated with UV light under sterile conditions (365 nm at 10 mW cm⁻² for 8 min per side) to create a z-gradient in degradation, releasing modified PEG and decreasing the polymer density around the cells in the regions closest to the incident irradiation. As controls, the remaining portion of photodegradable gels were not irradiated to elucidate the effect of non-specific cell-induced degradation, while the non-degradable gels were irradiated to elucidate the effect of non-specific light-induced degradation. Morphology of cells labeled with cell tracker green for each of these gel conditions was observed over 4 days (Day 1, 2, 3, and 4) in confocal fluorescence and in brightfield (Zeiss 710, 40x objective). Cell area was quantified from confocal projections of cell tracker green images with Image J. To quantify cell area by z-position, 100- μ m z-stacks were split into 20- μ m increment z-projections (top 20 μ m section = position 1). Note that since the average cell diameter within the upper regions of the degraded gels is larger than 20 μ m (\sim 30 μ m based on a cell area of 706 μ m²), most large cells that appear in position 1 images (depth = 0 - 20 μ m) also appear in position 2 images (depth = 21 - 40 μ m), insignificantly increasing the cell area observed in position 2 as compared to position 1.

In addition, cell-gel constructs were stained for viability or f-actin (Supplemental text, **Figure 6.5** and **6.7**), and uniform presentation of fibronectin throughout the degraded gels over 4 days was verified (Supplemental text, **Figure 6.8**). In this study, we examine the influence of gel crosslinking density on cell morphology assuming that the density of an adhesion molecule (i.e, fibronectin) is independent of crosslinking density. It should be noted that high extents of gel degradation may release fibronectin from the gel, thereby altering its density. However, calculations of the gel mesh size and images of fibronectin presentation support the assumption that fibronectin was retained over the wide range of gel crosslinking densities that were investigated in this study ($\rho_x / \rho_{x0} = 0.09$ to 1).

6.5.2 Supplemental text

Human mesenchymal stem cells (hMSCs) were encapsulated in photodegradable PEG hydrogels or non-degradable PEG hydrogels with entrapped fibronectin. Upon irradiation and degradation, cells encapsulated in the photodegradable hydrogel were viable (**Figure 6.5**), indicating that the irradiation conditions and degradation products are cytocompatible. In addition, cell spreading over 4 days was observed in photodegradable hydrogels with irradiation on Day 1 of culture, as discussed in the manuscript text. To verify that this spreading was not due to non-specific cell-induced or light-induced degradation of the gel, cell spreading in irradiated photodegradable gels was compared to two controls: (i) photodegradable gels without irradiation, as discussed in the manuscript text, and (ii) non-degradable gels with irradiation. No significant cell spreading is observed in the non-degradable gels over 4 days, indicating that neither cells nor light are non-specifically degrading the gel (**Figure 6.6**). This same trend is observed in control (i), photodegradable gels without irradiation, further supporting that cell spreading in the photodegradable hydrogel with irradiation is a response to light-induced cleavage of the gel crosslinks. While cell area does not change over 4 days in control (i) or (ii), cell area in the non-degradable gel is slightly smaller than in the photodegradable gels. This non-statistical difference is likely caused by small differences in the gel polymerization conditions due to free-radical inhibition by the photolabile group.

To examine the progression of cell spreading with and without photodegradation, confocal z-stacks of encapsulated cells within the top 100 μm of the gel were taken on Day 1, 2, 3, and 4 in culture (**Figure 6.7**). Prior to irradiation on Day 1, cells were rounded and small in the photodegradable gels and in the non-degradable gels. After irradiation, limited change in cell

morphology was observed on Day 2, whereas cell spreading was observed by Day 3 and 4. In contrast, little change in cell morphology is observed in the two controls over 4 days. In addition to spreading, the cell cytoskeleton was stained in each of these gel compositions (f-actin labeled red and overlaid with brightfield). While increased cell area was observed for cells in irradiated photodegradable gels, a diffuse cytoskeleton was observed in all gel conditions. For future studies of the influence of gel properties on cytoskeletal organization, longer culture time points will likely be needed to observe changes in the cytoskeletal organization.

Last, fibronectin presentation within the gel was examined to verify that differences in cell spreading with degradation were not convoluted by loss of fibronectin. Fibronectin was fluorescently-labeled and entrapped during encapsulation within a cell-laden gel. Fibronectin presence was subsequently verified with confocal z-stacks (**Figure 6.8**), where diffuse fibronectin as well as fibronectin clusters were observed. No statistical difference in fibronectin fluorescence was observed before (Day 1) or after irradiation (Day 4), indicating that the fibronectin concentration within the gel does not change with irradiation and degradation. Further, the mesh size of the photodegradable hydrogel with 8 min of irradiation was estimated to be 126 Å, which is smaller than an estimated average hydrodynamic radius for fibronectin in different solution conformations of 141 Å.¹⁰ This calculation supports that fibronectin should remain entrapped within the hydrogel with 8 min of irradiation and corresponding degradation.

6.5.3 Supplemental experimental

6.5.3a Encapsulation and spreading cells within gradient hydrogel

As described in the manuscript text, cells were encapsulated within a photodegradable hydrogel or a non-degradable hydrogel with entrapped fibronectin. To examine cell

morphology, cells were fluorescently labeled with Cell Tracker Green (5 μ M, 30 min, Invitrogen) prior to encapsulation; to examine cell viability or cytoskeletal organization, cells were encapsulated without any prior labeling. Upon encapsulation, the hydrogel constructs were transferred to fresh growth media, which was refreshed after 30 min, 12 h, and subsequently twice per week. On Day 1, the cell-gel constructs were flood irradiated with UV light under sterile conditions (365 nm at 10 mW cm^{-2} for 8 min per side, Novacure, EFOS) to create a z-gradient in degradation, releasing modified PEG and decreasing the polymer density surrounding cells in the regions closest to the incident irradiation. Similarly, on Day 1, a portion of the photodegradable gels was not irradiated, and the non-degradable gels were irradiated as controls. A live/dead assay (30 min staining, LIVE/DEAD Viability/Cytotoxicity Kit, Invitrogen) was used to examine cell viability after irradiation and degradation, where live cells fluoresce green and dead cells fluoresce red. Cell viability and morphology within the top 100 μ m of the gel were observed with and without degradation with a confocal laser scanning microscope (LSM, Zeiss Pascal or Zeiss 710, respectively) over 4 days. Cell area was quantified from cell tracker green images using Image J. To examine cell cytoskeletal organization, cell-gel constructs were fixed with 10% buffered formalin, permeabilized in 0.05 wt% Tween 20, stained with phalloidin-tetramethylrhodamine B isothiocyanate (Sigma-Aldrich), washed with phosphate buffered saline (PBS) (3x over 24 h), and imaged with a confocal LSM (Zeiss 710).

6.5.3b Fibronectin labeling, entrapment, and imaging

Fibronectin (FN, human, BD Biosciences) was labeled with a fluorophore (FITC-isocyanate, Invitrogen) per the manufacturer instructions for amine-reactive probes. Briefly, 1 mg of protein was dissolved in 0.1 M sodium bicarbonate (aqueous, pH \sim 9.16) to produce a 2

mg/mL solution. FITC-isocyanate was dissolved in dimethyl sulfoxide (10 mg/mL), added to the protein solution (10 μ L, 0.1 mg dye), and reacted while stirring for 1 h at room temperature. Unreacted fluorophore was removed from the reaction mixture by gel filtration (PD-10, Sephadex G-25M, GE Healthcare) in PBS per manufacturer instructions. Modification of the protein was verified by UV-visible spectroscopy per manufacturer instructions (absorbance at 280 nm and 494 nm). Photodegradable gels were created as described in the manuscript with FITC-FN (100 nM). Half of the samples with FITC-FN were irradiated for 8 min.

Gel fluorescence was examined with confocal microscopy (Zeiss 710). The gel surface was imaged (100 μ m z-scan), and the z-stack was summed over the 100 μ m stack to capture total fluorescence of the region, as a measure of FN content. Similar fluorescence was observed for the FITC-FN gels with no irradiation and 8 min irradiation. This fluorescence was quantified with Metamorph software. To further evaluate the retention of FN, gel crosslinking density was calculated using rubber elasticity theory,¹¹ and the gel mesh size was subsequently estimated [4], using the initial modulus of the gel (13.6 kPa), its equilibrium volumetric swelling ratio (13.0), and known constants for PEG-based hydrogels.⁴

6.5.4 Supporting references

1. Kloxin, A. M., Kasko, A. M., Salinas, C. N. & Anseth, K. S. Photodegradable hydrogels for dynamic tuning of physical and chemical properties. *Science* 324, 59–63 (2009).
2. Young, R. & Lovell, P. *Introduction to polymers*. (Chapman & Hall: London, UK, 1991).
3. Odian, G. *Principles of Polymerization*. (John Wiley & Sons, Inc.: Hoboken, NJ, 2004).
4. Bryant, S. Photopolymerization of hydrogel scaffolds. *Scaffolding in Tissue Engineering* 1–21 (2006).
5. Reddy, S., Anseth, K. & Bowman, C. Modeling of network degradation in mixed step-chain growth polymerizations. *Polymer* 46, 4212–4222 (2005).

6. Metters, A., Bowman, C. & Anseth, K. A statistical kinetic model for the bulk degradation of PLA-b-PEG-b-PLA hydrogel networks. *J Phys Chem B* 104, 7043–7049 (2000).
7. Johnson, P., Reynolds, T., Stansbury, J. & Bowman, C. High throughput kinetic analysis of photopolymer conversion using composition and exposure time gradients. *Polymer* 46, 3300–3306 (2005).
8. Domke, J. & Radmacher, M. Measuring the elastic properties of thin polymer films with the atomic force microscope. *Langmuir* 14, 3320–3325 (1998).
9. Wang, M. & Hill, R. J. Anomalous bulk viscosity of polymer-nanocomposite melts. *Soft Matter* 5, 3940–3953 (2009).
10. Rocco, M., Infusini, E., Daga, M., Gogioso, L. & Cuniberti, C. Models of Fibronectin. *Embo J* 6, 2343–2349 (1987).
11. Salinas, C. N. & Anseth, K. S. Mixed mode thiol-acrylate photopolymerizations for the synthesis of PEG-peptide hydrogels. *Macromolecules* 41, 6019–6026 (2008).

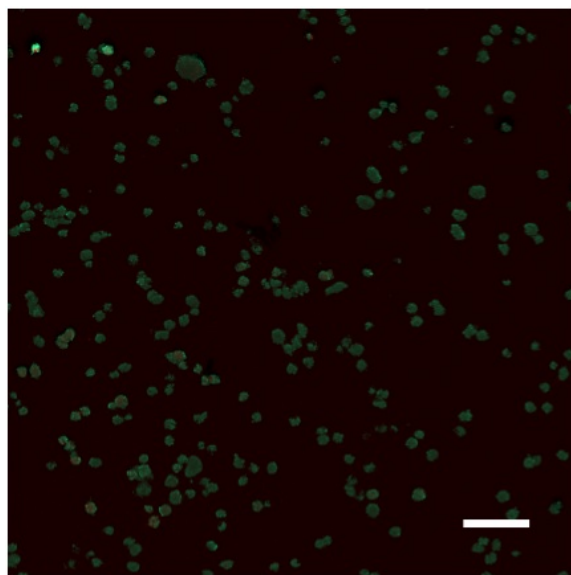


Figure 6.5 Cell viability with photodegradation. hMSCs encapsulated in photodegradable PEGdiPDA hydrogels were exposed to flood irradiation (365 nm at 10 mW cm^{-2} for 8 min). Upon exposure to light, cell viability is maintained throughout the hydrogel, where live cells fluoresce green and dead cells fluoresce red (top down view of confocal LSM stack). Scale bar is $100\text{ }\mu\text{m}$.

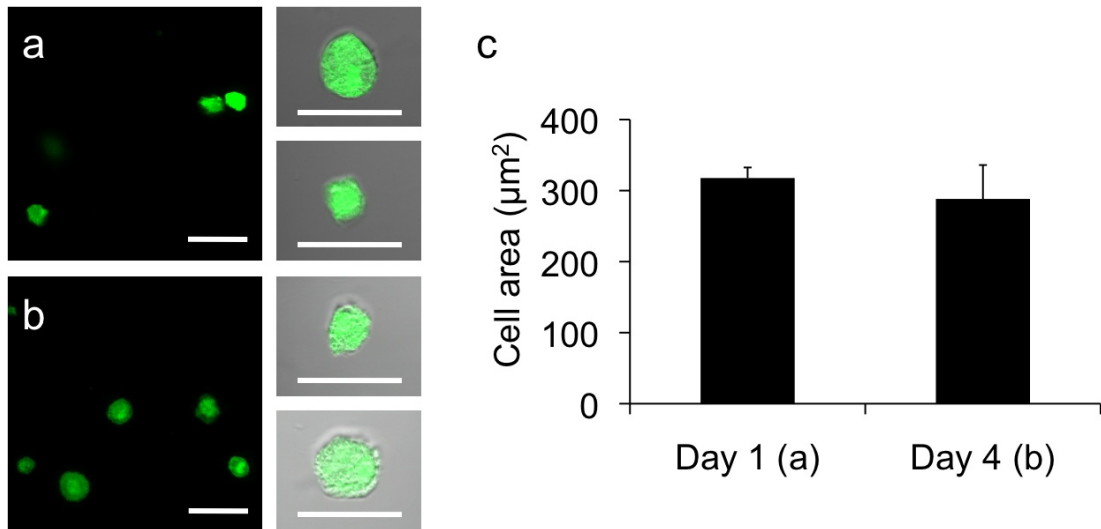


Figure 6.6 Cell morphology in non-degradable hydrogel. (a) hMSCs were encapsulated in non-degradable PEGDA hydrogels and exposed to flood irradiation (365 nm at 10 mW cm^{-2} for 8 min). Prior to light exposure (Day 1), cells exhibit small and rounded morphologies (left, top down view of confocal LSM stack; right, representative cells imaged with brightfield and fluorescence), where cells are fluorescently labeled green. (b) After light exposure (Day 4), cells persist in their small and rounded morphologies. (c) No significant difference in cell area is observed between encapsulated hMSCs in non-degradable PEGDA hydrogels at Day 1 (prior to light exposure) and at Day 4 (after light exposure). Scale bars are $50\ \mu\text{m}$.

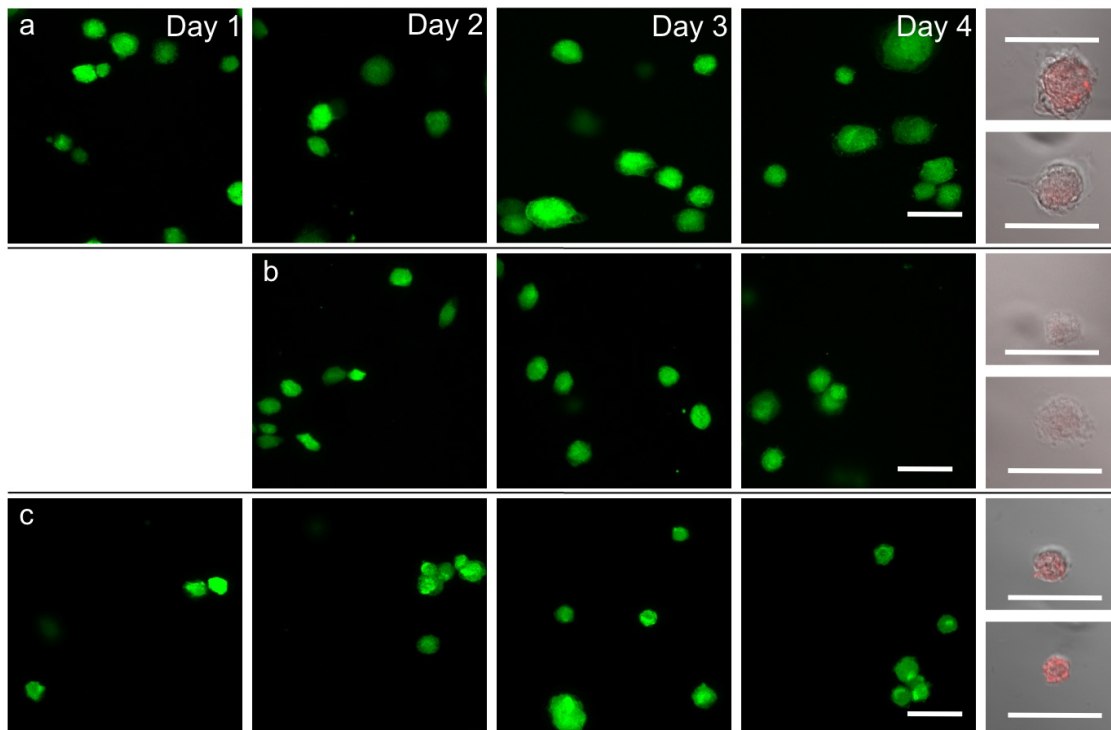


Figure 6.7 Cell morphology progression. hMSCs were encapsulated in photodegradable PEGdiPDA (a,b) and non-degradable PEGDA (c) hydrogels. The progression of cell morphology over the course of four days in culture was monitored by confocal LSM imaging of cell morphology on each day, where cells are fluorescently labeled green, and of phalloidin staining for the presence of f-actin (red) coupled with brightfield imaging on day 4. (a) hMSCs encapsulated in photodegradable hydrogels that were exposed to flood irradiation (365 nm at 10 mW cm⁻² for 8 min) exhibit a small and rounded morphology prior to light exposure (Day 1). After light exposure (Days 2-4), the cells begin to spread and increase in cell area. hMSCs encapsulated in photodegradable hydrogels that were not exposed to flood irradiation (b) and in non-degradable hydrogels that were exposed to flood irradiation (365 nm at 10 mW cm⁻² for 8 min) (c) persist in a small and rounded morphology throughout the four days in culture. Corresponding phalloidin staining on Day 4 (right) indicates diffuse f-actin presence around the exterior of the cells for all conditions. Scale bars are 50 μm.

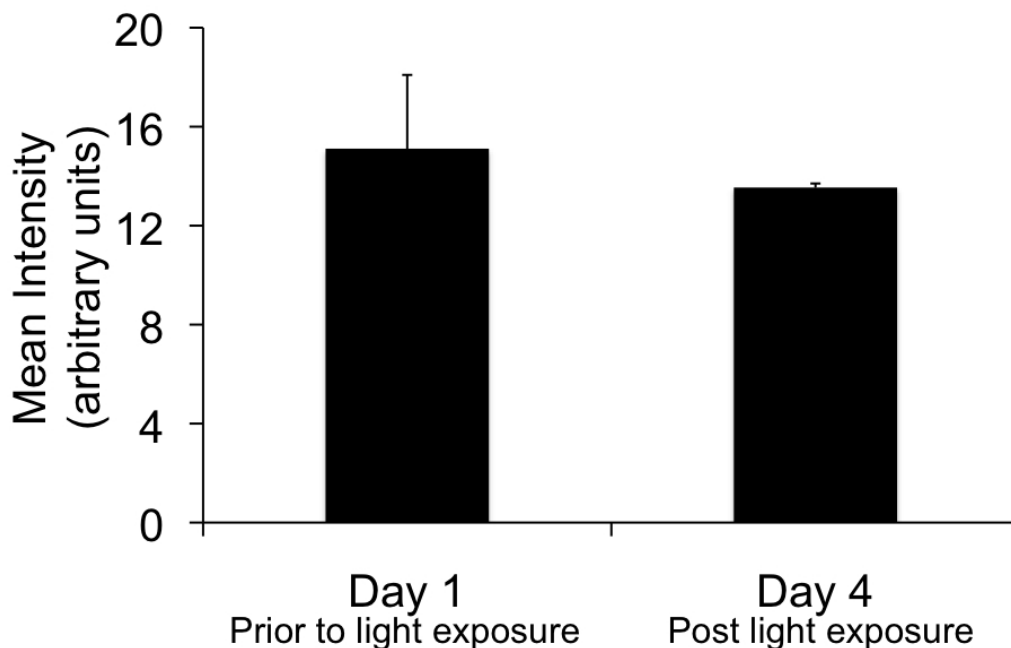


Figure 6.8 Fibronectin presentation with degradation. Fluorescein labeled fibronectin was entrapped in photodegradable PEGdiPDA hydrogels and confocal image stacks of the fibronectin presence were taken prior to (Day 1) and post (Day 4) light exposure. Image analysis of the mean fluorescent intensity of the LSM stacks reveals no significant difference in fibronectin presentation between the PEGdiPDA hydrogel prior to light exposure (Day 1) and after light exposure (Day 4).

CHAPTER VII

CONTROLLED TWO-PHOTON DEGRADATION OF PEG HYDROGELS TO STUDY AND MANIPULATE SUBCELLULAR INTERACTIONS ON SOFT MATERIALS

As published in *Soft Matter*, 6, 5100-5108 (2010)

7.1 Abstract

Cell adhesion and detachment to and from the extracellular matrix (ECM) are critical regulators of cell function and fate due to the exchange of mechanical signals between the cell and its microenvironment. To study this cell mechanobiology, researchers have developed several innovative methods to investigate cell adhesion *in vitro*; however, most of these culture platforms are unnaturally stiff or static. To better capture the soft, dynamic nature of the ECM, we present a PEG-based hydrogel in which the context and geometry of the extracellular space can be precisely controlled *in situ* via two-photon induced erosion. Here, we characterize the two-photon erosion process, demonstrate its efficacy in the presence of cells, and subsequently exploit it to induce subcellular detachment from soft hydrogels. A working space was established for a range of laser powers required to induce complete erosion of the gel, and these data are plotted with model predictions. From this working space, two-photon irradiation parameters were selected for complete erosion in the presence of cells. Micron-scale features were eroded on and within a gel to demonstrate the resolution of patterning with these irradiation conditions. Lastly, two-photon irradiation was used to erode the material at the cell-gel interface

to remove cell adhesion sites selectively, and cell retraction was monitored to quantify the mesenchymal stem cell (MSC) response to subcellular detachment from soft materials.

7.2 Introduction

Approaches to expand and culture progenitor cells in vitro often focus on the role of soluble media additives to control cell function, such as proliferation and differentiation. For example, multipotent mesenchymal stem cells (MSCs) can be differentiated into chondrocytes with the exogenous addition of transforming growth factor- β 3 (TGF- β 3) or osteoblasts with the addition of dexamethasone, β -glycerol phosphate, and ascorbate.¹ Less attention is given to the role of the cellular microenvironment in this process, but it may be equally important for regulating cell function; for MSCs, chondrogenesis is conducted in pellet culture while osteogenesis is conducted in high cell density plate culture.¹ Further, the elasticity of the culture substrate has been shown to influence cell proliferation, adhesion, morphology, and migration and to direct MSC differentiation,²⁻⁶ while patterning of substrates to control cell geometry has been shown to regulate relative cell growth and apoptotic rates.^{7, 8} These results illustrate that a myriad of epigenetic factors, beyond soluble media additives, contribute to the control of cell function.^{9, 10} In particular, the extracellular matrix (ECM) serves as a major regulator of cell phenotype¹¹ by presenting mechanical cues and interacting with the cell through integrin binding.^{12, 13} Mechanotransduction relays these physical signals via dynamic focal adhesion formation and cytoskeletal organization, which regulate cell morphology, proliferation, migration, differentiation, and apoptosis via changes in gene expression.^{12, 14-16}

Seminal studies in cellular mechanobiology^{5, 7} have effectively linked ECM mechanics and cell-material interactions to cell function, but this work has been conducted primarily on static

substrates that fail to capture the active nature of the native ECM. In vivo, the ECM undergoes continual restructuring by ECM-cleaving molecules, such as matrix metalloproteinases, and cellular deposition of ECM components, creating a dynamic adhesive landscape.¹⁷ This landscape directs attachment and detachment to and from the ECM, controls the geometry of the cell niche, and regulates cytoskeletal organization, which all influence tissue formation, cell fate, wound repair, and cancer metastasis.¹⁸ In short, cells exert contractile forces as they actively engage with the ECM introducing tensile stresses in the cytoskeleton that originate at focal adhesions and it is now evident that both dynamic adhesion and force generation play a major role in directing cell function.¹⁴

Researchers have developed several in vitro techniques to investigate the mechanisms of cell adhesion and cytoskeletal tension on the cellular level, including the cell-spreading assay,^{19, 20} laser-induced ablation of actin stress fibers,^{21,22} pharmacological treatment to disrupt microtubules,²³ and trypsin-induced detachment.²⁴ In complementary approaches, investigators have developed responsive material substrates that can trigger changes in surface chemistry to temporally manipulate adhesive ligand presentation^{25,26} and cell attachment.^{27,28} For example, Wildt et al. presented a strategy to induce subcellular detachment by electrochemically releasing the fibronectin-derived adhesive ligand RGD from micropatterned gold features on glass and reported quantitative analysis of the detachment dynamics.²⁸ This technique allows the user to control adhesion dynamically on stiff substrates in predefined geometries.

Building from these studies, we sought to engineer soft, yet tunable, photodegradable substrates that would allow user-defined manipulation of cell-material interactions at any location, over any area, and at any point in time. Photoactive polymeric biomaterials that can be manipulated exogenously with light have emerged in recent literature as a class of materials that

provide unprecedented spatial and temporal control of both chemical and mechanical properties.²⁹⁻³² Out of this work, photodegradable hydrogels have been developed that are fully compatible with cell culture.^{6,30,33,34} Studies with these materials have demonstrated control of the biochemical nature of the ECM to direct MSC differentiation,³⁰ channel formation to direct cancer cell migration,³⁰ and control of ECM elasticity to mediate the myofibroblast-to-fibroblast transition³⁴ or to direct cell morphology in 2D⁶ and 3D.³³

In this manuscript, our objective is to employ a poly(ethylene glycol) (PEG)-based photodegradable hydrogel to study the dynamics of subcellular detachment from soft materials by spatially-defined substrate erosion. First, we demonstrate how the focal point of a mode-locked, femtosecond pulsed two-photon laser can be rastered directly below cells seeded on photodegradable hydrogels to erode the underlying substrate completely and disrupt cell-material interactions. Second, a simple model is presented to determine the irradiation conditions that afford complete erosion via two-photon excitation. Laser-induced degradation, and ultimately complete erosion, is demonstrated over a broad range of pulse energies, and features are generated within the gel on size scales relevant to cells. As a final proof of principle, surface erosion is conducted in the presence of cells to analyze quantitatively the retraction dynamics of erosion-induced subcellular detachment.

7.3 Results and Discussion

7.3.1 Preparation of a two-photon degradable hydrogel

Photodegradable hydrogels were formed by redox initiated, free-radical chain polymerization of a photolabile PEG-based crosslinker (PEGdiPDA, $M_n \sim 4070$ g/mol, **Figure 7.1a**) with a monoacrylated PEG macromer (PEGA, $M_n \sim 400$ g/mol) in phosphate buffered

saline (PBS). Since PEG-based materials are bioinert and present a poorly adhesive substrate for cells,³⁵ fibronectin (300 nM, $R_g \sim 14\text{nm}$ ³⁶) was included in the macromer solution used for all cell experiments; by this method, the adhesive protein is entrapped within or covalently attached to the hydrogel (mesh size $\xi \sim 10\text{nm}$, as approximated using rubber elasticity and Flory-Rehner theories) and presents integrin-binding adhesive sites. By this approach, cells sense the hydrogel's adhesive context and geometry, spread on the surface, and form an organized cytoskeleton (**Figure 7.3b**).

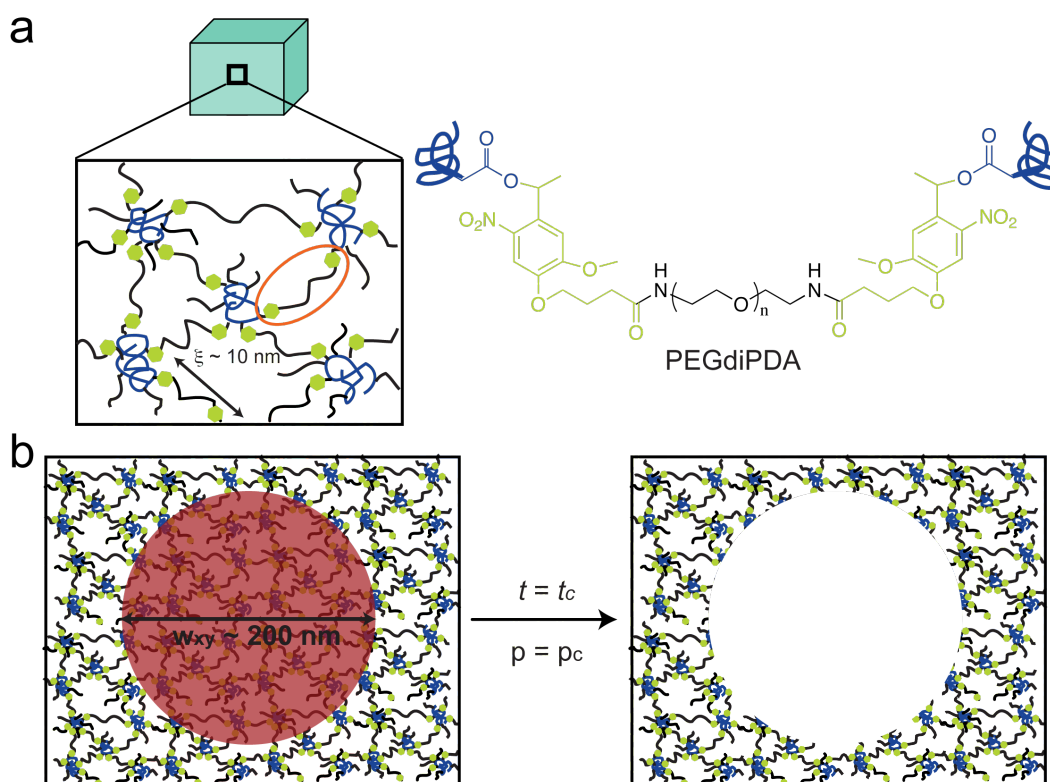


Figure 7.1 Two-photon induced degradation and complete erosion of photodegradable hydrogels. (a) Poly(ethylene glycol) (PEG)-based photodegradable hydrogels were formed (a, left) by redox-initiated free radical chain polymerization of PEGdiPDA (a, right) with PEGA. The crosslinking density of these gels corresponds to a mesh size (ξ) of approximately 10 nm (a, left), and the gels allow fibronectin to be physically entrapped within or covalently linked to the gel structure. (b) Focused, two-photon irradiation induces complete gel erosion when the focal point (red circle) dwells for enough time ($t = t_c$) such that a sufficient fraction of PEGdiPDA crosslinks can be cleaved locally ($p = p_c$) for a given average laser power. This photocleavage releases the polymer chains that comprise the hydrogel selectively from irradiated regions (b, right).

The crosslinker, PEGdiPDA, was rendered photoactive by attaching an acrylated *ortho*-nitrobenzylether (NBE) moiety to both sides of a PEG-*bis*-amine, as previously described.³⁰ This moiety was chosen due to its capability of undergoing two-photon photolysis³⁷ (at 740nm the two-photon cross section $\delta_u\Phi_u \approx 0.01$ to 0.03 GM^{38}) and its previous use in biological systems.³⁹ Upon two-photon excitation, PEGdiPDA cleaves between the NBE and acrylate functionalities, releasing modified PEG and polyacrylate chains with pendant PEG. Previous studies have shown that the degradation products of this hydrogel formulation are cytocompatible.^{30, 33, 34}

While the ability to erode completely NBE modified PEG-based hydrogels with two-photon excitation has been demonstrated,^{30, 31} these experiments were not performed in the presence of cells. Here, we sought to better understand how these materials might provide a unique substrate for probing cell-material interactions and to exploit this knowledge to direct cell function *in vitro*. Towards this end, there are critical aspects of the photodegradation process that need to be understood: (i) complete two-photon erosion should occur with micron-scale resolution; (ii) features should be generated on relevant time scales (ms to s); and (iii) the irradiation conditions should not disrupt normal cell function. For example, two-photon erosion can be used to define the geometry of the stem cell niche only if the features are formed rapidly on the cellular size scale *and* the cell is not affected solely by the irradiation. Therefore, we first characterized the resolution and time-scale of two-photon erosion within PEGdiPDA hydrogels, and subsequently employed previously reported cytocompatible irradiation conditions to induce subcellular detachment of MSCs.

7.3.2 Resolution of two-photon erosion of PEGdiPDA hydrogels

Mode-locked, pulsed laser directed two-photon excitation induces degradation within PEGdiPDA hydrogels over multiple length scales from (μm to mm) by cleaving the NBE moieties within the PEGdiPDA crosslinks (**Figure 7.1b**). The spatial resolution of patterning within the gel is theoretically limited by the focal volume, which for a Gaussian laser beam is governed by the lateral (w_{xy}) and axial (w_z) $1/e$ radii.⁴⁰ The focal radii are dictated by the numerical aperture (NA), the wavelength of irradiation (λ), and the refractive index of the material (n) as given by⁴⁰

$$w_{xy} = \frac{0.325\lambda}{\sqrt{2\text{NA}^{0.91}}}, \text{NA} > 0.7 \quad (1)$$

$$w_z = \frac{0.532\lambda}{\sqrt{2}} \left[\frac{1}{n - \sqrt{n^2 - \text{NA}^2}} \right] \quad (2)$$

For the experiments in this study with $\text{NA} = 1.0$, $\lambda = 740\text{nm}$, and $n = 1.33$, w_{xy} is 170nm , and w_z is 610nm . The theoretical diameter for the focal volume is an order of magnitude larger than the approximate mesh size of the hydrogels (**Figure 7.1b**), confirming that the focal point is the limiting factor for spatial resolution of degradation and not the material itself. Further, this focal volume confirms that micron-scale patterning is attainable in both the x-y and z-dimensions, which is demonstrated in experimental results found in Figs. 7.2c & 3.

7.3.3 Critical exposure time for two-photon erosion

A statistical-kinetic model of two-photon degradation and reverse gelation was developed to determine the critical exposure times needed to completely erode the focal volume within this material. In this manuscript, we use the terms degrade or degradation to refer to the cleavage of individual PEGdiPDA crosslinks due to two-photon excitation and the term reverse gelation to refer to the critical extent of degradation when the gel undergoes a solid-to-liquid transition, releasing soluble PEG crosslinks and polyacrylate chains with pendant PEG into solution. The release of these soluble fragments from the gel leads to mass loss, which we term erosion. Thus, reverse gelation refers to the point at which features are formed within the material through complete erosion and degradation is the process of cleaving bonds that ultimately leads to reverse gelation.

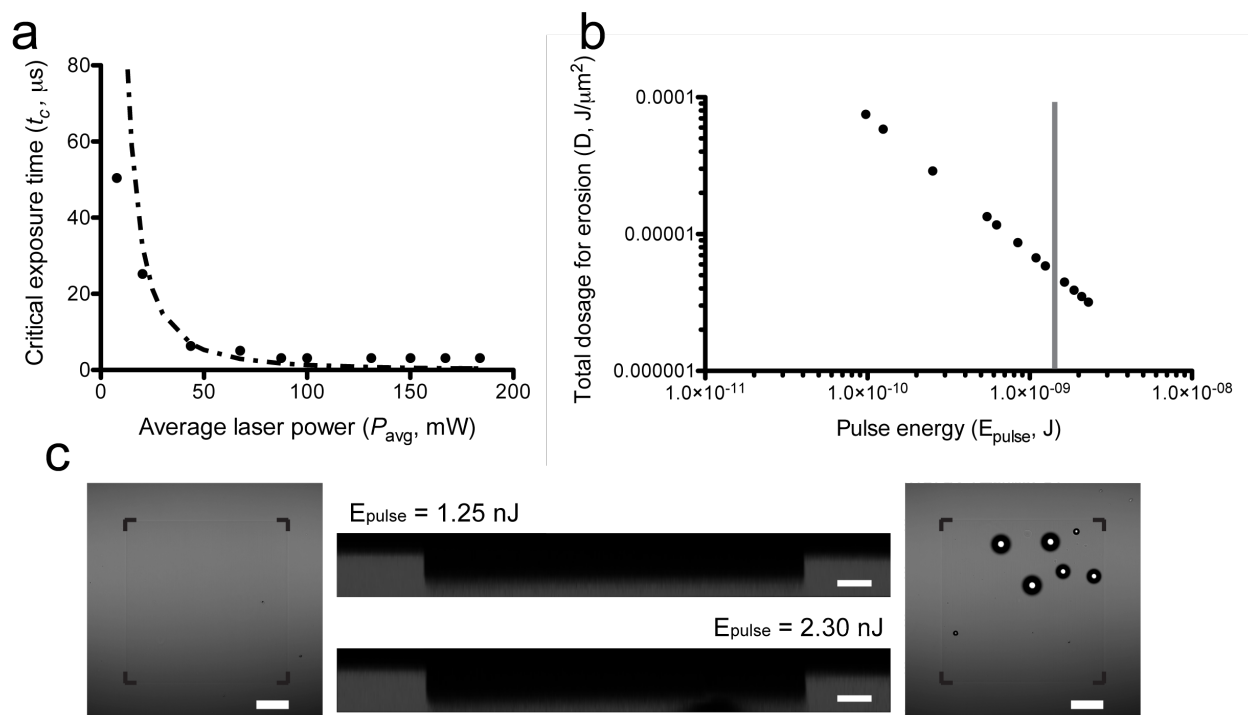


Figure 7.2 Parameter space for two-photon induced erosion of PEGdiPDA hydrogels. (a) Critical exposure times (t_c) for irradiation to induce complete erosion of PEGdiPDA hydrogels were determined experimentally for a broad range of average laser powers (P_{avg}) (solid circles) and plotted with model predictions (dashed line). (b) The pulse energy (E_{pulse}) for each average laser power used was calculated and combined with t_c to determine the total dosage required to erode the material and these data were plotted (solid circles). Previous studies have concluded

that pulse energies above 1.5 nJ thermally ablate intracellular components (gray vertical line), demonstrating that complete erosion can be performed below the cut-off for laser-induced ablation of intracellular components. (c) Locally confined erosion of PEGdiPDA hydrogels was imaged in brightfield (outside images, black corner marks indicate the region of erosion) and with cross-sections of fluorescent confocal stacks (central images) and was confirmed with profilometry (data not shown). For the pulse energy used in cells studies and feature formation ($E_{\text{pulse}} = 1.25$ nJ, left outside image and top central image), selective erosion was achieved with an average depth of 8 ± 1 μm for 7 μm deep scans. At the highest pulse energies studied ($E_{\text{pulse}} = 2.3$ nJ, right outside image and bottom central image), nonspecific erosion was induced with an average depth of 11 ± 1 μm for 7 μm deep scans. Furthermore, cavitation was observed within the hydrogels at such high pulse energies as evidenced by bubble formation in the material. Scale bars represent 20 μm in the fluorescent images and 50 μm in the brightfield images.

To reach reverse gelation, such that the gel erodes completely and undergoes a solid-to-liquid transition, a critical fraction of the NBE molecules must be degraded within the focal point. Based on a statistical treatment of chain growth networks, the critical extent of cleavage (p_c) is dictated by the weight average number of crosslinks per polyacrylate kinetic chain ($N = 20$ for this system³³), such that $p_c = \frac{1}{\sqrt{N-1}}$.⁴¹ The degradation reaction as a function of irradiation time (t) is modeled as a first-order process as previously described^{38,42}:

$$\frac{d[\text{NBE}]}{dt} = -k_e[\text{NBE}] \quad (3)$$

with

$$k_e = 1.17\delta_u\Phi_u \frac{T}{\tau_p} \left(\frac{\lambda}{\pi h c w_{xy}^2} \right)^2 P_{\text{avg}}^2 VF \quad (4)$$

Here, $\delta_u\Phi_u$ is the two-photon cross section; T is the period of the laser pulses (12.5 ns); τ_p is the duration of the laser pulses (140 fs); h is Planck's constant; c is the speed of light; P_{avg} is the

average laser power; and VF is a volume factor (0.63 for an axial cylinder).^{38, 42} For these studies, a conservative estimate of 0.01 GM for the two-photon cross section was used based on previous literature.³⁸ Equation (3) was solved to give a form for the extent of degradation (p):

$$p = \frac{[\text{NBE}]}{[\text{NBE}]_0} = e^{-k_e t} \quad (5)$$

such that one can combine Eqns. (4) and (5) for the relationship between the critical exposure time ($t = t_c$) required to erode the material completely ($p = p_c$) and the average laser power (P_{avg}). Solving this expression for P_{avg} one arrives at

$$P_{\text{avg}} = \sqrt{-\frac{\ln p_c}{\alpha t_c}} \quad (6)$$

where $\alpha = 1.17\delta_u\Phi_u \frac{T}{\tau_p} \left(\frac{\lambda}{\pi h c w_{xy}^2} \right)^2 VF$. This relationship combines photodegradation kinetics, two-photon physics, and statistical models of reverse gelation to predict the exposure time required for complete hydrogel erosion. Accordingly, this model provides a working parameter space for two-photon induced erosion of PEGdiPDA hydrogels (**Figure 7.2a**) and a methodology for determining critical exposure times (t_c) for two-photon labile materials based on P_{avg} . Experimentally determined critical exposure times required to erode the material completely were plotted with the statistical-kinetic model (**Figure 7.2a**) over a broad range of average laser powers (7.8 to 183.8 mW). Experimentally determined critical exposure times agree well with the model over the range of P_{avg} from 20.2 to 87.5 mW (*i.e.*, the absolute value of the deviation =

$(t_{cexperimental} - t_{cpredicted})/t_{cexperimental} < 0.5$). Outside of this range, larger deviations are observed at high P_{avg} because of the limitation of the fastest scan speed on the LSM and at low P_{avg} because of excitation from other planes that can lead to out-of-plane excitation at slower pixel dwell times. Using this approach, the critical exposure time for erosion of any photolabile network can be predicted for a broad range of irradiation conditions. In addition, this information can be used rationally to select irradiation parameters for modifying gel properties and thus the cell microenvironment.

7.3.4 Irradiation conditions for *in situ* degradation

An array of laser powers results in erosion of PEGdiPDA hydrogels (**Figure 7.2a**), but the end application of erosion in the *presence* of cells limits the user to cytocompatible irradiation conditions. Focused two-photon irradiation has been used previously to thermally ablate intracellular components, such as actin stress fibers,^{22, 43, 44} neurofilaments,⁴⁵ and mitochondria.^{44, 46} These investigations have demonstrated that femtosecond pulsed two-photon irradiation can be used in the presence of cells, but that there is a pulse energy (E_{pulse}) threshold for photo-induced ablation and a threshold for maintaining cell viability. It was reported that pulse energies below 1.5 nJ fail to induce intracellular ablation⁴⁴ and that cells remain viable when exposed to pulse energies at or below 4 nJ.⁴⁶ In other words, to prevent non-specific ablation of intracellular components, such as the actin cytoskeleton, and to maintain high cell viability the user should operate below the pulse energy threshold of 1.5 nJ.

The pulse energy for a specific laser system is the energy delivered by each femtosecond laser pulse and is calculated as $E_{pulse} = P_{peak}\tau_p$, where $P_{peak} = P_{avg} \frac{T}{\tau_p}$ is the peak energy delivered by the laser ($\tau_p = 140$ fs for the laser used in this study). To explore the relationship between

pulse energy and gel erosion, the pulse energies were determined for the irradiation conditions used in this study (**Figure 7.2b**). From these energies and the t_c , the total dosage (D) required to erode the material was also calculated, $D = \frac{E_{\text{pulse}} t_c}{A_{\text{focal}} T}$ with $A_{\text{focal}} = \pi \left(\frac{w_{xy}}{2} \right)^2$. This analysis demonstrates that higher pulse energies require less total dosage to erode the material (**Figure 7.2b**). However, sufficiently high pulse energies (2.3 nJ) induce cavitation within the PEGdiPDA hydrogels causing non-specific, uncontrolled degradation (**Figure 7.2c**). At lower pulse energies ($E_{\text{pulse}} < 2.0$ nJ), no cavitation was observed (**Figure 7.2c**). Based on previous findings for the cellular response to pulse energies^{44, 46} and our characterization of photoerosion in PEGdiPDA hydrogels, a working space for achieving complete gel erosion while not affecting cell function is established. Correspondingly, gel erosion in this study was conducted with a laser pulse energy of 1.25 nJ to minimize the total dosage while avoiding ablation of cellular components and uncontrolled gel erosion due to cavitation. Further, exposure to this pulse energy of 1.25 nJ does not affect the normal function of cells seeded on non-degradable PEGDA hydrogels (Supplementary Information, **Figure 7.5**).

7.3.5 Two-photon control of ECM context and geometry

Studies of the cellular response to dynamic changes in the ECM necessitate modifying the adhesive landscape on size scales relevant to the cell (~1-100 μm) in a spatially and temporally defined manner. Recently, this has been achieved in predefined geometries on the surface of glass with an array of gold features that electrochemically releases RGD.²⁸ In addition, adhesive ligands have been photochemically exposed on glass via single and two-photon irradiation of photoactive SAMs.^{25, 26, 37} Here, two-photon induced photodegradation of PEGdiPDA hydrogels offers a soft substrate with tunable elasticity and user-defined geometrical

and temporal control of the ECM landscape at *both* the surface of 2D hydrogel scaffolds and within 3D hydrogels. In each case, erosion is achieved by rastering the focal point for the critical exposure time (a pixel dwell time of 1.58 μs) given the pulse energy (1.25 nJ) at each focal volume within the desired geometries (**Figure 7.3a**). Due to the short pixel dwell time, features can be formed rapidly within the gel: ~ 10 ms for a 10 μm wide square and ~ 4 s for a 250 μm diameter circle. As such, this platform is appropriate to study (i) erosion-induced motility and the dynamics of subcellular detachment on 2D substrates and (ii) migration through channels and the effect of the geometry of the cell niche on cell function within 3D scaffolds.

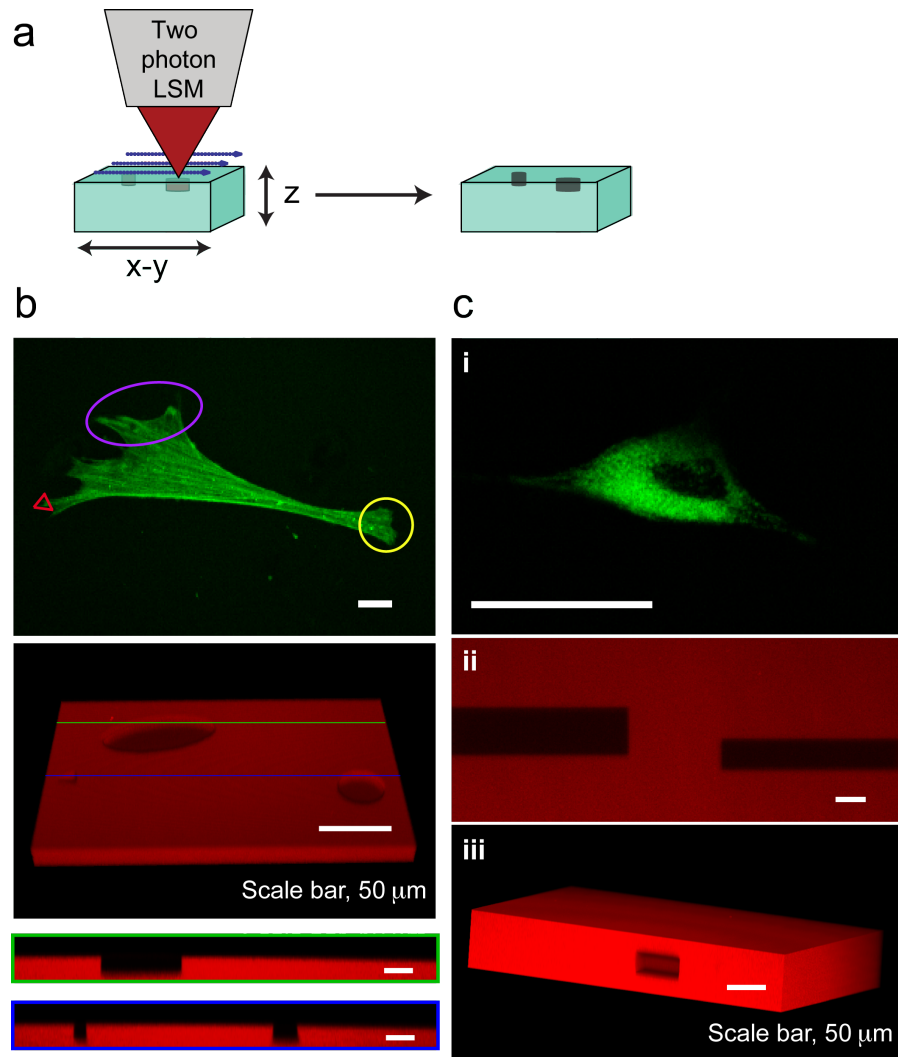


Figure 7.3 Feature formation to control ECM context and geometry. (a) Defined features can be patterned at the surface or within PEGdiPDA hydrogels by rastering the focal point of a two-photon laser scanning microscope (LSM, Zeiss LSM 710) through specific geometries using region of interest software. (b) Surface feature formation can be performed on size scales relevant to the cell ($\sim 1\text{-}100\ \mu\text{m}$) and spatially confined to desired regions to disrupt adhesion at the anterior or posterior of adhered cells (purple oval and yellow circle) or to disrupt adhesion at individual filopodia (red triangle). To demonstrate this strategy, feature formation was performed in the absence of cells on the order of microns (red triangle) to $100\ \mu\text{m}$ (purple oval) and was monitored with confocal microscopy (3D renderings of fluorescent confocal stacks and the corresponding cross-sections, green and blue lines). (c) Features were also patterned within the bulk of PEGdiPDA hydrogels to motivate the utility of this approach for directing encapsulated cells (c.i) to migrate down specific channels (c.ii) or for defining the geometry of the cell niche (c.iii). $20\ \mu\text{m}$ and $30\ \mu\text{m}$ wide channels were patterned into PEGdiPDA gels (c.ii) for representative channel formation, and a $45\ \mu\text{m}$ wide square cylinder was patterned into a gel (c.iii) as a representative change to the geometry of the cell niche. Scale bars represent $20\ \mu\text{m}$, except as noted.

Based on the degradation parameters outlined above, pulsed two-photon laser excitation was used to spatially direct feature formation at the surface of a PEGdiPDA hydrogel (**Figure 7.3a**), demonstrating selective removal of specific cell-material interactions. This technique allows for spatiotemporal removal of the ECM associated with the anterior or posterior of polarized cells (**Fig. 7.3b**, purple oval and yellow circle), which has implications in understanding the mechanisms of cell motility, as well as individual filopodia (**Figure 7.3b**, triangle) to study the dynamics of subcellular detachment. Further, this material allows for three-dimensional scaffold erosion within the gel, which could be used to direct cell migration and connectivity or to define the geometry of the cell niche. A cell's geometrical constraints have been shown to influence relative growth and apoptotic rates on 2D substrates,^{7, 8} but due to material limitations, this has been difficult to study in 3D. Here, we demonstrate the ability to pattern channels on relevant size scales or geometric niches within 3D scaffolds using cytocompatible irradiation conditions (**Figure 7.3c**). This method presents a unique approach that provides full spatial and temporal control of the ECM context for hypothesis testing of how the adhesive landscape on 2D and within 3D soft materials affects cell function.

7.3.6 Erosion of PEGdiPDA hydrogels to study subcellular detachment

Cell adhesion and morphology are important regulators of cell function and fate. To demonstrate the efficacy and utility of this material for cell studies, subcellular adhesion was controlled dynamically by selective two-photon irradiation. Specifically, MSCs were transfected with a GFP-actin construct for real time monitoring of cytoskeletal organization and morphology. These cells were seeded on 2D PEGdiPDA hydrogels and given time (~48 hr) to attach to the substrate, spread, and form an organized cytoskeleton. Subsequently, regions of the scaffold were eroded to disrupt cell-material interactions selectively (less than 20% of the initial cell area was eroded in all cases, **Figure 7.4a**). Removal of the substrate material just at the cell interface induces subcellular detachment (**Figure 7.4**, Supporting Information), which was initiated at the site of scaffold erosion and was followed by cellular retraction. The morphological response of each cell was tracked over an elapsed time between 10 and 60 minutes using confocal microscopy (**Figure 7.4a**). Control MSCs seeded on non-degradable PEG diacrylate (PEGDA) gels exposed to the same irradiation conditions did not detach or undergo cytoskeletal reorganization (Supporting Information, **Figure 7.5**).

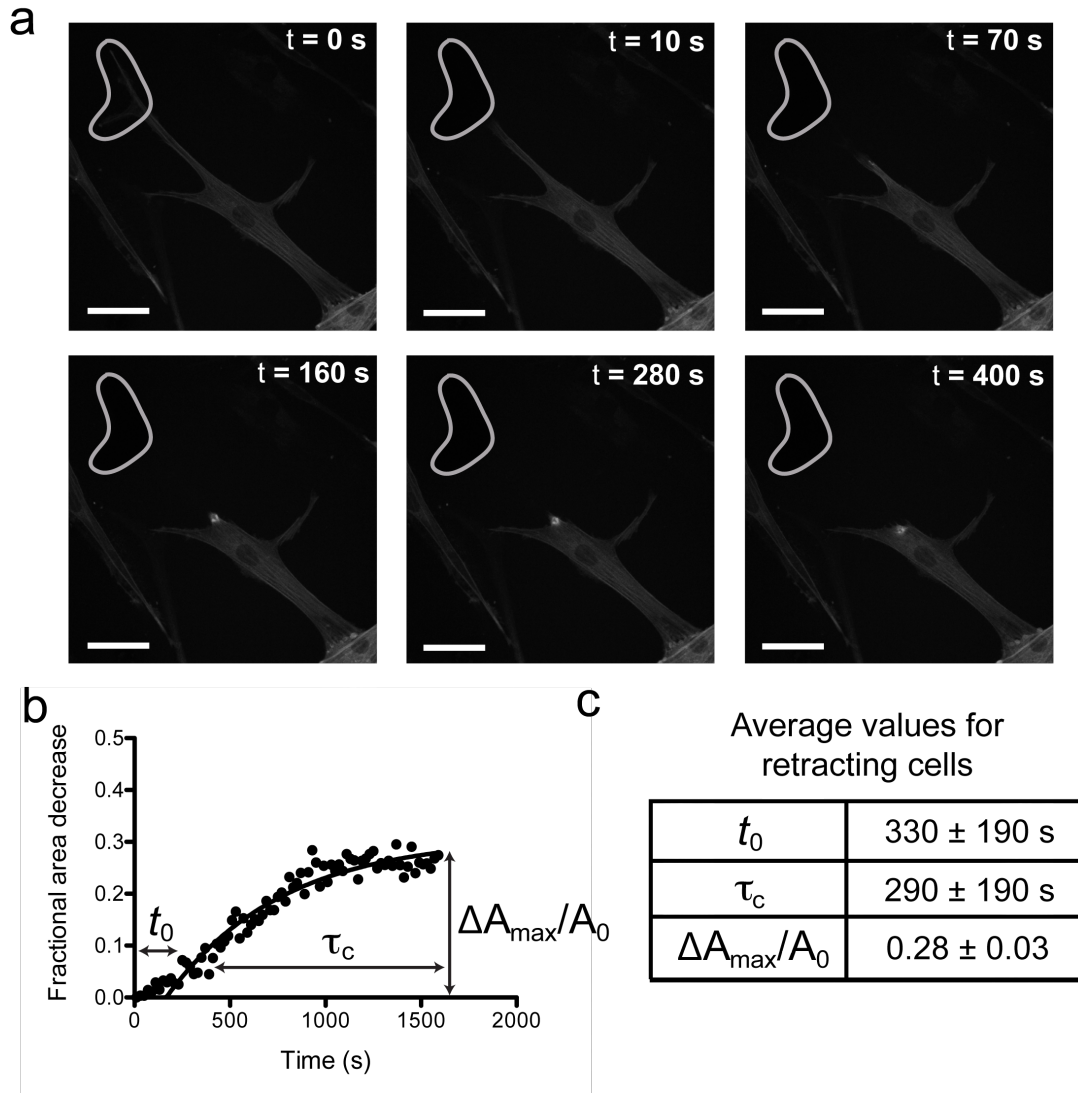


Figure 7.4 Two-photon erosion of PEG substrates induces subcellular detachment. (a) Specific regions of cell-material interactions between GFP-actin transfected MSCs and PEGdiPDA hydrogels were disrupted by two-photon erosion ($t = 0$ s, region outlined in gray). This spatiotemporal erosion induced cell retraction, which was monitored with confocal microscopy (representative images of the first 400 s for an individual cell are shown). (b) Using confocal microscopy, cell area was monitored in response to subcellular detachment, and a fractional area decrease ($\Delta A(t)/A_0$) was calculated via image analysis. The solid line is a fit to the equation $\Delta A(t)/A_0 = \Delta A_{\max}/A_0[1 - \exp(-(t-t_0)/\tau_c)]$, and good agreement is observed. (c) Average values for the induction time (t_0), retraction time (τ_c), and the maximum fractional area change ($\Delta A_{\max}/A_0$) were compiled for retracting cells ($n = 6$, mean \pm s.e.m), where slowed induction and retraction times were observed on these soft hydrogels as compared to stiff culture substrates.²⁸ Scale bars represent 20 μm .

To quantify the dynamics of subcellular detachment from PEGdiPDA hydrogels, the fractional area decrease of each cell was followed as $\Delta A(t)/A_0$ (**Figure 7.4b**), where $\Delta A(t)$ is the change in cell area at time t ($A_0 - A(t)$) and A_0 is the initial cell area, similar to the approach of Wildt et al.²⁸ The following expression that describes the relationship between cell area and retraction time was fit to the data corresponding to each retracting cell:

$$\frac{\Delta A(t)}{A_0} = \frac{\Delta A_{\max}}{A_0} \left[1 - \exp\left(-\frac{t - t_0}{\tau_c}\right) \right] \quad (7)$$

where ΔA_{\max} is the maximum change in cell area; t_0 is the induction time prior to retraction during which $A \cong A_0$; and τ_c is the characteristic retraction time for the cell.²⁸ The fit to this model (**Figure 7.4b**) suggests that the cell is under tension prior to detachment and undergoes damped retraction.^{22, 24, 28} For the cell population examined in this study, cells responded with an average t_0 of 330 ± 190 s (mean \pm s.e.m.), an average τ_c of 290 ± 70 s, and an average $\Delta A_{\max}/A_0$ of 0.28 ± 0.03 . The values for t_0 and τ_c are approximately 6-fold larger than the values reported for contractile cells on rigid substrates,^{24, 28} indicating that the dynamics of subcellular detachment are slowed on soft materials. These data agree with the proposed theory that subcellular detachment dynamics are dictated by the elasticity of the cell prior to detachment and indicate the importance of studying dynamic cell adhesion and cytoskeletal organization on substrates with moduli similar to soft tissues. Further, this method disrupts adhesive junctions, allowing the user to investigate the full signaling cascade induced by subcellular detachment, complementing other approaches that target specific segments of the cascade.

7.4 Conclusion

A strategy is presented that allows users to manipulate precisely the context and geometry of a cell's underlying substrate or surrounding microenvironment at any point in space and time via two-photon irradiation of a photodegradable PEG-based hydrogel. A statistical-kinetic model of gel erosion was combined with previous literature to determine a cytocompatible parameter space for spatiotemporal two-photon induced erosion of PEGdiPDA hydrogels. Based on this parameter space, irradiation conditions were selected that preclude uncontrolled erosion and nonspecific ablation of intracellular components while minimizing the total light dosage. These cytocompatible irradiation parameters were subsequently employed to generate features at the surface and within the bulk of PEGdiPDA gels. Subsequently, surface erosion was exploited to disrupt the cell-material interface and induce subcellular detachment. Using this approach we quantified subcellular detachment of MSCs from soft materials, which was observed to be ~6 fold slower than detachment from stiffer substrates.²⁸ PEGdiPDA hydrogels combined with two-photon induced erosion are useful tools for studying cell adhesion and detachment to and from soft substrates with tunable elasticity, and these materials should facilitate fundamental investigations of the dynamics of cell mechanobiology in both 2D and 3D culture.

7.5 Experimental

7.5.1 Synthesis of a photodegradable crosslinker

A nitrobenzyl-based photodegradable monomer, photodegradable acrylate (PDA), was synthesized by acrylation of ethyl 4-(4-(1-hydroxyethyl)-2-methoxy-5-nitrophenoxy)butanoic acid and subsequent purification as previously described.³⁰ Through a pendant carboxylic acid,

this photodegradable monomer can easily be coupled to any primary amine containing molecule, such as amine functionalized PEG and peptides. A divinyl crosslinking macromer (PEGdiPDA) was synthesized by coupling the PDA to PEG-bis-amine ($M_n \sim 3400$ g/mol, Laysan Bio).³⁰ Briefly, in a glass scintillation vial, PDA (6 mmol) was dissolved in n-methylpyrrolidone (NMP, 156 mmol, Applied Biosystems). 2-(1H-benzotriazole-1-yl)-1,1,3,3-tetramethyluronium hexafluorophosphate (HBTU, 6.5 mmol, Anaspec) and 1-hydroxybenzotriazole (HOBt, 6.5 mmol, Anaspec) were added and the solution was heated intermittently with vortexing into complete dissolution of all components. Diisopropylethylamine (DIEA, 11.8 mmol, Anaspec) was subsequently added to the solution and stirred for 5 min. In a single-neck round bottom flask with argon purge, PEG-*bis*-amine (0.6 mmol) was dissolved in NMP (104 mmol) by intermittent heating and stirring. The activated acid solution was added to this PEG-*bis*-amine solution, and the flask was purged with argon and stirred overnight at room temperature. The reaction solution was precipitated in cold ethyl ether (0°C on ice, Fisher Scientific). The precipitated product was recovered by centrifugation (5 min at 3000 rpm) and washed twice with cold ethyl ether. After the final wash, ether was decanted, and the pelleted product was stored under vacuum overnight to remove any remaining ether. The crude product (< 10 wt%) was dissolved in deionized water (DI water, 18 MΩ-cm, Barnstead NANOpure II). The resulting mixture was centrifuged (30 min at 3000 rpm) to remove any soluble by products that remained from the reaction. The dissolved product was subsequently dialyzed (SpectraPor 7, CO 1000 g/mol) and lyophilized. The purity of the PEGdiPDA was verified with proton NMR (> 85% modification of PEG-*bis*-amine with the PDA). ¹H NMR ((CD₃)₂SO): δ=8.0 (t, C(=O)NHCH₂CH₂O), δ= 7.6 (s, Aromatic-H), δ=7.2 (s, Aromatic-H), δ=6.4, 6.05 (d, d, OC(=O)CH=CH₂), δ=6.35 (m, Aromatic-CH(CH₃)OC(=O)CH=CH₂), δ=6.25 (m,

OC(=O)CH=CH₂), $\delta=4.1$ (t, Aromatic-OCH₂CH₂CH₂CO₂H), $\delta=3.9$ (s, Aromatic-OCH₃), $\delta=3.5$ (m, [CH₂CH₂O]_n, n~77), $\delta=2.75$ (t, NH₂CH₂CH₂O), $\delta=2.4$ (t, Aromatic-OCH₂CH₂CH₂CO₂H), $\delta=2.0$ (m, Aromatic-OCH₂CH₂CH₂CO₂H), and $\delta=1.4$ (d, Aromatic-CHCH₃).

7.5.2 Fabrication of PEGdiPDA hydrogels

Photodegradable hydrogels were synthesized using redox-initiated free radical chain polymerization as previously described.³³ Briefly, stock solutions of each component were prepared, sterile filtered, and diluted to final concentrations of 8.2 wt% PEGdiPDA, 6.8 wt% PEG monoacrylate (PEGA, Mn ~ 400 g/mol, Monomer-Polymer and Dajac Labs), and 0.2 M ammonium persulfate (Acros) in phosphate buffered saline (PBS, pH ~ 7.4, Invitrogen) to make the gel-forming monomer solution. This monomer solution was aliquoted into individual tubes for each gel sample. To initiate polymerization, tetraethylmethylenediamine (0.1 M in PBS, Sigma Aldrich) was added to an aliquot of the monomer solution while vortexing and quickly pipetted into a mold between glass cover slips (0.25 mm thick spacer, McMaster Carr; 25 mm x 25 mm cover glass, No. 2, Fisher Scientific). To aid in handling, one of these coverslips was modified with an acrylate silane to covalently link the gel to the cover slip during polymerization. Cover slip modification was performed as previously described:³⁴ the slip was cleaned with Piranha (30 min), rinsed with DI water, dried with an acetone rinse, and modified by chemical vapor deposition with (3-acryloxypropyl)-trimethoxysilane (120 μ L, Gelest) in a sealed chamber at 60°C for 3 h. For gels used in cell culture, fibronectin (FN, human, BD Biosciences) was added to the monomer solution (300 nM in PBS) for entrapment within the gel during polymerization. For gels used in demonstrations of feature formation, methacryloxyethyl thiocarbamoyl rhodamine B (Polysciences, Inc.) was added to the monomer solution (300 μ M in

PBS, sterile filtered) to covalently modify the polymer network with a fluorophore for subsequent pattern imaging.

7.5.3 Culture and transfection of hMSCs

Adult human mesenchymal stem cells (MSCs) (Cambrex Bio Science) were plated on 15 cm diameter tissue culture polystyrene Petri dishes (BD Bioscience) at 5,000 cells/cm². The MSCs were cultured in low-glucose DMEM containing 10% fetal bovine serum, 1 µg/mL amphotericin B, 50 units/mL penicillin, and 50 µg/mL streptomycin (Invitrogen). The cells were grown at standard cell culture conditions (incubated at 37 °C with 5% CO₂) and the media was refreshed every third day. Cells were passaged at ~75-85% confluency and MSCs at passage 2 or 3 were used in this study. To monitor the cytoskeletal and morphological responses to subcellular detachment, MSCs were transfected with a GFP-actin plasmid (BD Biosciences), which is a mammalian expression vector that encodes a fusion protein of the green fluorescent protein (GFP) from *Aequorea coerulea* to human cytoplasmic β-actin. Transfections were conducted with 1.25 to 1.5x10⁶ cells and 1.8 µg of the GFP-actin plasmid in 100 µL of Human MSC Nucleofector® Solution (Lonza) with an Amaxa Nucleofector® II. Upon transfection, cells were seeded on PEGdiPDA hydrogels at 40,000 cells/cm², based on hemocytometer counts prior to transfection. Cells were given ~ 48 hr to adhere to the hydrogels, spread on the surface, and express the GFP-actin plasmid. Subsequently, the gels were transferred to a custom imaging chamber for two-photon irradiation and monitoring of the cell response.

7.5.4 Laser setup and power measurement

Two-photon induced photoerosion of PEGdiPDA hydrogels was carried out on a LSM 710 (Zeiss) with a modelocked Ti:Sapphire, femtosecond pulsed, multiphoton laser (Chameleon Ultra II, Coherent, Inc.) at a wavelength of 740 nm. A 20x water immersion objective (NA = 1.0, Plan-Apochromat) was used for all eroding scans. ZEN region of interest (ROI) software (Zeiss) was used to raster the focal point through defined geometries of the in-focus x-y plane. Features were patterned into the surface of PEGdiPDA hydrogels by rastering the focal point through desired ROIs and scanning in the z-direction from the surface of the gel to 7 μm below the surface of the gel with a step size of 1 μm . Similarly, features were patterned within the bulk of PEGdiPDA hydrogels by scanning through selected z-dimensions with a step size of 1 μm . A pixel dwell time of 1.58 μs and an average laser power of 0.1 W was used for pattern formation and to ensure complete erosion each scan was performed twice. The average power of the laser through the objective was measured with a power meter (FieldMaxII-TO, Coherent, Inc.) for all two-photon irradiation conditions used. Imaging of pattern formation and cells was also performed on the LSM 710.

7.5.5 Gel characterization

Rhodamine-labeled PEGdiPDA hydrogels were imaged on the LSM 710 before and after feature formation. Both brightfield and fluorescent images were taken to monitor two-photon induced erosion and the height (z-dimension) of feature formation was monitored with fluorescent confocal z-stacks. Feature formation and height measurements were confirmed by profilometry (DekTak 6M Stylus Profiler).

7.5.6 Quantification of subcellular detachment

Confocal microscopy (LSM 710, Zeiss) was used to monitor cell area as a function of time post-irradiation. Specifically, a time-series of images ($\Delta t = 15$ or 30 s) of each cell was captured for an elapsed time between 10 and 60 minutes. A MATLAB® script was written using the Image Processing Toolbox to quantify the cell area over the course of the time-series corresponding to each cell.

7.5.7 Statistical analysis

All data are represented as mean \pm standard error of the mean (s.e.m.). GraphPad© software was used for curve fitting, plotting, and data analysis.

7.6 References

1. Pittenger, M. *et al.* Multilineage potential of adult human mesenchymal stem cells. *Science* **284**, 143–147 (1999).
2. Pelham, R. & Wang, Y. Cell locomotion and focal adhesions are regulated by substrate flexibility. *P Natl Acad Sci Usa* **94**, 13661–13665 (1997).
3. Discher, D., Janmey, P. & Wang, Y. Tissue cells feel and respond to the stiffness of their substrate. *Science* **310**, 1139–1143 (2005).
4. Georges, P. & Janmey, P. Cell type-specific response to growth on soft materials. *J Appl Physiol* **98**, 1547–1553 (2005).
5. Engler, A. J., Sen, S., Sweeney, H. L. & Discher, D. E. Matrix elasticity directs stem cell lineage specification. *Cell* **126**, 677–689 (2006).
6. Frey, M. T. & Wang, Y.-L. A photo-modulatable material for probing cellular responses to substrate rigidity. *Soft Matter* **5**, 1918–1924 (2009).
7. Chen, C. S. Geometric Control of Cell Life and Death. *Science* **276**, 1425–1428 (1997).
8. Singhvi, R. *et al.* Engineering Cell-Shape and Function. *Science* **264**, 696–698 (1994).
9. Tibbitt, M. W. & Anseth, K. S. Hydrogels as Extracellular Matrix Mimics for 3D Cell Culture. *Biotechnol Bioeng* **103**, 655–663 (2009).

10. Freytes, D. O., Wan, L. Q. & Vunjak-Novakovic, G. Geometry and Force Control of Cell Function. *J Cell Biochem* **108**, 1047–1058 (2009).
11. Guilak, F. *et al.* Control of Stem Cell Fate by Physical Interactions with the Extracellular Matrix. *Cell Stem Cell* **5**, 17–26 (2009).
12. Schwartz, M., Schaller, M. & Ginsberg, M. Integrins: Emerging paradigms of signal transduction. *Annu Rev Cell Dev Bi* **11**, 549–599 (1995).
13. Giancotti, F. & Ruoslahti, E. Integrin signaling. *Science* **285**, 1028–1032 (1999).
14. Ingber, D. E. Tensegrity-based mechanosensing from macro to micro. *Prog Biophys Mol Bio* **97**, 163–179 (2008).
15. Mammoto, A. *et al.* A mechanosensitive transcriptional mechanism that controls angiogenesis. *Nature* **457**, 1103–U57 (2009).
16. Birgersdotter, A., Sandberg, R. & Ernberg, I. Gene expression perturbation in vitro - A growing case for three-dimensional (3D) culture systems. *Semin Cancer Biol* **15**, 405–412 (2005).
17. Daley, W. P., Peters, S. B. & Larsen, M. Extracellular matrix dynamics in development and regenerative medicine. *J Cell Sci* **121**, 255–264 (2008).
18. Lauffenburger, D. & Horwitz, A. Cell migration: A physically integrated molecular process. *Cell* **84**, 359–369 (1996).
19. Raucher, D. & Sheetz, M. Cell spreading and lamellipodial extension rate is regulated by membrane tension. *J Cell Biol* **148**, 127–136 (2000).
20. Dobereiner, H., Dubin-Thaler, B., Giannone, G., Xenias, H. & Sheetz, M. Dynamic phase transitions in cell spreading. *Phys Rev Lett* **93**, – (2004).
21. Rajfur, Z., Roy, P., Otey, C., Romer, L. & Jacobson, K. Dissecting the link between stress fibres and focal adhesions by CALI with EGFP fusion proteins. *Nat Cell Biol* **4**, 286–293 (2002).
22. Kumar, S. *et al.* Viscoelastic retraction of single living stress fibers and its impact on cell shape, cytoskeletal organization, and extracellular matrix mechanics. *Biophys J* **90**, 3762–3773 (2006).
23. Ezratty, E. J., Partridge, M. A. & Gundersen, G. G. Microtubule-induced focal adhesion disassembly is mediated by dynamin and focal adhesion kinase. *Nat Cell Biol* **7**, 581–590 (2005).

24. Sen, S. & Kumar, S. Cell-Matrix De-Adhesion Dynamics Reflect Contractile Mechanics. *Cell Mol Bioeng* **2**, 218–230 (2009).
25. Petersen, S. *et al.* Phototriggering of cell adhesion by caged cyclic RGD peptides. *Angew Chem Int Edit* **47**, 3192–3195 (2008).
26. Ohmuro-Matsuyama, Y. & Tatsu, Y. Photocontrolled cell adhesion on a surface functionalized with a caged arginine-glycine-aspartate peptide. *Angew Chem Int Edit* **47**, 7527–7529 (2008).
27. Yeo, W.-S. & Mrksich, M. Electroactive self-assembled monolayers that permit orthogonal control over the adhesion of cells to patterned substrates. *Langmuir* **22**, 10816–10820 (2006).
28. Wildt, B., Wirtz, D. & Searson, P. C. Programmed subcellular release for studying the dynamics of cell detachment. *Nat Meth* **6**, 211–213 (2009).
29. Johnson, J. A., Baskin, J. M., Bertozzi, C. R., Koberstein, J. T. & Turro, N. J. Copper-free click chemistry for the in situ crosslinking of photodegradable star polymers. *Chem Commun* 3064–3066 (2008).
30. Kloxin, A. M., Kasko, A. M., Salinas, C. N. & Anseth, K. S. Photodegradable hydrogels for dynamic tuning of physical and chemical properties. *Science* **324**, 59–63 (2009).
31. Wong, D. Y., Griffin, D. R., Reed, J. & Kasko, A. M. Photodegradable Hydrogels to Generate Positive and Negative Features over Multiple Length Scales. *Macromolecules* **43**, 2824–2831 (2010).
32. Murayama, S. & Kato, M. Photocontrol of Biological Activities of Protein by Means of a Hydrogel. *Anal. Chem.* **82**, 2186–2191 (2010).
33. Kloxin, A. M., Tibbitt, M. W., Kasko, A. M., Fairbairn, J. A. & Anseth, K. S. Tunable Hydrogels for External Manipulation of Cellular Microenvironments through Controlled Photodegradation. *Adv Mater* **22**, 61–66 (2010).
34. Kloxin, A. M., Benton, J. A. & Anseth, K. S. In situ elasticity modulation with dynamic substrates to direct cell phenotype. *Biomaterials* **31**, 1–8 (2010).
35. Peppas, N., Hilt, J., Khademhosseini, A. & Langer, R. Hydrogels in biology and medicine: From molecular principles to bionanotechnology. *Adv Mater* **18**, 1345–1360 (2006).
36. Rocco, M., Infusini, E., Daga, M., Gogioso, L. & Cuniberti, C. Models of Fibronectin. *Embo J* **6**, 2343–2349 (1987).
37. Álvarez, M. *et al.* Single-Photon and Two-Photon Induced Photocleavage for Monolayers of an Alkyltriethoxysilane with a Photoprotected Carboxylic Ester. *Adv Mater* **20**, 4563–

- 4567 (2008).
38. Aujard, I. *et al.* o-Nitrobenzyl photolabile protecting groups with red-shifted absorption: Syntheses and uncaging cross-sections for one- and two-photon excitation. *Chem-Eur J* **12**, 6865–6879 (2006).
 39. Zhao, Y. *et al.* New caged coumarin fluorophores with extraordinary uncaging cross sections suitable for biological imaging applications. *J Am Chem Soc* **126**, 4653–4663 (2004).
 40. Zipfel, W., Williams, R. & Webb, W. Nonlinear magic: multiphoton microscopy in the biosciences. *Nat Biotechnol* **21**, 1368–1376 (2003).
 41. Reddy, S., Anseth, K. & Bowman, C. Modeling of network degradation in mixed step-chain growth polymerizations. *Polymer* **46**, 4212–4222 (2005).
 42. Kiskin, N., Chillingworth, R., McCray, J., Piston, D. & Ogden, D. The efficiency of two-photon photolysis of a “caged” fluorophore, o-1-(2-nitrophenyl)ethylpyranine, in relation to photodamage of synaptic terminals. *Eur Biophys J Biophys* **30**, 588–604 (2002).
 43. Heisterkamp, A. *et al.* Pulse energy dependence of subcellular dissection by femtosecond laser pulses. *Opt Express* **13**, 3690–3696 (2005).
 44. Shen, N. *et al.* Ablation of cytoskeletal filaments and mitochondria in live cells using a femtosecond laser nanoscissor. *Mech Chem Biosyst* **2**, 17–25 (2005).
 45. Yanik, M. F. *et al.* Neurosurgery: functional regeneration after laser axotomy. *Nature* **432**, 822 (2004).
 46. Watanabe, W. *et al.* Femtosecond laser disruption of subcellular organelles in a living cell. *Opt Express* **12**, 4203–4213 (2004).

7.7 Supplemental Information

MSCs, transfected with a GFP-actin plasmid, were seeded on non-photodegradable PEG diacrylate (PEGDA) hydrogels to control for possible irradiation-induced retraction. When exposed to identical irradiation conditions as the degradable PEGdiPDA hydrogels ($E_{\text{pulse}} = 1.25$ nJ and $t_c = 1.58$ μs), PEGDA gels do not undergo erosion (data not shown) and control cells seeded on the surface remain attached and spread and do not exhibit retraction over similar elapsed times (**Figure 7.5**). These data suggest that, under these irradiation conditions, retraction

is not induced by laser exposure, but exclusively by the selective removal of cell-material interactions.

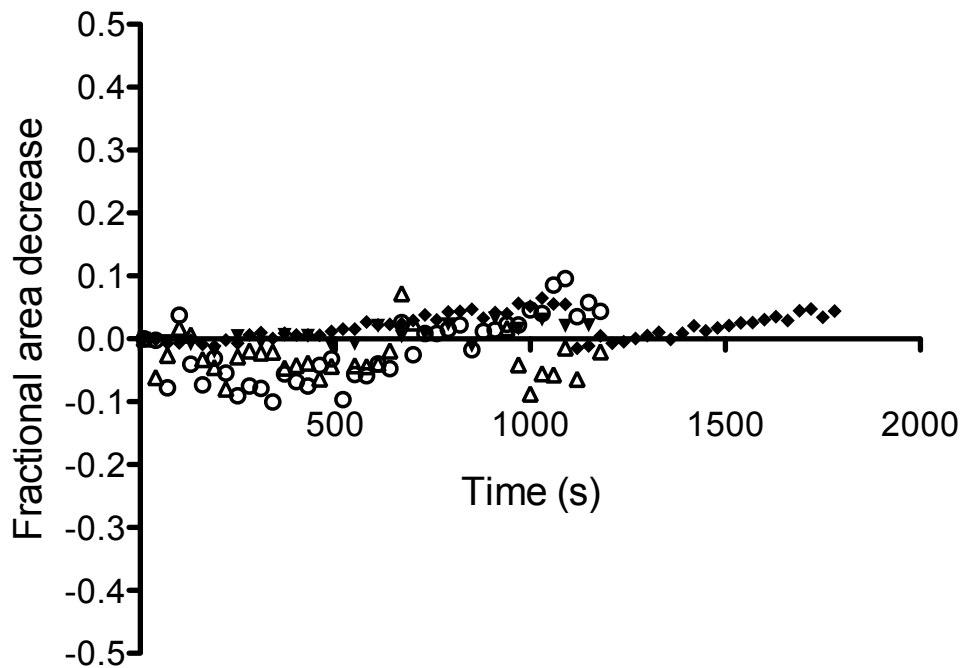


Figure 7.5 MSCs on non-photodegradable PEG hydrogels exhibit no retraction in response to light exposure. Here, we present the fractional decrease in cell area for each of the control cells studied ($n = 4$) and in each scenario there is no retraction observed. Instead, the cells undergo fluctuations in cell area as expected for cells actively sensing a substrate. The average maximum fractional area change ($\Delta A_{\max}/A_0$) was -0.02 ± 0.04 (mean \pm s.e.m.), which is not significantly different from zero, indicating random fluctuations in cell area and not a concerted retraction mechanism.

CHAPTER VIII

DYNAMIC SUBSTRATES TO PROBE MESENCHYMAL STEM CELL MECHANOTRANSDUCTION AND PLASTICITY

8.1 Introduction

Increasing evidence suggests that cells sense and respond to mechanical signals from the extracellular matrix (ECM). It is hypothesized that integrin-binding serves as the link between cells and the ECM, enabling the cells to integrate mechanical cues and convert them to biochemical signals that influence cell function – a process known as mechanotransduction.^{1,2} For example, cells cultured *in vitro* on substrates with varying elastic moduli have displayed marked differences in motility,³ cytoskeletal organization,⁴ and differentiation.⁵ Furthermore, cell function in diseased states has been shown to depend on substrate mechanics, as fibroblasts activate to myofibroblasts in stiffened wound-healing environments⁶ and cancer cell metastasis is related to cell and environment mechanics.⁷ While the importance of mechanotransduction as a regulator of cell function is clear, the mechanisms of how physical signals are interpreted by the cell and converted to biochemical outputs is not fully elucidated.

To study mechanotransduction in defined culture systems, researchers have developed an array of hydrogel systems that recapitulate tissue-like elasticities to investigate the physical influence on specific cell functions. Specifically, discrete polyacrylamide-based hydrogels of different moduli have been employed to study mechanically-driven process extension in neural

cells⁸ and differentiation in myotubes and mesenchymal stem cells.^{4,5} Similarly, discrete poly(ethylene glycol)-based gels have been utilized to investigate smooth muscle cell spreading, cytoskeletal organization, and phenotype.⁹ These discrete samples require a different precursor solution to be prepared for each sample, limiting the throughput of these studies. To circumvent this limitation, samples with gradients in mechanical properties have been developed using microfluidic or photolithographic techniques to generate a single sample with a range of elasticities.¹⁰⁻¹³ These materials have enabled investigations of mechanically induced fibroblast migration¹⁰ and vascular smooth muscle spreading.¹¹

While these studies in mechanobiology have provided a nascent understanding of the relationship between ECM mechanics and cell function, these analyses have been conducted on static substrates that fail to capture the dynamic nature of the *in vivo* ECM. Natively, the ECM is continually restructured by ECM-cleaving molecules, such as matrix metalloproteinases, and cellular deposition of ECM components, creating a dynamic landscape varying in adhesivity and elasticity.¹⁴ Cell processes, such as proliferation, migration, and differentiation, are also dynamic and cell decision-making is based on reciprocal interactions with this dynamic environment. To study mechanotransduction in this context, cytocompatible, photoresponsive hydrogels have been developed to investigate the cell response to dynamic changes in the mechanical properties of the extracellular matrix.¹⁵⁻¹⁸ These materials have begun to elucidate how mesenchymal stem cells differentiate on stiffening matrices^{18,19}, that fibroblast activation is dependent on substrate modulus,¹³ and that cells respond dynamically to changes in their adhesive environment.^{20,21}

Seminal studies have indicated that mesenchymal stem cells (MSCs) differentiate selectively based on the elasticity of the underlying substrate, specifically MSCs favored a

neurogenic lineage on very soft substrates ($E \sim 0.1 - 1$ kPa), a myogenic lineage on medium substrates ($E \sim 8 - 15$ kPa), and an osteogenic lineage on stiff substrates ($E \sim 25-40$ kPa).⁵ However, our understanding of mechanotransduction is still limited in that most studies have been conducted on static substrates that fail to recapitulate the dynamics of the *in vivo* environment. Recently, Burdick *et al.* reported a photoresponsive, stiffening hydrogel platform to investigate the differentiation of MSCs into adipogenic and osteogenic lineages in response to dynamic increases in the material elasticity.¹⁸ Here, we extend this work to investigate the myogenic and osteogenic differentiation of MSCs on softening hydrogels to investigate MSC plasticity and the underlying mechanisms that regulate MSC mechanotransduction.

Specifically, a photodegradable hydrogel culture platform is presented in which the elasticity can be softened from $E \sim 32$ kPa to $E \sim 7$ kPa in a controlled fashion and in real-time with light. Preliminary studies employed the material to investigate how *in situ* changes in substrate modulus influence mesenchymal stem cell differentiation. Specifically, a step change in substrate modulus from 32 kPa to 7 kPa was used to explore how cells preferentially differentiate toward given lineages and to probe if MSCs differentiation is plastic based solely on substrate mechanics – that is can MSCs change their differentiation state in response to mechanical cues. Moreover, this material should facilitate an improved understanding of how MSCs sense the mechanical environment and transform these signals into the biochemical activity that directs differentiation.

8.2 Materials and Methods

All reagents were purchased from Sigma-Aldrich except as otherwise noted.

8.2.1 Hydrogel preparation

A photodegradable crosslinker (PEGdiPDA) was synthesized as previously published.¹⁵ To fabricate photodegradable hydrogels, PEGdiPDA ($M_n \sim 4070$ g/mol, 8.2 wt%) was copolymerized with a monoacrylated PEG (PEGA, $M_n \sim 400$ g/mol, 6.8 wt%, Monomer-Polymer and Dajac Laboratories, Inc.) in PBS via redox initiated free-radical chain polymerization with 0.2 M ammonium persulfate and 0.1 M triethylmethylenediamine. The triethylmethylenediamine was added last to a mixture of the other precursor components in order to initiate the polymerization. The polymerization was complete in 5 minutes, based on storage modulus evolution quantified by rheometry. For rheometric experiments, the hydrogels were formed *in situ*. For cell culture experiments, 100 nM fibronectin was included in the precursor solution so that it would become entrapped within the gel network to present adhesive ligands to the cells. Then, 1 cm x 1 cm hydrogels were polymerized between two coverslips separated by a 250 μ m spacer. To immobilize the hydrogel to a solid support, one of the coverslips was acrylated to allow covalent attachment between the hydrogel and the coverslip. To functionalize the glass with acrylates, coverslips were first flame-treated to clean the surface and then immersed in a liquid deposition solution of (3-acryloxypropyl) trimethoxysilane, cleaned with ethanol, and heated to 80 °C for 15 minutes. After preparation gels were rinsed with PBS, which was refreshed twice in the first 24 hours.

8.2.2 Hydrogel film characterization with rheometry

The photodegradation of PEGdiPDA hydrogels was quantified *via* photorheometry ($\gamma = 10\%$, $\omega = 10$ rad/s for the linear viscoelastic regime, ARES, TA). Thin PEGdiPDA hydrogels were polymerized *in situ* between an 8 mm quartz plate and a temperature-controlled Peltier plate (25 °C). After complete polymerization, the sample was hydrated and then exposed to UV

light ($\lambda = 365 \text{ nm}$; $I_0 = 10 \text{ mW/cm}^2$) while the shear storage modulus (G') was monitored. The shear storage modulus was converted to Young's modulus (E), where $E = 2G(1+\nu)$, assuming a Poisson's ratio (ν) of 0.5.²²

8.2.3 Cell culture

Human mesenchymal stem cells (hMSCs) were isolated from human bone marrow aspirates (Lonza). Red blood cells were lysed per the manufacturer's instructions using an Ammonium Chloride Solution (Stem Cell Technologies). Remaining cells were plated on tissue culture polystyrene in growth media (low-glucose DMEM, 10% fetal bovine serum (FBS), 1 ng/ml recombinant human fibroblast growth factor-basic (FGF-2, Peprotech), 50 U/ml each penicillin/streptomycin, 1 mg/ml Fungizone antimycotic). hMSCs were isolated as the adherent cell population, and cells were cultured for no more than three passages. hMSCs were seeded on PEGdiPDA hydrogels in 6-well culture plates at 40,000 cells/cm² or 384,000 cells/well in growth media. Cell-gel constructs were culture at 37 °C and 5% CO₂.

8.2.4 Immunostaining for myogenic and osteogenic lineages

At desired time points, cell-gel constructs were fixed with 4% paraformaldehyde, permeabilized with 0.5 wt% Triton-X 100, blocked with 3 v% GS/1 wt% BSA, and incubated with rabbit anti-MyoD (Santa Cruz Biotechnology) or mouse anti-RunX2 (abcam). Samples were then washed and incubated with goat-anti-rabbit or goat-anti-mouse Alexa Fluor 594 (Invitrogen) to image the anti-MyoD or anti-RunX2 staining. Cell nuclei were counter-stained with DAPI, and the samples were imaged on an upright confocal microscope (Zeiss LSM 710 NLO) with 20x magnification objective. To quantify relative fluorescence, all samples from a

given experiment were stained and imaged at the same time using the same imaging protocol. A program was written in MATLAB (MathWorks®) using the Image Processing Toolbox to identify the nuclear regions of cells and average the intensity of the anti-MyoD or anti-RunX2 staining that was co-localized to the nucleus.

8.2.5 Statistics

All data are presented as mean \pm standard error of the mean. A Student's *t*-test was used to compare data sets.

8.3 Results and Discussion

8.3.1 Fabrication of photodegradable hydrogels with tunable mechanics *via* light

Mesenchymal stem cell (MSC) differentiation to myogenic or osteogenic lineages has been shown to be mechanosensitive, in that the differentiation state depends on the elasticity of the underlying substrate.⁵ It is important to understand the fundamentals of MSC mechanobiology and differentiation toward the development of regenerative medicine therapeutics, but also as a prototypical mechanosensitive biological system. To investigate the effect of substrate elasticity variation on MSC differentiation, we fabricated photodegradable hydrogels through the co-polymerization of PEGdiPDA^{15,20} with PEGA in PBS (**Figure 8.1a**). The modulus of thin PEGdiPDA hydrogels, which replicate the region of the gel probed by a cell, was quantified via *in situ* rheometry. The films were irradiated on the rheometer and the light-induced change in modulus was monitored (**Figure 8.1b**). Since the modulus is directly proportional to the density of elastically active network strands and the photocleavage of a PEGdiPDA molecule breaks an elastically active network strand, modulus decays with

increasing irradiation time. In this manner, irradiation can be used to tailor elasticity at the surface of PEGdiPDA films with light.

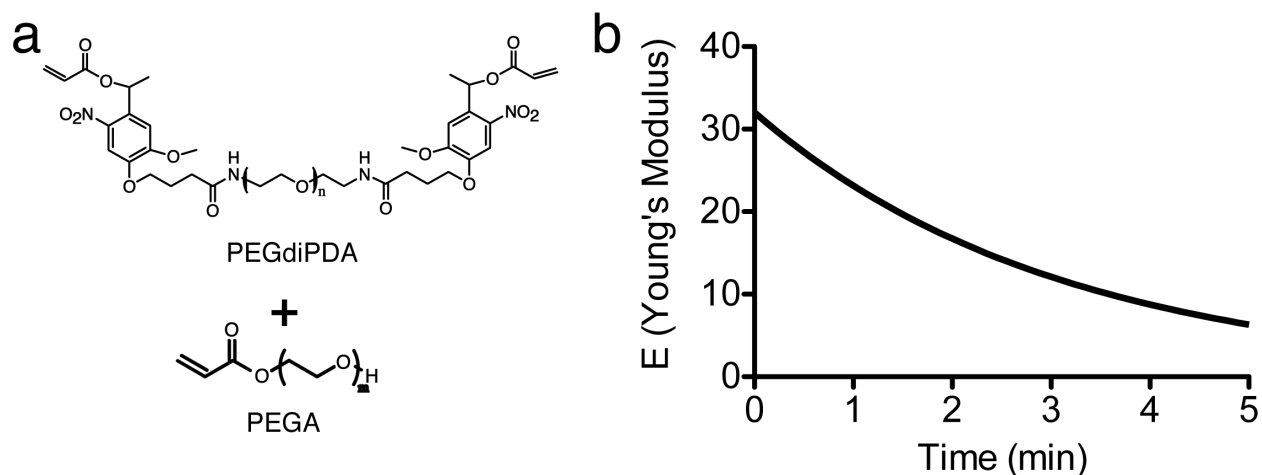


Figure 8.1 Fabrication of PEGdiPDA hydrogels with tunable elasticity. (a) Photodegradable hydrogels were fabricated *via* the co-polymerization of PEGdiPDA with PEGA under redox-initiated, free radical chain polymerization. (b) The initial elasticity of these samples was $E \sim 32$ kPa and irradiation ($\lambda = 365$ nm; $I_0 = 10$ mW/cm²) lead to a monotonic decrease in substrate elasticity. With 5 minutes of irradiation, samples with a softer elasticity, $E \sim 7$ kPa, were formed.

8.3.2 Dynamic moduli to direct MSC plasticity

To probe the mechanical plasticity of hMSCs – that is the ability of the cells to transdifferentiate based on physical cues alone – cultured on stiff substrates, PEGdiPDA hydrogels were prepared at $E \sim 32$ kPa to be softened *in situ* with light to soft substrates. Since stiff substrates favored osteogenic differentiation and soft substrates favored myogenic differentiation,⁵ it was hypothesized that hMSCs could be transdifferentiated from a pre-osteogenic lineage to a pre-myogenic lineage by softening the underlying culture substrate. Further, it was hypothesized that at some time during the differentiation process the cells would be committed to an osteogenic differentiation and would no longer respond to alterations in the elasticity of the culture substrate. To test this hypothesis, an experiment was designed where

hMSCs were seeded onto stiff PEGdiPDA hydrogels that were subsequently softened at different time points and the cells were cultured on these soft substrates prior to final differentiation analysis (**Figure 8.2**).

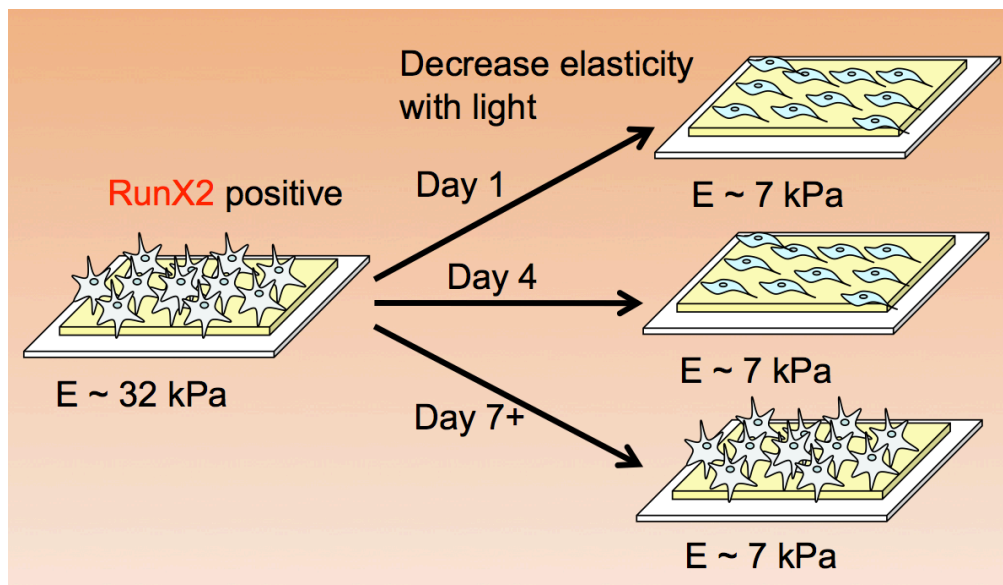


Figure 8.2 Experimental design for probing hMSC plasticity. Cells were seeded on stiff PEGdiPDA samples at Day 0, where they remain RunX2 positive. At Day 1, 4, or 7+, a subset of the gels was softened *in situ* with light to generate soft substrates. After another 3-14 Days in culture, cells were assayed for osteogenic or myogenic transcription factors and compared to Day 0 levels.

Specifically, we investigated cell-gel constructs that were softened after 1 day of culture on the stiff substrate and assessed differentiation preference 7, 10, and 14 days after softening (**Figure 8.3**). As hypothesized, the expression of the myogenic transcription factor, MyoD, was upregulated by day 7 after softening of the gel. Further, the expression of the osteogenic transcription factor, RunX2, was downregulated by day 14 after softening of the gel. These preliminary data suggest that hMSCs can respond plastically to dynamic changes in substrate elasticity.

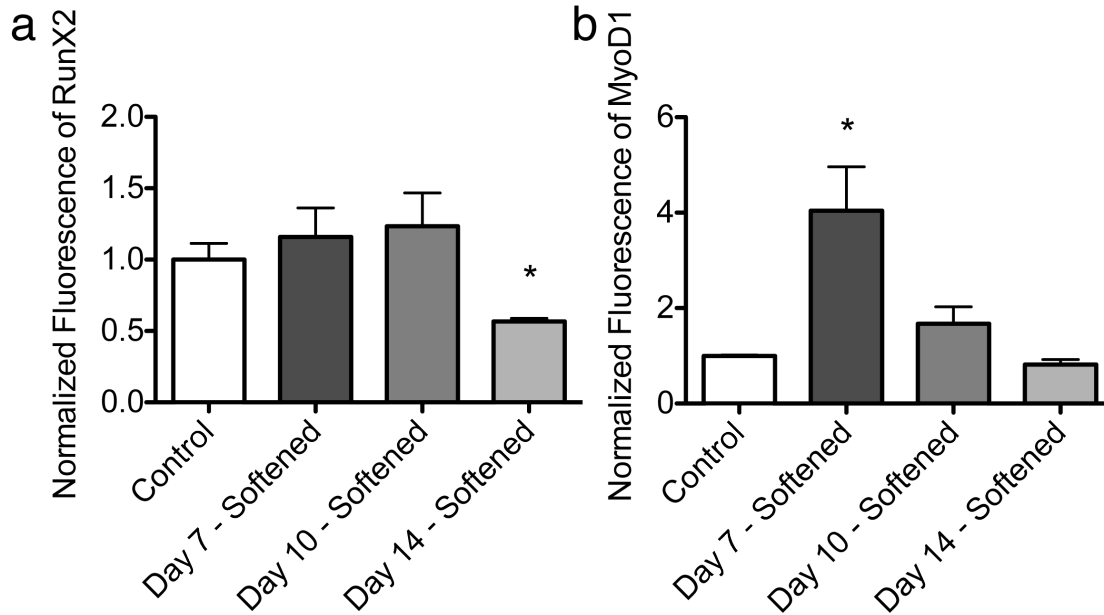


Figure 8.3 Dynamic elasticity changes induce a cell differentiation response. (a) hMSC expression of RunX2, an early osteogenic transcription factor, was monitored over the course of two weeks after stiff substrates were softened *in situ* to generate soft substrates. Nuclear co-localization of RunX2 was compared to control samples, cells on a stiff substrate at Day 1. By Day 14, the RunX2 expression was suppressed on soft substrates. **(b)** hMSC expression of MyoD1, an early myogenic transcription factor, was monitored over the course of two weeks after stiff substrates were softened *in situ* to generate soft substrates. Nuclear co-localization of MyoD1 was compared to control sample, cells on a stiff substrate at Day1. On Day 7, the MyoD1 expression was upregulated on soft substrates but returned to basal levels by Day 14. (* indicates significance, $p < 0.05$)

8.4 Current and future work

Ongoing work is focusing on the timescale over which hMSCs can be cultured on a stiff substrate and still transdifferentiate. Specifically, hMSCs are cultured on stiff substrates for 2-14 days and then the substrate is softened *in situ* and cultured for a subsequent 3-14 days to assess the transdifferentiation capability of the cells. To date, the analysis has relied on immunostaining of a single transcription factor for both myogenic (MyoD1) and osteogenic (RunX2) lineage. To corroborate these preliminary results, we are also analyzing RNA isolated from samples at the end time points to assess for a cadre of osteogenic and myogenic markers

(COL1A1, COL3A1, CBFA1, and SMAD4 for osteogenic markers and MYOD1, MYOG, CDH15 for myogenic markers).

In parallel, studies are being conducted to investigate the biochemical pathways through which the mechanical signals are converted into cellular differentiation. For instance, recent work has implicated the transcription factors YAP and TAZ as important in mechanotransduction pathways²³. and these pathways are being explored with respect to hMSC mechano-transdifferentiation. While phenomenological observations of cell differentiation in response to microenvironmental stiffness have been reported in the literature, very little is known about how mechanical signals influence cellular function at the transcription level. Such a molecular level understanding would be an important advancement for the field.

8.5 Conclusion

In sum, dynamically responsive, photodegradable hydrogels were fabricated to probe the mechanotransduction and differentiation of hMSCs. PEGdiPDA hydrogels were formed at a stiff ($E \sim 32$ kPa) elasticity, on which hMSCs preferentially expressed a marker for osteogenic differentiation. These same hydrogels were softened with light to generate soft substrates ($E \sim 7$ kPa), on which hMSCs preferentially expressed a marker for myogenic differentiation. Finally, the influence of dynamic changes in elasticity on hMSC differentiation was investigated by decreasing the modulus of the culture substrate *in situ* with light from stiff to soft. These studies suggest that hMSCs respond to dynamic changes in elasticity by trans-differentiating and future studies are elucidating the complete story and mechanism of this process.

8.6 References

1. Wang, N., Butler, J. & Ingber, D. Mechanotransduction Across the Cell-Surface and Through the Cytoskeleton. *Science* **260**, 1124–1127 (1993).
2. Chen, C. S. Mechanotransduction - a field pulling together? *J Cell Sci* **121**, 3285–3292 (2008).
3. Wong, J. Y., Velasco, A., Rajagopalan, P. & Pham, Q. Directed Movement of Vascular Smooth Muscle Cells on Gradient-Compliant Hydrogels. *Langmuir* **19**, 1908–1913 (2003).
4. Engler, A. J. *et al.* Myotubes differentiate optimally on substrates with tissue-like stiffness: pathological implications for soft or stiff microenvironments. *J Cell Biol* **166**, 877–887 (2004).
5. Engler, A. J., Sen, S., Sweeney, H. L. & Discher, D. E. Matrix elasticity directs stem cell lineage specification. *Cell* **126**, 677–689 (2006).
6. Hinz, B. *et al.* The myofibroblast - One function, multiple origins. *Am J Pathol* **170**, 1807–1816 (2007).
7. Swaminathan, V. *et al.* Mechanical Stiffness Grades Metastatic Potential in Patient Tumor Cells and in Cancer Cell Lines. *Cancer Res* **71**, 5075–5080 (2011).
8. Leach, J. B., Brown, X. Q., Jacot, J. G., Dimilla, P. A. & Wong, J. Y. Neurite outgrowth and branching of PC12 cells on very soft substrates sharply decreases below a threshold of substrate rigidity. *Journal of neural engineering* **4**, 26–34 (2007).
9. Peyton, S. R., Raub, C. B., Keschrurnus, V. P. & Putnam, A. J. The use of poly(ethylene glycol) hydrogels to investigate the impact of ECM chemistry and mechanics on smooth muscle cells. *Biomaterials* **27**, 4881–4893 (2006).
10. Lo, C. M., Wang, H. B., Dembo, M. & Wang, Y. L. Cell movement is guided by the rigidity of the substrate. *Biophys J* **79**, 144–152 (2000).
11. Zaari, N., Rajagopalan, P., Kim, S., Engler, A. & Wong, J. Photopolymerization in microfluidic gradient generators: Microscale control of substrate compliance to manipulate cell response. *Adv Mater* **16**, 2133 (2004).
12. Genzer, J. & Bhat, R. R. Surface-Bound Soft Matter Gradients. *Langmuir* **24**, 2294–2317 (2008).
13. Kloxin, A. M., Benton, J. A. & Anseth, K. S. In situ elasticity modulation with dynamic substrates to direct cell phenotype. *Biomaterials* **31**, 1–8 (2010).
14. Daley, W. P., Peters, S. B. & Larsen, M. Extracellular matrix dynamics in development and regenerative medicine. *J Cell Sci* **121**, 255–264 (2008).

15. Kloxin, A. M., Tibbitt, M. W. & Anseth, K. S. Synthesis of photodegradable hydrogels as dynamically tunable cell culture platforms. *Nat Protoc* **5**, 1867–1887 (2010).
16. Frey, M. T. & Wang, Y.-L. A photo-modulatable material for probing cellular responses to substrate rigidity. *Soft Matter* **5**, 1918–1924 (2009).
17. Khetan, S., Katz, J. S. & Burdick, J. A. Sequential crosslinking to control cellular spreading in 3-dimensional hydrogels. *Soft Matter* **5**, 1601–1606 (2009).
18. Guvendiren, M. & Burdick, J. A. Stiffening hydrogels to probe short- and long-term cellular responses to dynamic mechanics. *Nat Commun* **3**, – (2012).
19. Khetan, S. & Burdick, J. A. Patterning network structure to spatially control cellular remodeling and stem cell fate within 3-dimensional hydrogels. *Biomaterials* **31**, 8228–8234 (2010).
20. Kloxin, A. M., Kasko, A. M., Salinas, C. N. & Anseth, K. S. Photodegradable hydrogels for dynamic tuning of physical and chemical properties. *Science* **324**, 59–63 (2009).
21. Tibbitt, M. W., Kloxin, A. M., Dyamenahalli, K. U. & Anseth, K. S. Controlled two-photon photodegradation of PEG hydrogels to study and manipulate subcellular interactions on soft materials. *Soft Matter* **6**, 5100–5108 (2010).
22. Bryant, S. Photopolymerization of hydrogel scaffolds. *Scaffolding in Tissue Engineering* 1–21 (2006).
23. Dupont, S. *et al.* Role of YAP/TAZ in mechanotransduction. *Nature* **474**, 179–183 (2011).

CHAPTER IX

SYNTHESIS AND APPLICATION OF PHOTODEGRADABLE MICROSPHERES FOR SPATIOTEMPORAL CONTROL OF PROTEIN DELIVERY

As published in *Journal of Biomedical Materials Research - Part A*, **100A**, 1647-1654 (2012)

9.1 Abstract

Here, we present a photodegradable microparticle system that can be employed to entrap and deliver bioactive proteins to cells during culture. By using a photosensitive delivery system, experimenters can achieve a wide variety of spatiotemporally regulated release profiles with a single microparticle formulation, thereby enabling one to probe many questions as to how protein presentation can be manipulated to regulate cell function. Photodegradable microparticles were synthesized via inverse suspension polymerization with a mean diameter of 22 μm , and degradation was demonstrated upon exposure to several irradiation conditions. The protein-loaded depots were incorporated into cell cultures and release of bioactive protein was quantified during the photodegradation process. This phototriggered release allowed for the delivery of TGF- β 1 to stimulate PE25 cells and for the delivery of fluorescently labeled Annexin V to assay apoptotic 3T3 fibroblasts during culture. By incorporating these photoresponsive protein delivery depots into cell culture, new types of experiments are now possible to test hypotheses about how individual or multiple soluble factors might affect cell function when presented in a uniform, temporally varying, or gradient manner.

9.2 Introduction

Signaling proteins influence a myriad of critical cell functions, including differentiation, migration, and cell fate decisions, and many of these effects are pleiotropic depending on the dose and persistence of the signal.¹⁻⁴ Thus, spatiotemporal control over protein presentation is critical to study and understand the role that these biomacromolecules play in dynamic cellular processes. Toward this end, a prevalent method to protect, target, and locally deliver proteins and other therapeutics is to load such factors in polymeric microspheres.^{5,6} Such delivery vehicles enable the release of high doses of protein at specific locales, as well as controlled release over a desired time course.^{7,8}

Microsphere systems, typically formed from hydrolytically degradable polymers with pre-determined release profiles, have been used in numerous controlled release applications, including *in vitro* delivery of factors that influence the differentiation of embryoid bodies⁹ or *in vivo* delivery of osteogenic factors to encourage robust bone growth.¹⁰ Corresponding to the increase in the discovery of biological factors that direct stem cell differentiation, treat a range of diseases, and encourage proper tissue morphogenesis, there has been a focus on developing advanced materials that offer precise control over the delivery of such molecules. To date, full spatiotemporal control over the release and presentation of these factors during cell culture has been limited and few systems allow experimenters to direct release in real time. As a result of the lack of more sophisticated protein delivery vehicles, it has become increasingly difficult and time consuming to determine appropriate doses and release profiles of biomacromolecules for specific applications. Further, advanced understanding of wound healing and developmental processes underscore the importance of the proper presentation of multiple cues, including

proteins and co-factors or morphogen pairs, which is exceedingly difficult with current methods. Finally, few material systems allow the experimenter to introduce spatially heterogeneous gradients at any point in time that could be used to investigate how morphogens act during development and to fashion complex tissue structures *ex vivo*.

To circumvent these limitations and complement existing microsphere technologies, a unique delivery vehicle based on photolabile networks is presented that offers the experimenter control of entrapped biomolecule delivery in real time and in a manner that is compatible with 2D and 3D cell culture. Specifically, photodegradable, poly(ethylene glycol) (PEG) based hydrogel microspheres are fabricated that entrap and, subsequently, deliver proteins of interest on demand by exposure to selected wavelengths of light. Such delivery systems should prove beneficial for testing hypotheses related to how temporal and spatial protein presentation affects local cell function and have applied benefits for the controlled expansion and differentiation of stem cells.

The microsphere formulation includes PEGdiPDA (poly(ethylene glycol) di-photodegradable-acrylate)¹¹ to render photodegradable, protein-loaded microspheres, on account of the *o*-nitrobenzyl ether moieties in the PEGdiPDA structure. Nitrobenzyl ethers (NBEs) undergo an irreversible cleavage upon irradiation, causing the network to degrade in response to specific wavelengths of light (**Figure 9.1**). Similar macromers have been employed to form photoactive monolithic materials for applications ranging from cell culture¹²⁻¹⁵ to drug delivery.¹⁶⁻¹⁹ However, none of these approaches have combined microsphere processing techniques with the ability to deliver bioactive proteins to cells during culture with full spatiotemporal control.

The photodegradable microspheres described herein degrade upon single photon or multiphoton irradiation, which induces swelling and, ultimately, complete erosion and particle dissolution. During swelling, the entrapped protein diffuses into the surrounding environment and upon dissolution the total payload is released. In this system, the experimenter retains full control over the spatial and temporal presentation of the protein release by directing the irradiation. We demonstrate that biologically relevant proteins, namely TGF- β 1 and Annexin V, can be entrapped within the microspheres and released on demand to direct or detect cell function. In total, we describe an innovative method to generate pre-loaded depots of protein agents, which can be employed to release bioactive proteins in the presence of cells.

9.3 Materials and Methods

9.3.1 Microsphere preparation

Poly (ethylene glycol) di-photodegradable-acrylate (PEGdiPDA; $M_n \sim 4,070$ Da) was synthesized as previously described.^{11,12} Poly (ethylene glycol) tetrathiol (PEG4SH; $M_n \sim 5,000$ Da) was synthesized as previously described.²⁰ Photodegradable microparticles were prepared via inverse suspension polymerization, in which PEGdiPDA was copolymerized with PEG4SH via base-catalyzed Michael addition in an aqueous phase that was suspended in an organic phase. Briefly, the organic phase was comprised of 5 ml of hexane containing 150 mg of a 3:1 ratio by weight of sorbitan monooleate (Span 80, Sigma-Aldrich) and poly (ethylene glycol)-sorbitan monooleate (Tween 80, Sigma-Aldrich).²¹ The volume of the aqueous phase was 0.25 mL comprised of 300 mM triethanolamine (Sigma-Aldrich) at pH 8.0 with 6.2 wt % of PEGdiPDA, 3.8 wt % PEG4SH, and protein. Bovine serum albumin labeled with Alexa Fluor 488 or Alexa Fluor 594 (BSA-488 or BSA-594; Invitrogen) were entrapped at 0.8 mg/ml, TGF- β 1 (Peprotech)

was entrapped at 0.4 $\mu\text{g/ml}$, and the fluorescently labeled Annexin-V (Invitrogen) was entrapped at 20 v/v % Annexin-V conjugate solution. All of the components of the aqueous phase except for the PEG4SH solution were combined in a 1.7 ml microcentrifuge tube while the organic phase was added to a 20 ml scintillation vial with a stir bar. To initiate polymerization, the PEG4SH was added to the aqueous phase, which was subsequently vortexed for 10 s and quickly added to the organic phase. Mixing on a stir plate formed and maintained the inverse suspension between the two phases and the polymerization was allowed to proceed overnight.

Upon completion of the polymerization, the suspension was centrifuged (Eppendorf Centrifuge Model 5702) at 1000 rcf for 10 minutes and the supernatant was decanted. The microparticles were washed twice with hexanes and recovered with the same centrifugation conditions and once in 2-propanol and centrifuged at 2000 rcf for 10 minutes. The particles were then suspended in 1x PBS and washed three times by centrifuging (Eppendorf Centrifuge Model 5418) at 16,873 rcf for 15 minutes. The recovered particles were stored in PBS at 4°C and a portion was imaged on a low vacuum scanning electron microscope (LVSEM, JSM-6480LV).

9.3.2 Absorbance of PEGdiPDA

The molar absorptivity of the nitrobenzyl ether (NBE) moiety was calculated by measuring the absorbance of solutions of NBE in a water:DMSO (80:20 v/v) blend at concentrations of 110, 82.5, 55, and 27.5 μM . The absorbance was measured on a UV-visible spectrophotometer (NanoDrop Spectrophotometer ND-1000) for each solution and the molar absorptivity was calculated from these absorbance profiles.

9.3.3 Microsphere characterization with image analysis

Microparticles loaded with BSA-488 were used to characterize the size distribution of the particles. Particles were suspended in PBS and sealed between a glass slide and a cover slip in a rubber gasket, and imaged on an epifluorescent microscope (Nikon Eclipse TE2000-S). ImageJ (NIH) was used to threshold the images and the Analyze Particles plug-in was employed to determine the diameter of each microsphere. A total of 3130 particles were analyzed to determine the particle diameter distribution.

9.3.4 Degradation of microspheres

BSA-488 loaded microparticles were suspended in PBS in a sealed rubber gasket and exposed to 365 nm ($I_0 = 13.5 \pm 0.5$ mW/cm²; EXFO Omnicure 1000) or 400-500 nm ($I_0 = 20.0 \pm 0.5$ mW/cm²; EXFO Novacure) irradiation to induce degradation and erosion. To quantify the degradation induced changes in material properties, a time series of images was captured with an epifluorescent microscope. The images were analyzed with ImageJ by bounding each particle with a manually drawn circle to determine the particle diameter at each timepoint during irradiation. The diameters were used to calculate the ratio of the actual volume relative to the initial volume (V/V_0) as a function of time for each particle, and data for the respective irradiation condition was plotted as an average of three particles.

To demonstrate focused irradiation induced degradation and erosion, BSA-488 and BSA-594 loaded microparticles were suspended in PBS in a sealed rubber gasket and placed on the stage of an overhead confocal laser-scanning microscope (Zeiss 710 NLO LSM). Particles were exposed to 405 nm (single photon; $P = 1$ mW) or 740 nm (two-photon; $P = 100$ mW) irradiation to degrade and, ultimately, erode the particles. Degradation and erosion were monitored by direct imaging on the LSM.

9.3.5 Quantification of BSA-488 release

To quantify the release profile of entrapped BSA-488 from the particles, BSA-488 loaded microspheres were exposed to flood irradiation ($\lambda = 400\text{-}500\text{ nm}$; $I_0 = 20.0 \pm 0.5\text{ mW/cm}^2$) for 0 min to 15 min. Samples were collected at each time point and centrifuged to separate the soluble protein in the supernatant from intact particles in solution. The fluorescence of the supernatant was measured on a plate reader (BioTek Synergy H1 Hybrid Reader) to determine the relative amount of BSA-488 in the supernatant for each sample.

9.3.6 Diffusion in fibrin gels

Fibrin gels were formed by combining 50 μl of fibrin (20 mg/ml), 1 μl of thrombin (0.5 U/ml), and 150 μl PBS with BSA-488 and BSA-594 loaded particles (2 mg of particles/ml). The solution was allowed to gel at 37°C for 10 minutes in a sealed rubber gasket. The gels, with encapsulated particles, were imaged while the particles were degraded using an LSM (Zeiss 710 NLO LSM). Fluorescence intensity of the diffusing BSA-488 was quantified using the Image Processing Toolbox in MATLAB (MathWorks).

9.3.7 Cell culture

All cell culture reagents were purchased from Invitrogen except where otherwise noted. PE25 cells, a cell line that produces luciferase in response to TGF- β 1 exposure in a dose-dependent manner²² were cultured in low glucose DMEM supplemented with 10% FBS, 1% penicillin/streptomycin, and 0.2% fungizone. PE25 cells were passaged every 2-3 days and maintained at less than 80% confluency. Passage 4-6 PE25 cells were used for TGF- β 1

bioactivity assays. 3T3 fibroblasts were cultured in high glucose DMEM supplemented with 10% FBS, 1% penicillin/streptomycin, and 0.2% fungizone. 3T3 cells were passaged every 2-3 days and maintained at less than 70% confluency. P5 3T3 cells were used for the apoptosis assays.

9.3.8 TGF- β 1 delivery

For the TGF- β 1 bioactivity assays, PE25 cells were plated on 24-well culture plates at 80,000 cells/well and allowed to adhere overnight. The following day, media with soluble TGF- β 1 (2 ng/ml), media with TGF- β 1 loaded particles (10 mg of particles/ml of media, which equates to 4 ng/ml TGF- β 1 with complete release of the protein), media with blank particles (10 mg of protein-free particles/ml of media), and media were placed on the plated cells. Half of the wells were irradiated to degrade the particles ($\lambda = 365$ nm; $I_0 = 13.5 \pm 0.5$ mW/cm²) for 5 minutes to ensure complete erosion, while a duplicate set of conditions was not exposed to light. The solutions were left on the PE25 cells in an incubator for 16 hours. The following day, 200 μ l of Glo-Lysis Buffer (Promega) was added to each well to lyse the cells and release any luciferase that had been produced. After 15 minutes, 50 μ l of the lysis solution was combined with 50 μ l of luciferin substrate in triplicate. The solutions were immediately quantified for luminescence on a plate reader (BioTek Synergy H1 Hybrid Reader).

9.3.9 Fluorescently labeled Annexin V delivery

Particles were synthesized that were loaded with AlexaFluor-594 Annexin V (Invitrogen) at 5 μ l of Annexin V solution per 250 μ l of particle solution. 3T3 cells were plated on a 6-well plate at 100,000 cells/well and allowed to adhere overnight. The following day, half of the wells

were treated with (+)camptothecin (Sigma) at 10 μ M for 6 hours to induce apoptosis. After the treatment, the media was removed and substituted with 400 μ l of Annexin V binding buffer (10 mM HEPES, 140 mM NaCl, 2.5 mM CaCl₂ at a pH 7.4) containing soluble Annexin V (3 μ l per 400 μ l buffer) or Annexin V loaded particles (12.5 mg of particles/ml). A set of wells with Annexin V loaded particles was irradiated to release Annexin V ($\lambda = 365$ nm; $I_0 = 13.5 \pm 0.5$ mW/cm²) for 5 minutes. After 15 minutes, the samples were imaged on an LSM (Zeiss 710 LSM NLO).

9.4 Results and Discussion

9.4.1 Synthesis and characterization of microspheres

Photodegradable microparticles were fabricated by reacting PEGdiPDA ($M_n \sim 4,000$ Da) with poly(ethylene glycol) tetrathiol (PEG4SH; $M_n \sim 5,000$ Da) via base-catalyzed Michael addition in an inverse-phase, microsuspension polymerization (**Figure 9.1a**). The polymerization was carried out with the protein of interest included in the aqueous, macromer solution, which was suspended in an organic phase of hexanes with surfactants.²¹ This approach allowed the target protein to be entrapped within the particles upon gelation. Subsequently, the particles were purified via centrifugation, resulting in smooth, protein-loaded hydrogel microspheres (**Figure 9.1a**).

As a representative protein, fluorescently labeled bovine serum albumin (BSA-488) was incorporated into the macromer solution (**Figure 9.2a**) during polymerization and entrapped homogeneously within the microsphere network. BSA-488 loaded particles were employed to characterize the size distribution of the particles via image analysis ($n = 3130$ particles). The microspheres were synthesized with diameters on the order of 10 μ m or greater, and more than

80% of the particles had a diameter less than 50 μm (**Figure 9.2b**, inset). The distribution had a first moment (D_n) = 22 μm , a second moment (D_w) = 42 μm , and a polydispersity index (PDI) = 1.9 (**Figure 9.2b**). This size distribution is appropriate for the delivery of a substantial local dose of protein with rapid light-triggered degradation.

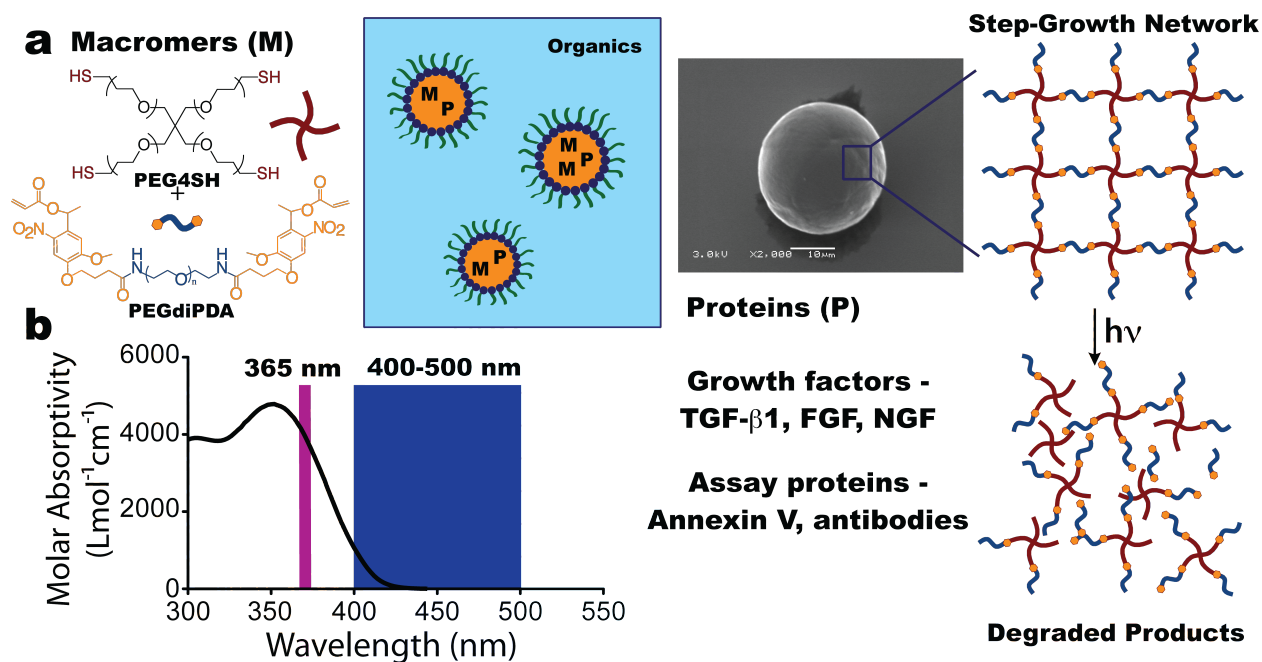


Figure 9.1 Photodegradable microparticle fabrication. (a) Photodegradable particles were synthesized by reacting PEG4SH with PEGdiPDA via base-catalyzed Michael addition in an inverse-phase, suspension polymerization. The aqueous phase, consisting of macromers, the base catalyst triethanolamine, and the target protein, was suspended in an organic phase of hexanes and stabilized by surfactants. Upon completion of the polymerization, the particles were purified via centrifugation resulting in spherical particles, as imaged by SEM. The reaction of the PEG4SH with the PEGdiPDA forms a step-growth network, and owing to the presence of nitrobenzyl ether (NBE) moieties in the PEGdiPDA, the network degrades in response to light. (b) The NBE moiety absorbs light strongly at 365 nm with a tail out past 405 nm. This allows both single photon irradiation at 365 nm or 400-500 nm to be used to degrade the particles, as well as two-photon irradiation using a wavelength of 740 nm.

9.4.2 Photodegradation of microspheres

Since the *o*-nitrobenzyl ether (NBE) moiety in the PEGdiPDA macromer is susceptible to cleavage with single photon or multiphoton excitation,^{23,24} a broad range of irradiation conditions can be used to erode the microspheres and release the entrapped payload on the order of

milliseconds to minutes. This process works as the NBE moieties in the PEGdiPDA structure introduce a photolabile linker into the network backbone of the microspheres. NBE moieties absorb light strongly in the UV (peak at 365 nm) with a tail that extends into the visible (**Figure 9.1b**) and may undergo an irreversible cleavage upon absorption of light at these wavelengths, as well as absorption of two-photon irradiation centered at 740 nm. When a NBE is cleaved, the corresponding bond in the particle backbone is also cleaved. This process, which will be referred to as degradation, induces swelling in the particle as bonds are cleaved in the microsphere and the crosslinking density is decreased. Eventually, when a sufficient fraction of the bonds have been cleaved, erosion (*i.e.*, mass loss) occurs and at these later stages of degradation, the microsphere is no longer a network, but soluble branched polymers that dissolve.

To demonstrate degradation and protein release in response to single photon irradiation, BSA-488 loaded microspheres were irradiated with collimated light ($\lambda = 365$ nm or 400-500 nm). Particles swelled initially, as bonds were cleaved throughout the network, as quantified by the increase in V/V_0 with irradiation time (**Figure 9.2c,d**). Ultimately, the microspheres eroded completely when a sufficient number of bonds in the network were cleaved ($p_c = 0.42$; the critical fraction of bonds that need to be cleaved to dissolve the network as determined by the Flory-Stockmayer equation) (**Figure 9.2c,d**). For 365 nm irradiation at an intensity of 13.5 ± 0.5 mW/cm², the microspheres swelled prior to eroding into solution over the course of 55 ± 5 s. Whereas 400-500 nm irradiation at an intensity of 20.0 ± 0.5 mW/cm² induced swelling and erosion over the course of 300 ± 30 s. The fractional release of entrapped BSA-488 from the microspheres followed the degradation-induced swelling profile at short times and for the first 30% of release, while the bulk of the payload was released after complete particle dissolution

(Figure 9.2e). In this manner, collimated irradiation provides the user with temporal control over protein release within a culture system.

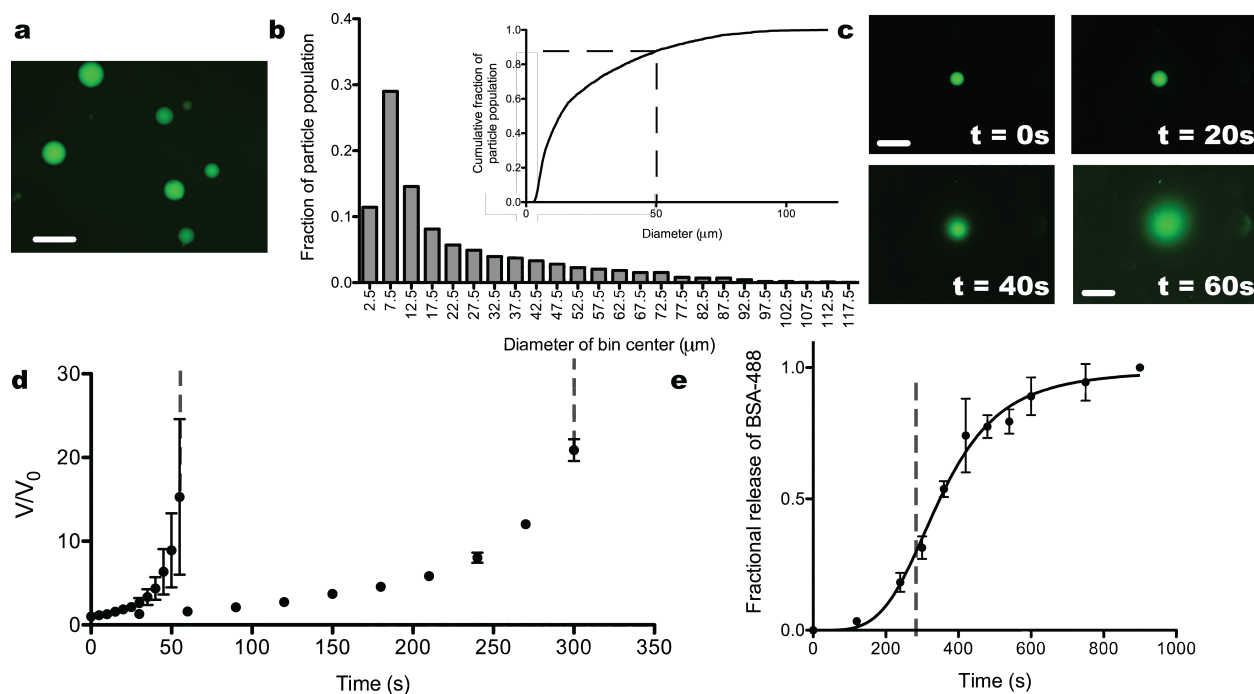


Figure 9.2 Size and degradation characteristics of photodegradable microparticles. (a) BSA-488 was entrapped within photodegradable microspheres. **(b)** Image analysis was used to quantify the size distribution of the particles synthesized by this method ($n = 3130$). The particles were formed with a number average diameter of $22 \mu\text{m}$ and a diameter average diameter of $42 \mu\text{m}$, which resulted in a polydispersity index of 1.9. Over 80% of the particles had a diameter less than $50 \mu\text{m}$. **(c)** Photodegradable particles swell and, ultimately, erode in response to flood irradiation ($\lambda = 365 \text{ nm}$; $I_0 = 13.5 \pm 0.5 \text{ mW/cm}^2$) over the time course of a minute. **(d)** The swelling was quantified with image analysis and plotted as normalized volume (V/V_0) as a function of irradiation time. Particles were exposed to 365 nm ($I_0 = 13.5 \pm 0.5 \text{ mW/cm}^2$; circles) and $400\text{-}500 \text{ nm}$ ($I_0 = 20.0 \pm 0.5 \text{ mW/cm}^2$; triangles) irradiation, and the particles eroded at $55 \pm 5 \text{ s}$ and $300 \pm 30 \text{ s}$ for the two conditions, respectively (indicated by the dashed gray lines). **(e)** The release of BSA-488 as a function of irradiation time was quantified as the particles swelled and dissolved. Prior to dissolution (indicated by the dashed gray line), BSA-488 began diffusing out as the particles swelled, and after dissolution the majority of the payload was released into solution. Scale bars, $100 \mu\text{m}$.

9.4.3 Selective release of proteins

Oftentimes the release of multiple factors within a single culture system is desirable, as cells respond *in vivo* to combinations of factors. For example, opposing gradients of

transcriptional repressors, Hunchback and Knirps, direct proper development in *Drosophila*.²⁵ Light responsive protein release affords the unique ability to deliver multiple factors selectively within a single system. To demonstrate this concept, photodegradable microspheres were loaded with BSA-594 (BSA labeled with Alexa Fluor 594) and combined with BSA-488 loaded particles. A mixture of BSA-488 and BSA-594 spheres were plated and imaged on a confocal LSM (**Figure 9.3a**). Focused irradiation ($\lambda = 405$ nm single photon or 740 nm multiphoton) was employed to erode individual particles in sequence to release each desired protein (**Figure 9.3a**). Initially, $t = t_1$, the focused irradiation ($\lambda = 740$ nm; $P = 100$ mW) was used to selectively erode a BSA-594 loaded microsphere. At a subsequent point in time, $t = t_2$, focused irradiation was employed to selective erode a microsphere containing a second entrapped protein, BSA-488. In this manner, different growth factors or cytokines could be delivered locally and in combination over short distances to specific locations during culture. This system should prove useful for studies aimed at the investigation of synergistic protein interactions or to elucidate how multiple and/or opposing gradients influence cell fate or function, such as chemotaxis or tissue morphogenesis.

9.4.4 Release of proteins in 3D culture platforms

Advanced three-dimensional culture platforms are increasingly employed for the study of cell biology and pathophysiology *ex vivo*.²⁶⁻²⁸ Accompanying these advances is the need for methods to deliver proteins within these platforms in sophisticated manners, systematically introducing cues that recapitulate aspects of the native extracellular environment. Photoresponsive, pre-loaded depots of proteins were encapsulated within fibrin hydrogels (**Figure 9.3b,c**) to demonstrate how this system might be used to deliver factors during 3D

culture. Focused irradiation ($\lambda = 405$ nm; $P = 1$ mW) from a confocal LSM was used to dissolve individual particles, allowing the entrapped payload to release and diffuse through the gel (9.9.3b). The released protein diffused, at a detectable level, ~ 50 μm radially from the edge of the particle (Figure 9.3c). As was demonstrated in 2D, multiple proteins were released selectively within a single hydrogel to motivate combinatorial studies in 3D (Figure 9.3d). In this manner, signaling proteins of interest can be delivered locally within a 3D cell culture scaffold. This light-controlled release and diffusion can be tailored to cell binding and uptake levels to influence cells and their function over reasonable length scales

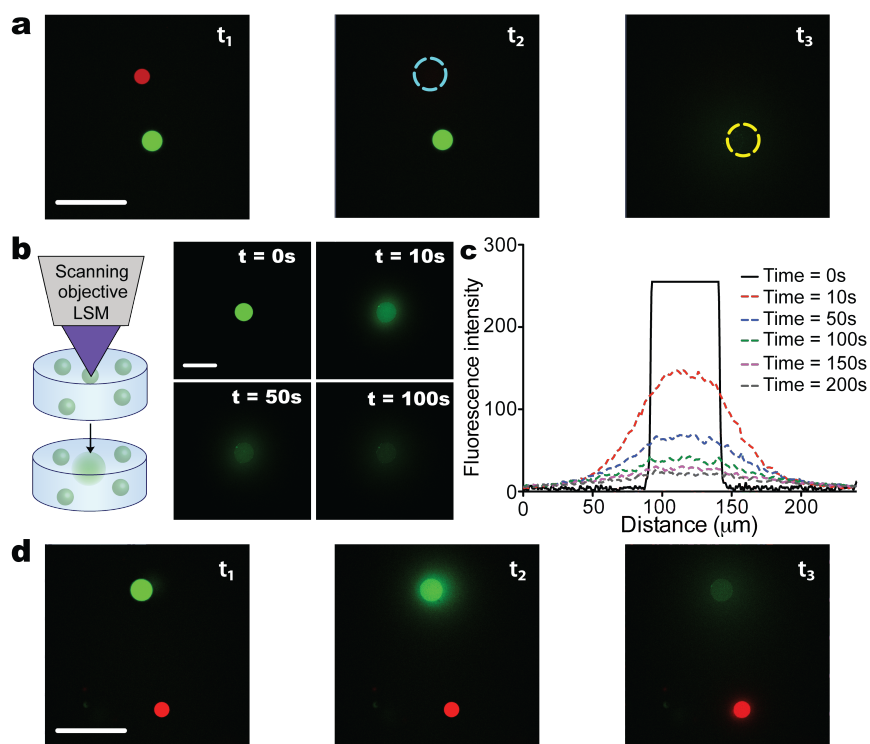


Figure 9.3 Spatially controlled degradation of photodegradable particles. (a) BSA-488 loaded microparticles were combined with BSA-594 loaded particles in a single system and focused irradiation from an LSM ($\lambda = 740$ nm; two-photon) was used to erode individual particles selectively. Here, a BSA-594 loaded particle was dissolved (t_1 to t_2) followed by the erosion of a BSA-488 loaded particle (t_2 to t_3) without disrupting neighboring particles. (b) Photodegradable particles can also be encapsulated within three-dimensional hydrogels and selectively photodegraded with focused light from an LSM ($\lambda = 405$ nm). Here, BSA-488 loaded particles were encapsulated within fibrin hydrogels and eroded with focused LSM irradiation after the image $t = 0$ s was taken. Images were captured after erosion to monitor diffusion of the

protein through the fibrin gel. **(c)** Profiles of the diffusing protein were quantified over the time course of imaging and demonstrate that the BSA-488 diffused radially at a detectable level to a distance of 50 μm from the edge of the original particle. **(d)** Multiple protein loaded particle populations were encapsulated within a single fibrin gel and individual particles were eroded selectively as was demonstrated in 2D. Scale bars, 100 μm .

9.4.5 Release of bioactive proteins to direct cell function

The microsphere formulation was designed to accommodate a broad range of proteins including growth factors, cytokines, antibodies, and extracellular matrix components. To demonstrate that bioactive proteins can be incorporated and released from the photodegradable particles in the presence of cells, we entrapped a common and potent growth factor, TGF- β 1,²⁹ within the microspheres. TGF- β 1 loaded particles, as well as blank particles, were delivered to plated PE25 cells, a reporter cell line that produces luciferase in response to TGF- β 1 exposure. The particles were dissolved with collimated irradiation ($\lambda = 365 \text{ nm}$, $I_0 = 13.5 \pm 0.5 \text{ mW/cm}^2$) for 5 minutes to release the TGF- β 1. PE25 cells that were exposed to TGF- β 1 loaded particles significantly up-regulated luciferase production as compared to blank particles and media control (**Figure 9.4a**). This demonstrates that the majority of the TGF- β 1 remains bioactive upon entrapment and subsequent release. Furthermore, viability, as measured by a membrane integrity assay, was greater than 90% for all conditions (data not shown) indicating that the irradiation conditions and microsphere degradation products do not adversely affect cell function.

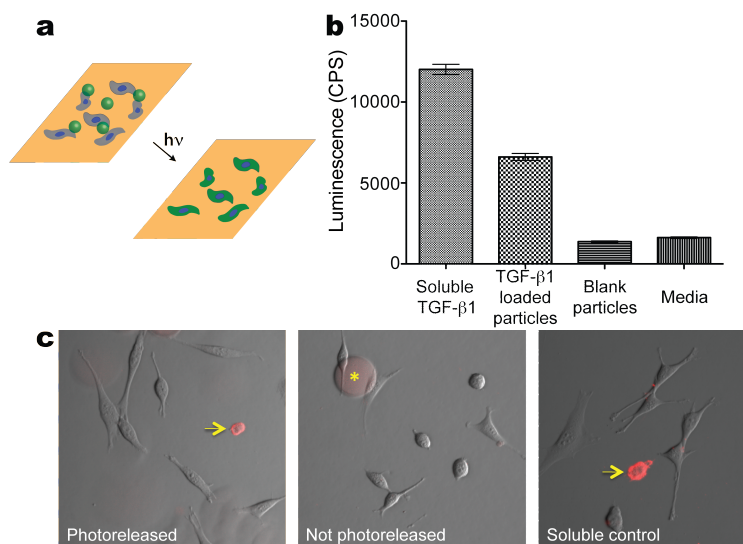


Figure 9.4 Release of bioactive proteins in the presence of cells. (a) Protein-loaded, photodegradable microparticles were incorporated into cell culture with plated cells. Collimated irradiation ($\lambda = 365 \text{ nm}$; $I_0 = 13.5 \pm 0.5 \text{ mW/cm}^2$) was used to release the entrapped protein to direct or detect cell function. (b) TGF- β 1 loaded particles were added to the media of plated PE25 cells, a TGF- β 1 responsive reporter cell line, and compared to conditions: media with blank particles, media with soluble TGF- β 1, and plain media. All samples were irradiated with the same dose used to erode particles and release the TGF- β 1, and the response of the PE25 cells was compared between each condition. The TGF- β 1 loaded particles had a significantly higher response than negative controls (blank particles and media alone), though not as strong a response as the positive control of soluble TGF- β 1. This demonstrates that a significant fraction of the TGF- β 1 remained bioactive upon entrapment and photorelease. (c) Fluorescently-labeled Annexin V loaded particles were added to the media on plated 3T3 cells. (+)Camptothecin was used to induce apoptosis and selected samples were irradiated to release the Annexin V. The samples were imaged to visualize cells labeled as apoptotic. Samples exposed to soluble Annexin V and photoreleased Annexin V stained positively for apoptosis (indicated by arrows at regions of red staining on the cell membranes), while there was no staining in the sample that was exposed to particles that were not photoreleased (particles are still visible in this image, denoted by the asterisk). Scale bar, 100 μm .

9.4.6 Release of bioactive proteins to assay cell function

A further difficulty of *in vitro* culture is assaying a specific cell's functions during culture, and this can be especially challenging when culturing cells in 3D. To illustrate how photodegradable microspheres can be employed as protein loaded depots for assaying cell function, fluorescently conjugated Annexin V was loaded into microspheres. Annexin V loaded

particles were delivered to plated NIH 3T3 fibroblasts, and the protein was photoreleased to identify apoptotic cells (**Figure 9.4c**). Camptothecin was dosed to the cells prior to release to increase the rate of apoptosis in culture. Annexin V staining on the membranes of apoptotic cells was observed in the samples with photoreleased Annexin V and soluble Annexin V, whereas no membrane staining was observed in the sample in which the microspheres were not irradiated. To circumvent the challenge of assaying cell function during 3D culture, protein-loaded microspheres could be included in cell encapsulations so that the assay protein of interest can be delivered at a later time during culture.

9.5 Conclusion

The synthesis of photodegradable, PEG-based microspheres was demonstrated and these microspheres were employed to entrap and release soluble proteins. Cytocompatible irradiation conditions were determined to dissolve the particles with light, and the corresponding release of the entrapped payload was quantified during the degradation and erosion process. Multiple factors were loaded into batches of microspheres and focused irradiation was used to degrade individual particles selectively to release specific proteins of interest. TGF- β 1 was loaded into the microspheres and was released with light to a reporter cell line to demonstrate that the entrapped and released protein remained bioactive. Similarly, Annexin V was loaded into particles to illustrate that protein-loaded depots could be incorporated into cell cultures to assay local cell function. By incorporating protein loaded, photoresponsive microspheres within cell aggregates, in media fed to plated cells, or in cell-laden scaffolds, the externally controlled and on-demand release of entrapped biological signals will allow experimenters to answer complex questions regarding the influence of sequential protein presentation on stem cell function or the

response of cells to local gradients of chemokines or cytokines.

9.6 References

1. Dekanty, A. & Milán, M. The interplay between morphogens and tissue growth. *Embo Rep* **12**, 1003–1010 (2011).
2. Leung, D. W., Cachianes, G., Kuang, W. J., Goeddel, D. V. & Ferrara, N. Vascular endothelial growth factor is a secreted angiogenic mitogen. *Science* **246**, 1306–1309 (1989).
3. Plouet, J., Schilling, J. & Gospodarowicz, D. Isolation and Characterization of a Newly Identified Endothelial-Cell Mitogen Produced by Att-20 Cells. *Embo J* **8**, 3801–3806 (1989).
4. Engler, A. J. *et al.* Embryonic cardiomyocytes beat best on a matrix with heart-like elasticity: scar-like rigidity inhibits beating. *J Cell Sci* **121**, 3794–3802 (2008).
5. Freiberg, S. & Zhu, X. X. Polymer microspheres for controlled drug release. *Int J Pharm* **282**, 1–18 (2004).
6. Peppas, N. A., Bures, P., Leobandung, W. & Ichikawa, H. Hydrogels in pharmaceutical formulations. *Eur J Pharm Biopharm* **50**, 27–46 (2000).
7. Timko, B. P. *et al.* Advances in Drug Delivery. *Annu Rev Mater Res* **41**, 1–20 (2011).
8. Berkland, C., King, M., Cox, A., Kim, K. & Pack, D. W. Precise control of PLG microsphere size provides enhanced control of drug release rate. *J Control Release* **82**, 137–147 (2002).
9. Carpenedo, R. L. *et al.* Homogeneous and organized differentiation within embryoid bodies induced by microsphere-mediated delivery of small molecules. *Biomaterials* **30**, 2507–2515 (2009).
10. Saito, N. *et al.* A biodegradable polymer as a cytokine delivery system for inducing bone formation. *Nat Biotechnol* **19**, 332–335 (2001).
11. Kloxin, A. M., Tibbitt, M. W. & Anseth, K. S. Synthesis of photodegradable hydrogels as dynamically tunable cell culture platforms. *Nat Protoc* **5**, 1867–1887 (2010).
12. Kloxin, A. M., Kasko, A. M., Salinas, C. N. & Anseth, K. S. Photodegradable hydrogels for dynamic tuning of physical and chemical properties. *Science* **324**, 59–63 (2009).
13. Kloxin, A. M., Tibbitt, M. W., Kasko, A. M., Fairbairn, J. A. & Anseth, K. S. Tunable

- Hydrogels for External Manipulation of Cellular Microenvironments through Controlled Photodegradation. *Adv Mater* **22**, 61–66 (2010).
14. Kloxin, A. M., Benton, J. A. & Anseth, K. S. In situ elasticity modulation with dynamic substrates to direct cell phenotype. *Biomaterials* **31**, 1–8 (2010).
 15. Tibbitt, M. W., Kloxin, A. M., Dyamenahalli, K. U. & Anseth, K. S. Controlled two-photon photodegradation of PEG hydrogels to study and manipulate subcellular interactions on soft materials. *Soft Matter* **6**, 5100–5108 (2010).
 16. Katz, J. S. *et al.* Modular synthesis of biodegradable diblock copolymers for designing functional polymersomes. *J Am Chem Soc* **132**, 3654–3655 (2010).
 17. Yesilyurt, V., Ramireddy, R. & Thayumanavan, S. Photoregulated release of noncovalent guests from dendritic amphiphilic nanocontainers. *Angew Chem Int Ed Engl* **50**, 3038–3042 (2011).
 18. Klinger, D. & Landfester, K. Photo-sensitive PMMA microgels: light-triggered swelling and degradation. *Soft Matter* **7**, 1426–1440 (2011).
 19. Peng, K. *et al.* Dextran based photodegradable hydrogels formed via a Michael addition. *Soft Matter* **7**, 4881–4887 (2011).
 20. Fairbanks, B. D., Singh, S. P., Bowman, C. N. & Anseth, K. S. Photodegradable, Photoadaptable Hydrogels via Radical-Mediated Disulfide Fragmentation Reaction. *Macromolecules* **44**, 2444–2450 (2011).
 21. Murthy, N. *et al.* A macromolecular delivery vehicle for protein-based vaccines: acid-degradable protein-loaded microgels. *P Natl Acad Sci Usa* **100**, 4995–5000 (2003).
 22. Clarke, D. C., Brown, M. L., Erickson, R. A., Shi, Y. & Liu, X. Transforming growth factor beta depletion is the primary determinant of Smad signaling kinetics. *Mol. Cell Biol.* **29**, 2443–2455 (2009).
 23. Zhao, Y. *et al.* New caged coumarin fluorophores with extraordinary uncaging cross sections suitable for biological imaging applications. *J Am Chem Soc* **126**, 4653–4663 (2004).
 24. Aujard, I. *et al.* o-Nitrobenzyl photolabile protecting groups with red-shifted absorption: Syntheses and uncaging cross-sections for one- and two-photon excitation. *Chem-Eur J* **12**, 6865–6879 (2006).
 25. Clyde, D. E. *et al.* A self-organizing system of repressor gradients establishes segmental complexity in *Drosophila*. *Nature* **426**, 849–853 (2003).
 26. Abbott, A. Cell culture: biology's new dimension. *Nature* **424**, 870–872 (2003).

27. Lutolf, M. P. & Hubbell, J. A. Synthetic biomaterials as instructive extracellular microenvironments for morphogenesis in tissue engineering. *Nat Biotechnol* **23**, 47–55 (2005).
28. Tibbitt, M. W. & Anseth, K. S. Hydrogels as Extracellular Matrix Mimics for 3D Cell Culture. *Biotechnol Bioeng* **103**, 655–663 (2009).
29. Shi, Y. & Massague, J. Mechanisms of TGF-beta signaling from cell membrane to the nucleus. *Cell* **113**, 685–700 (2003).

CHAPTER X

THREE-DIMENSIONAL CULTURE PLATFORMS FOR THE ENCAPSULATION AND RECOVERY OF MAMMALIAN CELLS

10.1 Introduction

Increasing evidence suggests that cells respond differently in two-dimensional (2D) and three-dimensional (3D) culture platforms, indicating that the context of the culture is relevant to the biological output.¹ As such, the assumption that culture templates serve as passive vehicles with which to study the relationship between cell function and gene expression is no longer valid. In fact, an abundance of evidence indicates that the spatially and temporally complex signaling domain presented by the cellular microenvironment directly influences cell behavior. Early work from the Bissell lab established that different functions can be observed from the same genotype solely due to interactions with the cellular microenvironment.² Specifically, they found that the dimensionality of culture directly influences the function and response to drugs in mammary epithelial cancer cells. Presumably, these differences in function arise as cells interact with 2D and 3D matrices very differently.

Cells on a 2D culture platform become polarized as a segment of the cell membrane interacts with the substrate or neighboring cells while the rest is exposed to the culture medium, generating inhomogenous interactions with soluble factors.³ Owing to this inherent polarization, integrin-binding and focal adhesion formation are confined to a region of the cell, which

ultimately influences mechanotransduction and intracellular signaling.⁴ Furthermore, this polarity confines the cell morphologies that can manifest, as generating complex three-dimensional tissue structures is prohibitively difficult in monolayer culture. Similarly, migration is limited to a plane and there is little to no resistance from a surrounding extracellular matrix in 2D culture, making phenomena such as cancer metastasis and tissue morphogenesis difficult to study in monolayer culture.^{5,6}

On account of these limitations of two-dimensional culture systems, recent research has focused on the development of defined, three-dimensional matrices that recapitulate critical aspects of the native extracellular matrix to study physiology, pathophysiology, and regenerative medicine *in vitro*.^{6,7} For example, Hubbell *et al.* have pioneered the use of peptide-functionalized, poly(ethylene glycol) (PEG) based hydrogels to encapsulate cells to study three-dimensional cell migration and neurite extension.^{8,9} Similar work from West *et al.* has employed PEG-based hydrogels to study angiogenesis in defined, three-dimensional culture.^{10,11} Increasing complexity has been built into these systems through the use of photochemical reactions to enable the addition and removal of biochemical and physical cues with full control in 3D space and time.¹²⁻¹⁵

Despite the significant advances in three-dimensional culture platforms for controlled investigations of cell biology *ex vivo*, there remain significant challenges in the downstream assaying of cell function as culture moves to the third dimension. For instance, immunostaining for proteins that indicate cell phenotype becomes increasingly challenging in 3D culture on account of diffusion limitations and increased non-specific binding. The imaging and assay of reporter cell lines becomes more difficult as light is scattered and attenuated in 3D platforms. Further difficulties arise in the isolation and purification of nucleic acids and proteins that are

used to determine cell function. Platforms that facilitate three-dimensional culture while enabling downstream processing and assaying of cell function will enable more complex biological studies in 3D culture systems.

To address this limitation, we present a unique, PEG-based hydrogel system that is formed *via* copper-free, click chemistry and enables cell encapsulation, culture, and subsequent recovery. The gel is functionalized so that it is degradable by both matrix metalloproteinases (MMPs) and light by the design of a linking peptide that contains an MMP labile sequence (GPQG↓IAGQ) and a photolabile moiety (*o*-nitrobenzyl ether). In this manner, cells can remodel the three-dimensional space by expressing surface-bound or secreted MMPs. Similarly, the user can alter the material through the controlled delivery of light that cleaves the *o*-nitrobenzyl ether group. By enabling the cells to remodel the material, this system facilitates cell migration, cell proliferation, and tissue morphogenesis over the course of days. Subsequently, the user-controlled handle can be used to erode regions of the material to recover cells for further analysis. We demonstrate that this process can be used to selectively isolate viable cells from a three-dimensional platform. This points toward the ability to employ this material to recover cells for nucleic acid or protein isolation for downstream analysis of cell populations cultured in defined, three-dimensional platforms.

10.2 Materials and Methods

All reagents were purchased from Sigma-Aldrich except as otherwise noted.

10.2.1 Synthesis of click-functionalized polymer precursors

Click-functionalized macromolecular precursors were first synthesized. An *o*-nitrobenzyl ether based azide (PLA) was synthesized as previously described.¹⁴ To synthesize the diazide-

functionalized photodegradable and MMP-degradable peptide, the peptide H-RRKGPQGIAGQGRK(dde)-NH₂ was synthesized via solid-phase peptide chemistry. 4-Azidobutanoic acid was then coupled to the N-terminus of the peptide and PLA was coupled to the ϵ -amino group of the C-terminal lysine after removal of Dde. The diazide peptide (MMPdiN₃) was cleaved and recovered in diethyl ether before being purified by reversed-phase high-performance liquid chromatography. A tetra-yne-functionalized PEG-based crosslinker (PEGtetra-yne) was synthesized by reacting dibenzylcyclooctyne-acid (Jena Biosciences) with a four-arm PEG tetraamine (M_n ~ 10,000 Da; JenKem). The PEGtetra-yne crosslinker was dialyzed and lyophilized prior to use. The adhesive peptides GRGDS and GYIGSR were synthesized via solid-phase peptide chemistry. 4-Azidobutanoic acid was coupled to the N-terminus of each peptide on-resin to azide functionalize these peptides. N₃-GRGDS and N₃-GYIGSR were cleaved from the resin, precipitated in ether, and reconstituted in PBS at 100 mM.

10.2.2 Hydrogel formation and photodegradation

Photodegradable, MMP-degradable hydrogels were formed by stoichiometrically reacting PEGtetra-yne with MMPdiN₃ in PBS or cell media at room temperature for 10 minutes at a total of 10 wt% macromolecular precursors. Gelation was monitored by polymerizing gels *in situ* on a rheometer (ARES, TA) to monitor shear storage modulus evolution as a function of time. Upon complete polymerization, gels were irradiated ($\lambda = 365 \text{ nm}$; $I_0 = 10 \text{ mW/cm}^2$) *in situ* on the rheometer to monitor shear storage modulus decrease as a function of photoinduced degradation time.

10.2.3 Cell culture

3T3 fibroblasts and human mesenchymal stem cells (hMSCs) were cultured in DMEM media with 10% FBS at 37°C with 5% CO₂. Neural progenitor cells were derived from mES embryoid bodies as previously described¹⁶ and cultured in AK media at 37°C with 5% CO₂. For cell encapsulation, 3T3s and hMSCs were encapsulated at 1 x 10⁶ cells/mL and motor neuron EBs were encapsulated at 500 EBs/mL.

10.3 Results and Discussion

PEG-based, MMP- and photo-degradable hydrogels were formed through the copolymerization of four-arm, dibenzylcyclooctyne (DBCO) -functionalized PEG (PEGtetra-*yne*) with a diazide MMP- and photo-labile peptide (MMPdiN₃) *via* strain-promoted azide-alkyne cycloaddition with a 1:1 stoichiometry at 10 wt% total macromolecule concentration to form a step polymerized hydrogel (**Figure 10.1**). The DBCO-azide reaction proceeds rapidly at room temperature in aqueous conditions without a catalyst and, thus, can be conducted in the presence of cells.¹⁷ Complete gelation occurred over the course of 10 minutes as determined by rheometric measurements of modulus evolution during polymerization with a final shear storage modulus, $G' = 1.7 \pm 0.2$ kPa (**Figure 10.2**). The use of the diazide peptide enables the incorporation of multiple degradation mechanisms into the hydrogel backbone. Namely, the GPQG↓IAGQ sequence allows the linking peptide to be degraded by cell-secreted MMPs^{18,19} (arrow indicated cleavage site), while the *o*-nitrobenzyl ether enables the linking peptide to be degraded by the experimenter with light (one-photon: $\lambda \sim 320$ -436 nm, two-photon: $\lambda \sim 740$ nm).

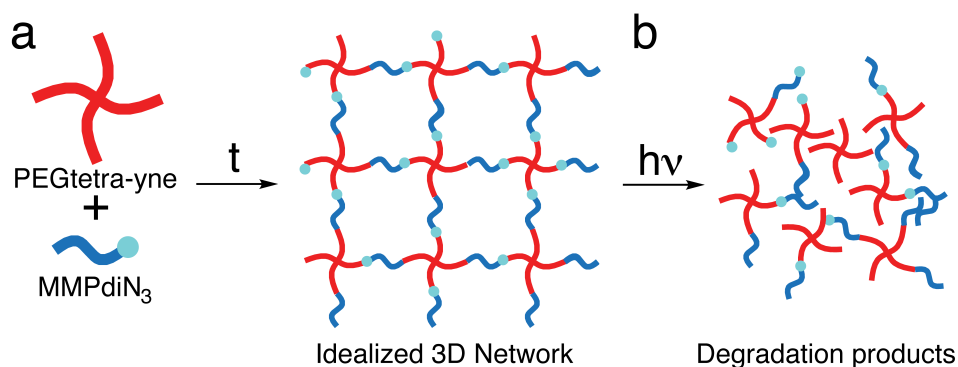


Figure 10.1. Formation of click-based hydrogels. (a) Photodegradable, MMP-degradable hydrogels were synthesized from the copolymerization of PEGtetra-yne and MMPdiN₃. (b) These gels were degraded with 365 nm light to fully erode the gel into soluble branched polymer chains, referred to as the degradation products.

Photodegradation of the click-based hydrogel was characterized *via* rheometry as the shear storage modulus (G') was monitored during exposure to UV light ($\lambda = 365$ nm; $I_0 = 10$ mW/cm²) over the irradiation time course. A monotonic decrease in G' is caused by breakage of elastically active network strands as *o*-nitrobenzyl ether moieties cleave in the backbone of the polymer network. The hydrogel can be formed and then fully eroded *via* irradiation, providing the user with full temporal control over hydrogel dissolution. Further, since light is used to erode the gel, photopatterning or focused light can be used to spatially control the gel erosion.

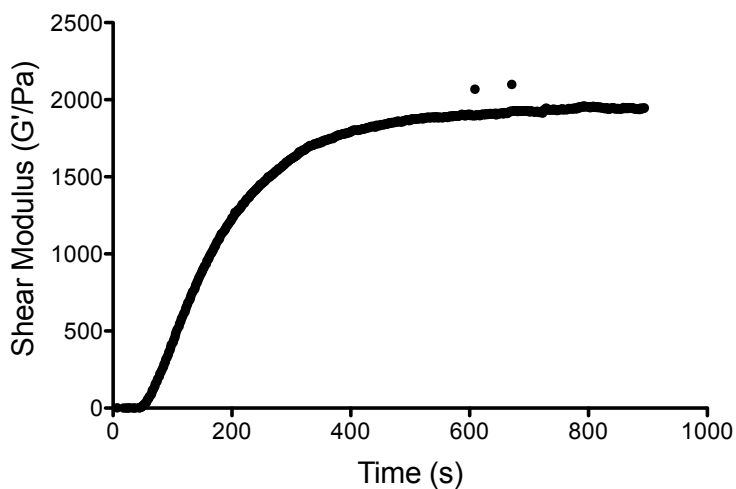


Figure 10.2 Polymerization of click-based hydrogels. Rheometric monitoring of the shear storage modulus (G') evolution during polymerization indicated that a gel is formed by combining the PEGtetra-yne and the MMPdiN₃ (10 wt% monomer reacted on stoichiometry) over the course of ~10 minutes with $G' = 1.7 \pm 0.2$ kPa. Should you give the specific formulation here? The time course should depend on concentration of functional group... and mention that it is ambient conditions?

To demonstrate that the bioorthogonal, click-based gel synthesis can be used for mammalian cell culture, NIH 3T3 fibroblasts were encapsulated at 1×10^6 cells/mL and remained viable after encapsulation (data not shown). To facilitate long term viability and cell function, integrin-binding peptide sequences (RGDS and YIGSR) were included into the gel formulation. RGD functionalized gels were used to encapsulate human mesenchymal stem cells (hMSCs), which have been shown to spread in MMP-degradable hydrogels.²⁰ Over the course of 24 hours, hMSCs spread within the gels (**Figure 10.3a**) and continued to spread, migrate, and proliferate during the time in culture. Similarly, neural precursor embryoid bodies were encapsulated in RGD and YIGSR functionalized gels. Over the course of 7 days, the EBs began extending axonal processes radially over 100s of microns from the embryoid body surface (**Figure 10.3b**). In each case, the ability to spread, migrate, proliferate, or extend processes was afforded by the MMP labile peptide linker, as cells encapsulated in control gels with a non-degradable linker did not manifest the same phenomena (data not shown).

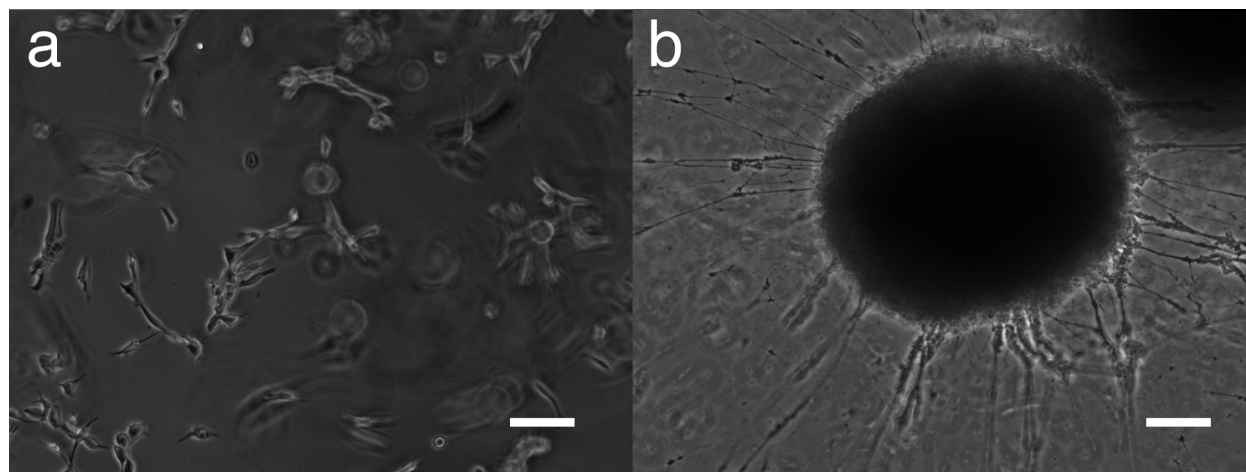


Figure 10.3 Cell culture in click-based hydrogels. (a) hMSCs (1×10^6 cells/mL) and (b) neural precursor embryoid bodies (500 EBs/mL) were encapsulated within the photodegradable, MMP-degradable hydrogels and spread after 24 h in the gel or extended axons during culture after 7 days in the gel, respectively. Scale bars, 50 μm

The inclusion of the *o*-nitrobenzyl ether moiety in the peptide linker provides the user with the additional handle of photodegradation to control material properties during culture. In this work, photodegradation was employed to rapidly erode the material to recover encapsulated cells for subsequent analysis. Taking advantage of the rapid degradation in this step polymerized gel, a 40 μL hydrogel was fully eroded in ~ 20 minutes with 365 nm light at an intensity of 10 mW/cm^2 , releasing the encapsulated cells back in to solution. The liberated cells were recovered, centrifuged, and re-seeded on TCPS plates to demonstrate the cytocompatibility of this process (**Figure 10.4**).

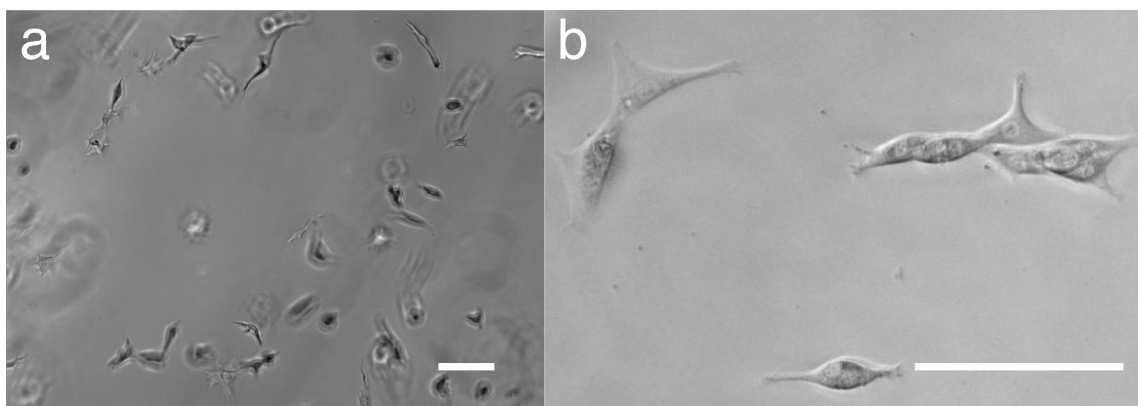


Figure 10.4 Cell recovery from click-based hydrogels. (a) hMSCs encapsulated within photodegradable, MMP-degradable hydrogels can be liberated from the gel with light ($\lambda = 365$ nm; $I_0 = 10 \text{ mW}/\text{cm}^2$). (b) 6 hours after liberation from the gel, hMSCs begin to spread on tissue-culture polystyrene, indicating viability and functionality after the recovery process. Scale bars, 50 μm

10.4 Current and future work

To demonstrate the full utility of this system, current work is focusing on the isolation and purification of proteins and nucleic acids from recovered cells to monitor the phenotype of

encapsulated cells. Traditionally, the assessment of cell function in three-dimensional culture systems is limited to whole mount immunostaining, which can be time consuming when the diffusion lengths are long, is difficult to quantify, and provides limited information. Current methods to recover protein and nucleic acids from 3D culture systems result in low-yields and impure samples, owing to contamination of the samples with material from the culture platform itself. Here, we recover viable cells free of polymer contaminants, as demonstrated above that can be used to isolate pure proteins or nucleic acids for analysis of cell function. Further, the ability to spatially define regions of the gel from which cells are to be liberated enables multiple time-point sampling.

Another convenient assay of cell populations in two-dimensional culture is fluorescent assisted cell sorting. While whole mount immunostaining attempts to enable similar assays in 3D, the throughput is low and staining is difficult. Here, we exploit the photodegradation of the click-based hydrogels to recover cells for subsequent fluorescent assisted cell sorting. In this manner, quantitative assays of the differentiation state of stem cell populations during three-dimensional culture treated with various factors can be assessed more facilely.

10.5 Conclusion

Photodegradable and MMP-degradable, PEG-based hydrogels were synthesized *via* strain-promoted azide-alkyne cycloaddition to encapsulate mammalian cells. These gels were formed by reacting a strained cyclooctyne-functionalized four-arm PEG (PEGtetra-yne) with a diazide MMP-degradable and photodegradable peptide linker (MMPdiN3). NIH 3T3 fibroblasts, human mesenchymal stem cells (hMSCs), and neural precursor embryoid bodies were encapsulated within the click-based hydrogels with high viability. On account of the MMP-

degradable peptide, hMSCs spread in RGD-functionalized gels and neural precursor embryoid bodies extended axonal processes in RGD- and YIGSR-functionalized gels. Since the gels were also photodegradable, light was employed to successfully liberate cells from the three-dimensional hydrogel and to recover them for subsequent culture. Uniquely, this recovery is achieved without the use of enzymes, *e.g.*, collagenase or MMPs, that can alter cell surface receptors and cell phenotype. This system is being employed to recover cells for phenotype analyses that are prohibitively difficult in three-dimensional culture.

10.6 References

1. Abbott, A. Cell culture: biology's new dimension. *Nature* **424**, 870–872 (2003).
2. Petersen, O. W., Rønnov-Jessen, L., Howlett, A. R. & Bissell, M. J. Interaction with basement membrane serves to rapidly distinguish growth and differentiation pattern of normal and malignant human breast epithelial cells. *P Natl Acad Sci Usa* **89**, 9064–9068 (1992).
3. Zhang, S., Zhao, X. & Spirio, L. PuraMatrix: Self-assembling peptide nanofiber scaffolds. *Scaffolding in tissue engineering* 217–238 (2005).
4. Gieni, R. S. & Hendzel, M. J. Mechanotransduction from the ECM to the genome: Are the pieces now in place? *J Cell Biochem* **104**, 1964–1987 (2008).
5. Cushing, M. C. & Anseth, K. S. Hydrogel cell cultures. *Science* **316**, 1133–1134 (2007).
6. Tibbitt, M. W. & Anseth, K. S. Hydrogels as Extracellular Matrix Mimics for 3D Cell Culture. *Biotechnol Bioeng* **103**, 655–663 (2009).
7. Lutolf, M. P. & Hubbell, J. A. Synthetic biomaterials as instructive extracellular microenvironments for morphogenesis in tissue engineering. *Nat Biotechnol* **23**, 47–55 (2005).
8. Raeber, G. P., Lutolf, M. P. & Hubbell, J. A. Mechanisms of 3-D migration and matrix remodeling of fibroblasts within artificial ECMs. *Acta Biomater* **3**, 615–629 (2007).
9. Schense, J., Bloch, J., Aebischer, P. & Hubbell, J. Enzymatic incorporation of bioactive peptides into fibrin matrices enhances neurite extension. *Nat Biotechnol* **18**, 415–419 (2000).

10. Saik, J. E., Gould, D. J., Keswani, A. H., Dickinson, M. E. & West, J. L. Biomimetic hydrogels with immobilized ephrinA1 for therapeutic angiogenesis. *Biomacromolecules* **12**, 2715–2722 (2011).
11. Leslie-Barbick, J. E., Saik, J. E., Gould, D. J., Dickinson, M. E. & West, J. L. The promotion of microvasculature formation in poly(ethylene glycol) diacrylate hydrogels by an immobilized VEGF-mimetic peptide. *Biomaterials* **32**, 5782–5789 (2011).
12. Kloxin, A. M., Kasko, A. M., Salinas, C. N. & Anseth, K. S. Photodegradable hydrogels for dynamic tuning of physical and chemical properties. *Science* **324**, 59–63 (2009).
13. Tibbitt, M. W., Kloxin, A. M., Dyamenahalli, K. U. & Anseth, K. S. Controlled two-photon photodegradation of PEG hydrogels to study and manipulate subcellular interactions on soft materials. *Soft Matter* **6**, 5100–5108 (2010).
14. Deforest, C. A. & Anseth, K. S. Cytocompatible click-based hydrogels with dynamically tunable properties through orthogonal photoconjugation and photocleavage reactions. *Nat Chem* **3**, 925–931 (2011).
15. Deforest, C. A. & Anseth, K. S. Photoreversible Patterning of Biomolecules within Click-Based Hydrogels. *Angew Chem Int Ed Engl* **51**, 1816–1819 (2012).
16. Peljto, M. & Wichterle, H. Programming embryonic stem cells to neuronal subtypes. *Curr Opin Neurobiol* **21**, 43–51 (2011).
17. Gordon, C. G. *et al.* Reactivity of Biarylazacyclooctynones in Copper-Free Click Chemistry. *J Am Chem Soc* **134**, 9199–9208 (2012).
18. Fairbanks, B. D. *et al.* A Versatile Synthetic Extracellular Matrix Mimic via Thiol-Norbornene Photopolymerization. *Adv Mater* **21**, 5005–5010 (2009).
19. Patterson, J. & Hubbell, J. A. Enhanced proteolytic degradation of molecularly engineered PEG hydrogels in response to MMP-1 and MMP-2. *Biomaterials* **31**, 7836–7845 (2010).
20. Anderson, S. B., Lin, C.-C., Kuntzler, D. V. & Anseth, K. S. The performance of human mesenchymal stem cells encapsulated in cell-degradable polymer-peptide hydrogels. *Biomaterials* **32**, 3564–3574 (2011).

CHAPTER XI

MICROFLUIDIC DEVICES FOR THE SELECTIVE CAPTURE AND RELEASE OF MAMMALIAN CELLS WITH PHOTODEGRADABLE HYDROGELS

11.1 Introduction

Microfluidic devices with affinity labels enable unique opportunities for the capture and sorting of mammalian cells from complex aqueous solutions, such as culture medium or whole blood, with minimal preprocessing.¹ For example, antibody-functionalized microfluidic devices have been employed to capture EpCAM-expressing cancer cells spiked into whole blood² and CD4⁺ T-cells from HIV+ subjects.³ A traditional limitation of microfluidic devices is that they can only process nanoliter to microliter scale volumes; however, recent work from Toner *et al.* has demonstrated that adjustments to device geometry enable the processing of milliliters of whole blood to capture exceptionally rare circulating tumor cells (CTCs).^{2,4,5} Further improvements on the geometry of antibody-functionalized microfluidic capture devices have facilitated clinical applications in cancer diagnostics through the capture of CTCs directly from patient blood.^{6,7} Despite these advances, capture devices are still limited in the ability to analyze and process captured cells downstream. Current methods to confirm the identity of captured cells are confined to on-chip labeling, *e.g.*, FISH or immunocytochemistry, owing to the inability to remove desired cells from the capture surface. Developing materials that enable selective

capture and release of individual cells to allow genome-wide analysis of single cells, *in vitro* culture, and *in vivo* testing will enable a better understanding of rare cell populations such as circulating tumor cells and certain stem cell populations, as well as better point-of-care diagnostics.

Initial work to recover cells from capture surfaces has focused on the use of chemical or mechanical dislocation. In these examples, chemical gradients or shear forces were employed to disrupt cell-material interactions and to elute captured cells.^{8,9} However, strong chemical treatment and shear forces are known to damage cells or at a minimum rapidly alter gene expression, limiting the application of these techniques.¹⁰ More recent studies have focused on the fabrication of microfluidic capture devices with phase changing materials, through the application of temperature,¹¹ ions,¹² or enzymes,¹⁰ that enable the disruption of cell-material interactions and subsequent recovery of captured cells. Specifically, Murthy *et al.* employed sacrificial alginate layers to capture endothelial progenitor cells from blood that could be released through the treatment and dissolution of the alginate capture layer with Ca^{2+} ions.¹² This treatment is limited in that it cannot be conducted in the presence of calcium chelating ligands, *e.g.*, EDTA and citrates, and calcium treatment can alter cell signaling on short time scales.^{10,13}

The use of alginate layers has been extended by Toner *et al.* to enable capture of cancer cells and their subsequent release with alginate lysase.¹⁰ While this method is cytocompatible and enables highly efficient recovery of captured cells, it is still limited in that the whole capture surface becomes disrupted with the application of the enzyme and the experimenter is unable to recover selected cells as the whole population of captured cells is released. Captured cell populations are often heterogeneous, for example circulating tumor cells from a given tumor can

have different genotypes and rare stem cells can exist in asymmetric states. Therefore, individual cell release and recovery are desired to better analyze the cells that are captured with these devices and to characterize fully rare cell populations. This ability requires spatial control over cell release from the capture surface, which is possible with light-based release mechanisms.

Here, we present the fabrication of microfluidic capture devices with antibody-functionalized, thin film, photodegradable hydrogels as the capture surface. Photolabile, poly(ethylene glycol) (PEGdiPDA) based hydrogels are polymerized within microfluidic chambers using visible wavelength photoinitiation, which allows for longwave UV light induced gel erosion with both spatial and temporal precision. Acrylated-NeutrAvidin is included in the hydrogel formulation to facilitate subsequent functionalization with a variety of biotinylated antibodies, for example anti-EpCAM. Mammalian cells are selectively captured on the surface of antibody-functionalized gels within the microfluidic devices and subsequently released with cytocompatible, UV light exposure. This platform offers the unique ability to capture and selectively release mammalian cells toward the individual culture and analysis of circulating tumor cells and isolation of rare stem cells.

11.2 Materials and Methods

All reagents were purchased from Sigma Aldrich except as otherwise noted.

11.2.1 Hydrogel precursor synthesis

Poly(ethylene glycol) diphotodegradable acrylate (PEGdiPDA) was synthesized as previously described.¹⁴ Lithium phenyl-2,4,6-trimethylbenzoylphosphinate (LAP) was synthesized as previously described.¹⁵ Acrylated NeutrAvidin was synthesized based on a

previously published acrylation procedure.¹⁶ Briefly, NeutrAvidin (Life Technologies) was acrylated by reacting the NeutrAvidin (2 mg/mL) with 3400 Da Acryl-PEG-NHS (Laysan Bio) at a 1:40 molar ratio, respectively, in 50 mM sodium bicarbonate buffer, pH 8.4. The reaction proceeded for 4 h at room temperature under constant rocking. Unreacted Acryl-PEG-NHS was removed by passing the solution through a Zeba Spin Desalting Column (7K MWCO; Thermo Scientific), and the solution was lyophilized to recover acrylated-NeutrAvidin (AcryINA). AcryINA was resuspended at 10 mg/mL in PBS after lyophilization.

11.2.2 PEGdiPDA hydrogel fabrication

Stock solutions of PEGdiPDA (20 wt% in PBS), poly(ethylene glycol) monoacrylate (PEGA, $M_n \sim 400$ Da; 40 wt% in PBS; Monomer-Polymer and Dajac Labs), LAP (8 wt % in PBS), and AcryINA (10mg/mL in PBS) were prepared. The gel forming monomer solution (13.2 wt% monomer) was formulated with PEGdiPDA (8.2 wt%), PEGA (5 wt%), LAP (3 wt%), and AcryINA (0.9 mg/mL), and the solution was mixed with a vortex. PEGdiPDA hydrogels were photopolymerized using collimated visible light ($\lambda = 400\text{-}500$ nm; $I_0 \sim 20$ mW/cm²; EFOS Novacure with liquid light guide and collimating lens). The gels were polymerized for 2 min to minimize cleavage of the *o*-nitrobenzyl ether groups in the PEGdiPDA at the photoinitiating wavelengths.

11.2.3 Hydrogel fabrication in microfluidic devices

Clean glass slides were functionalized with an acrylated silane to enable covalent attachment between the PEGdiPDA hydrogel and the glass surface. To acrylate the glass slides, they were submerged in a mixture of 30 mL ethanol (95% in DIH₂O), acetic acid (enough to

lower the solution pH to 4.5-5.5), and 170 μL (3-Acryloxypropyl)trimethoxy silane (APTS). Poly(dimethylsiloxane) (PDMS) channels were placed on top of the cleaned glass slides, and the location of the channel was marked to allow for future alignment of microfluidic channels over the formed gels. The microfluidic channel was then filled with the APTS solution, which was allowed to react with the glass for ~ 3 min. The APTS solution was then flushed out of the channel, the glass slide was rinsed in ethanol (95% in DIH_2O); and the prepared slides were placed in an oven (80°C) for ~ 15 min. Fresh microfluidic channels were placed over the silanized region of the glass slide, filled with the PEGdiPDA gel precursor solution ($\sim 10\ \mu\text{L}$), and quickly placed under the collimated visible light to polymerize the gel for 2 min. The microfluidic channels were removed, and PEGdiPDA gels attached to glass slides were immersed in PBS overnight prior to use.

11.2.4 Fabrication of multifaceted PEGdiPDA hydrogels

Multifaceted gels were created as described above, except that the AcryINA was replaced with BSA-Alexa Fluor 488 (BSA-488) or BSA-Alexa Fluor 594 (BSA-594), final concentration of 0.45 mg/mL. Dual-inlet microfluidic channels were placed over silanized glass slides with each inlet reserved for either the BSA-488 or the BSA-594 PEGdiPDA gel precursor solutions. The channels were filled with a glycerol solution (40 v% in DIH_2O). Once the channel was completely filled with the glycerol solution, the two labeled PEGdiPDA precursor solutions were loaded into the device through the microfluidic channel. After the channel was filled with the two solutions, the gel was polymerized for 2 min; the microfluidic channel was removed; and the gels were immersed in PBS overnight prior to imaging. Multifaceted PEGdiPDA films were imaged on an upright confocal laser scanning microscope (Zeiss LSM 710 NLO).

11.2.5 PEGdiPDA hydrogel functionalization

PEGdiPDA gels were formed as described above with varying concentrations of AcrylNA (0 mg/mL to 0.9 mg/mL). Circular gaskets (~ 0.5 mm in height) with a diameter of ~ 1 cm were used to form the gels. The gels were rinsed in PBS for 1 h and then blocked in a 3% BSA solution in PBS for 1 h. After blocking, the gels were exposed to a biotinylated fluorescein (Life Technologies) for 1 h. Gels were then rinsed with PBS overnight to remove any unreacted biotinylated fluorescein. The gels were imaged with an upright confocal laser scanning microscope (Zeiss LSM 710 NLO) to monitor the fluorescein intensity, which was quantified with ImageJ (NIH). For cell capture experiments, PEGdiPDA gels with 0.9 mg/mL AcrylNA were functionalized with a biotinylated anti-EpCAM antibody (R&D Systems BAF960, 20 $\mu\text{g/mL}$ in 1% BSA) to capture EpCAM expressing cells.

11.2.6 Cell culture, capture, and release

PC3 prostate cancer (ATCC) cells were cultured in F-12K medium with 10% FBS at 37°C and 5% CO₂. Static cell capture experiments were conducted by seeding PC3 cells on anti-EpCAM functionalized and blank PEGdiPDA gels. For the flow capture experiments, PBS spiked with PC3s (1×10^6 cells/mL) was flowed (2 $\mu\text{L/min}$) through a microfluidic channel over an anti-EpCAM functionalized PEGdiPDA thin film. After the cells were flowed over the PEGdiPDA gel, the device was rinsed with 10x volumes of PBS (20 $\mu\text{L/min}$). For release, cell capture devices were placed on an inverted epifluorescent microscope (Nikon TE 2000), and regions of the gel were exposed to UV light using the DAPI filter cube ($\lambda \sim 350\text{-}370$ nm) under flow (1 $\mu\text{L/min}$). The devices were imaged during light exposure to monitor degradation-

induced cell release.

11.3 Results and Discussion

11.3.1 Photopolymerization of PEGdiPDA films

A photolabile, macromolecular monomer, poly(ethylene glycol) diphotodegradable acrylate (PEGdiPDA)^{14,17} was employed to fabricate photopolymerized, photodegradable hydrogels (**Figure 11.1a**). Lithium phenyl-2,4,6-trimethylbenzoylphosphinate (LAP)[CITE Fairbanks Biomaterials] enabled visible light ($\lambda = 400\text{-}500$ nm; $I_0 = 20$ mW/cm²) initiation of polymerization with minimal cleavage of the photolabile *o*-nitrobenzyl ether (NBE) moieties (**Figure 11.1b**) owing to the differences in quantum yield and molar absorptivity between LAP and NBE.^{15,18} Complete polymerization as assessed by *in situ* rheometry ($G' = 8200 \pm 200$ Pa) occurred in ~ 2 min, during which time the concentration of photolabile NBE moieties remained at $\sim 90\%$ of its initial concentration.¹⁸ Upon photopolymerization with LAP, PEGdiPDA hydrogels were still able to degrade completely, as demonstrated by monitoring the shear modulus decrease during continued irradiation with visible light (**Figure 11.1c**; $\lambda = 400\text{-}500$ nm). Similarly, UV light exposure from an inverted epifluorescent microscope ($\lambda = 350\text{-}370$ nm; Nikon TE2000 FS) rapidly eroded regions of the PEGdiPDA films (**Figure 11.4b**).

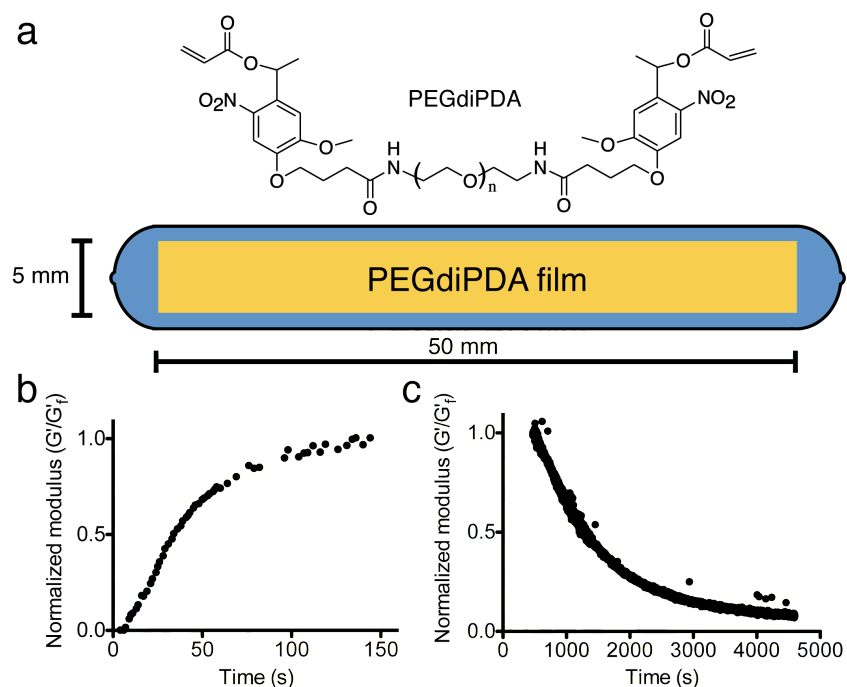


Figure 11.1 Photopolymerization of PEGdiPDA hydrogels for microfluidic capture devices. (a) PEGdiPDA-based, photodegradable hydrogels were photopolymerized using the visible light photoinitiator LAP within microfluidic channels to develop selective capture and release devices. (b) PEGdiPDA hydrogels (13.2 wt% monomer; 3 wt% LAP) were photopolymerized with 2 min of visible light exposure ($\lambda = 400\text{-}500\text{ nm}$; $I_0 = 20\text{ mW/cm}^2$) resulting in a final shear modulus $G' = 8200 \pm 200\text{ Pa}$. (c) After complete polymerization, continued exposure of PEGdiPDA gels to light exposure ($\lambda = 400\text{-}500\text{ nm}$; $I_0 = 20\text{ mW/cm}^2$) completely degraded the film over the course of an hour, demonstrated by the monotonic decrease in the normalized shear modulus.

11.3.2 Functionalizing gels with biotinylated molecules

Reactive NeutrAvidin groups were covalently incorporated into PEGdiPDA hydrogel films to facilitate subsequent functionalization with biotinylated molecules. Acrylated-NeutrAvidin (AcryINA) was included in the hydrogel precursor solution so that the pendant acrylate group would react with growing kinetic chains during network formation. To monitor the incorporation of AcryINA into PEGdiPDA films, films with a range of AcryINA concentrations in the precursor solution were exposed to a biotinylated probe (Biotin-fluorescein; Life Technologies). Confocal microscopy confirmed that the biotinylated fluorophore reacted with and became bound to AcryINA functionalized gels in a dose-dependent manner (**Figure**

11.2a). The level of incorporation of AcrylNA into the precursor solution can control the degree of functionalization, but high-affinity capture devices (10 mg/mL AcrylNA) were used for the cell capture experiments. For static cell culture experiments, PEGdiPDA gels were functionalized with biotinylated anti-EpCAM. These experiments confirmed the bioavailability of functional molecules incorporated into the gels, as EpCAM expressing cancer cells adhered to anti-EpCAM functionalized gels and not to control, blank gels (**Figure 11.2b**).

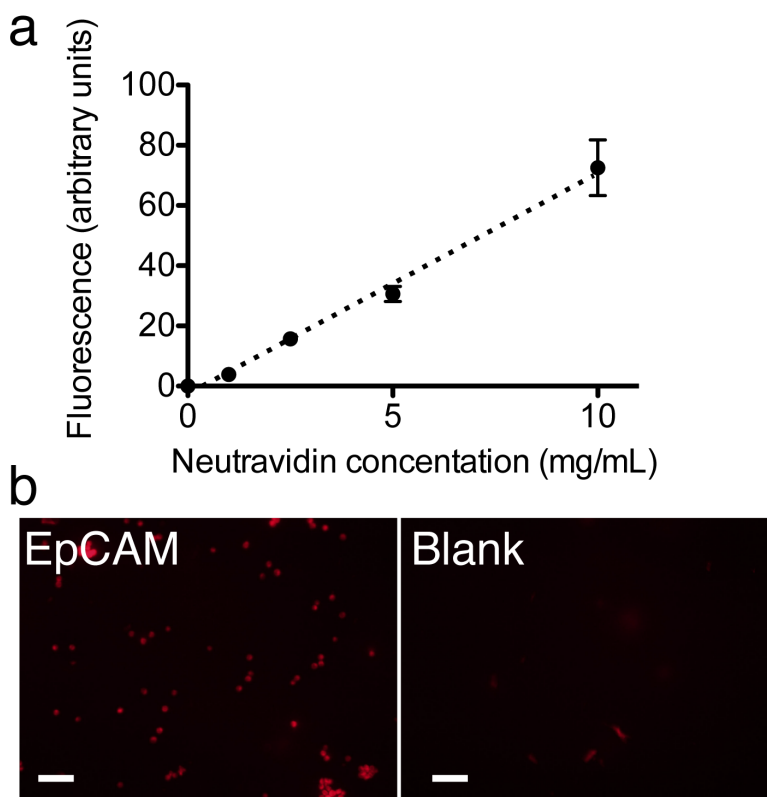


Figure 11.2 Functionalization of PEGdiPDA hydrogel films. (a) Acrylated-NeutrAvidin (AcrylNA) was incorporated into PEGdiPDA hydrogels at a range of concentrations (0 to 0.9 mg/mL). Biotinylated-fluorescein was coupled to the available AcrylNA in the gels, and the incorporation of NeutrAvidin led to a dose-dependent increase in biotin binding. This demonstrates that a range of concentrations in surface functionality can be presented using AcrylNA into PEGdiPDA hydrogels. (b) PEGdiPDA hydrogels were also functionalized with a cell capture antibody (biotinylated anti-EpCAM), and EpCAM expressing cancer cells (1×10^6 cells/mL) were only captured on anti-EpCAM functionalized gels in static capture experiments. Scale bars, 100 μ m.

11.3.3 Multifaceted capture devices

Current microfluidic capture devices have demonstrated the efficient capture of single cell subtypes;^{2,3,6,10} however, it would be beneficial to capture multiple cell populations within a single device and recover them sequentially for cell purification or increased capture throughput. Multifaceted PEGdiPDA hydrogels were fabricated to demonstrate that the use of photopolymerization within microfluidic devices enables the facile generation of multifaceted devices. Two precursor solutions (PEGdiPDA with BSA-488 and PEGdiPDA with BSA-594) were drawn into a two-inlet microfluidic device to create side-by-side PEGdiPDA gels (**Figure 11.3**). There was minimal mixing ($\sim 100 \mu\text{m}$) at the interface of the two solutions during the polymerization time, resulting in a clearly defined interface. In principle, this technique can be extended to fabricate multifaceted surfaces with increased numbers of unique capture surfaces by designing microfluidic devices with more inlets, and employing this same technique.

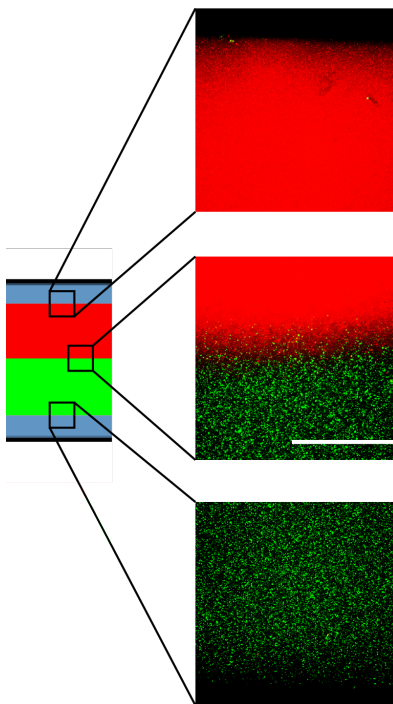


Figure 11.3 Multifaceted capture devices. Dual-layer PEGdiPDA hydrogels were photopolymerized into the microfluidic channels functionalized with BSA-488 (green) and BSA-594 (red), demonstrating the ability to present multiple, disparate surfaces to a cell suspension during flow. In this manner, the ability to spatially capture separate populations of cells from a

single cell suspension could be realized. Scale bar, 400 μm .

11.3.4 Flow capture and release of cells

EpCAM-expressing prostate cancer cells (PC3) were captured by and released from anti-EpCAM functionalized PEGdiPDA gels in a continuous-flow microfluidic capture device. PC3 cells were captured on hydrogel surfaces within the device under flow (2 $\mu\text{L}/\text{min}$) and remained attached after rinsing the device with PBS (20 $\mu\text{L}/\text{min}$). UV light was focused through the 20x objective of an inverted epifluorescent microscope ($\lambda = 350\text{-}370\text{ nm}$; Nikon TE2000) to erode a selective region of the gel under flow and release captured PC3 cells (**Figure 11.4a**). During release under flow, captured cells began to detach from the gel as it was photodegraded; captured cells (**Figure 11.4a-i**) first detached from the capture surface (**Figure 11.4a-ii**), then rolled slowly along the surface (**Figure 11.4a-iii**), and finally became entrained in the flow path and were removed from the device (**Figure 11.4a-iv**). All cells in the region of UV light induced degradation released from the gel over the course of 30 seconds, while cells remained adhered to regions of the gel that were not photodegraded (**Figure 11.4b**).

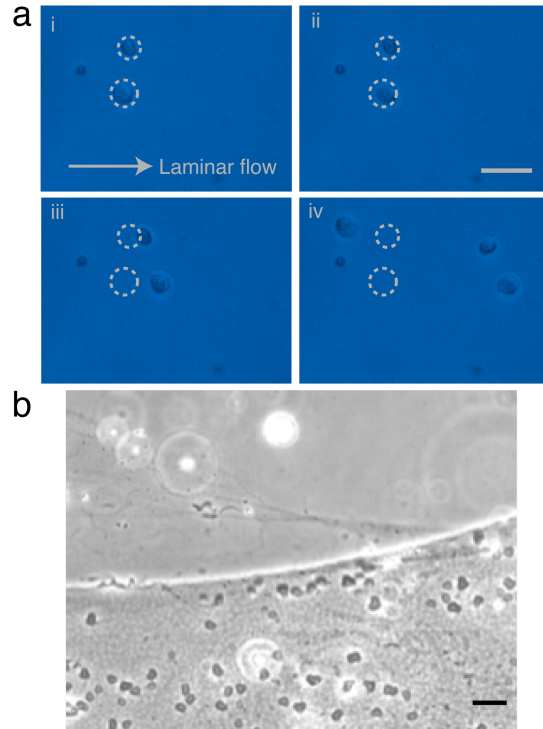


Figure 11.4 Cell capture and release with PEGdiPDA microfluidic devices. (a) PC3 prostate cancer cells, which express EpCAM, were captured with anti-EpCAM functionalized PEGdiPDA hydrogels under continuous flow (i). UV light ($\lambda = 350\text{-}370\text{ nm}$) was employed to degrade the thin film selectively under specific cells to release them from the capture surface. Cells initially began to release from the capture location (ii), then began to roll away in the direction of continuous flow (iii), and finally became entrained in the flow for full release (iv). (b) PC3 cells were completely released in regions of degradation, curved feature on the top of the picture, but remained attached to the non-degraded regions of the film. Scale bars, $60\ \mu\text{m}$.

11.3.5 Current studies and future directions

This work has illustrated the utility of PEGdiPDA hydrogels for the capture and subsequent release of mammalian cells within microfluidic capture devices. Current work is focusing on the use of the multifaceted hydrogel films to capture multiple cell subtypes in single flow experiments and to demonstrate the ability to release and recover single cells. To employ these devices in clinically relevant settings, it is necessary to form capture surface with more efficient geometries, such as the herringbone topography.¹⁹ Preliminary studies have shown that this geometry is amenable to the techniques in this paper (data not shown), but they have not

been tested to capture rare cells from whole blood. Future work will apply PEGdiPDA herringbone devices to capture and recover rare cells from whole blood to demonstrate ability of these materials to perform in the presence of more complex biological fluids, which is important to test the clinical relevance of these devices. The culture of released cells will also be conducted to analyze the captured cells more fully downstream from the capture device. Specifically, the culture of individual circulating tumor cells would enable unprecedented experiments to be conducted on a relatively characterized population of cells. Capture and release of individual circulating tumor cells would enable clonal expansion for *in vitro* analysis, such as single cell genomics, and *in vivo* assessment of tumorigenicity.

11.4 Conclusion

A photodegradable hydrogel based microfluidic capture device was presented that enabled the unique ability to selectively capture and release mammalian cells under continuous flow. Acrylated-NeutrAvidin was included in the gel precursor solution to covalently link this reactive handle into the gel. The PEGdiPDA films were functionalized with biotinylated molecules, *e.g.*, fluorescein and anti-EpCAM antibody, to quantify the degree of functionalization and to capture EpCAM expressing PC3 prostate cancer cells. Multifaceted films were fabricated pointing toward the ability to capture multiple cell subtypes within a single microfluidic device. Finally, PC3 cells were captured on hydrogel surfaces within the microfluidic device under continuous flow and subsequently released with UV light exposure. PEGdiPDA offer unique abilities in the development of microfluidic devices for cell sorting and diagnostics, in that cells can be captured and individually released for downstream culture and analysis.

11.5 References

1. Evanko, D. Microfluidics and a garden hose. *Nat Meth* **5**, 124–124 (2008).
2. Nagrath, S. *et al.* Isolation of rare circulating tumour cells in cancer patients by microchip technology. *Nature* **450**, 1235–1239 (2007).
3. Cheng, X. *et al.* A microfluidic device for practical label-free CD4(+) T cell counting of HIV-infected subjects. *Lab Chip* **7**, 170–178 (2007).
4. Cristofanilli, M. *et al.* Circulating tumor cells, disease progression, and survival in metastatic breast cancer. *New Engl J Med* **351**, 781–791 (2004).
5. Braun, S. & Marth, C. Circulating tumor cells in metastatic breast cancer--toward individualized treatment? *N. Engl. J. Med.* **351**, 824–826 (2004).
6. Stott, S. L. *et al.* Isolation and characterization of circulating tumor cells from patients with localized and metastatic prostate cancer. *Sci Transl Med* **2**, 25ra23 (2010).
7. Maheswaran, S. *et al.* Detection of mutations in EGFR in circulating lung-cancer cells. *N. Engl. J. Med.* **359**, 366–377 (2008).
8. Pappas, D. & Wang, K. Cellular separations: a review of new challenges in analytical chemistry. *Anal. Chim. Acta* **601**, 26–35 (2007).
9. Wang, K., Marshall, M. K., Garza, G. & Pappas, D. Open-tubular capillary cell affinity chromatography: single and tandem blood cell separation. *Anal. Chem.* **80**, 2118–2124 (2008).
10. Shah, A. M. *et al.* Biopolymer system for cell recovery from microfluidic cell capture devices. *Anal. Chem.* **84**, 3682–3688 (2012).
11. Cooperstein, M. A. & Canavan, H. E. Biological cell detachment from poly(N-isopropyl acrylamide) and its applications. *Langmuir* **26**, 7695–7707 (2010).
12. Hatch, A., Hansmann, G. & Murthy, S. K. Engineered alginate hydrogels for effective microfluidic capture and release of endothelial progenitor cells from whole blood. *Langmuir* **27**, 4257–4264 (2011).
13. Machaca, K. Ca(2+) signaling, genes and the cell cycle. *Cell Calcium* **48**, 243–250 (2010).
14. Kloxin, A. M., Tibbitt, M. W. & Anseth, K. S. Synthesis of photodegradable hydrogels as dynamically tunable cell culture platforms. *Nat Protoc* **5**, 1867–1887 (2010).

15. Fairbanks, B. D., Schwartz, M. P., Bowman, C. N. & Anseth, K. S. Photoinitiated polymerization of PEG-diacrylate with lithium phenyl-2,4,6-trimethylbenzoylphosphinate: polymerization rate and cytocompatibility. *Biomaterials* **30**, 6702–6707 (2009).
16. Hume, P. S. & Anseth, K. S. Inducing local T cell apoptosis with anti-Fas-functionalized polymeric coatings fabricated via surface-initiated photopolymerizations. *Biomaterials* **31**, 3166–3174 (2010).
17. Kloxin, A. M., Kasko, A. M., Salinas, C. N. & Anseth, K. S. Photodegradable hydrogels for dynamic tuning of physical and chemical properties. *Science* **324**, 59–63 (2009).
18. Tibbitt, M. W., Kloxin, A. M. & Anseth, K. S. Modeling Photodegradation in Optically Thick Polymer Networks for the Predictable Control of Network Evolution. *Macromolecules* **In Review**
19. Stott, S. L. *et al.* Isolation of circulating tumor cells using a microvortex-generating herringbone-chip. *P Natl Acad Sci Usa* **107**, 18392–18397 (2010).

CHAPTER XII

CONCLUSIONS AND FUTURE DIRECTIONS

Mammalian cell functions, such as proliferation, differentiation, migration, or morphogenesis, are intimately connected to the myriad biochemical and mechanical signals that are displayed dynamically by the local extracellular matrix (ECM).^{1,2} This complex and bidirectional signaling environment integrates with the cell's predetermined genetic state to enable rapid decision making through biochemical pathways that control cell phenotype.^{3,4} In recent years, the paradigm that cell culture platforms simply enable experimenters to study the relationship between genotype and phenotype *in vitro* has been refuted, and it is now clear that the context in which a cell is cultured directly influences its biological function.^{5,6} It is hypothesized that the biochemical and mechanical cues presented outside of the cell generate the functional differences in cell behavior. Unfortunately, it is difficult to isolate the effect that individual signals from the ECM have on cell signaling and behavior *in vivo*, as cells reside in a highly complex and ever-changing milieu. Therefore, materials that enable *in vitro* cell culture for the systematic study of the relationship between dynamic ECM signals and cell behavior are becoming more and more advantageous and allowing researchers to begin to build up this knowledge. Related to this point, this thesis has presented the development of photoresponsive, synthetic hydrogels to investigate specific questions regarding the effect that spatiotemporally

modulated microenvironmental cues have on cell function. Specifically, the quantifiable characterization and modeling of light-induced changes in the synthetic hydrogels is exploited to vary individual mechanical and biochemical cues in the presence of cells for hypothesis testing of their role in biological output.

First, a photolabile monomer was developed, poly(ethylene glycol) diphotodegradable acrylate (PEGdiPDA), to fabricate chain polymerized photodegradable, PEG-based hydrogels for cell culture (Chapter III). PEG was selected as the base material on account of its hydrophilicity and bioinert characteristics, and it can be formed into three-dimensional materials with tissue-like elasticity and reasonable transport of molecules to serve as blank slate culture platforms. A photolabile moiety, *o*-nitrobenzyl ether (NBE), was synthetically incorporated into the PEGdiPDA crosslinking monomer to imbue hydrogels with a photoreactive handle. Polymerizing the macromolecular precursors in a cytocompatible fashion then allowed for either encapsulation during gelation or cell seeding after gelation. The light-induced property changes in the PEGdiPDA hydrogels, *e.g.*, degradation, mass loss, and complete erosion, were measured with one-photon and two-photon irradiation and a statistical-kinetic model of photodegradation was developed (Chapters III, IV). This enabled quantifiable characterization of the structure and function of PEGdiPDA hydrogels during and post-irradiation.

Additionally, the PEGdiPDA monomer was reacted with a four-arm, thiol-functionalized PEG based macromolecular precursor (PEGtetraSH) *via* base-catalyzed, Michael addition; a step polymerization yielding a more ideal structure of the photodegradable network (Chapter V). Measurements of the mechanical integrity and photodegradation of chain polymerized and step polymerized gels further elucidated the structure-function relationship in these materials. Subsequently, photodegradable hydrogels were employed to introduce dynamic mechanical

signals to two-dimensional (2D) and three-dimensional (3D) culture platforms to investigate their influence on selected cell functions (Chapters VI, VII, VIII). Specifically, dynamically presented gradients in the elasticity of 3D cell-gel constructs were employed to investigate the relationship between gel density and cell spreading and morphology (Chapter VI). Further, micron-scale regions of 2D photodegradable gels were eroded to disrupt cell adhesion on the subcellular size scale and study the dynamic cell's cytoskeletal response to changes in the ECM's adhesive environment (Chapter VII). Complementary to these studies, changes in the surface elasticity of 2D culture substrates was used to study human mesenchymal stem cell (hMSC) mechanotransduction and plasticity of hMSC differentiation (Chapter VIII).

A unique processing of step polymerized, photodegradable hydrogels into protein-laden microspheres enabled the systematic study of cell response to spatially and temporally defined presentation of chemical factors (Chapter IX). Cell function was directed by the release of the potent chemokine TGF- β 1 and assayed through the release of the apoptosis marker Annexin V. Further advances in step polymerized, photodegradable hydrogels led to the development of peptide-functionalized, click-based hydrogels that are both enzymatically degradable and photodegradable to enable 3D culture and recovery of mammalian cells (Chapter X). While numerous publications tout the importance of 3D cell culture systems, few address the complexities in performing biological analyses in 3D, and this work sought to demonstrate some of the useful properties of photodegradation to address these limitations. Finally, visible light photopolymerization was used to form PEGdiPDA films within microfluidic capture devices to selectively capture and release mammalian cells under continuous flow for cell purification and rare cell isolation (Chapter XI). These hydrogel surfaces were combined with microfluidic devices to selectively capture and release PC3 prostate cancer cells under continuous flow.

The overall design of this thesis research is outlined in **Figure 12.1**. The general approach was to develop a fundamental and quantifiable understanding of how light-induced changes control the structure and function of hydrogel matrices through both experimental characterization and modeling. From this detailed understanding, we then introduced predictable and defined changes in a more complex system, *i.e.*, the cellular microenvironment, to gain unique insight as to how cells sense extracellular changes in the ECM and how this influences key biological functions. While several conclusions have been made regarding both materials-based and biological questions, many still remain unstudied or incomplete. In this chapter, ongoing research and recommended additional studies with these photodegradable hydrogels will be presented and discussed, toward the goal of addressing increasingly complex biological problems with synthetic cell culture platforms.

Spatiotemporal control of the cell microenvironment

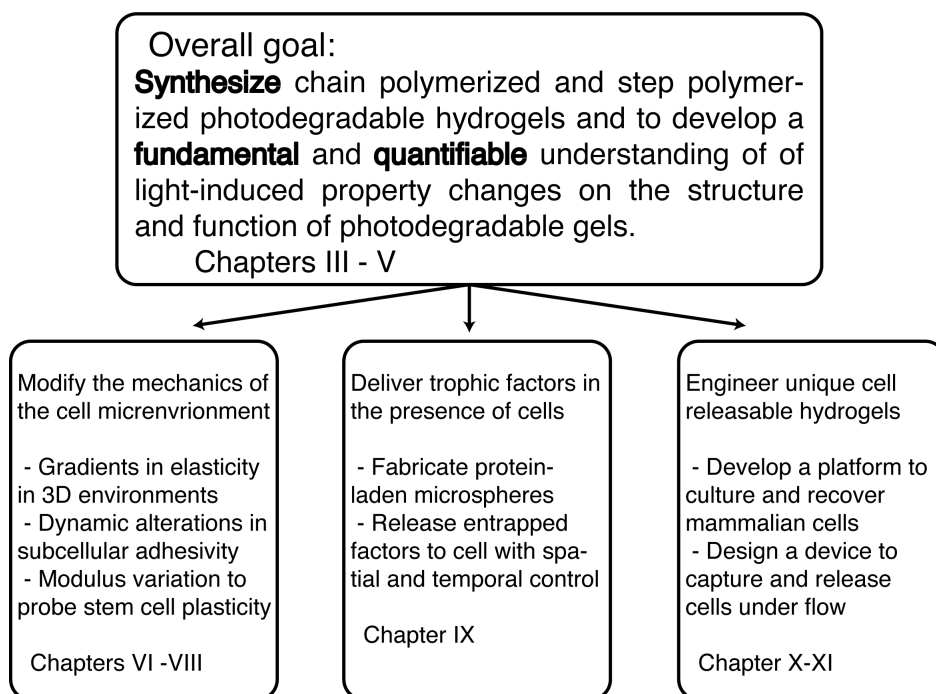


Figure 12.1 Photodegradable hydrogels for spatiotemporal control of the cell microenvironment thesis organization. This thesis focused on the development of photodegradable hydrogels that enable user-defined control over the mechanics and biochemical

nature of the cell microenvironment. The general approach was to develop a fundamental and quantifiable understanding of light-induced property changes on the structure and function of photodegradable gels through characterization and modeling. Using this knowledge, photodegradable hydrogels were employed to probe the cellular response to dynamic mechanical signals, to direct and assay cell function through the spatiotemporally controlled release of trophic factors, and to engineer unique materials for the culture and capture of mammalian cells that enable subsequent cell release.

In Chapter III, a method was presented to synthesize the photolabile monomer, PEGdiPDA, with which PEG-based, photodegradable hydrogels were formed *via* cytocompatible, redox initiated, free-radical chain polymerization. Collimated and focused irradiation were used to modulate gel structure through the cleavage of NBE moieties within the network crosslinks, which was demonstrated to alter gel modulus or geometry. Cells were cultured on or within these photodegradable hydrogels to achieve dynamic, photoresponsive cell culture templates. While both one-photon and two-photon light were employed to modify the PEGdiPDA hydrogels in the presence of cells, the degradation kinetics are inherently limited by the photophysical properties of the NBE moiety. Since PEGdiPDA hydrogels have a demonstrated utility in modulating a cell's microenvironment *in situ*, it would be advantageous to extend these techniques to new, cytocompatible photolabile molecules that are being developed currently, such as nitrobenzyl-based or coumarin-based photocleavable moieties (**Figure 12.2**).^{7,8} In this manner, a broad range of photodegradable hydrogels for cell culture can be developed based on the principles employed to fabricate PEGdiPDA hydrogels with specific degradation properties.

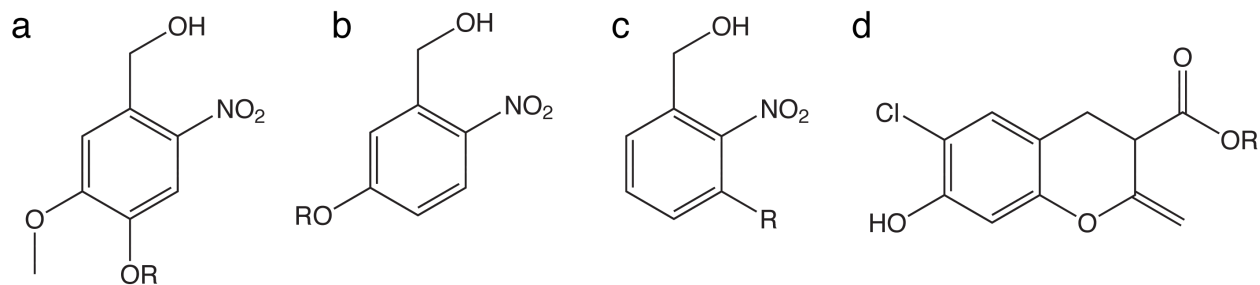


Figure 12.2 Subset of photocleavable moieties for photodegradable hydrogel synthesis. Organic synthesis is enabling the development of a broad range of cytocompatible, photolabile molecules, based on nitrobenzyl ether (**a-c**)⁸ or coumarin chemistries (**d**)⁷, that can be used to form photodegradable gels similar to the PEGdiPDA gels presented in this work. Similar fundamental characterization should be applied to these gels as they become synthetically available.

In Chapter IV, a statistical-kinetic model of photodegradation in optically thick hydrogels was presented to better characterize the fundamental physical process of photodegradation induced material property changes. Briefly, numerical methods were employed to solve a set of coupled partial differential equations that describe the attenuation of light within the gel and the kinetics of the photocleavage reaction. This information was combined with mean-field descriptions of network connectivity to describe light-induced changes in crosslinking density, mass loss, and, ultimately, reverse gelation. While this statistical-kinetic model predicted the experimental observations of material property changes for PEGdiPDA hydrogels, it has only been tested for NBE based hydrogels and it assumes that the degraded products instantaneously diffuse through the gel and dissolve into a sink at the surface. As new photodegradable hydrogels are developed, the statistical-kinetic model should also be applied to these materials. Instantaneous diffusion may be a reasonable assumption for slowly degrading materials; however, as the timescale of degradation approaches that of diffusion both phenomena will need to be taken into account and further iterations of the statistical-kinetic model should include diffusion and dissolution where appropriate (**Figure 12.3a**).

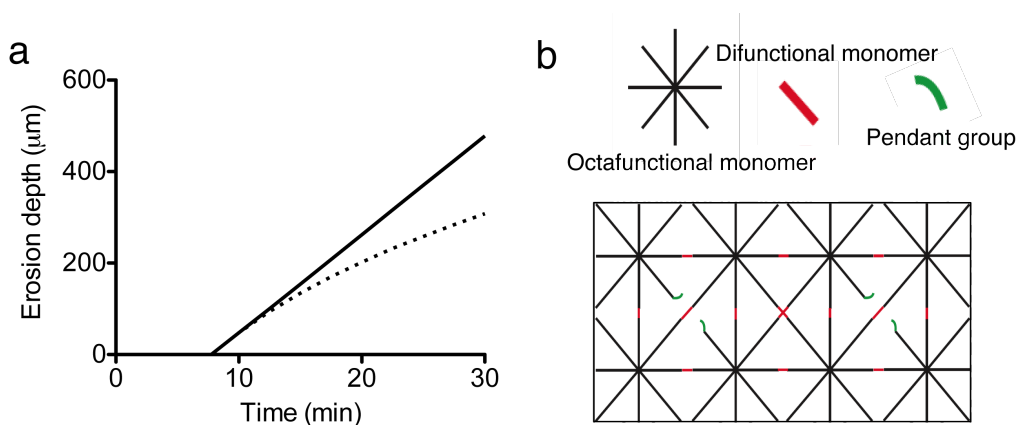


Figure 12.3 Modifications to statistical-kinetic model of photodegradation. (a) Erosion depth is predicted to trend linearly with irradiation time when diffusion and dissolution are assumed to occur instantaneously (solid black line); however, the inclusion of a simple dissolution assumption (dashed black line) changes the qualitative shape of the erosion depth trend line as well as the quantitative rate of erosion. These assumptions should be included in future developments of statistical-kinetic models of photodegradation. (b) Step polymerized gels are being developed from many multifunctional monomers, such as eight-arm norbornene-functionalized PEG and difunctional thiol-terminated PEG,⁹ and as photodegradable gels are synthesized with these network connectivities, new characterization and modeling should be applied to these systems.

In Chapter V, chain polymerized and step polymerized hydrogels were fabricated from the PEGdiPDA monomer to better understand the structure-function relationship in photolabile hydrogels. As was observed previously,^{10,11} step polymerized hydrogels demonstrated increased mechanical integrity as compared to the chain polymerized gels owing to the increased network cooperativity in these more ideal hydrogels. Differences in network connectivity also led to more rapid erosion in step polymerized hydrogels, allowing for the facile generation of patterned features in these gels or low dosage erosion of these gels. While the behavior of chain polymerized PEGdiPDA hydrogels was compared to the step polymerization of a tetrafunctional monomer with a difunctional monomer, photodegradable hydrogels with other network connectivities, such as an octafunctional monomer reacting with a difunctional monomer (**Figure 12.3b**) or double network hydrogels could prove beneficial and require further investigation.

One of the driving forces behind the material design was a critical consideration of the cytocompatibility of the macromers, initiation mechanisms, resulting polymers, and degradation products. While these restrictions greatly limit the choice of chemistries, it also enables a plethora of biological questions to be studied and answered. In Chapter VI, human mesenchymal stem cells (hMSCs) were encapsulated within 3D PEGdiPDA hydrogels and gradients in elasticity were patterned through the z-dimension of the gel using collimated light. Cells were imaged over the course of days to monitor the hMSC response to the gradient, and by Day 4 hMSCs spread significantly in regions of decreased gel density as compared to control samples at a higher gel density. This simple experiment demonstrated that encapsulated cells respond to dynamic changes in the mechanics of the microenvironment. Future studies should explore the relationship between gel density and cell spreading with hMSC differentiation. Several studies have implicated gel mechanics with hMSC differentiation on 2D substrates,^{12,13} yet little is known about how hMSCs respond to dynamic changes in elasticity in 3D culture.

In Chapter VII, 2D PEGdiPDA gels were used to study the dynamic response of hMSCs to changes in the adhesive nature of the ECM on subcellular length scales. Specifically, two-photon irradiation was used to erode precisely micron-scale features into PEGdiPDA gels, and the irradiation parameters to achieve two-photon erosion were quantified and characterized. This technique was applied at the cell-material interface to disrupt local cell adhesion and the cell retraction response was observed. The cells displayed damped viscoelastic retractions in response to disruption of cell adhesion, indicating that the cells were pre-stressed on the substrates prior to subcellular detachment. The time constants of retraction were significantly longer than those for similar experiments conducted on glassy substrates, indicating that the cells were able to sense the soft mechanics of the underlying hydrogel substrate. Uniquely, this

method of two-photon erosion is amenable to generating controlled micron-scale features in 3D, and further studies should explore the use of two-photon erosion within 3D PEGdiPDA hydrogels to explore how 3D geometry influences cell fate decisions (**Figure 12.4a**).¹⁴

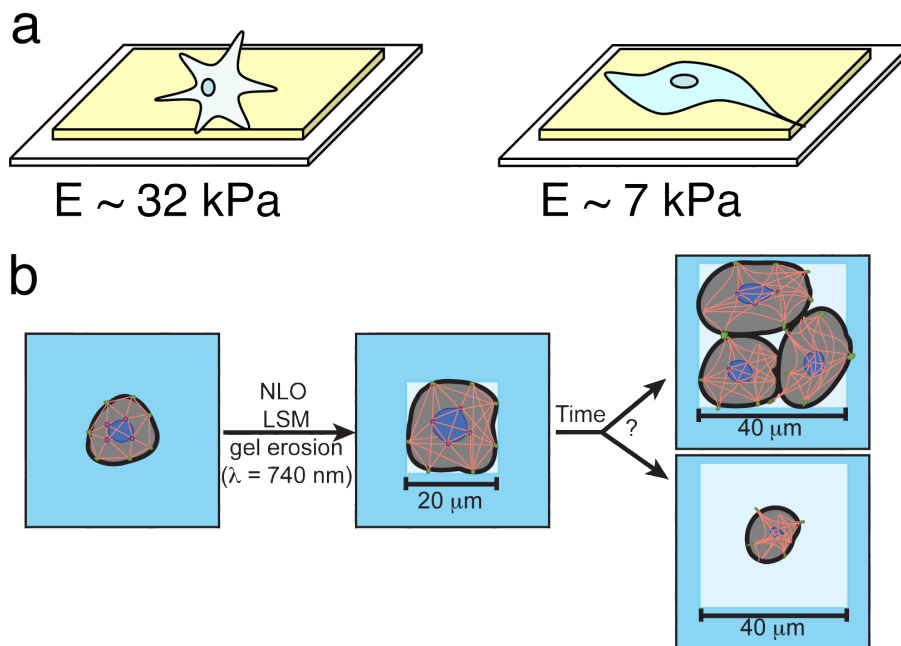


Figure 12.4 Single cell analyses with photodegradable hydrogels. (a) Softening of 2D substrate modulus should be combined with single-cell analyses to further investigate the molecular mechanisms by which mammalian cells integrate mechanical signals from the extracellular matrix. (b) Micron-scale two-photon erosion of 3D hydrogels proximal to encapsulated cells should be explored to investigate how cells respond to changes in cell geometry in a 3D context.

In Chapter VIII, modulation of surface elasticity of 2D PEGdiPDA hydrogels was employed to study hMSC mechanotransduction and differentiation plasticity. hMSCs were seeded onto stiff PEGdiPDA hydrogel surfaces ($E \sim 32$ kPa), and the surface elasticity was dynamically softened ($E \sim 7$ kPa) with light in the presence of cells to explore the differentiation response of the cells. As has been observed in static culture systems, osteogenic differentiation was preferred on stiff substrates, and uniquely, these osteogenic primed cells upregulated a myogenic transcription factor (MyoD1) after the stiff substrates were softened on Day 1 in culture. These preliminary experiments suggest that hMSCs respond biochemically to dynamic

mechanical signals in the ECM; however, the signaling pathways are not fully understood. To elucidate these mechanisms further, current work is exploring the role of mechanotransduction pathways through the YAP and TAZ transcription factors¹⁵ and other signaling molecules that are not yet understood. Similarly, studies are focusing on the single cell response to dynamic softening of substrate modulus and how this affects cytoskeletal organization and differentiation, as some observations are obscured when the whole population is studied (**Figure 12.4b**). To date, the literature provides numerous examples of phenomenological observations of the role of substrate elasticity and its influence on macroscopic cellular functions, *e.g.*, apoptosis, differentiation, morphology. While these studies have highlighted the importance of mechanotransduction in dictating cell fate, a basic understanding of how mechanical signals are translated from the matrix to the nucleus remains understudied and largely not understood.

In Chapter IX, step polymerized, PEGdiPDA hydrogels were processed in a unique manner to fabricate protein-loaded microspheres through an inverse-phase microemulsion polymerization for spatial and temporal control over protein delivery. Photodegradable microspheres were shown to degrade in response to one-photon and two-photon irradiation in a similar fashion to the bulk PEGdiPDA hydrogels. Furthermore, the release of entrapped and bioactive proteins was demonstrated in both 2D and 3D culture systems toward the application of photoresponsive release in the presence of mammalian cells. TGF- β 1 was loaded into the microspheres and released in the presence of PE25 cells (a TGF- β 1 responsive mink lung epithelial cell line) to stimulate the production of luciferase. Similarly, the apoptosis assay protein, Annexin V, was released to detect apoptotic cells with spatiotemporal control during 2D culture. Current studies on the release of bioactive proteins in the presence of cells is focusing on the differentiation of neural precursor cells into motor neurons and the directed migration of

hMSCs in 3D fibrin hydrogels. Specifically, the neurotrophic factor sonic hedgehog (Shh) is being loaded into photodegradable microspheres and released to stimulate proper ventralization of mouse embryonic stem cell derived motor neurons (**Figure 12.5a**). In parallel, the chemotactic factor SDF-1 α is being entrapped within photodegradable microspheres and subsequently loaded into a fibrin clot. An hMSC-laden fibrin gel is fabricated that surrounds this small fibrin clot, and the SDF-1 α is subsequently released with light to stimulate directed migration toward the chemotactic source (**Figure 12.5b**). Future studies should corroborate these preliminary results and continue to demonstrate and explore applications for the spatiotemporal release of protein delivery in the presence of mammalian cells. Numerous opportunities exist to perform basic *in vitro* experiments that would deliver nanoliter quantities of preloaded cytokines, chemokines, antibodies, and small molecules, and to study how the on demand delivery of these cues can be used to manipulate desired cell behavior.

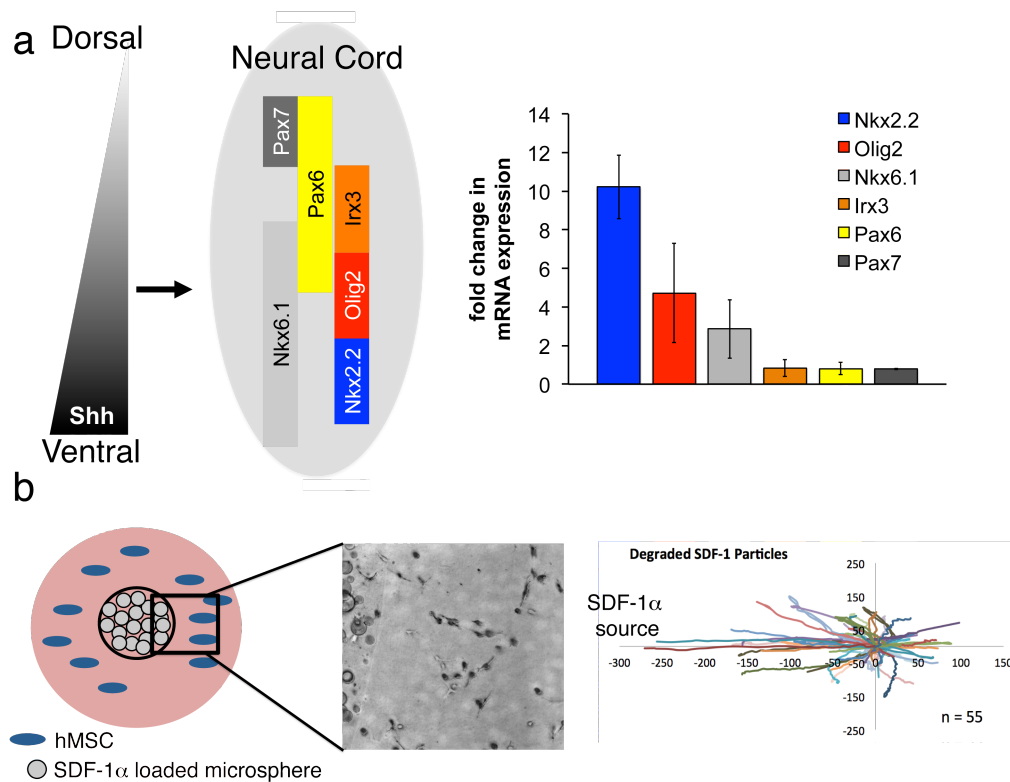


Figure 12.5 Delivery of trophic factors from photodegradable microspheres. (a) Sonic hedgehog (Shh) loaded particles were employed to release Shh in the presence of neural precursor embryoid bodies to direct them toward a ventral motor neuron phenotype. *In vivo*, Shh patterns the CNS from ventral to dorsal with a gradient of Shh. Similarly, Shh released from photodegradable microspheres upregulated ventral genes (Nkx2.2, Olig2, and Nkx6.1) compared to un-treated, control embryoid bodies. *Work done in collaboration with Quinn Fleming and Mirza Peljto. (b) The chemokine SDF-1 α was loaded into photodegradable microspheres to develop a system to study hMSC chemotaxis in response to spatial release of SDF-1 α . SDF-1 α loaded microspheres were encapsulated in a small fibrin clot, which was surrounded by an hMSC laden fibrin gel. The SDF-1 α was released with photodegradation of the microspheres and the hMSCs preferentially migrated in the direction of released chemokine. *Work done in collaboration with Bruce Han and Kyle Kyburz.

The photodegradable microspheres are also being employed to generate cyst-like structures with lung epithelial cells to facilitate proper morphogenesis of alveoli to study the physiology and pathophysiology of lung tissue *in vitro*. Here, extracellular matrix proteins, *e.g.*, fibronectin or laminin, are entrapped within the mesh of the photodegradable microspheres. These adhesive particles are then cultured with A549 cells to coat the particle surface with a monolayer of cells. Cell-microsphere constructs are then encapsulated within RGD-functionalized, 3D hydrogels and the microspheres are photoeroded to generate an encapsulated cyst-like structure (**Figure 12.6**). Currently, immunocytochemistry is being used to characterize the integrity and polarization of the cyst-like structures, while proper formulations for the microsphere template and surrounding encapsulating gel are being developed. Future studies will be conducted to fabricate cyst-like structures with primary lung epithelial cells so that fabricated alveoli can be used to study epithelial – endothelial interactions and the behavior of alveoli interfaces with air. While numerous methods exist in the literature to form and culture cell aggregates of controlled sizes, cyst-like structures are more difficult to assemble. The ability to create cysts in 3D is important for many applications of epithelial cells, and the unique microenvironment may very well be critical for establishing cell polarity and corresponding functional properties.

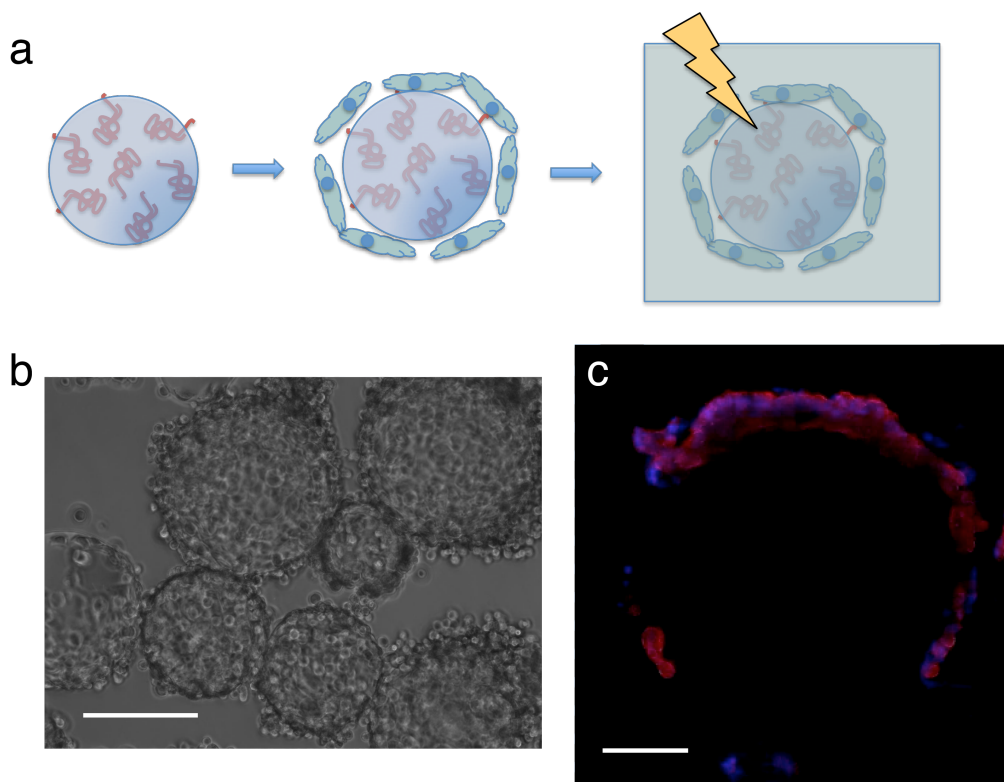


Figure 12.6 Templated cyst-like structures from photodegradable microspheres. (a) Adhesive proteins, such as fibronectin and laminin, were entrapped within photodegradable hydrogels to enable coating with A549 cells. These cell coated particles were entrapped within MMP-degradable and RGD-functionalized hydrogels and the inner photodegradable microspheres were ablated to generate hollow, cyst-like structures. (b) A549 cells coat particles over the course of 18 h and remain attached during encapsulation. (c) Immunostaining for cytoskeleton (red = actin) and nuclei (blue = nuclei) illustrated that the cyst-like structures remain intact after cell encapsulation and photodegradation of the microspheres. *Work done in collaboration with Katie Lewis and Dr. Vivek Balasubramaniam.

In Chapter X, a unique formulation of step polymerized, photodegradable hydrogels was fabricated *via* strain-promoted azide-alkyne cycloaddition (SPAAC) between a four-arm, octyne-functionalized PEG monomer and a diazide-functionalized peptide. The peptide was formed from a matrix metalloproteinase (MMP) susceptible sequence (GPQG↓IAGQ) and an *o*-nitrobenzyl ether moiety rendering the gel both MMP-degradable and photodegradable. In this manner, the gels formed from these macromolecular monomers can be dynamically remodeled by cells through the expression of MMPs and by the user through the controlled delivery of light.

Thus, the system allows one to observe cells in an environment that mimics the native extracellular matrix, while simultaneously allowing one to recover cells at any time point during culture for further analysis of cell function through photoerosion. NIH 3T3 fibroblasts, hMSCs, and neural precursor embryoid bodies were encapsulated within MMP-degradable and photodegradable hydrogels demonstrating that the reaction is fully cytocompatible. hMSCs spread within the gel over the course of 24 h, as MMPs locally degraded the gel and neural precursor embryoid bodies extended axonal projection over the course of 7 days. Cells were liberated from the gel with light, recovered, and plated on TCPS demonstrating that cells released from the gel remain viable. Current work is employing these gels to culture hMSCs and embryoid bodies for the spatial recovery of cells and downstream analysis of cell phenotype through nucleic acid and protein extraction that is traditionally quite difficult in 3D culture templates (**Figure 12.7**)

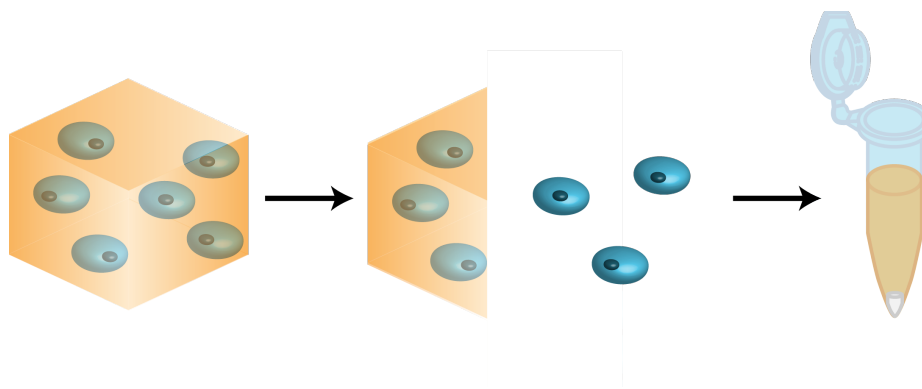


Figure 12.7 Selective recovery of encapsulated cells for downstream analysis. Cells encapsulated in MMP-degradable and photodegradable, click-based hydrogels are selectively released by photodegradation of regions of the gel. Released cells are then recovered for subsequent culture or analysis.

In Chapter XI, thin films of PEGdiPDA were photopolymerized in microfluidic channels to develop selective capture and release devices for cell purification and rare cell isolation. Acrylated-NeutrAvidin was incorporated into films upon polymerization to provide a reactive

handle for subsequent biofunctionalization. Specifically, a biotinylated anti-EpCAM was bound to the surface of PEGdiPDA thin films and demonstrated to capture EpCAM expressing cells while non-functionalized gels failed to capture cells. As a more rigorous test using a continuous flow microfluidic device, PEGdiPDA films captured PC3 prostate cancer cells and these cells could be subsequently released *via* photodegradation of the thin film. Current studies are demonstrating that these recovered cells remain viable after release and are extending the capture devices to purify multiple cell populations in a single device and to isolate rare circulating tumor cells from whole blood.

In summary, through the synthesis of a photodegradable monomer (PEGdiPDA), cell compatible hydrogel scaffolds were fabricated and used to modify dynamically the mechanical and biochemical properties of the cellular microenvironments with full spatial and temporal control with the ultimate goal of influencing cell function. A fundamental and quantifiable characterization of the relationship between light-induced property changes and the structure and function of these photodegradable hydrogels was developed through both experimental and modeling approaches. From this detailed understanding, defined changes were introduced in the cellular microenvironment to hypothesis test as to how specific properties of the ECM influence certain biological outputs. The methodology and experiments described in this thesis contribute to the field's basic understanding as to how cells integrate complex and spatiotemporally varying signals from the ECM, which will enable a better understanding of fundamental biology and the improved engineering of biomaterials for cell culture, cell delivery, and regenerative medicine.

12.1 References

1. Daley, W. P., Peters, S. B. & Larsen, M. Extracellular matrix dynamics in development and regenerative medicine. *J Cell Sci* **121**, 255–264 (2008).

2. Tibbitt, M. W. & Anseth, K. S. Hydrogels as Extracellular Matrix Mimics for 3D Cell Culture. *Biotechnol Bioeng* **103**, 655–663 (2009).
3. Stevens, M. M. & George, J. H. Exploring and Engineering the Cell Surface Interface. *Science* **310**, 1135–1138 (2005).
4. Birgersdotter, A., Sandberg, R. & Ernberg, I. Gene expression perturbation in vitro - A growing case for three-dimensional (3D) culture systems. *Semin Cancer Biol* **15**, 405–412 (2005).
5. Abbott, A. Cell culture: biology's new dimension. *Nature* **424**, 870–872 (2003).
6. Petersen, O. W., Rønnov-Jessen, L., Howlett, A. R. & Bissell, M. J. Interaction with basement membrane serves to rapidly distinguish growth and differentiation pattern of normal and malignant human breast epithelial cells. *P Natl Acad Sci Usa* **89**, 9064–9068 (1992).
7. Wong, D. Y., Griffin, D. R., Reed, J. & Kasko, A. M. Photodegradable Hydrogels to Generate Positive and Negative Features over Multiple Length Scales. *Macromolecules* **43**, 2824–2831 (2010).
8. Griffin, D. R. & Kasko, A. M. Photodegradable macromers and hydrogels for live cell encapsulation and release. *JACS Accepted*
9. Gould, S. T., Darling, N. J. & Anseth, K. S. Small peptide functionalized thiol-ene hydrogels as culture substrates for understanding valvular interstitial cell activation and de novo tissue deposition. *Acta Biomater* (2012).
10. Malkoch, M. *et al.* Synthesis of well-defined hydrogel networks using Click chemistry. *Chem Commun* 2774–2776 (2006).
11. Yang, T. *et al.* Characterization of Well-Defined Poly(ethylene glycol) Hydrogels Prepared by Thiol-ene Chemistry. *J Polym Sci Pol Chem* **49**, 4044–4054 (2011).
12. Engler, A. J., Sen, S., Sweeney, H. L. & Discher, D. E. Matrix elasticity directs stem cell lineage specification. *Cell* **126**, 677–689 (2006).
13. Guvendiren, M. & Burdick, J. A. Stiffening hydrogels to probe short- and long-term cellular responses to dynamic mechanics. *Nat Commun* **3**, – (2012).
14. Chen, C. S. Geometric Control of Cell Life and Death. *Science* **276**, 1425–1428 (1997).
15. Dupont, S. *et al.* Role of YAP/TAZ in mechanotransduction. *Nature* **474**, 179–183 (2011).

CHAPTER XIII

BIBLIOGRAPHY

CHAPTER I -

1. Jaiswal, N., Haynesworth, S., Caplan, A. & Bruder, S. Osteogenic differentiation of purified, culture-expanded human mesenchymal stem cells in vitro. *J Cell Biochem* **64**, 295–312 (1997).
2. Schnaper, H. *et al.* Type-Iv Collagenase(S) and Timps Modulate Endothelial-Cell Morphogenesis in-Vitro. *J. Cell. Physiol.* **156**, 235–246 (1993).
3. Engler, A. J., Sen, S., Sweeney, H. L. & Discher, D. E. Matrix elasticity directs stem cell lineage specification. *Cell* **126**, 677–689 (2006).
4. Engler, A. J., Rehfeldt, F., Sen, S. & Discher, D. E. Microtissue elasticity: Measurements by atomic force microscopy and its influence on cell differentiation. *Method Cell Biol* **83**, 521 (2007).
5. Singhvi, R. *et al.* Engineering Cell-Shape and Function. *Science* **264**, 696–698 (1994).
6. Chen, C. S. Geometric Control of Cell Life and Death. *Science* **276**, 1425–1428 (1997).
7. Petersen, O. W., Rønnov-Jessen, L., Howlett, A. R. & Bissell, M. J. Interaction with basement membrane serves to rapidly distinguish growth and differentiation pattern of normal and malignant human breast epithelial cells. *P Natl Acad Sci Usa* **89**, 9064–9068 (1992).
8. Tanaka, H. *et al.* Chondrogenic differentiation of murine embryonic stem cells: Effects of culture conditions and dexamethasone. *J Cell Biochem* **93**, 454–462 (2004).
9. Birgersdotter, A., Sandberg, R. & Ernberg, I. Gene expression perturbation in vitro - A growing case for three-dimensional (3D) culture systems. *Semin Cancer Biol* **15**, 405–412 (2005).

10. Zhang, S., Zhao, X. & Spirio, L. PuraMatrix: Self-assembling peptide nanofiber scaffolds. *Scaffolding in tissue engineering* 217–238 (2005).
11. Gieni, R. S. & Hendzel, M. J. Mechanotransduction from the ECM to the genome: Are the pieces now in place? *J Cell Biochem* **104**, 1964–1987 (2008).
12. Ashe, H. & Briscoe, J. The interpretation of morphogen gradients. *Development* **133**, 385–394 (2006).
13. Le Beyec, J. *et al.* Cell shape regulates global histone acetylation in human mammary epithelial cells. *Exp Cell Res* **313**, 3066–3075 (2007).
14. Kilian, K. A., Bugarija, B., Lahn, B. T. & Mrksich, M. Geometric cues for directing the differentiation of mesenchymal stem cells. *P Natl Acad Sci Usa* **107**, 4872–4877 (2010).
15. Shea, L., Smiley, E., Bonadio, J. & Mooney, D. DNA delivery from polymer matrices for tissue engineering. *Nat Biotechnol* **17**, 551–554 (1999).
16. Levenberg, S. *et al.* Differentiation of human embryonic stem cells on three-dimensional polymer scaffolds. *P Natl Acad Sci Usa* **100**, 12741–12746 (2003).
17. Yim, E. & Leong, K. Proliferation and differentiation of human embryonic germ cell derivatives in bioactive polymeric fibrous scaffold. *J Biomat Sci-Polym E* **16**, 1193–1217 (2005).
18. Semino, C., Merok, J., Crane, G., Panagiotakos, G. & Zhang, S. Functional differentiation of hepatocyte-like spheroid structures from putative liver progenitor cells in three-dimensional peptide scaffolds. *Differentiation* **71**, 262–270 (2003).
19. Silva, G. A. *et al.* Selective differentiation of neural progenitor cells by high-epitope density nanofibers. *Science* **303**, 1352–1355 (2004).
20. Peppas, N., Hilt, J., Khademhosseini, A. & Langer, R. Hydrogels in biology and medicine: From molecular principles to bionanotechnology. *Adv Mater* **18**, 1345–1360 (2006).
21. Saha, K., Pollock, J. F., Schaffer, D. V. & Healy, K. E. Designing synthetic materials to control stem cell phenotype. *Curr Opin Chem Biol* **11**, 381–387 (2007).
22. Nguyen, K. T. & West, J. L. Photopolymerizable hydrogels for tissue engineering applications. *Biomaterials* **23**, 4307–4314 (2002).
23. Lutolf, M. P. & Hubbell, J. A. Synthetic biomaterials as instructive extracellular microenvironments for morphogenesis in tissue engineering. *Nat Biotechnol* **23**, 47–55 (2005).

24. Lee, K. Y. & Mooney, D. J. Hydrogels for Tissue Engineering. *Chem Rev* **101**, 1869–1880 (2001).
25. Slaughter, B. V., Khurshid, S. S., Fisher, O. Z., Khademhosseini, A. & Peppas, N. A. Hydrogels in Regenerative Medicine. *Adv Mater* **21**, 3307–3329 (2009).
26. Butcher, J. & Nerem, R. Porcine aortic valve interstitial cells in three-dimensional culture: Comparison of phenotype with aortic smooth muscle cells. *J Heart Valve Dis* **13**, 478–485 (2004).
27. Eyrich, D. *et al.* Long-term stable fibrin gels for cartilage engineering. *Biomaterials* **28**, 55–65 (2007).
28. Masters, K., Shah, D., Walker, G., Leinwand, L. & Anseth, K. Designing scaffolds for valvular interstitial cells: Cell adhesion and function on naturally derived materials. *J Biomed Mater Res A* **71A**, 172–180 (2004).
29. Chung, C. & Burdick, J. A. Influence of three-dimensional hyaluronic Acid microenvironments on mesenchymal stem cell chondrogenesis. *Tissue engineering Part A* **15**, 243–254 (2009).
30. Azab, A. *et al.* Crosslinked chitosan implants as potential degradable devices for brachytherapy: In vitro and in vivo analysis. *J Control Release* **111**, 281–289 (2006).
31. Barralet, J. *et al.* Comparison of bone marrow cell growth on 2D and 3D alginate hydrogels. *J Mater Sci-Mater M* **16**, 515–519 (2005).
32. Huebsch, N. *et al.* Harnessing traction-mediated manipulation of the cell/matrix interface to control stem-cell fate. *Nat Mater* **9**, 518–526 (2010).
33. Augst, A. *et al.* Effects of chondrogenic and osteogenic regulatory factors on composite constructs grown using human mesenchymal stem cells, silk scaffolds and bioreactors. *Journal of The Royal Society Interface* **5**, 929–939 (2008).
34. Dawson, E., Mapili, G., Erickson, K., Taqvi, S. & Roy, K. Biomaterials for stem cell differentiation. *Adv Drug Deliv Rev* **60**, 215–228 (2008).
35. Cushing, M. C. & Anseth, K. S. Hydrogel cell cultures. *Science* **316**, 1133–1134 (2007).
36. Sawhney, A. S., Pathak, C. P. & Hubbell, J. A. Bioerodible hydrogels based on photopolymerized poly(ethylene glycol)-co-poly(.alpha.-hydroxy acid) diacrylate macromers. *Macromolecules* **26**, 581–587 (1993).
37. Martens, P. & Anseth, K. Characterization of hydrogels formed from acrylate modified poly(vinyl alcohol) macromers. *Polymer* **41**, 7715–7722 (2000).

38. Chirila, T. *et al.* Poly(2-Hydroxyethyl Methacrylate) Sponges as Implant Materials - In vivo and In vitro Evaluation of Cellular Invasion. *Biomaterials* **14**, 26–38 (1993).
39. Bryant, S. J. & Anseth, K. S. Hydrogel properties influence ECM production by chondrocytes photoencapsulated in poly(ethylene glycol) hydrogels. *J Biomed Mater Res A* **59**, 63–72 (2002).
40. Shu, X. Z., Ahmad, S., Liu, Y. & Prestwich, G. D. Synthesis and evaluation of injectable, in situ crosslinkable synthetic extracellular matrices for tissue engineering. *J Biomed Mater Res A* **79A**, 902–912 (2006).
41. West, J. L. Bioactive hydrogels: Mimicking the ECM with synthetic materials. *Scaffolding in tissue engineering* (2005).
42. Daley, W. P., Peters, S. B. & Larsen, M. Extracellular matrix dynamics in development and regenerative medicine. *J Cell Sci* **121**, 255–264 (2008).
43. Griffith, L. G. & Naughton, G. Tissue Engineering--Current Challenges and Expanding Opportunities. *Science* **295**, 1009–1014 (2002).
44. Lee, S.-H., Moon, J. J. & West, J. L. Three-dimensional micropatterning of bioactive hydrogels via two-photon laser scanning photolithography for guided 3D cell migration. *Biomaterials* **29**, 2962–2968 (2008).
45. Salinas, C. N. & Anseth, K. S. The enhancement of chondrogenic differentiation of human mesenchymal stem cells by enzymatically regulated RGD functionalities. *Biomaterials* **29**, 2370–2377 (2008).
46. Mann, B. & West, J. Cell adhesion peptides alter smooth muscle cell adhesion, proliferation, migration, and matrix protein synthesis on modified surfaces and in polymer scaffolds. *J Biomed Mater Res A* **60**, 86–93 (2002).
47. West, J. & Hubbell, J. Polymeric biomaterials with degradation sites for proteases involved in cell migration. *Macromolecules* **32**, 241–244 (1999).
48. Wang, N., Butler, J. & Ingber, D. Mechanotransduction Across the Cell-Surface and Through the Cytoskeleton. *Science* **260**, 1124–1127 (1993).
49. Giancotti, F. & Ruoslahti, E. Integrin signaling. *Science* **285**, 1028–1032 (1999).
50. Howe, A., Aplin, A., Alahari, S. & Juliano, R. Integrin signaling and cell growth control. *Curr Opin Cell Biol* **10**, 220–231 (1998).
51. Weber, L. M., Hayda, K. N. & Anseth, K. S. Cell-Matrix Interactions Improve beta-Cell Survival and Insulin Secretion in Three-Dimensional Culture. *Tissue engineering Part A* **14**, 1959–1968 (2008).

52. Ruoslahti, E. RGD and other recognition sequences for integrins. *Annu Rev Cell Dev Bi* **12**, 697–715 (1996).
53. Nuttelman, C., Tripodi, M. & Anseth, K. Synthetic hydrogel niches that promote hMSC viability. *Matrix Biol* **24**, 208–218 (2005).
54. Park, K., Na, K. & Chung, H. Enhancement of the adhesion of fibroblasts by peptide containing an Arg-Gly-Asp sequence with poly(ethylene glycol) into a thermo-reversible hydrogel as a synthetic extracellular matrix. *Biotechnol Lett* **27**, 227–231 (2005).
55. Patel, P., Gobin, A., West, J. & Patrick, C. Poly(ethylene glycol) hydrogel system supports preadipocyte viability, adhesion, and proliferation. *Tissue Eng* **11**, 1498–1505 (2005).
56. Massia, S. & Hubbell, J. An Rgd Spacing of 440nm Is Sufficient for Integrin Alpha-v-Beta-3-Mediated Fibroblast Spreading and 140nm for Focal Contact and Stress Fiber Formation. *J Cell Biol* **114**, 1089–1100 (1991).
57. Gobin, A. & West, J. Cell migration through defined, synthetic extracellular matrix analogues. *Faseb J* **16**, 751 (2002).
58. Khire, V. S., Benoit, D. S. W., Anseth, K. S. & Bowman, C. N. Ultrathin gradient films using thiol-ene polymerizations. *J Polym Sci Pol Chem* **44**, 7027–7039 (2006).
59. Rydholm, A. E., Held, N. L., Benoit, D. S. W., Bowman, C. N. & Anseth, K. S. Modifying network chemistry in thiol-acrylate photopolymers through postpolymerization functionalization to control cell-material interactions. *J Biomed Mater Res A* **86A**, 23–30 (2008).
60. Salinas, C. N. & Anseth, K. S. Mixed mode thiol-acrylate photopolymerizations for the synthesis of PEG-peptide hydrogels. *Macromolecules* **41**, 6019–6026 (2008).
61. Sekiya, I., Vuoristo, J., Larson, B. & Prockop, D. In vitro cartilage formation by human adult stem cells from bone marrow stroma defines the sequence of cellular and molecular events during chondrogenesis. *P Natl Acad Sci Usa* **99**, 4397–4402 (2002).
62. Ramirez, F. & Rifkin, D. Cell signaling events: a view from the matrix. *Matrix Biol* **22**, 101–107 (2003).
63. Chen, R. & Mooney, D. Polymeric growth factor delivery strategies for tissue engineering. *Pharm Res-Dord* **20**, 1103–1112 (2003).
64. Yamaguchi, N. & Kiick, K. Polysaccharide-poly(ethylene glycol) star copolymer as a scaffold for the production of bioactive hydrogels. *Biomacromolecules* **6**, 1921–1930 (2005).

65. Willerth, S. M. *et al.* Rationally designed peptides for controlled release of nerve growth factor from fibrin matrices. *J Biomed Mater Res A* **80A**, 13–23 (2007).
66. Zisch, A. *et al.* Cell-demanded release of VEGF from synthetic, biointeractive cell-growth matrices for vascularized tissue growth. *Faseb J* **17**, 2260 (2003).
67. Raeber, G. P., Lutolf, M. P. & Hubbell, J. A. Mechanisms of 3-D migration and matrix remodeling of fibroblasts within artificial ECMs. *Acta Biomater* **3**, 615–629 (2007).
68. Mahoney, M. & Anseth, K. Three-dimensional growth and function of neural tissue in degradable polyethylene glycol hydrogels. *Biomaterials* **27**, 2265–2274 (2006).
69. Metters, A., Anseth, K. & Bowman, C. Fundamental studies of a novel, biodegradable PEG-b-PLA hydrogel. *Polymer* **41**, 3993–4004 (2000).
70. Nuttelman, C. R., Kloxin, A. M. & Anseth, K. S. Temporal changes in peg hydrogel structure influence human mesenchymal stem cell proliferation and matrix mineralization. *Adv. Exp. Med. Biol.* **585**, 135–149 (2006).
71. Lutolf, M. *et al.* Synthetic matrix metalloproteinase-sensitive hydrogels for the conduction of tissue regeneration: Engineering cell-invasion characteristics. *P Natl Acad Sci Usa* **100**, 5413–5418 (2003).
72. Hartgerink, J. D., Beniash, E. & Stupp, S. I. Self-Assembly and Mineralization of Peptide-Amphiphile Nanofibers. *Science* **294**, 1684–1688 (2001).
73. Palsson, B. & Bhatia, S. N. *Tissue engineering*. (Pearson Prentice Hall: Upper Saddle River, NJ, 2004).
74. Deforest, C. A., Polizzotti, B. D. & Anseth, K. S. Sequential click reactions for synthesizing and patterning three-dimensional cell microenvironments. *Nat Mater* **8**, 659–664 (2009).
75. Kloxin, A. M., Kasko, A. M., Salinas, C. N. & Anseth, K. S. Photodegradable hydrogels for dynamic tuning of physical and chemical properties. *Science* **324**, 59–63 (2009).
76. Langer, R. & Tirrell, D. A. Designing materials for biology and medicine. *Nature* **428**, 487–492 (2004).
77. Ratner, B. & Bryant, S. Biomaterials: Where we have been and where we are going. *Annu Rev Biomed Eng* **6**, 41–75 (2004).
78. Martens, P., Bryant, S. & Anseth, K. Tailoring the degradation of hydrogels formed from multivinyl poly(ethylene glycol) and poly(vinyl alcohol) macromers for cartilage tissue engineering. *Biomacromolecules* **4**, 283–292 (2003).

79. Fairbanks, B. D. *et al.* A Versatile Synthetic Extracellular Matrix Mimic via Thiol-Norbornene Photopolymerization. *Adv Mater* **21**, 5005–5010 (2009).
80. Odian, G. *Principles of Polymerization*. (John Wiley & Sons, Inc.: Hoboken, NJ, 2004).
81. Hoyle, C. E. & Bowman, C. N. Thiol-Ene Click Chemistry. *Angew Chem Int Edit* **49**, 1540–1573 (2010).
82. Anseth, K.S., Wang, C. & Bowman, C. Reaction Behavior and Kinetic Constants for Photopolymerizations of Multi(Meth)Acrylate Monomers. *Polymer* **35**, 3243–3250 (1994).
83. Quick, D. J. & Anseth, K. S. DNA delivery from photocrosslinked PEG hydrogels: encapsulation efficiency, release profiles, and DNA quality. *Journal of controlled release* **96**, 341–351 (2004).
84. McCall, J. D., Lin, C.-C. & Anseth, K. S. Affinity peptides protect transforming growth factor beta during encapsulation in poly(ethylene glycol) hydrogels. *Biomacromolecules* **12**, 1051–1057 (2011).
85. Lin-Gibson, S., Jones, R., Washburn, N. & Horkay, F. Structure-property relationships of photopolymerizable poly(ethylene glycol) dimethacrylate hydrogels. *Macromolecules* **38**, 2897–2902 (2005).
86. Matsunaga, T., Sakai, T., Akagi, Y., Chung, U.-I. & Shibayama, M. Structure Characterization of Tetra-PEG Gel by Small-Angle Neutron Scattering. *Macromolecules* **42**, 1344–1351 (2009).
87. Sakai, T. *et al.* Design and fabrication of a high-strength hydrogel with ideally homogeneous network structure from tetrahedron-like macromonomers. *Macromolecules* **41**, 5379–5384 (2008).
88. Malkoch, M. *et al.* Synthesis of well-defined hydrogel networks using Click chemistry. *Chem Commun* 2774–2776 (2006).
89. Elbert, D., Pratt, AB, Lutolf, M., Halstenberg, S. & Hubbell, J. Protein delivery from materials formed by self-selective conjugate addition reactions. *J Control Release* **76**, 11–25 (2001).
90. Johnson, J. A., Finn, M. G., Koberstein, J. T. & Turro, N. J. Synthesis of photocleavable linear macromonomers by ATRP and star macromonomers by a tandem ATRP-click reaction: Precursors to photodegradable model networks. *Macromolecules* **40**, 3589–3598 (2007).
91. Johnson, J. A., Baskin, J. M., Bertozzi, C. R., Koberstein, J. T. & Turro, N. J. Copper-free click chemistry for the in situ crosslinking of photodegradable star polymers. *Chem*

- Commun* 3064–3066 (2008).
92. Yang, T. *et al.* Characterization of Well-Defined Poly(ethylene glycol) Hydrogels Prepared by Thiol-ene Chemistry. *J Polym Sci Pol Chem* **49**, 4044–4054 (2011).
 93. Flory, P. J. *Principles of Polymer Chemistry*. (Cornell University Press: Ithaca, NY, 1953).
 94. Bryant, S.J. & Anseth, K.S. Photopolymerization of hydrogel scaffolds. *Scaffolding in Tissue Engineering* 1–21 (2006).
 95. Anseth, K.S., Bowman, C.N. & BrannonPeppas, L. Mechanical properties of hydrogels and their experimental determination. *Biomaterials* **17**, 1647–1657 (1996).
 96. Metters, A., Bowman, C. & Anseth, K.S. Verification of scaling laws for degrading PLA-b-PEG-b-PLA hydrogels. *Aiche J* **47**, 1432–1437 (2001).
 97. Mason, M., Metters, A., Bowman, C. & Anseth, K. Predicting controlled-release behavior of degradable PLA-b-PEG-b-PLA hydrogels. *Macromolecules* **34**, 4630–4635 (2001).
 98. Flory, P. & Rehner, J. Statistical mechanics of cross-linked polymer networks I Rubberlike elasticity. *J Chem Phys* **11**, 512–520 (1943).
 99. Nicodemus, G. D. & Bryant, S. J. Cell encapsulation in biodegradable hydrogels for tissue engineering applications. *Tissue Engineering Part B: Reviews* **14**, 149–165 (2008).
 100. Metters, A., Bowman, C. & Anseth, K. A statistical kinetic model for the bulk degradation of PLA-b-PEG-b-PLA hydrogel networks. *J Phys Chem B* **104**, 7043–7049 (2000).
 101. Reddy, S., Anseth, K. & Bowman, C. Modeling of network degradation in mixed step-chain growth polymerizations. *Polymer* **46**, 4212–4222 (2005).
 102. Rydholm, A. E., Reddy, S. K., Anseth, K. S. & Bowman, C. N. Development and Characterization of Degradable Thiol-Allyl Ether Photopolymers. *Polymer* **48**, 4589–4600 (2007).
 103. Johnson, J. A., Turro, N. J., Koberstein, J. T. & Mark, J. E. Some hydrogels having novel molecular structures. *Prog Polym Sci* **35**, 332–337 (2010).
 104. Burdick, J. A. & Anseth, K. S. Photoencapsulation of osteoblasts in injectable RGD-modified PEG hydrogels for bone tissue engineering. *Biomaterials* **23**, 4315–4323 (2002).
 105. Hahn, M. S., Miller, J. S. & West, J. L. Three-Dimensional Biochemical and

- Biomechanical Patterning of Hydrogels for Guiding Cell Behavior. *Adv Mater* **18**, 2679–2684 (2006).
106. Luo, Y. & Shoichet, M. S. A photolabile hydrogel for guided three-dimensional cell growth and migration. *Nat Mater* **3**, 249–253 (2004).
 107. Polizzotti, B. D., Fairbanks, B. D. & Anseth, K. S. Three-dimensional biochemical patterning of click-based composite hydrogels via thiolene photopolymerization. *Biomacromolecules* **9**, 1084–1087 (2008).
 108. Wylie, R. G. *et al.* Spatially controlled simultaneous patterning of multiple growth factors in three-dimensional hydrogels. *Nat Mater* **10**, 799–806 (2011).
 109. Khetan, S., Katz, J. S. & Burdick, J. A. Sequential crosslinking to control cellular spreading in 3-dimensional hydrogels. *Soft Matter* **5**, 1601–1606 (2009).
 110. Khetan, S. & Burdick, J. A. Patterning network structure to spatially control cellular remodeling and stem cell fate within 3-dimensional hydrogels. *Biomaterials* **31**, 8228–8234 (2010).
 111. Guvendiren, M. & Burdick, J. A. Stiffening hydrogels to probe short- and long-term cellular responses to dynamic mechanics. *Nat Commun* **3**, – (2012).
 112. Anseth, K. S. *et al.* In situ forming degradable networks and their application in tissue engineering and drug delivery. *Journal of Controlled Release* **78**, 199–209 (2002).
 113. Rydholm, A. E., Reddy, S. K., Anseth, K. S. & Bowman, C. N. Controlling network structure in degradable thiol-acrylate biomaterials to tune mass loss behavior. *Biomacromolecules* **7**, 2827–2836 (2006).
 114. Bryant, S. & Anseth, K. Controlling the spatial distribution of ECM components in degradable PEG hydrogels for tissue engineering cartilage. *J Biomed Mater Res A* **64A**, 70–79 (2003).
 115. Benoit, D. S. W., Durney, A. R. & Anseth, K. S. Manipulations in hydrogel degradation behavior enhance osteoblast function and mineralized tissue formation. *Tissue Eng* **12**, 1663–1673 (2006).
 116. Lutolf, M., Raeber, G., Zisch, A., Tirelli, N. & Hubbell, J. Cell-responsive synthetic hydrogels. *Adv Mater* **15**, 888 (2003).
 117. Anderson, S. B., Lin, C.-C., Kuntzler, D. V. & Anseth, K. S. The performance of human mesenchymal stem cells encapsulated in cell-degradable polymer-peptide hydrogels. *Biomaterials* **32**, 3564–3574 (2011).
 118. Rice, M. A., Sanchez-Adams, J. & Anseth, K. S. Exogenously Triggered, Enzymatic

- Degradation of Photopolymerized Hydrogels with Polycaprolactone Subunits: Experimental Observation and Modeling of Mass Loss Behavior. *Biomacromolecules* **7**, 1968–1975 (2006).
119. Jo, Y. S. *et al.* Biomimetic PEG hydrogels crosslinked with minimal plasmin-sensitive tri-amino acid peptides. *J Biomed Mater Res A* **93A**, 870–877 (2010).
 120. Patterson, J. & Hubbell, J. A. Enhanced proteolytic degradation of molecularly engineered PEG hydrogels in response to MMP-1 and MMP-2. *Biomaterials* **31**, 7836–7845 (2010).
 121. Andreopoulos, F. *et al.* Photoscissable hydrogel synthesis via rapid photopolymerization of novel PEG-based polymers in the absence of photoinitiators. *J Am Chem Soc* **118**, 6235–6240 (1996).
 122. Zheng, Y. *et al.* PEG-based hydrogel synthesis via the photodimerization of anthracene groups. *Macromolecules* **35**, 5228–5234 (2002).
 123. Frey, M. T. & Wang, Y.-L. A photo-modulatable material for probing cellular responses to substrate rigidity. *Soft Matter* **5**, 1918–1924 (2009).
 124. Zhao, Y. *et al.* New caged coumarin fluorophores with extraordinary uncaging cross sections suitable for biological imaging applications. *J Am Chem Soc* **126**, 4653–4663 (2004).
 125. Holmes, C. & Jones, D. Reagents for Combinatorial Organic-Synthesis - Development of a New O-Nitrobenzyl Photolabile Linker for Solid-Phase Synthesis. *J Org Chem* **60**, 2318–2319 (1995).
 126. Holmes, C. Model studies for new o-nitrobenzyl photolabile linkers: Substituent effects on the rates of photochemical cleavage. *J Org Chem* **62**, 2370–2380 (1997).
 127. Whitehouse, D., Savinov, S. & Austin, D. An improved synthesis and selective coupling of a hydroxy based photolabile linker for solid phase organic synthesis. *Tetrahedron Lett* **38**, 7851–7852 (1997).
 128. Deiters, A. Principles and Applications of the Photochemical Control of Cellular Processes. *Chembiochem* **11**, 47–53 (2010).
 129. Ohmuro-Matsuyama, Y. & Tatsu, Y. Photocontrolled cell adhesion on a surface functionalized with a caged arginine-glycine-aspartate peptide. *Angew Chem Int Edit* **47**, 7527–7529 (2008).
 130. Kaneko, S. *et al.* Photocontrol of cell adhesion on amino-bearing surfaces by reversible conjugation of poly(ethylene glycol) via a photocleavable linker. *Phys Chem Chem Phys* **13**, 4051–4059 (2011).

131. Kloxin, A. M., Benton, J. A. & Anseth, K. S. In situ elasticity modulation with dynamic substrates to direct cell phenotype. *Biomaterials* **31**, 1–8 (2010).

CHAPTER II -

1. Weibel, D. B., DiLuzio, W. R. & Whitesides, G. M. Microfabrication meets microbiology. *Nat Rev Microbiol* **5**, 209–218 (2007).
2. Langer, R. & Peppas, N. Advances in biomaterials, drug delivery, and bionanotechnology. *Aiche J* **49**, 2990–3006 (2003).
3. Liechty, W. B., Kryscio, D. R., Slaughter, B. V. & Peppas, N. A. Polymers for drug delivery systems. *Annu Rev Chem Biomol Eng* **1**, 149–173 (2010).
4. Lutolf, M. P. & Hubbell, J. A. Synthetic biomaterials as instructive extracellular microenvironments for morphogenesis in tissue engineering. *Nat Biotechnol* **23**, 47–55 (2005).
5. Tibbitt, M. W. & Anseth, K. S. Hydrogels as Extracellular Matrix Mimics for 3D Cell Culture. *Biotechnol Bioeng* **103**, 655–663 (2009).
6. Stevens, M. M. & George, J. H. Exploring and Engineering the Cell Surface Interface. *Science* **310**, 1135–1138 (2005).
7. Metters, A. & Hubbell, J. Network formation and degradation behavior of hydrogels formed by Michael-type addition reactions. *Biomacromolecules* **6**, 290–301 (2005).
8. Nicodemus, G. D. & Bryant, S. J. Cell encapsulation in biodegradable hydrogels for tissue engineering applications. *Tissue Engineering Part B: Reviews* **14**, 149–165 (2008).
9. Lutolf, M., Raeber, G., Zisch, A., Tirelli, N. & Hubbell, J. Cell-responsive synthetic hydrogels. *Adv Mater* **15**, 888 (2003).
10. Rice, M. A., Sanchez-Adams, J. & Anseth, K. S. Exogenously Triggered, Enzymatic Degradation of Photopolymerized Hydrogels with Polycaprolactone Subunits: Experimental Observation and Modeling of Mass Loss Behavior. *Biomacromolecules* **7**, 1968–1975 (2006).
11. Fairbanks, B. D. *et al.* A Versatile Synthetic Extracellular Matrix Mimic via Thiol-Norbornene Photopolymerization. *Adv Mater* **21**, 5005–5010 (2009).
12. Johnson, J. A., Finn, M. G., Koberstein, J. T. & Turro, N. J. Synthesis of photocleavable linear macromonomers by ATRP and star macromonomers by a tandem ATRP-click reaction: Precursors to photodegradable model networks. *Macromolecules* **40**, 3589–3598 (2007).

13. Johnson, J. A., Baskin, J. M., Bertozzi, C. R., Koberstein, J. T. & Turro, N. J. Copper-free click chemistry for the in situ crosslinking of photodegradable star polymers. *Chem Commun* 3064–3066 (2008).
14. Kloxin, A. M., Kasko, A. M., Salinas, C. N. & Anseth, K. S. Photodegradable hydrogels for dynamic tuning of physical and chemical properties. *Science* **324**, 59–63 (2009).
15. Frey, M. T. & Wang, Y.-L. A photo-modulatable material for probing cellular responses to substrate rigidity. *Soft Matter* **5**, 1918–1924 (2009).
16. Deforest, C. A., Polizzotti, B. D. & Anseth, K. S. Sequential click reactions for synthesizing and patterning three-dimensional cell microenvironments. *Nat Mater* **8**, 659–664 (2009).

CHAPTER III -

1. Lutolf, M.P. & Hubbell, J.A. Synthetic biomaterials as instructive extracellular microenvironments for morphogenesis in tissue engineering. *Nat. Biotechnol.* **23**, 47-55 (2005).
2. Liu, S.Q. et al. Synthetic hydrogels for controlled stem cell differentiation. *Soft Matter* **6**, 67-81 (2010).
3. Tibbitt, M.W. & Anseth, K.S. Hydrogels as Extracellular Matrix Mimics for 3D Cell Culture. *Biotechnol. Bioeng.* **103**, 655-663 (2009).
4. Guilak, F. et al. Control of Stem Cell Fate by Physical Interactions with the Extracellular Matrix. *Cell Stem Cell* **5**, 17-26 (2009).
5. Hwang, N.S., Varghese, S. & Elisseeff, J. Controlled differentiation of stem cells. *Adv. Drug Deliv. Rev.* **60**, 199-214 (2008).
6. Wolf, K. et al. Multi-step pericellular proteolysis controls the transition from individual to collective cancer cell invasion. *Nat. Cell Biol.* **9**, 893-U839 (2007).
7. Tayalia, P., Mendonca, C.R., Baldacchini, T., Mooney, D.J. & Mazur, E. 3D Cell-Migration Studies using Two-Photon Engineered Polymer Scaffolds. *Adv. Mater.* **20**, 4494-4498 (2008).
8. Kloxin, A.M., Kasko, A.M., Salinas, C.N. & Anseth, K.S. Photodegradable Hydrogels for Dynamic Tuning of Physical and Chemical Properties. *Science* **324**, 59-63 (2009).
9. Jay, S.M. & Saltzman, W.M. Shining light on a new class of hydrogels. *Nat. Biotechnol.* **27**, 543-544 (2009).

10. Lutolf, M.P. Spotlight on hydrogels. *Nat. Mater.* **8**, 451-453 (2009).
11. Yu, H.T., Li, J.B., Wu, D.D., Qiu, Z.J. & Zhang, Y. Chemistry and biological applications of photo-labile organic molecules. *Chem. Soc. Rev.* **39**, 464-473 (2010).
12. Holmes, C.P. Model studies for new o-nitrobenzyl photolabile linkers: Substituent effects on the rates of photochemical cleavage. *Journal Of Organic Chemistry* **62**, 2370-2380 (1997).
13. Akerblom, E.B., Nygren, A.S. & Agback, K.H. Six new photolabile linkers for solid-phase synthesis. 1. Methods of preparation. *Mol. Divers.* **3**, 137-148 (1998).
14. Zhao, Y.R. et al. New caged coumarin fluorophores with extraordinary uncaging cross sections suitable for biological imaging applications. *Journal Of The American Chemical Society* **126**, 4653-4663 (2004).
15. Alvarez, M. et al. Single-Photon and Two-Photon Induced Photocleavage for Monolayers of an Alkyltriethoxysilane with a Photoprotected Carboxylic Ester. *Adv. Mater.* **20**, 4563-4567 (2008).
16. Pelliccioli, A.P. & Wirz, J. Photoremovable protecting groups: reaction mechanisms and applications. *Photochem. Photobiol. Sci.* **1**, 441-458 (2002).
17. Deiters, A. Principles and Applications of the Photochemical Control of Cellular Processes. *ChemBioChem* **11**, 47-53 (2010).
18. Luo, Y. & Shoichet, M.S. A photolabile hydrogel for guided three-dimensional cell growth and migration. *Nat. Mater.* **3**, 249-253 (2004).
19. Wosnick, J.H. & Shoichet, M.S. Three-dimensional chemical Patterning of transparent hydrogels. *Chem. Mat.* **20**, 55-60 (2008).
20. Ohmuro-Matsuyama, Y. & Tatsu, Y. Photocontrolled cell adhesion on a surface functionalized with a caged arginine-glycine-aspartate peptide. *Angew. Chem.-Int. Edit.* **47**, 7527-7529 (2008).
21. Nakanishi, J. et al. Spatiotemporal control of cell adhesion on a self-assembled monolayer having a photocleavable protecting group. *Anal. Chim. Acta* **578**, 100-104 (2006).
22. Johnson, J.A., Finn, M.G., Koberstein, J.T. & Turro, N.J. Synthesis of photocleavable linear macromonomers by ATRP and star macromonomers by a tandem ATRP-Click reaction: precursors to photodegradable model networks. *Macromolecules* **40**, 3589-3598 (2007).

23. Johnson, J.A., Baskin, J.M., Bertozzi, C.R., Koberstein, J.T. & Turro, N.J. Copper-free click chemistry for the in situ crosslinking of photodegradable star polymers. *Chemical Communications*, 3064-3066 (2008).
24. Kikuchi, Y. et al. Grafting Poly(ethylene glycol) to a Glass Surface via a Photocleavable Linker for Light-induced Cell Micropatterning and Cell Proliferation Control. *Chem. Lett.* **37**, 1062-1063 (2008).
25. Frey, M.T. & Wang, Y.L. A photo-modulatable material for probing cellular responses to substrate rigidity. *Soft Matter* **5**, 1918-1924 (2009).
26. Kloxin, A.M., Benton, J.A. & Anseth, K.S. In situ elasticity modulation with dynamic substrates to direct cell phenotype. *Biomaterials* **31**, 1-8 (2010).
27. Kloxin, A.M., Tibbitt, M.W., Kasko, A.M., Fairbairn, J.F. & Anseth, K.S. Tunable hydrogels for external manipulation of cellular microenvironments through controlled photodegradation. *Adv. Mater.* **22**, 61-66 (2010).
28. Engler, A.J., Sen, S., Sweeney, H.L. & Discher, D.E. Matrix elasticity directs stem cell lineage specification. *Cell* **126**, 677-689 (2006).
29. Chowdhury, F. et al. Material properties of the cell dictate stress-induced spreading and differentiation in embryonic stem cells. *Nat. Mater.* **9**, 82-88 (2010).
30. Wong, J.Y., Velasco, A., Rajagopalan, P. & Pham, Q. Directed movement of vascular smooth muscle cells on gradient-compliant hydrogels. *Langmuir* **19**, 1908-1913 (2003).
31. Khetan, S., Katz, J.S. & Burdick, J.A. Sequential crosslinking to control cellular spreading in 3-dimensional hydrogels. *Soft Matter* **5**, 1601-1606 (2009).
32. Gillette, B.M., Jensen, J.A., Wang, M.X., Tchao, J. & Sia, S.K. Dynamic Hydrogels: Switching of 3D Microenvironments Using Two-Component Naturally Derived Extracellular Matrices. *Adv. Mater.* **22**, 686 (2010).
33. Murayama, S. & Kato, M. Photocontrol of Biological Activities of Protein by Means of a Hydrogel. *Analytical Chemistry* **82**, 2186-2191 (2010).
34. Benoit, D.S.W., Nuttelman, C.R., Collins, S.D. & Anseth, K.S. Synthesis and characterization of a fluvastatin-releasing hydrogel delivery system to modulate hMSC differentiation and function for bone regeneration. *Biomaterials* **27**, 6102-6110 (2006).
35. Salinas, C.N. & Anseth, K.S. The enhancement of chondrogenic differentiation of human mesenchymal stem cells by enzymatically regulated RGD functionalities. *Biomaterials* **29**, 2370 (2008).

36. Wong, D.Y., Griffin, D.R., Reed, J. & Kasko, A.M. Photodegradable Hydrogels to Generate Positive and Negative Features over Multiple Length Scales. *Macromolecules* **43**, 2824-2831 (2010).
37. Yeo, W.S. & Mrksich, M. Electroactive self-assembled monolayers that permit orthogonal control over the adhesion of cells to patterned substrates. *Langmuir* **22**, 10816-10820 (2006).
38. Yamato, M. et al. Temperature-responsive cell culture surfaces for regenerative medicine with cell sheet engineering. *Prog. Polym. Sci.* **32**, 1123-1133 (2007).
39. Williams, C. et al. Aligned Cell Sheets Grown on Thermo-Responsive Substrates with Microcontact Printed Protein Patterns. *Adv. Mater.* **21**, 2161 (2009).
40. Mohammed, J.S. & Murphy, W.L. Bioinspired Design of Dynamic Materials. *Adv. Mater.* **21**, 2361-2374 (2009).
41. Nowatzki, P.J., Franck, C., Maskarinec, S.A., Ravichandran, G. & Tirrell, D.A. Mechanically tunable thin films of photosensitive artificial proteins: Preparation and characterization by nanoindentation. *Macromolecules* **41**, 1839-1845 (2008).
42. Andreopoulos, F.M. & Persaud, I. Delivery of basic fibroblast growth factor (bFGF) from photoresponsive hydrogel scaffolds. *Biomaterials* **27**, 2468-2476 (2006).
43. Trenor, S.R., Shultz, A.R., Love, B.J. & Long, T.E. Coumarins in polymers: From light harvesting to photo-cross-linkable tissue scaffolds. *Chem. Rev.* **104**, 3059-3077 (2004).
44. Nuttelman, C.R., Tripodi, M.C. & Anseth, K.S. In vitro osteogenic differentiation of human mesenchymal stem cells photoencapsulated in PEG hydrogels. *J. Biomed. Mater. Res. Part A* **68A**, 773-782 (2004).
45. Salinas, C.N. & Anseth, K.S. The influence of the RGD peptide motif and its contextual presentation in PEG gels on human mesenchymal stem cell viability. *J. Tissue Eng. Regen. Med.* **2**, 296-304 (2008).
46. Salinas, C.N., Cole, B.B., Kasko, A.M. & Anseth, K.S. Chondrogenic differentiation potential of human mesenchymal stem cells photoencapsulated within poly(ethylene glycol)-arginine-glycine-aspartic acid-serine thiol-methacrylate mixed-mode networks. *Tissue Eng.* **13**, 1025-1034 (2007).
47. Chan, W.C. & White, P.D. (eds.) *Fmoc Solid Phase Peptide Synthesis*. (Oxford University Press, Inc., New York; 2000).

CHAPTER IV -

1. Peppas, N., Hilt, J., Khademhosseini, A. & Langer, R. Hydrogels in biology and medicine: From molecular principles to bionanotechnology. *Adv Mater* **18**, 1345–1360 (2006).
2. Liechty, W. B., Kryscio, D. R., Slaughter, B. V. & Peppas, N. A. Polymers for drug delivery systems. *Annu Rev Chem Biomol Eng* **1**, 149–173 (2010).
3. Tibbitt, M. W. & Anseth, K. S. Hydrogels as Extracellular Matrix Mimics for 3D Cell Culture. *Biotechnol Bioeng* **103**, 655–663 (2009).
4. Lutolf, M. P. & Hubbell, J. A. Synthetic biomaterials as instructive extracellular microenvironments for morphogenesis in tissue engineering. *Nat Biotechnol* **23**, 47–55 (2005).
5. Hilt, J. Z., Gupta, A. K., Bashir, R. & Peppas, N. A. Ultrasensitive Biomems Sensors Based on Microcantilevers Patterned with Environmentally Responsive Hydrogels. *Biomedical Microdevices* **5**, 177–184 (2003).
6. Dong, L. & Jiang, H. Autonomous microfluidics with stimuli-responsive hydrogels. *Soft Matter* **3**, 1223 (2007).
7. Johnson, J. A., Finn, M. G., Koberstein, J. T. & Turro, N. J. Synthesis of photocleavable linear macromonomers by ATRP and star macromonomers by a tandem ATRP-click reaction: Precursors to photodegradable model networks. *Macromolecules* **40**, 3589–3598 (2007).
8. Johnson, J. A., Baskin, J. M., Bertozzi, C. R., Koberstein, J. T. & Turro, N. J. Copper-free click chemistry for the in situ crosslinking of photodegradable star polymers. *Chem Commun* 3064–3066 (2008).doi:10.1039/b803043j
9. Luo, Y. & Shoichet, M. S. A photolabile hydrogel for guided three-dimensional cell growth and migration. *Nat Mater* **3**, 249–253 (2004).
10. Kloxin, A. M., Kasko, A. M., Salinas, C. N. & Anseth, K. S. Photodegradable hydrogels for dynamic tuning of physical and chemical properties. *Science* **324**, 59–63 (2009).
11. Frey, M. T. & Wang, Y.-L. A photo-modulatable material for probing cellular responses to substrate rigidity. *Soft Matter* **5**, 1918–1924 (2009).
12. Tibbitt, M. W., Kloxin, A. M., Dyamenahalli, K. U. & Anseth, K. S. Controlled two-photon photodegradation of PEG hydrogels to study and manipulate subcellular interactions on soft materials. *Soft Matter* **6**, 5100–5108 (2010).
13. Deforest, C. A. & Anseth, K. S. Cytocompatible click-based hydrogels with dynamically tunable properties through orthogonal photoconjugation and photocleavage reactions. *Nat Chem* **3**, 925–931 (2011).

14. Wong, D. Y., Griffin, D. R., Reed, J. & Kasko, A. M. Photodegradable Hydrogels to Generate Positive and Negative Features over Multiple Length Scales. *Macromolecules* **43**, 2824–2831 (2010).
15. Peng, K. *et al.* Dextran based photodegradable hydrogels formed via a Michael addition. *Soft Matter* **7**, 4881–4887 (2011).
16. Nicodemus, G. D. & Bryant, S. J. Cell encapsulation in biodegradable hydrogels for tissue engineering applications. *Tissue Engineering Part B: Reviews* **14**, 149–165 (2008).
17. Metters, A., Bowman, C. & Anseth, K. A statistical kinetic model for the bulk degradation of PLA-b-PEG-b-PLA hydrogel networks. *J Phys Chem B* **104**, 7043–7049 (2000).
18. Reddy, S., Anseth, K. & Bowman, C. Modeling of network degradation in mixed step-chain growth polymerizations. *Polymer* **46**, 4212–4222 (2005).
19. Slaughter, B. V., Khurshid, S. S., Fisher, O. Z., Khademhosseini, A. & Peppas, N. A. Hydrogels in Regenerative Medicine. *Adv Mater* **21**, 3307–3329 (2009).
20. Kloxin, A. M., Tibbitt, M. W., Kasko, A. M., Fairbairn, J. A. & Anseth, K. S. Tunable Hydrogels for External Manipulation of Cellular Microenvironments through Controlled Photodegradation. *Adv Mater* **22**, 61–66 (2010).
21. Kloxin, A. M., Benton, J. A. & Anseth, K. S. In situ elasticity modulation with dynamic substrates to direct cell phenotype. *Biomaterials* **31**, 1–8 (2010).
22. Griffin, D. R., Patterson, J. T. & Kasko, A. M. Photodegradation as a mechanism for controlled drug delivery. *Biotechnol Bioeng* **107**, 1012–1019 (2010).
23. Tibbitt, M. W., Han, B. W., Kloxin, A. M. & Anseth, K. S. Synthesis and application of photodegradable microspheres for spatiotemporal control of protein delivery. *J Biomed Mater Res A* **100**, 1647–1654 (2012).
24. Wong, D. Y., Griffin D. R., Reed J. & Kasko, A. M. Photodegradably hydrogels to generate positive and negative features over multiple length scales. *Macromolecules* **43**, 2824–2831 (2010).
25. Andreopoulos, F. M. & Persaud, I. Delivery of basic fibroblast growth factor (bFGF) from photoresponsive hydrogel scaffolds. *Biomaterials* **27**, 2468–2476 (2006).
26. Trenor, S., Shultz, A., Love, B. & Long, T. Coumarins in polymers: From light harvesting to photo-cross-linkable tissue scaffolds. *Chem Rev* **104**, 3059–3077 (2004).
27. Martens, P., Metters, A., Anseth, K. & Bowman, C. A generalized bulk-degradation model for hydrogel networks formed from multivinyl cross-linking molecules. *J Phys Chem B* **105**, 5131–5138 (2001).

28. Rydholm, A. E., Reddy, S. K., Anseth, K. S. & Bowman, C. N. Development and Characterization of Degradable Thiol-Allyl Ether Photopolymers. *Polymer* **48**, 4589–4600 (2007).
29. Kloxin, A. M., Tibbitt, M. W. & Anseth, K. S. Synthesis of photodegradable hydrogels as dynamically tunable cell culture platforms. *Nat Protoc* **5**, 1867–1887 (2010).
30. Odian, G. *Principles of Polymerization*. (John Wiley & Sons, Inc.: Hoboken, NJ, 2004).
31. Miller, G., Gou, L., Narayanan, V. & Scranton, A. Modeling of photobleaching for the photoinitiation of thick polymerization systems. *J Polym Sci Pol Chem* **40**, 793–808 (2002).
32. Wegscheider, R. Z. *Physical Chemistry* **103**, 273–306 (1923).
33. Terrones, G. & Pearlstein, A. Effects of optical attenuation and consumption of a photobleaching initiator on local initiation rates in photopolymerizations. *Macromolecules* **34**, 3195–3204 (2001).
34. Macosko, C. W. & Miller, D. R. A new derivation of average molecular weights of nonlinear polymers. *Macromolecules* **9**, 199–206 (1976).
35. Miller, D. R. & Macosko, C. W. A new derivation of post gel properties of network polymers. *Macromolecules* **9**, 206–211 (1976).
36. Nuttelman, C. R., Kloxin, A. M. & Anseth, K. S. Temporal changes in peg hydrogel structure influence human mesenchymal stem cell proliferation and matrix mineralization. *Adv. Exp. Med. Biol.* **585**, 135–149 (2006).
37. Bryant, S. Photopolymerization of hydrogel scaffolds. *Scaffolding in Tissue Engineering* 1–21 (2006).

CHAPTER V -

1. Lutolf, M. P. & Hubbell, J. A. Synthetic biomaterials as instructive extracellular microenvironments for morphogenesis in tissue engineering. *Nat Biotechnol* **23**, 47–55 (2005).
2. Tibbitt, M. W. & Anseth, K. S. Hydrogels as Extracellular Matrix Mimics for 3D Cell Culture. *Biotechnol Bioeng* **103**, 655–663 (2009).
3. Magin, C. M. *et al.* Antifouling performance of cross-linked hydrogels: refinement of an attachment model. *Biomacromolecules* **12**, 915–922 (2011).
4. Kidane, A., Szabocsik, J. & Park, K. Accelerated study on lysozyme deposition on poly(HEMA) contact lenses. *Biomaterials* **19**, 2051–2055 (1998).
5. Liechty, W. B., Kryscio, D. R., Slaughter, B. V. & Peppas, N. A. Polymers for drug

- delivery systems. *Annu Rev Chem Biomol Eng* **1**, 149–173 (2010).
6. Peppas, N., Hilt, J., Khademhosseini, A. & Langer, R. Hydrogels in biology and medicine: From molecular principles to bionanotechnology. *Adv Mater* **18**, 1345–1360 (2006).
 7. Sawhney, A. S., Pathak, C. P. & Hubbell, J. A. Bioerodible hydrogels based on photopolymerized poly(ethylene glycol)-co-poly(.alpha.-hydroxy acid) diacrylate macromers. *Macromolecules* **26**, 581–587 (1993).
 8. Anseth, K., Bowman, C. & BrannonPeppas, L. Mechanical properties of hydrogels and their experimental determination. *Biomaterials* **17**, 1647–1657 (1996).
 9. West, J. L. & Hubbell, J. A. Polymeric Biomaterials with Degradation Sites for Proteases Involved in Cell Migration. *Macromolecules* **32**, 241–244 (1999).
 10. Hoyle, C. E. & Bowman, C. N. Thiol-Ene Click Chemistry. *Angew Chem Int Edit* **49**, 1540–1573 (2010).
 11. Anseth, K., WANG, C. & Bowman, C. Reaction Behavior and Kinetic Constants for Photopolymerizations of Multi(Meth)Acrylate Monomers. *Polymer* **35**, 3243–3250 (1994).
 12. Quick, D. J. & Anseth, K. S. DNA delivery from photocrosslinked PEG hydrogels: encapsulation efficiency, release profiles, and DNA quality. *Journal of controlled release : official journal of the Controlled Release Society* **96**, 341–351 (2004).
 13. McCall, J. D., Lin, C.-C. & Anseth, K. S. Affinity peptides protect transforming growth factor beta during encapsulation in poly(ethylene glycol) hydrogels. *Biomacromolecules* **12**, 1051–1057 (2011).
 14. Lin-Gibson, S., Jones, R., Washburn, N. & Horkay, F. Structure-property relationships of photopolymerizable poly(ethylene glycol) dimethacrylate hydrogels. *Macromolecules* **38**, 2897–2902 (2005).
 15. Sakai, T. *et al.* Design and fabrication of a high-strength hydrogel with ideally homogeneous network structure from tetrahedron-like macromonomers. *Macromolecules* **41**, 5379–5384 (2008).
 16. Malkoch, M. *et al.* Synthesis of well-defined hydrogel networks using Click chemistry. *Chem Commun* 2774–2776 (2006).doi:10.1039/b603438a
 17. Matsunaga, T., Sakai, T., Akagi, Y., Chung, U.-I. & Shibayama, M. Structure Characterization of Tetra-PEG Gel by Small-Angle Neutron Scattering. *Macromolecules* **42**, 1344–1351 (2009).
 18. Yang, T. *et al.* Characterization of Well-Defined Poly(ethylene glycol) Hydrogels Prepared by Thiol-ene Chemistry. *J Polym Sci Pol Chem* **49**, 4044–4054 (2011).

19. Elbert, D., Pratt, A.B., Lutolf, M., Halstenberg, S. & Hubbell, J. Protein delivery from materials formed by self-selective conjugate addition reactions. *J Control Release* **76**, 11–25 (2001).
20. Lutolf, M., Raeber, G., Zisch, A., Tirelli, N. & Hubbell, J. Cell-responsive synthetic hydrogels. *Adv Mater* **15**, 888–+ (2003).
21. Johnson, J. A., Baskin, J. M., Bertozzi, C. R., Koberstein, J. T. & Turro, N. J. Copper-free click chemistry for the in situ crosslinking of photodegradable star polymers. *Chem Commun* 3064–3066 (2008).doi:10.1039/b803043j
22. Johnson, J. A., Finn, M. G., Koberstein, J. T. & Turro, N. J. Synthesis of photocleavable linear macromonomers by ATRP and star macromonomers by a tandem ATRP-click reaction: Precursors to photodegradable model networks. *Macromolecules* **40**, 3589–3598 (2007).
23. Fairbanks, B. D. *et al.* A Versatile Synthetic Extracellular Matrix Mimic via Thiol-Norbornene Photopolymerization. *Adv Mater* **21**, 5005–5010 (2009).
24. Deforest, C. A., Polizzotti, B. D. & Anseth, K. S. Sequential click reactions for synthesizing and patterning three-dimensional cell microenvironments. *Nat Mater* **8**, 659–664 (2009).
25. Kloxin, A. M., Kasko, A. M., Salinas, C. N. & Anseth, K. S. Photodegradable hydrogels for dynamic tuning of physical and chemical properties. *Science* **324**, 59–63 (2009).
26. Frey, M. T. & Wang, Y.-L. A photo-modulatable material for probing cellular responses to substrate rigidity. *Soft Matter* **5**, 1918–1924 (2009).
27. Kloxin, A. M., Tibbitt, M. W. & Anseth, K. S. Synthesis of photodegradable hydrogels as dynamically tunable cell culture platforms. *Nat Protoc* **5**, 1867–1887 (2010).
28. Wong, D. Y., Griffin, D. R., Reed, J. & Kasko, A. M. Photodegradable Hydrogels to Generate Positive and Negative Features over Multiple Length Scales. *Macromolecules* **43**, 2824–2831 (2010).
29. Deforest, C. A. & Anseth, K. S. Cytocompatible click-based hydrogels with dynamically tunable properties through orthogonal photoconjugation and photocleavage reactions. *Nat Chem* **3**, 925–931 (2011).
30. Kloxin, A. M., Benton, J. A. & Anseth, K. S. In situ elasticity modulation with dynamic substrates to direct cell phenotype. *Biomaterials* **31**, 1–8 (2010).
31. Kloxin, A. M., Tibbitt, M. W., Kasko, A. M., Fairbairn, J. A. & Anseth, K. S. Tunable Hydrogels for External Manipulation of Cellular Microenvironments through Controlled Photodegradation. *Adv Mater* **22**, 61–66 (2010).
32. Tibbitt, M. W., Kloxin, A. M., Dyamenahalli, K. U. & Anseth, K. S. Controlled two-

- photon photodegradation of PEG hydrogels to study and manipulate subcellular interactions on soft materials. *Soft Matter* **6**, 5100–5108 (2010).
33. Deforest, C. A. & Anseth, K. S. Photoreversible Patterning of Biomolecules within Click-Based Hydrogels. *Angew Chem Int Ed Engl* **51**, 1816–1819 (2012).
 34. Peng, K. *et al.* Dextran based photodegradable hydrogels formed via a Michael addition. *Soft Matter* **7**, 4881–4887 (2011).
 35. Tibbitt, M. W., Han, B. W., Kloxin, A. M. & Anseth, K. S. Synthesis and application of photodegradable microspheres for spatiotemporal control of protein delivery. *J Biomed Mater Res A* **100**, 1647–1654 (2012).
 36. Fairbanks, B. D., Singh, S. P., Bowman, C. N. & Anseth, K. S. Photodegradable, Photoadaptable Hydrogels via Radical-Mediated Disulfide Fragmentation Reaction. *Macromolecules* **44**, 2444–2450 (2011).
 37. Tibbitt, M. W., Kloxin, A. M. & Anseth, K. S. Modeling Photodegradation in Optically Thick Polymer Networks for the Predictable Control of Network Evolution. *Macromolecules* **In Review**.
 38. Griffin, D. R., Patterson, J. T. & Kasko, A. M. Photodegradation as a mechanism for controlled drug delivery. *Biotechnol Bioeng* **107**, 1012–1019 (2010).
 39. Gould, S. T., Darling, N. J. & Anseth, K. S. Small peptide functionalized thiol-ene hydrogels as culture substrates for understanding valvular interstitial cell activation and de novo tissue deposition. *Acta Biomater* (2012).
 40. Flory, P. J. *Principles of Polymer Chemistry*. (Cornell University Press, 1953).
 41. Flory, P. & Rehner, J. Statistical mechanics of cross-linked polymer networks I Rubberlike elasticity. *J Chem Phys* **11**, 512–520 (1943).
 42. Macosko, C. W. & Miller, D. R. A new derivation of average molecular weights of nonlinear polymers. *Macromolecules* **9**, 199–206 (1976).
 43. Miller, D. R. & Macosko, C. W. A new derivation of post gel properties of network polymers. *Macromolecules* **9**, 206–211 (1976).
 44. Reddy, S., Anseth, K. & Bowman, C. Modeling of network degradation in mixed step-chain growth polymerizations. *Polymer* **46**, 4212–4222 (2005).
 45. Kloxin, A. M. *et al.* Responsive culture platform to examine the influence of microenvironmental geometry on cell function in 3D. *Integr. Biol.* **4**, 1540–1549 (2012).
 46. Anderson, S. B., Lin, C.-C., Kuntzler, D. V. & Anseth, K. S. The performance of human mesenchymal stem cells encapsulated in cell-degradable polymer-peptide hydrogels. *Biomaterials* **32**, 3564–3574 (2011).

47. Bryant, S. & Anseth, K. Controlling the spatial distribution of ECM components in degradable PEG hydrogels for tissue engineering cartilage. *J Biomed Mater Res A* **64A**, 70–79 (2003).

CHAPTER VI -

1. Drury, J. & Mooney, D. Hydrogels for tissue engineering: scaffold design variables and applications. *Biomaterials* **24**, 4337–4351 (2003).
2. Nuttelman, C. R. *et al.* Macromolecular Monomers for the Synthesis of Hydrogel Niches and Their Application in Cell Encapsulation and Tissue Engineering. *Prog Polym Sci* **33**, 167–179 (2008).
3. Wang, D.-A. *et al.* Multifunctional chondroitin sulphate for cartilage tissue-biomaterial integration. *Nat Mater* **6**, 385–392 (2007).
4. Peppas, N., Hilt, J., Khademhosseini, A. & Langer, R. Hydrogels in biology and medicine: From molecular principles to bionanotechnology. *Adv Mater* **18**, 1345–1360 (2006).
5. Benoit, D. S. W., Nuttelman, C. R., Collins, S. D. & Anseth, K. S. Synthesis and characterization of a fluvastatin-releasing hydrogel delivery system to modulate hMSC differentiation and function for bone regeneration. *Biomaterials* **27**, 6102–6110 (2006).
6. Hahn, M. S., Miller, J. S. & West, J. L. Three-Dimensional Biochemical and Biomechanical Patterning of Hydrogels for Guiding Cell Behavior. *Adv Mater* **18**, 2679–2684 (2006).
7. Tayalia, P., Mendonca, C. R., Baldacchini, T., Mooney, D. J. & Mazur, E. 3D Cell-Migration Studies using Two-Photon Engineered Polymer Scaffolds. *Adv Mater* **20**, 4494–4498 (2008).
8. Raeber, G. P., Lutolf, M. P. & Hubbell, J. A. Mechanisms of 3-D migration and matrix remodeling of fibroblasts within artificial ECMs. *Acta Biomater* **3**, 615–629 (2007).
9. Mahoney, M. & Anseth, K. Three-dimensional growth and function of neural tissue in degradable polyethylene glycol hydrogels. *Biomaterials* **27**, 2265–2274 (2006).
10. Adeloew, C., Segura, T., Hubbell, J. A. & Frey, P. The effect of enzymatically degradable poly(ethylene glycol) hydrogels on smooth muscle cell phenotype. *Biomaterials* **29**, 314–326 (2008).
11. Metters, A., Anseth, K. & Bowman, C. Fundamental studies of a novel, biodegradable PEG-b-PLA hydrogel. *Polymer* **41**, 3993–4004 (2000).
12. Nuttelman, C. R., Kloxin, A. M. & Anseth, K. S. Temporal changes in peg hydrogel structure influence human mesenchymal stem cell proliferation and matrix mineralization.

- Adv. Exp. Med. Biol.* **585**, 135–149 (2006).
13. Davis, K. A. & Anseth, K. S. Controlled release from crosslinked degradable networks. *Crit Rev Ther Drug Carrier Syst* **19**, 385–423 (2002).
 14. Seliktar, D., Zisch, A. H., Lutolf, M. P., Wrana, J. L. & Hubbell, J. A. MMP-2 sensitive, VEGF-bearing bioactive hydrogels for promotion of vascular healing. *J Biomed Mater Res A* **68**, 704–716 (2004).
 15. Andreopoulos, F. *et al.* Photocrosslinkable hydrogel synthesis via rapid photopolymerization of novel PEG-based polymers in the absence of photoinitiators. *J Am Chem Soc* **118**, 6235–6240 (1996).
 16. Zheng, Y. *et al.* PEG-based hydrogel synthesis via the photodimerization of anthracene groups. *Macromolecules* **35**, 5228–5234 (2002).
 17. Luo, Y. & Shoichet, M. S. A photolabile hydrogel for guided three-dimensional cell growth and migration. *Nat Mater* **3**, 249–253 (2004).
 18. Kloxin, A. M., Kasko, A. M., Salinas, C. N. & Anseth, K. S. Photodegradable hydrogels for dynamic tuning of physical and chemical properties. *Science* **324**, 59–63 (2009).
 19. Zhao, Y. *et al.* New caged coumarin fluorophores with extraordinary uncaging cross sections suitable for biological imaging applications. *J Am Chem Soc* **126**, 4653–4663 (2004).
 20. Holmes, C. Model studies for new o-nitrobenzyl photolabile linkers: Substituent effects on the rates of photochemical cleavage. *J Org Chem* **62**, 2370–2380 (1997).
 21. Metters, A., Bowman, C. & Anseth, K. A statistical kinetic model for the bulk degradation of PLA-b-PEG-b-PLA hydrogel networks. *J Phys Chem B* **104**, 7043–7049 (2000).
 22. Odian, G. *Principles of Polymerization*. (John Wiley & Sons, Inc.: Hoboken, NJ, 2004).
 23. Young, R. & Lovell, P. *Introduction to polymers*. (Chapman & Hall: London, UK, 1991).
 24. Bryant, S., Nuttelman, C. & Anseth, K. Cytocompatibility of UV and visible light photoinitiating systems on cultured NIH/3T3 fibroblasts in vitro. *J Biomat Sci-Polym E* **11**, 439–457 (2000).
 25. Hudalla, G. A., Eng, T. S. & Murphy, W. L. An approach to modulate degradation and mesenchymal stem cell behavior in poly(ethylene glycol) networks. *Biomacromolecules* **9**, 842–849 (2008).
 26. Bryant, S. J., Bender, R. J., Durand, K. L. & Anseth, K. S. Encapsulating chondrocytes in degrading PEG hydrogels with high modulus: engineering gel structural changes to

facilitate cartilaginous tissue production. *Biotechnol Bioeng* **86**, 747–755 (2004).

CHAPTER VII -

1. Pittenger, M. *et al.* Multilineage potential of adult human mesenchymal stem cells. *Science* **284**, 143–147 (1999).
2. Pelham, R. & Wang, Y. Cell locomotion and focal adhesions are regulated by substrate flexibility. *P Natl Acad Sci Usa* **94**, 13661–13665 (1997).
3. Discher, D., Janmey, P. & Wang, Y. Tissue cells feel and respond to the stiffness of their substrate. *Science* **310**, 1139–1143 (2005).
4. Georges, P. & Janmey, P. Cell type-specific response to growth on soft materials. *J Appl Physiol* **98**, 1547–1553 (2005).
5. Engler, A. J., Sen, S., Sweeney, H. L. & Discher, D. E. Matrix elasticity directs stem cell lineage specification. *Cell* **126**, 677–689 (2006).
6. Frey, M. T. & Wang, Y.-L. A photo-modulatable material for probing cellular responses to substrate rigidity. *Soft Matter* **5**, 1918–1924 (2009).
7. Chen, C. S. Geometric Control of Cell Life and Death. *Science* **276**, 1425–1428 (1997).
8. Singhvi, R. *et al.* Engineering Cell-Shape and Function. *Science* **264**, 696–698 (1994).
9. Tibbitt, M. W. & Anseth, K. S. Hydrogels as Extracellular Matrix Mimics for 3D Cell Culture. *Biotechnol Bioeng* **103**, 655–663 (2009).
10. Freytes, D. O., Wan, L. Q. & Vunjak-Novakovic, G. Geometry and Force Control of Cell Function. *J Cell Biochem* **108**, 1047–1058 (2009).
11. Guilak, F. *et al.* Control of Stem Cell Fate by Physical Interactions with the Extracellular Matrix. *Cell Stem Cell* **5**, 17–26 (2009).
12. Schwartz, M., Schaller, M. & Ginsberg, M. Integrins: Emerging paradigms of signal transduction. *Annu Rev Cell Dev Bi* **11**, 549–599 (1995).
13. Giancotti, F. & Ruoslahti, E. Integrin signaling. *Science* **285**, 1028–1032 (1999).
14. Ingber, D. E. Tensegrity-based mechanosensing from macro to micro. *Prog Biophys Mol Bio* **97**, 163–179 (2008).
15. Mammoto, A. *et al.* A mechanosensitive transcriptional mechanism that controls angiogenesis. *Nature* **457**, 1103–U57 (2009).

16. Birgersdotter, A., Sandberg, R. & Ernberg, I. Gene expression perturbation in vitro - A growing case for three-dimensional (3D) culture systems. *Semin Cancer Biol* **15**, 405–412 (2005).
17. Daley, W. P., Peters, S. B. & Larsen, M. Extracellular matrix dynamics in development and regenerative medicine. *J Cell Sci* **121**, 255–264 (2008).
18. Lauffenburger, D. & Horwitz, A. Cell migration: A physically integrated molecular process. *Cell* **84**, 359–369 (1996).
19. Raucher, D. & Sheetz, M. Cell spreading and lamellipodial extension rate is regulated by membrane tension. *J Cell Biol* **148**, 127–136 (2000).
20. Dobereiner, H., Dubin-Thaler, B., Giannone, G., Xenias, H. & Sheetz, M. Dynamic phase transitions in cell spreading. *Phys Rev Lett* **93**, – (2004).
21. Rajfur, Z., Roy, P., Otey, C., Romer, L. & Jacobson, K. Dissecting the link between stress fibres and focal adhesions by CALI with EGFP fusion proteins. *Nat Cell Biol* **4**, 286–293 (2002).
22. Kumar, S. *et al.* Viscoelastic retraction of single living stress fibers and its impact on cell shape, cytoskeletal organization, and extracellular matrix mechanics. *Biophys J* **90**, 3762–3773 (2006).
23. Ezratty, E. J., Partridge, M. A. & Gundersen, G. G. Microtubule-induced focal adhesion disassembly is mediated by dynamin and focal adhesion kinase. *Nat Cell Biol* **7**, 581–590 (2005).
24. Sen, S. & Kumar, S. Cell-Matrix De-Adhesion Dynamics Reflect Contractile Mechanics. *Cell Mol Bioeng* **2**, 218–230 (2009).
25. Petersen, S. *et al.* Phototriggering of cell adhesion by caged cyclic RGD peptides. *Angew Chem Int Edit* **47**, 3192–3195 (2008).
26. Ohmuro-Matsuyama, Y. & Tatsu, Y. Photocontrolled cell adhesion on a surface functionalized with a caged arginine-glycine-aspartate peptide. *Angew Chem Int Edit* **47**, 7527–7529 (2008).
27. Yeo, W.-S. & Mrksich, M. Electroactive self-assembled monolayers that permit orthogonal control over the adhesion of cells to patterned substrates. *Langmuir* **22**, 10816–10820 (2006).
28. Wildt, B., Wirtz, D. & Searson, P. C. Programmed subcellular release for studying the dynamics of cell detachment. *Nat Meth* **6**, 211–213 (2009).
29. Johnson, J. A., Baskin, J. M., Bertozzi, C. R., Koberstein, J. T. & Turro, N. J. Copper-free

- click chemistry for the in situ crosslinking of photodegradable star polymers. *Chem Commun* 3064–3066 (2008).
30. Kloxin, A. M., Kasko, A. M., Salinas, C. N. & Anseth, K. S. Photodegradable hydrogels for dynamic tuning of physical and chemical properties. *Science* **324**, 59–63 (2009).
 31. Wong, D. Y., Griffin, D. R., Reed, J. & Kasko, A. M. Photodegradable Hydrogels to Generate Positive and Negative Features over Multiple Length Scales. *Macromolecules* **43**, 2824–2831 (2010).
 32. Murayama, S. & Kato, M. Photocontrol of Biological Activities of Protein by Means of a Hydrogel. *Anal. Chem.* **82**, 2186–2191 (2010).
 33. Kloxin, A. M., Tibbitt, M. W., Kasko, A. M., Fairbairn, J. A. & Anseth, K. S. Tunable Hydrogels for External Manipulation of Cellular Microenvironments through Controlled Photodegradation. *Adv Mater* **22**, 61–66 (2010).
 34. Kloxin, A. M., Benton, J. A. & Anseth, K. S. In situ elasticity modulation with dynamic substrates to direct cell phenotype. *Biomaterials* **31**, 1–8 (2010).
 35. Peppas, N., Hilt, J., Khademhosseini, A. & Langer, R. Hydrogels in biology and medicine: From molecular principles to bionanotechnology. *Adv Mater* **18**, 1345–1360 (2006).
 36. Rocco, M., Infusini, E., Daga, M., Gogioso, L. & Cuniberti, C. Models of Fibronectin. *Embo J* **6**, 2343–2349 (1987).
 37. Álvarez, M. *et al.* Single-Photon and Two-Photon Induced Photocleavage for Monolayers of an Alkyltriethoxysilane with a Photoprotected Carboxylic Ester. *Adv Mater* **20**, 4563–4567 (2008).
 38. Aujard, I. *et al.* o-Nitrobenzyl photolabile protecting groups with red-shifted absorption: Syntheses and uncaging cross-sections for one- and two-photon excitation. *Chem-Eur J* **12**, 6865–6879 (2006).
 39. Zhao, Y. *et al.* New caged coumarin fluorophores with extraordinary uncaging cross sections suitable for biological imaging applications. *J Am Chem Soc* **126**, 4653–4663 (2004).
 40. Zipfel, W., Williams, R. & Webb, W. Nonlinear magic: multiphoton microscopy in the biosciences. *Nat Biotechnol* **21**, 1368–1376 (2003).
 41. Reddy, S., Anseth, K. & Bowman, C. Modeling of network degradation in mixed step-chain growth polymerizations. *Polymer* **46**, 4212–4222 (2005).
 42. Kiskin, N., Chillingworth, R., McCray, J., Piston, D. & Ogden, D. The efficiency of two-photon photolysis of a “caged” fluorophore, o-1-(2-nitrophenyl)ethylpyranine, in relation

- to photodamage of synaptic terminals. *Eur Biophys J Biophys* **30**, 588–604 (2002).
43. Heisterkamp, A. *et al.* Pulse energy dependence of subcellular dissection by femtosecond laser pulses. *Opt Express* **13**, 3690–3696 (2005).
 44. Shen, N. *et al.* Ablation of cytoskeletal filaments and mitochondria in live cells using a femtosecond laser nanoscissor. *Mech Chem Biosyst* **2**, 17–25 (2005).
 45. Yanik, M. F. *et al.* Neurosurgery: functional regeneration after laser axotomy. *Nature* **432**, 822 (2004).
 46. Watanabe, W. *et al.* Femtosecond laser disruption of subcellular organelles in a living cell. *Opt Express* **12**, 4203–4213 (2004).

CHAPTER VIII -

1. Wang, N., Butler, J. & Ingber, D. Mechanotransduction Across the Cell-Surface and Through the Cytoskeleton. *Science* **260**, 1124–1127 (1993).
2. Chen, C. S. Mechanotransduction - a field pulling together? *J Cell Sci* **121**, 3285–3292 (2008).
3. Wong, J. Y., Velasco, A., Rajagopalan, P. & Pham, Q. Directed Movement of Vascular Smooth Muscle Cells on Gradient-Compliant Hydrogels †. *Langmuir* **19**, 1908–1913 (2003).
4. Engler, A. J. *et al.* Myotubes differentiate optimally on substrates with tissue-like stiffness: pathological implications for soft or stiff microenvironments. *J Cell Biol* **166**, 877–887 (2004).
5. Engler, A. J., Sen, S., Sweeney, H. L. & Discher, D. E. Matrix elasticity directs stem cell lineage specification. *Cell* **126**, 677–689 (2006).
6. Hinz, B. *et al.* The myofibroblast - One function, multiple origins. *Am J Pathol* **170**, 1807–1816 (2007).
7. Swaminathan, V. *et al.* Mechanical Stiffness Grades Metastatic Potential in Patient Tumor Cells and in Cancer Cell Lines. *Cancer Res* **71**, 5075–5080 (2011).
8. Leach, J. B., Brown, X. Q., Jacot, J. G., Dimilla, P. A. & Wong, J. Y. Neurite outgrowth and branching of PC12 cells on very soft substrates sharply decreases below a threshold of substrate rigidity. *Journal of neural engineering* **4**, 26–34 (2007).
9. Peyton, S. R., Raub, C. B., Keschrums, V. P. & Putnam, A. J. The use of poly(ethylene glycol) hydrogels to investigate the impact of ECM chemistry and mechanics on smooth muscle cells. *Biomaterials* **27**, 4881–4893 (2006).

10. Lo, C. M., Wang, H. B., Dembo, M. & Wang, Y. L. Cell movement is guided by the rigidity of the substrate. *Biophys J* **79**, 144–152 (2000).
11. Zaari, N., Rajagopalan, P., Kim, S., Engler, A. & Wong, J. Photopolymerization in microfluidic gradient generators: Microscale control of substrate compliance to manipulate cell response. *Adv Mater* **16**, 2133 (2004).
12. Genzer, J. & Bhat, R. R. Surface-Bound Soft Matter Gradients. *Langmuir* **24**, 2294–2317 (2008).
13. Kloxin, A. M., Benton, J. A. & Anseth, K. S. In situ elasticity modulation with dynamic substrates to direct cell phenotype. *Biomaterials* **31**, 1–8 (2010).
14. Daley, W. P., Peters, S. B. & Larsen, M. Extracellular matrix dynamics in development and regenerative medicine. *J Cell Sci* **121**, 255–264 (2008).
15. Kloxin, A. M., Tibbitt, M. W. & Anseth, K. S. Synthesis of photodegradable hydrogels as dynamically tunable cell culture platforms. *Nat Protoc* **5**, 1867–1887 (2010).
16. Frey, M. T. & Wang, Y.-L. A photo-modulatable material for probing cellular responses to substrate rigidity. *Soft Matter* **5**, 1918–1924 (2009).
17. Khetan, S., Katz, J. S. & Burdick, J. A. Sequential crosslinking to control cellular spreading in 3-dimensional hydrogels. *Soft Matter* **5**, 1601–1606 (2009).
18. Guvendiren, M. & Burdick, J. A. Stiffening hydrogels to probe short- and long-term cellular responses to dynamic mechanics. *Nat Commun* **3**, – (2012).
19. Khetan, S. & Burdick, J. A. Patterning network structure to spatially control cellular remodeling and stem cell fate within 3-dimensional hydrogels. *Biomaterials* **31**, 8228–8234 (2010).
20. Kloxin, A. M., Kasko, A. M., Salinas, C. N. & Anseth, K. S. Photodegradable hydrogels for dynamic tuning of physical and chemical properties. *Science* **324**, 59–63 (2009).
21. Tibbitt, M. W., Kloxin, A. M., Dyamenahalli, K. U. & Anseth, K. S. Controlled two-photon photodegradation of PEG hydrogels to study and manipulate subcellular interactions on soft materials. *Soft Matter* **6**, 5100–5108 (2010).
22. Bryant, S. Photopolymerization of hydrogel scaffolds. *Scaffolding in Tissue Engineering* 1–21 (2006).
23. Dupont, S. *et al.* Role of YAP/TAZ in mechanotransduction. *Nature* **474**, 179–183 (2011).

CHAPTER IX -

1. Dekanty, A. & Milán, M. The interplay between morphogens and tissue growth. *Embo Rep* **12**, 1003–1010 (2011).
2. Leung, D. W., Cachianes, G., Kuang, W. J., Goeddel, D. V. & Ferrara, N. Vascular endothelial growth factor is a secreted angiogenic mitogen. *Science* **246**, 1306–1309 (1989).
3. Plouet, J., Schilling, J. & Gospodarowicz, D. Isolation and Characterization of a Newly Identified Endothelial-Cell Mitogen Produced by Att-20 Cells. *Embo J* **8**, 3801–3806 (1989).
4. Engler, A. J. *et al.* Embryonic cardiomyocytes beat best on a matrix with heart-like elasticity: scar-like rigidity inhibits beating. *J Cell Sci* **121**, 3794–3802 (2008).
5. Freiberg, S. & Zhu, X. X. Polymer microspheres for controlled drug release. *Int J Pharm* **282**, 1–18 (2004).
6. Peppas, N. A., Bures, P., Leobandung, W. & Ichikawa, H. Hydrogels in pharmaceutical formulations. *Eur J Pharm Biopharm* **50**, 27–46 (2000).
7. Timko, B. P. *et al.* Advances in Drug Delivery. *Annu Rev Mater Res* **41**, 1–20 (2011).
8. Berkland, C., King, M., Cox, A., Kim, K. & Pack, D. W. Precise control of PLG microsphere size provides enhanced control of drug release rate. *J Control Release* **82**, 137–147 (2002).
9. Carpenedo, R. L. *et al.* Homogeneous and organized differentiation within embryoid bodies induced by microsphere-mediated delivery of small molecules. *Biomaterials* **30**, 2507–2515 (2009).
10. Saito, N. *et al.* A biodegradable polymer as a cytokine delivery system for inducing bone formation. *Nat Biotechnol* **19**, 332–335 (2001).
11. Kloxin, A. M., Tibbitt, M. W. & Anseth, K. S. Synthesis of photodegradable hydrogels as dynamically tunable cell culture platforms. *Nat Protoc* **5**, 1867–1887 (2010).
12. Kloxin, A. M., Kasko, A. M., Salinas, C. N. & Anseth, K. S. Photodegradable hydrogels for dynamic tuning of physical and chemical properties. *Science* **324**, 59–63 (2009).
13. Kloxin, A. M., Tibbitt, M. W., Kasko, A. M., Fairbairn, J. A. & Anseth, K. S. Tunable Hydrogels for External Manipulation of Cellular Microenvironments through Controlled Photodegradation. *Adv Mater* **22**, 61–66 (2010).
14. Kloxin, A. M., Benton, J. A. & Anseth, K. S. In situ elasticity modulation with dynamic substrates to direct cell phenotype. *Biomaterials* **31**, 1–8 (2010).

15. Tibbitt, M. W., Kloxin, A. M., Dyamenahalli, K. U. & Anseth, K. S. Controlled two-photon photodegradation of PEG hydrogels to study and manipulate subcellular interactions on soft materials. *Soft Matter* **6**, 5100–5108 (2010).
16. Katz, J. S. *et al.* Modular synthesis of biodegradable diblock copolymers for designing functional polymersomes. *J Am Chem Soc* **132**, 3654–3655 (2010).
17. Yesilyurt, V., Ramireddy, R. & Thayumanavan, S. Photoregulated release of noncovalent guests from dendritic amphiphilic nanocontainers. *Angew Chem Int Ed Engl* **50**, 3038–3042 (2011).
18. Klinger, D. & Landfester, K. Photo-sensitive PMMA microgels: light-triggered swelling and degradation. *Soft Matter* **7**, 1426–1440 (2011).
19. Peng, K. *et al.* Dextran based photodegradable hydrogels formed via a Michael addition. *Soft Matter* **7**, 4881–4887 (2011).
20. Fairbanks, B. D., Singh, S. P., Bowman, C. N. & Anseth, K. S. Photodegradable, Photoadaptable Hydrogels via Radical-Mediated Disulfide Fragmentation Reaction. *Macromolecules* **44**, 2444–2450 (2011).
21. Murthy, N. *et al.* A macromolecular delivery vehicle for protein-based vaccines: acid-degradable protein-loaded microgels. *P Natl Acad Sci Usa* **100**, 4995–5000 (2003).
22. Clarke, D. C., Brown, M. L., Erickson, R. A., Shi, Y. & Liu, X. Transforming growth factor beta depletion is the primary determinant of Smad signaling kinetics. *Mol. Cell Biol.* **29**, 2443–2455 (2009).
23. Zhao, Y. *et al.* New caged coumarin fluorophores with extraordinary uncaging cross sections suitable for biological imaging applications. *J Am Chem Soc* **126**, 4653–4663 (2004).
24. Aujard, I. *et al.* o-Nitrobenzyl photolabile protecting groups with red-shifted absorption: Syntheses and uncaging cross-sections for one- and two-photon excitation. *Chem-Eur J* **12**, 6865–6879 (2006).
25. Clyde, D. E. *et al.* A self-organizing system of repressor gradients establishes segmental complexity in *Drosophila*. *Nature* **426**, 849–853 (2003).
26. Abbott, A. Cell culture: biology's new dimension. *Nature* **424**, 870–872 (2003).
27. Lutolf, M. P. & Hubbell, J. A. Synthetic biomaterials as instructive extracellular microenvironments for morphogenesis in tissue engineering. *Nat Biotechnol* **23**, 47–55 (2005).
28. Tibbitt, M. W. & Anseth, K. S. Hydrogels as Extracellular Matrix Mimics for 3D Cell

Culture. *Biotechnol Bioeng* **103**, 655–663 (2009).

29. Shi, Y. & Massague, J. Mechanisms of TGF-beta signaling from cell membrane to the nucleus. *Cell* **113**, 685–700 (2003).

CHAPTER X -

1. Abbott, A. Cell culture: biology's new dimension. *Nature* **424**, 870–872 (2003).
2. Petersen, O. W., Rønnov-Jessen, L., Howlett, A. R. & Bissell, M. J. Interaction with basement membrane serves to rapidly distinguish growth and differentiation pattern of normal and malignant human breast epithelial cells. *P Natl Acad Sci Usa* **89**, 9064–9068 (1992).
3. Zhang, S., Zhao, X. & Spirio, L. PuraMatrix: Self-assembling peptide nanofiber scaffolds. *Scaffolding in tissue engineering* 217–238 (2005).
4. Gieni, R. S. & Hendzel, M. J. Mechanotransduction from the ECM to the genome: Are the pieces now in place? *J Cell Biochem* **104**, 1964–1987 (2008).
5. Cushing, M. C. & Anseth, K. S. Hydrogel cell cultures. *Science* **316**, 1133–1134 (2007).
6. Tibbitt, M. W. & Anseth, K. S. Hydrogels as Extracellular Matrix Mimics for 3D Cell Culture. *Biotechnol Bioeng* **103**, 655–663 (2009).
7. Lutolf, M. P. & Hubbell, J. A. Synthetic biomaterials as instructive extracellular microenvironments for morphogenesis in tissue engineering. *Nat Biotechnol* **23**, 47–55 (2005).
8. Raeber, G. P., Lutolf, M. P. & Hubbell, J. A. Mechanisms of 3-D migration and matrix remodeling of fibroblasts within artificial ECMs. *Acta Biomater* **3**, 615–629 (2007).
9. Schense, J., Bloch, J., Aebischer, P. & Hubbell, J. Enzymatic incorporation of bioactive peptides into fibrin matrices enhances neurite extension. *Nat Biotechnol* **18**, 415–419 (2000).
10. Saik, J. E., Gould, D. J., Keswani, A. H., Dickinson, M. E. & West, J. L. Biomimetic hydrogels with immobilized ephrinA1 for therapeutic angiogenesis. *Biomacromolecules* **12**, 2715–2722 (2011).
11. Leslie-Barbick, J. E., Saik, J. E., Gould, D. J., Dickinson, M. E. & West, J. L. The promotion of microvasculature formation in poly(ethylene glycol) diacrylate hydrogels by an immobilized VEGF-mimetic peptide. *Biomaterials* **32**, 5782–5789 (2011).
12. Kloxin, A. M., Kasko, A. M., Salinas, C. N. & Anseth, K. S. Photodegradable hydrogels

- for dynamic tuning of physical and chemical properties. *Science* **324**, 59–63 (2009).
13. Tibbitt, M. W., Kloxin, A. M., Dyamenahalli, K. U. & Anseth, K. S. Controlled two-photon photodegradation of PEG hydrogels to study and manipulate subcellular interactions on soft materials. *Soft Matter* **6**, 5100–5108 (2010).
 14. Deforest, C. A. & Anseth, K. S. Cytocompatible click-based hydrogels with dynamically tunable properties through orthogonal photoconjugation and photocleavage reactions. *Nat Chem* **3**, 925–931 (2011).
 15. Deforest, C. A. & Anseth, K. S. Photoreversible Patterning of Biomolecules within Click-Based Hydrogels. *Angew Chem Int Ed Engl* **51**, 1816–1819 (2012).
 16. Peljto, M. & Wichterle, H. Programming embryonic stem cells to neuronal subtypes. *Curr Opin Neurobiol* **21**, 43–51 (2011).
 17. Gordon, C. G. *et al.* Reactivity of Biarylazacyclooctynones in Copper-Free Click Chemistry. *J Am Chem Soc* **134**, 9199–9208 (2012).
 18. Fairbanks, B. D. *et al.* A Versatile Synthetic Extracellular Matrix Mimic via Thiol-Norbornene Photopolymerization. *Adv Mater* **21**, 5005–5010 (2009).
 19. Patterson, J. & Hubbell, J. A. Enhanced proteolytic degradation of molecularly engineered PEG hydrogels in response to MMP-1 and MMP-2. *Biomaterials* **31**, 7836–7845 (2010).
 20. Anderson, S. B., Lin, C.-C., Kuntzler, D. V. & Anseth, K. S. The performance of human mesenchymal stem cells encapsulated in cell-degradable polymer-peptide hydrogels. *Biomaterials* **32**, 3564–3574 (2011).

CHAPTER XI -

1. Evanko, D. Microfluidics and a garden hose. *Nat Meth* **5**, 124–124 (2008).
2. Nagrath, S. *et al.* Isolation of rare circulating tumour cells in cancer patients by microchip technology. *Nature* **450**, 1235–1239 (2007).
3. Cheng, X. *et al.* A microfluidic device for practical label-free CD4(+) T cell counting of HIV-infected subjects. *Lab Chip* **7**, 170–178 (2007).
4. Cristofanilli, M. *et al.* Circulating tumor cells, disease progression, and survival in metastatic breast cancer. *New Engl J Med* **351**, 781–791 (2004).
5. Braun, S. & Marth, C. Circulating tumor cells in metastatic breast cancer--toward individualized treatment? *N. Engl. J. Med.* **351**, 824–826 (2004).
6. Stott, S. L. *et al.* Isolation and characterization of circulating tumor cells from patients

- with localized and metastatic prostate cancer. *Sci Transl Med* **2**, 25ra23 (2010).
7. Maheswaran, S. *et al.* Detection of mutations in EGFR in circulating lung-cancer cells. *N. Engl. J. Med.* **359**, 366–377 (2008).
 8. Pappas, D. & Wang, K. Cellular separations: a review of new challenges in analytical chemistry. *Anal. Chim. Acta* **601**, 26–35 (2007).
 9. Wang, K., Marshall, M. K., Garza, G. & Pappas, D. Open-tubular capillary cell affinity chromatography: single and tandem blood cell separation. *Anal. Chem.* **80**, 2118–2124 (2008).
 10. Shah, A. M. *et al.* Biopolymer system for cell recovery from microfluidic cell capture devices. *Anal. Chem.* **84**, 3682–3688 (2012).
 11. Cooperstein, M. A. & Canavan, H. E. Biological cell detachment from poly(N-isopropyl acrylamide) and its applications. *Langmuir* **26**, 7695–7707 (2010).
 12. Hatch, A., Hansmann, G. & Murthy, S. K. Engineered alginate hydrogels for effective microfluidic capture and release of endothelial progenitor cells from whole blood. *Langmuir* **27**, 4257–4264 (2011).
 13. Machaca, K. Ca(2+) signaling, genes and the cell cycle. *Cell Calcium* **48**, 243–250 (2010).
 14. Kloxin, A. M., Tibbitt, M. W. & Anseth, K. S. Synthesis of photodegradable hydrogels as dynamically tunable cell culture platforms. *Nat Protoc* **5**, 1867–1887 (2010).
 15. Fairbanks, B. D., Schwartz, M. P., Bowman, C. N. & Anseth, K. S. Photoinitiated polymerization of PEG-diacrylate with lithium phenyl-2,4,6-trimethylbenzoylphosphinate: polymerization rate and cytocompatibility. *Biomaterials* **30**, 6702–6707 (2009).
 16. Hume, P. S. & Anseth, K. S. Inducing local T cell apoptosis with anti-Fas-functionalized polymeric coatings fabricated via surface-initiated photopolymerizations. *Biomaterials* **31**, 3166–3174 (2010).
 17. Kloxin, A. M., Kasko, A. M., Salinas, C. N. & Anseth, K. S. Photodegradable hydrogels for dynamic tuning of physical and chemical properties. *Science* **324**, 59–63 (2009).
 18. Tibbitt, M. W., Kloxin, A. M. & Anseth, K. S. Modeling Photodegradation in Optically Thick Polymer Networks for the Predictable Control of Network Evolution. *Macromolecules In Review*
 19. Stott, S. L. *et al.* Isolation of circulating tumor cells using a microvortex-generating herringbone-chip. *P Natl Acad Sci Usa* **107**, 18392–18397 (2010).

CHAPTER XII -

1. Daley, W. P., Peters, S. B. & Larsen, M. Extracellular matrix dynamics in development and regenerative medicine. *J Cell Sci* **121**, 255–264 (2008).
2. Tibbitt, M. W. & Anseth, K. S. Hydrogels as Extracellular Matrix Mimics for 3D Cell Culture. *Biotechnol Bioeng* **103**, 655–663 (2009).
3. Stevens, M. M. & George, J. H. Exploring and Engineering the Cell Surface Interface. *Science* **310**, 1135–1138 (2005).
4. Birgersdotter, A., Sandberg, R. & Ernberg, I. Gene expression perturbation in vitro - A growing case for three-dimensional (3D) culture systems. *Semin Cancer Biol* **15**, 405–412 (2005).
5. Abbott, A. Cell culture: biology's new dimension. *Nature* **424**, 870–872 (2003).
6. Petersen, O. W., Rønnov-Jessen, L., Howlett, A. R. & Bissell, M. J. Interaction with basement membrane serves to rapidly distinguish growth and differentiation pattern of normal and malignant human breast epithelial cells. *P Natl Acad Sci Usa* **89**, 9064–9068 (1992).
7. Wong, D. Y., Griffin, D. R., Reed, J. & Kasko, A. M. Photodegradable Hydrogels to Generate Positive and Negative Features over Multiple Length Scales. *Macromolecules* **43**, 2824–2831 (2010).
8. Griffin, D. R. & Kasko, A. M. Photodegradable macromers and hydrogels for live cell encapsulation and release. *JACS Accepted*
9. Gould, S. T., Darling, N. J. & Anseth, K. S. Small peptide functionalized thiol-ene hydrogels as culture substrates for understanding valvular interstitial cell activation and de novo tissue deposition. *Acta Biomater* (2012).
10. Malkoch, M. *et al.* Synthesis of well-defined hydrogel networks using Click chemistry. *Chem Commun* 2774–2776 (2006).
11. Yang, T. *et al.* Characterization of Well-Defined Poly(ethylene glycol) Hydrogels Prepared by Thiol-ene Chemistry. *J Polym Sci Pol Chem* **49**, 4044–4054 (2011).
12. Engler, A. J., Sen, S., Sweeney, H. L. & Discher, D. E. Matrix elasticity directs stem cell lineage specification. *Cell* **126**, 677–689 (2006).
13. Guvendiren, M. & Burdick, J. A. Stiffening hydrogels to probe short- and long-term cellular responses to dynamic mechanics. *Nat Commun* **3**, – (2012).
14. Chen, C. S. Geometric Control of Cell Life and Death. *Science* **276**, 1425–1428 (1997).
15. Dupont, S. *et al.* Role of YAP/TAZ in mechanotransduction. *Nature* **474**, 179–183 (2011).

